Theory and Phenomenology of Exclusive Rare B Decays

Matthias Beylich

München 2017

Theory and Phenomenology of Exclusive Rare B Decays

Dissertation
an der Fakultät für Physik
der Ludwig-Maximilians-Universität
München

vorgelegt von
Matthias Beylich
aus Hamburg

München, den 20. Juli 2017

Erstgutachter: Prof. Dr. Gerhard Buchalla
Zweitgutachter: Prof. Dr. Stefan Hofmann
Tag der mündlichen Prüfung: 18.09.2017

Zusammenfassung

Hauptgegenstand dieser Arbeit, bestehend aus einem theoretischen und einen phänomenologischen Teil, sind exklusive semileptonische B Zerfälle vom Typ $B \to M\ell^+\ell^-$. Da solche Zerfälle durch Flavour-ändernde neutrale Ströme bei sehr kurzen Abständen hervorgerufen werden, sind sie im Standardmodell stark unterdrückt, woraus sich vielversprechende Möglichkeiten für die indirekte Suche nach neuer Physik ergeben.

Im ersten, theoretischen Teil geht es um die Kontrolle der langreichweitigen Effekte der Quark-Loops. Diese gehen allein aus dem hadronischen Teil des schwachen Hamiltonians hervor, genauer gesagt, aus Pinguin-Diagrammen, bei denen zwei Quarks einer lokalen $(\bar{s}b)(\bar{q}q)$ Wechselwirkung über Photon-Austausch in $\ell^+\ell^-$ annihilieren.

Ein Problem stellt hierbei der Austausch weicher Gluonen zwischen dem Kaon und dem $\bar{q}q$-System dar. Während der etablierte Formalismus der QCD-Faktorisierung eine störungstheoretische Berechnung bei großem Kaon-Rückstoß erlaubt, ist der geeignete theoretische Rahmen bei kleinem Rückstoß ($q^2 \gtrsim 15\,\mathrm{GeV}^2$) durch die hier ausgearbeitete Operator-Produkt-Entwicklung (OPE) gegeben. Sie ermöglicht eine systematische Berechnung der Zerfalls-Amplitude in Potenzen von $\Lambda/\sqrt{q^2}$, wobei die Standard Formfaktoren zu allen Ordnungen in α_s ausreichen, um die hadronische Physik der führenden OPE-Terme zu beschreiben. Im chiralen Limes $m_s = 0$ sind die ersten Korrekturen bereits von relativer Ordnung $1/q^2$ und, wie eine quantitative Abschätzung der entsprechenden Matrixelemente zeigt, vernachlässigbar klein (ca. 0.5%).

Das andere Problem – die Verletzung der Quark-Hadron-Dualität – wird durch die Anwesenheit der Charmonium-Resonanzen verursacht und betrifft somit allein den Charm-Loop bei höherem q^2. Unter Verwendung von Shifmans auf Resonanzen basierendem Modell des hadronischen Korrelators werden die zugrunde liegenden Mechanismen, insbesondere die Verbindung zur Existenz der OPE, abgeklärt. Ferner wird der Einfluss Dualitäts-verletzender Effekte auf die über den Bereich hoher q^2 integrierte $B \to K\ell^+\ell^-$ Zerfallsrate explizit abgeschätzt ($\pm 2\%$).

Im zweiten, phänomenologischen Teil geht es dann um die langreichweitige Physik der hadronischen Matrixelemente. Vorhersagen für exklusive Zerfälle leiden noch immer an den großen Unsicherheiten ($\pm 15\%$), mit denen die Formfaktoren, welche der Beschreibung der hadronischen Physik dienen, behaftet sind. Andererseits sind Formfaktoren vergleichsweise universelle Größen und faktorisieren zudem von der spezifischeren kurzreichweitigen Physik, was durch eine gleichzeitige Betrachtung verwandter Zerfalls-Kanäle zur Konstruktion von Präzision-Observablen ausgenutzt werden kann.

Im einzelnen werden hier die drei Zerfalls-Paare $B^+ \to \pi^+\mu^+\mu^-$ und $\bar{B}^0 \to \pi^+\ell^-\bar{\nu}$, $B \to K^*\ell^+\ell^-$ und $B \to K^*\nu\bar{\nu}$, sowie $B \to K\ell^+\ell^-$ und $B \to K\nu\bar{\nu}$, betrachtet, wobei sich eine Reduktion der Formfaktor-Unsicherheit auf 1.6%, 1% und 0.3% in dem vollständig integrierten π, K^* bzw. K Verhältnis ergibt.

Abstract

The main subject of this thesis, which consists of a theoretical and a phenomenological part, are exclusive semileptonic B decays of the type $B \to M\ell^+\ell^-$. Since such decays are induced by flavour-changing neutral currents at very short distances, they are heavily suppressed in the Standard Model, which results in promising opportunities for the indirect search of new physics.

The first, theoretical part is about the control of the long-distance effects of the quark loops. They arise solely from the hadronic part of the weak Hamiltonian, more specifically, from penguin-type diagrams where two quarks of a local $(\bar{s}b)(\bar{q}q)$ interaction annihilate into $\ell^+\ell^-$ via virtual photon exchange.

One difficulty here is the exchange of soft gluons between the kaon and the $\bar{q}q$ system. While the established formalism of QCD factorization allows for a perturbative calculation at large kaon recoil, the appropriate framework for decays at low recoil ($q^2 \gtrsim 15\,\mathrm{GeV}^2$) is given by the operator product expansion (OPE) developed here. It allows for a systematic computation of the decay amplitude in powers of $\Lambda/\sqrt{q^2}$, whereat the standard form factors are, to all orders in α_s, sufficient to describe the hadronic physics of the leading-power matrix elements. In the chiral limit $m_s = 0$, the first subleading terms are already of relative order $1/q^2$ and, as a quantitative estimate of the corresponding matrix elements shows, negligibly small (roughly 0.5%).

The other difficulty – the violation of quark-hadron duality – is caused by the presence of charmonium resonances and consequently concerns only the charm-loop at higher q^2. Using Shifman's resonance-based model for the hadronic correlator, the systematics of duality violation, in particular the connection to the existence of the OPE, are clarified. Furthermore, we estimate explicitly the impact of duality violating effects on the $B \to K\ell^+\ell^-$ decay rate integrated over the high-q^2 region ($\pm 2\%$).

The second, phenomenological part addresses the long-distance dynamics of the hadronic matrix elements. Predictions for exclusive decays still suffer from the sizeable uncertainties ($\pm 15\%$) of the form factors used to describe the hadronic physics. Then again, form factors are rather universal quantities and factorize from the more specific short-distance dynamics, which can be exploited by a combined analysis of related decay channels for the construction of precision observables.

In detail, we consider here the three decay pairs $B^+ \to \pi^+\mu^+\mu^-$ and $\bar{B}^0 \to \pi^+\ell^-\bar{\nu}$, $B \to K^*\ell^+\ell^-$ and $B \to K^*\nu\bar{\nu}$, as well as $B \to K\ell^+\ell^-$ and $B \to K\nu\bar{\nu}$, finding a reduction of the form factor uncertainty to 1.6%, 1% and 0.3% in the fully integrated π, K^* and K ratio, respectively.

Contents

Part I

Introduction

Introduction

Standard Model – Success and Shortcomings

The *Standard Model* (SM) of particle physics [2, 3] is the most fundamental theory of nature at short distances we currently have. As a (renormalizable) *quantum field theory*, it has incorporated in its formalism the acknowledged principles of quantum mechanics and special relativity. It is further based on the general postulate of *local gauge invariance*, which is an elegant way to obtain interacting fields: The internal $SU(3) \otimes SU(2)_L \otimes U(1)_Y$ symmetry of the Lagrangian gives rise to the electromagnetic, the weak and the strong interaction, which are described by the exchange of gauge bosons.

At the same time, the experimental success of the SM is unprecedented. In particle accelerators and colliders all around the world, its predictions have been confirmed in countless experiments with extreme precision. The prime example for this is the anomalous magnetic moment of the electron a_e, where theory and experiment are consistent at an accuracy of roughly $1ppb$. Also, with the recent discovery of the *Higgs boson* at CERN, the last missing particle predicted by the SM has finally been found.

Nevertheless, despite its remarkable success, the SM is commonly considered to be incomplete, or rather the effective low-energy description of a more fundamental theory. This expectation is based mainly on the following considerations:

- The parameter space of the SM is widely seen as too arbitrary and unnatural for a truly final theory. The first criticism is based on the large number of independent parameters that must be determined experimentally before predictions can be made (at least 19, mostly fermion masses (9), CKM entries (4) and gauge couplings (3)). The second objection comes into play once the parameters have actually been measured: Fermion masses of different generations differ by many orders of magnitude; the entries of the CKM-matrix exhibit an, a priori, unexpected hierarchic structure, and the vacuum angle of *quantum chromodynamics* (QCD) θ_{QCD} is found to be extremely small. All of this indicates that the underlying principles are not fully understood.

- Quantum corrections to the squared mass of the Higgs boson m_H^2 are highly sensitive to physics at short distances – be it through the ultraviolet cutoff Λ_{UV} or the masses of virtual non-SM particles. The circumstance that the measured value for m_H is several orders of magnitude lower than the scales where the arrival of *new physics* (NP) is expected (e.g. the Planck scale) is known as the *hierarchy* or *fine tuning problem*. Strictly speaking, however, this is not a problem of the SM itself, but rather one that immediately arises once the existence of NP is assumed.

- Another shortcoming of the SM is related to the fourth fundamental force, gravity, which is usually neglected for its small impact. While in most cases an accurate description is given by Einstein's general relativity, quantum corrections can in principle be included consistently. There is, however, also the fact that the quantum field theory of gravity is non-renormalizable. This indicates the missing of the UV completion, which becomes relevant towards the Planck scale and thus hampers a profound understanding of black holes and the early universe.

- Finally, there are (mainly cosmological) observations that lack a proper explanation in the SM. This refers to the existence of dark matter and energy but also the unsettled question if the SM has sufficient sources of CP violation to account for the observed matter-antimatter asymmetry in the universe.

Search for New Physics with $B \to M\ell^+\ell^-$ Decays

In general, there are two different ways to search for physics beyond the SM:

Firstly, there is the *direct* approach: the production and subsequent detection of the unknown particles themselves. This method, however, is limited by the accessible energies in present colliders.

Secondly, at energies below their production threshold, the heavy unknown particles still have an influence on the SM decay channels through quantum effects, which can be exploited for an *indirect* detection. However, with the SM being such a well confirmed theory, this requires high precision in theoretical predictions and experimental measurements alike as well as the selection of particularly sensitive modes. In this respect, rare B decays of the type $B \to M\ell^+\ell^-$ are promising candidates, in particular as several modes already show some tension (up to 3.7σ) with the corresponding SM prediction [4, 5], indicating a reduction of the effective coefficient C_9 due to NP.

A short review of the most important properties of rare B decays – at the center of this work for the above reasons – is given below:

- As the top quark is not sufficiently stable, B mesons are the heaviest mesons, the decay of which can be studied. Apart from a large phase-space and a great diversity of decay channels, B decays therefore represent the most direct way to probe some of the less explored areas of the SM (notably in the flavour sector).

- *Rare B* decays are induced by *flavour-changing neutral currents* (FCNCs), which are heavily suppressed in the SM: They occur only at second order in the electroweak interaction and involve at least one off-diagonal element of the *Cabibbo-Kobayashi-Maskawa* (CKM)-matrix. In particular, this implies a small absolute uncertainty in theoretical predictions already at leading order in perturbation theory. The impact of NP, not necessarily suppressed in the same way, should therefore be easier to identify in these modes.

- In comparison to *inclusive* modes, such as $\bar{B} \to X_s \ell^+\ell^-$, where the problem can be reduced virtually to the one of free quarks, the *exclusive* $B \to M\ell^+\ell^-$ modes are theoretically less clean, as they necessarily involve the non-perturbative dynamics of the hadronization process. But then again, the exclusive decays, discussed in this work, are experimentally easier to handle, and consequently meaningful experimental results will be available for them earlier than for the inclusive decays.

- The different contributions to the $B \to M\ell^+\ell^-$ amplitude can be divided into two distinct categories:

  On the one hand, there are the matrix elements of the non-hadronic operators $\mathcal{O}_{7,9,10}$, which dominate the spectrum outside the domain of the narrow charmonium resonances due to the size of the semileptonic Wilson coefficients $C_{9,10}$. These contributions are theoretically also rather clean and simple, as short- and long-distance dynamics factorize completely into coefficient functions and standard $B \to M$ form factors, respectively.

  On the other hand, there are the theoretically more challenging, non-local contributions of the hadronic operators $\mathcal{O}_{1-6,8}$. These are typically penguin-type diagrams, where two quarks of a local $(\bar{s}b)(\bar{q}q)$ interaction annihilate into the final leptons via virtual photon exchange. Although small in comparison (about 10%), precise predictions require reliable results for these contributions as well.

- The properties (and with them the theoretical challenges and the treatment) of the non-local term strongly depend on the size of the dilepton invariant mass q^2:

  At low q^2, that is, at large kaon recoil, QCD factorization [6] represents the appropriate framework.

  In the middle part of the spectrum $7\,\mathrm{GeV}^2 \lesssim q^2 \lesssim 15\,\mathrm{GeV}^2$, the narrow charmonium resonances give rise to large violations of quark-hadron, which exceed the perturbative contributions by two orders of magnitude [7]. This part of the spectrum is therefore frequently removed by suitable cuts.

  The domain of high q^2, finally, is best addressed by performing an *operator product expansion* (OPE) for the non-leptonic part of the Hamiltonian. In addition, violations of duality – though (presumably) dampened by the broadening of the resonances – must still be quantified for (precise) theoretical predictions to be meaningful. Both these issues of the high-q^2 domain are discussed in the theoretical part of this work.

- As is apparent from the above, form factors are inherently non-perturbative quantities. Hence, their theoretical determination is limited to other, currently not very precise methods ($\pm 15\%$), such as lattice QCD [8] or QCD sum rules on the light-cone [9].

Then again, form factors are quite universal, which can be exploited by extracting the non-perturbative input needed for the prediction of one decay from the experimental data of another. Alternatively (which is also the general idea inspiring the phenomenological part of this work), one can take advantage of this by considering suitable ratios of related branching fractions, in which the form factor uncertainties are eliminated almost completely.

Structure of Thesis

This thesis is structured as follows:

The chapters 1 – 3 provide a brief review of the basic tools and concepts in B physics particularly relevant to the later discussed exclusive rare modes. In addition, this part serves as a summary of the employed conventions and notations for future reference. The individual chapters are about the kinematics and phase-space of 3-body decays (1), the formalism of effective weak Hamiltonians (2), and the treatment of the hadronic matrix elements encountered in $B \to M\ell^+\ell^-$ decays (3).

The actual work is divided into a theoretical part, which is based on [1], and a phenomenological part. In the first, theoretical part, consisting of the chapters 4 – 6, the two main theoretical issues of exclusive $b \to s\ell^+\ell^-$ transitions at low recoil are addressed. This includes a short review of the current correlator, responsible for the problems (4), the construction of an OPE, a suitable framework for calculations at high-q^2 (5), and the investigation of duality violating effects, caused by the presence of charmonium resonances (6).

The second, phenomenological part is devoted to the construction of precision observables virtually free of form factor uncertainties. To this end, in each of the chapters 7 – 9, two decays with similar long- but different short-distance dynamics are considered together. In detail, we perform a combined NLO analysis of $B^+ \to \pi^+\mu^+\mu^-$ and $\bar{B}^0 \to \pi^+\ell^-\bar{\nu}$ (7), $B \to K^*\nu\bar{\nu}$ and $B \to K^*\ell^+\ell^-$ (8), as well as a combined NNLO analysis of $B \to K\nu\bar{\nu}$ and $B \to K\ell^+\ell^-$ (9).

Finally, in the conclusions (V) the most important aspects and implications of this work are highlighted and summarized.

In the appendix, we give the numerical values of our input parameters (A) as well as the parametrizations employed for the $B \to K^{(*)}, \pi$ form factors and light-cone wave functions (B). Furthermore, it contains some rather technical details, such as the 3-loop beta-function (C), the RGE evolution of the Wilson coefficients (D), a proof for the completeness of the operator basis used in the OPE (E), and the calculation of some Feynman integrals, relevant to $B \to K\ell^+\ell^-$ at NNLO (F).

Part II

Fundamentals

1 Kinematics

This chapter is intended as a brief introduction to the kinematics of $B \to K^{(*)}\ell^+\ell^-$ decays. Special attention is given to the general structure of 3-body decay spectra.

1.1 Basic Formulas and Notation

The four-vectors (masses) of the B and $K^{(*)}$ meson are denoted as $p^\mu(m_B)$ and $k^\mu(m_K)$, respectively. The two momenta of the dilepton system, denoted as $q^\mu_{1,2}$, then satisfy

$$q_1^\mu + q_2^\mu \;\equiv\; q^\mu \;=\; p^\mu - k^\mu \tag{1.1}$$

and consequently the dilepton invariant mass squared attains values in the interval

$$4m_l^2 \;\approx\; 0 \;\leqslant\; q^2 \;\leqslant\; \left(m_B - m_K\right)^2 \tag{1.2}$$

To simplify the notation, one frequently makes use of the dimensionless invariants

$$s \;\equiv\; \frac{q^2}{m_B^2} \qquad\qquad r \;\equiv\; \frac{m_K^2}{m_B^2} \tag{1.3}$$

It is usually convenient to describe the decay in the center of mass frame, that is, in the rest frame of the B meson. In this frame of reference, the energy of the kaon is given as

$$E \;\equiv\; E_K \;=\; \frac{m_B}{2}\left[1 - \frac{q^2}{m_B^2} + \frac{m_K^2}{m_B^2}\right] \;=\; \frac{m_B}{2}\left(1 - s + r\right) \tag{1.4}$$

and thus, considering the boundaries of the dilepton mass (1.2), has a kinematically permitted range of

$$m_K \;\leqslant\; E \;\leqslant\; \frac{m_B}{2} + \frac{m_K^2}{2m_B} \tag{1.5}$$

At times, the clarity of presentation can also be improved by introducing the two light-like four-vectors (rest frame)

$$n_\pm^\mu \;\equiv\; (1,0,0,\pm 1) \tag{1.6}$$

which satisfy the invariant constraints

$$n_\pm^2 \;=\; 0 \qquad\qquad \text{and} \qquad\qquad n_\pm \cdot n_\mp \;=\; 2 \tag{1.7}$$

Without loss of generality, the meson momenta can then be written as

$$q^\mu \;=\; \frac{m_B - E}{2}\,(n_+^\mu + n_-^\mu) \;-\; \frac{|\vec{k}|}{2}\,(n_+^\mu - n_-^\mu) \tag{1.8}$$

$$k^\mu \;=\; \frac{E}{2}\,(n_+^\mu + n_-^\mu) \;+\; \frac{|\vec{k}|}{2}\,(n_+^\mu - n_-^\mu) \tag{1.9}$$

Vice versa, we have

$$\frac{m_B}{2}\,(n_+^\mu + n_-^\mu) \;\equiv\; m_B v^\mu \;=\; p^\mu \tag{1.10}$$

$$\frac{m_B}{2}\,(n_+^\mu - n_-^\mu) \;=\; \frac{m_B}{|\vec{k}|}\left[k^\mu \;-\; \frac{k\cdot p}{p^2}\,p^\mu\right] \tag{1.11}$$

Furthermore, in the case of a decay into a longitudinally polarized vector meson, the polarization vector can be expressed as

$$\varepsilon_\parallel^{*\mu} \;=\; \frac{|\vec{k}|}{2m_K}\,(n_+^\mu + n_-^\mu) \;+\; \frac{E}{2m_K}\,(n_+^\mu - n_-^\mu) \;=\; \frac{\sqrt{r}}{|\vec{k}|}\left[\frac{q\cdot k}{k^2}\,k^\mu \;-\; q^\mu\right] \tag{1.12}$$

which can be derived exploiting the invariant conditions $\varepsilon^2 = -1$ and $\varepsilon \cdot k = 0$. The above formula further implies

$$\varepsilon_\parallel^* \cdot q \;=\; \frac{|\vec{k}|}{\sqrt{r}} \tag{1.13}$$

Finally, there is a close relation between the spatial part of k^μ

$$|\vec{k}| \;=\; E\sqrt{1 - \left(\frac{m_K}{E}\right)^2} \;=\; \frac{\sqrt{(q\cdot k)^2 - q^2 k^2}}{m_B} \;=\; \frac{m_B}{2}\,\lambda^{1/2}(s) \tag{1.14}$$

and the phase-space function

$$\lambda(s) \;\equiv\; 1 + r^2 + s^2 - 2r - 2s - 2rs \tag{1.15}$$

The more prevalent (eponymous) interpretation of $\lambda(s)$, however, is given in the following section.

1.2 Phase-Space and Dilepton-Mass Spectra

The general structure of (partially integrated) $B \to M\ell^+\ell^-$ decay spectra is derived from first principles. Since the only information relevant to us is about particle interactions, all kinematic parameters on which the Feynman amplitude does not depend will be removed by integration. Furthermore, we assume vanishing lepton masses $m_l = 0$ and average over spin and polarization of outgoing particles. As we will see, this leads to dilepton mass spectra, constrained to a very specific form.

Taking into account the conservation of four-momentum as well as the energy-momentum relations, a 3-body decay may depend on five independent (kinematic) parameters. If, furthermore, rotational symmetry is exploited (e.g. by integration), the differential decay rate can be expressed in terms of just two variables, for instance

$$\frac{d\Gamma}{ds\,du} = \frac{m_B}{256\pi^3}\left|\overline{\mathcal{M}}(s,u)\right|^2 \qquad u = (p-q_1)^2/m_B^2 \tag{1.16}$$

This ultimately derives from the fact that only two independent variable Lorentz scalars can be build from the available momenta p,k,q_1 and q_2 (for $B \to V\ell^+\ell^-$, $\varepsilon^{*\mu}$ drops out once the polarization sum is taken), and consequently can appear in the (invariant) Feynman amplitude $\mathcal{M}$.

Besides, for a given s, the parameter u ranges within the boundaries

$$\frac{E}{m_B} - \frac{\lambda^{1/2}}{2} \leqslant u \leqslant \frac{E}{m_B} + \frac{\lambda^{1/2}}{2} \tag{1.17}$$

which also explains the name of the phase-space function $\lambda(s)$.

Next, the Feynman amplitude is decomposed into a vector and an axial vector component according to

$$i\mathcal{M}(s,u) \equiv \langle \bar{M}\ell^+\ell^-|\mathcal{H}_{\mathit{eff}}|\bar{B}\rangle = \mathcal{A}_V^\mu(s)\,\bar{u}(q_1)\gamma_\mu v(q_2) + \mathcal{A}_A^\mu(s)\,\bar{u}(q_1)\gamma_\mu\gamma_5 v(q_2) \tag{1.18}$$

After eliminating the lepton spinors $\bar{u}, v$ in the squared amplitude via spin summation, e.g. by using $\sum_s v^s\bar{v}^s \to \not{q}_2$, we have

$$|\overline{\mathcal{M}}|^2 = \left(\mathcal{A}_V^\mu\mathcal{A}_V^{*\nu} + \mathcal{A}_A^\mu\mathcal{A}_A^{*\nu}\right)\mathrm{tr}\left[\not{q}_1\gamma_\mu\not{q}_2\gamma_\nu\right] + 2\,\mathrm{Im}\left[\mathcal{A}_V^\mu\mathcal{A}_A^{*\nu}\right]\mathrm{tr}\left[\not{q}_1\gamma_\mu\not{q}_2\gamma_\nu\gamma_5\right] \tag{1.19}$$

It is usually sensible to consider just the leading contributions in the electroweak interaction. In this case, one can immediately rule out any dependence of the amplitudes $\mathcal{A}_{V,A}^\mu$ on the individual lepton momenta $q_{1,2}$ or, equivalently, on the parameter u. As a consequence, the u integration can then be performed, without further specifying the decay. By Lorentz invariance, one may thereby replace

$$12\int du\, q_1^\mu q_2^\nu = \left[2q^\mu q^\nu + q^2 g^{\mu\nu}\right]\int du = \left[2q^\mu q^\nu + q^2 g^{\mu\nu}\right]\lambda^{1/2}(s) \tag{1.20}$$

Thus, when integrating the squared amplitude over u, the different symmetry behaviour of the two terms in (1.19) under the exchange $q_1 \leftrightarrow q_2$ turns out to be crucial: The second term vanishes, and we obtain

$$\frac{d\Gamma}{ds}(B \to M\ell^+\ell^-) = \frac{m_B\,\lambda^{1/2}(s)}{192\pi^3}\left[q_\mu q_\nu - q^2 g_{\mu\nu}\right]\left(\mathcal{A}_V^\mu\mathcal{A}_V^{*\nu} + \mathcal{A}_A^\mu\mathcal{A}_A^{*\nu}\right) \tag{1.21}$$

1.2.1 $B \to P$ Decays

As the lepton masses are here neglected, a term in the partial amplitudes $\mathcal{A}^\mu_{V,A}$ proportional to q^μ gives no contribution to the decay rate. This can be seen by contracting q^μ into (1.18) and applying the equations of motion (e.o.m.) for the leptons. But then again, this property is already incorporated in the general form (1.21).

As far as decays into pseudoscalar mesons are concerned, one may thus assume

$$\mathcal{A}^\mu_{V,A}(s) \;=\; \mathcal{A}_{V,A}(s)\, p^\mu \tag{1.22}$$

Inserting in (1.21), the differential decay rate simplifies to

$$\frac{d\Gamma}{ds}\big(B \;\to\; P\ell^+\ell^-\big) \;=\; \frac{m_B^5\,\lambda^{3/2}(s)}{768\pi^3}\Big\{\big|\mathcal{A}_V(s)\big|^2 \,+\, \big|\mathcal{A}_A\big|^2\Big\} \tag{1.23}$$

where, in the SM, the axial amplitude $\mathcal{A}_A$ is a purely short-distance quantity, induced at the weak scale.

1.2.2 $B \to V$ Decays

Considering the strict separation of the two amplitudes $\mathcal{A}^\mu_{V,A}$ in (1.21), the branching fraction may be decomposed according to

$$\frac{d\Gamma}{ds}\big(B \;\to\; V\ell^+\ell^-\big) \;=\; \frac{d\Gamma_V}{ds} + \frac{d\Gamma_A}{ds} \tag{1.24}$$

which allows to restrict the explicit discussion to, for instance, just the vector component Γ_V.

Since there is now additionally the polarization vector $\varepsilon^{*\mu}$, on which the Feynman amplitude depends linearly, a general Lorentz decomposition of $\mathcal{A}^\mu_V$ is given by

$$\mathcal{A}^\mu_V\, m_B \;=\; 2\mathcal{V}(s)\, i\varepsilon^{\mu k p \varepsilon^*} \;-\; \mathcal{A}_1(s) m_B^2\, \varepsilon^{*\mu} \;+\; 2\mathcal{A}_2(s)(\varepsilon^*\!\cdot q)\,p^\mu \tag{1.25}$$

Once considering the squared amplitude, $\varepsilon^{*\mu}$ can be eliminated by taking the polarization sum

$$\sum_\varepsilon \varepsilon^{*\mu}\varepsilon^\nu \;\to\; -g^{\mu\nu} + \frac{k^\mu k^\nu}{k^2} \tag{1.26}$$

What then remains of the decomposition (1.25) is a characteristic kinematic prefactor, with which each partial amplitude appears in the differential decay rate

$$\frac{d\Gamma_V}{ds} \;=\; \frac{m_B^5\,\lambda^{1/2}(s)}{768\pi^3}\Big\{8s\Big(\big|\mathcal{V}\big|^2\lambda(s) + \big|\mathcal{A}_1\big|^2\Big) + \frac{1}{r}\Big|\mathcal{A}_2\lambda(s) \,-\, \frac{2k\cdot q}{m_B^2}\,\mathcal{A}_1\Big|^2\Big\} \tag{1.27}$$

As a final note, it is pointed out that the first term in (1.27) (round bracket) corresponds to a transversely, the second term to a longitudinally polarized vector meson.

2 Effective Weak Hamiltonians

B decays are by nature inseparably linked to two vastly different energy scales: Firstly, the scale of the inducing weak interaction and, secondly, the scale of the decaying B meson itself. Unfortunately, when calculating quantum corrections, the simultaneous presence of physics from such distinct scales gives rise to sizable logarithms $\ln M_W^2/m_b^2 \approx 6$, which thwarts the *direct* perturbative approach. This being said, both scales are still hard in comparison to the QCD scale Λ_{QCD}, which indicates that the perturbative breakdown at hand is not related to long-distance dynamics of the strong interaction. In other words, perturbation theory is *in principle* justified, even at the much lower scale m_b.

The problem is usually addressed by the construction of an effective weak Hamiltonian $\mathcal{H}_{\mathit{eff}}$, a procedure shortly described in the following sections. An exhaustive discussion of weak Hamiltonians, however, is certainly beyond the scope of this work. The interested reader is encouraged to consult the relevant literature [10, 11, 12].

2.1 OPE and RG Evolution

The intuitive understanding underlying the OPE is that low momenta $k^2 \sim m_b^2$ resolve the physics at short distances rather poorly. This train of thought naturally leads to the approximation illustrated in Fig. 2.1: The non-local W-exchange is described by a series of local operators $\mathcal{O}_i(\mu)$ with *Wilson coefficients* $C_i(\mu)$

$$(\bar{s}_L\gamma_\mu c)\,\frac{ig^{\mu\nu}}{k^2 - M_W^2}\,(\bar{c}_L\gamma_\nu b) + \text{QCD} \;\Rightarrow\; \sum_i C_i(M_W/\mu, \alpha_s)\mathcal{O}_i(\mu) + \mathcal{O}(k^2/M_W^2) \tag{2.1}$$

In the effective theory (r.h.s of (2.1)), the heavy particles no longer represent active degrees of freedom. What is left of them are the different induced interactions, in particular, the dependence of the corresponding coefficient functions on their masses.

Technically speaking, the OPE represents an expansion of the amplitude in the small parameter m_b^2/M_W^2. Thereby, the leading term consists of operators of energy dimension 6 – the contributions of higher dimensional operators are power suppressed and can in general be neglected.

As a first step, the coefficient functions are determined by *matching* the effective onto the full theory. This, however, can perturbatively be accomplished at a renormalization scale $\mu \sim M_W$ only. Admittedly, the coefficient functions, or rather the Hamiltonian, are actually needed at $\mu \sim m_b$, for this is the appropriate scale to renormalize the matrix

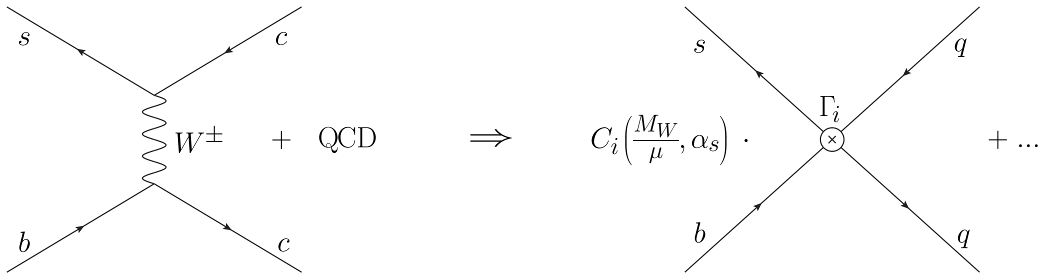

Figure 2.1: OPE at the weak scale: The non-local W-exchange is approximated by a series of local operators. The presence of QCD leads to a multitude of four-quark operators, which differ in their colour-, flavour- and/or Dirac-structure. Depending on the decay considered, local operators with less quark content may contribute as well.

elements of the local operators. That being so, the Wilson coefficients have then to be evolved down to lower energies. As further described in appendix D.1, this is accomplished by solving the relevant *renormalization group equation* (RGE)

$$\frac{d}{d\ln\mu}\vec{C}(\mu) \;=\; \hat{\gamma}^T\vec{C}(\mu) \tag{2.2}$$

In so doing, all contributions up to the considered order in the counting

$$\alpha_s^m(\alpha_s \ln m_b^2/M_W^2)^n \;\sim\; \mathcal{O}(\alpha_s^m) \tag{2.3}$$

are *resummed* in the coefficients $\vec{C}(m_b)$, which indicates that all (short-distance) dynamics above the scale $\mu \sim m_b$ (therefore also called *factorization* scale) are now absorbed into the coefficients. The matrix elements of the local operators, on the other hand, contain only (long-distance) dynamics below μ and thus, in particular, no longer suffer from large logarithms. This is clearly the most important feature of effective Hamiltonians: the systematic disentanglement of the physics governed by distinct scales.

Finally, it should be stressed that, as a matter of consistency, any arbitrariness must (to the given order) drop out in physical quantities. This refers in particular to the concrete choice of the scale μ. In order to ensure this, consistent usage of the same specific renormalization scheme is mandatory. Throughout this work, the *naive dimensional regularization* (NDR) [13] in combination with the modified *minimal subtraction* scheme ($\overline{MS}$ scheme) [14] is continuously put to use.

2.2 Flavour Structure

With respect to $b \to s(d)\ell^+\ell^-$ transitions, it is easily seen that all relevant SM processes are proportional to one of the CKM-combinations

$$\lambda_p \;\equiv\; V_{pq}^* V_{pb} \qquad \text{where} \qquad q \;=\; s(d) \tag{2.4}$$

Of course, this circumstance is also reflected in the general flavour structure of the effective weak $\Delta B = 1, \Delta C = 0$ Hamiltonian

$$\mathcal{H}_{\mathit{eff}} \;=\; \vec{C}^{\,T}_{ex}(0) \cdot \Big\{\lambda_u \vec{Q}^{\,u}_{ex} + \lambda_c \vec{Q}^{\,c}_{ex}\Big\} + \Big\{\big(\lambda_u + \lambda_c\big)\vec{C}^{\,T}_{in}(0) + \lambda_t \vec{C}^{\,T}_{in}(m_t)\Big\} \cdot \vec{Q}_{in} \tag{2.5}$$

Here the individual interactions of the Hamiltonian have been divided into two categories:

On the one hand, there are the (4-quark) operators $\vec{Q}^{\,u,c}_{ex}$ of the first term. They originate from current-current diagrams, where the weak interacting up-type quarks are *external* (ingoing/outgoing, that is). Thus, the corresponding contributions from the light quarks differ just by the replacement $u \leftrightarrow c$ in the induced local operators. Meanwhile, since the top quark is integrated out, there is no top equivalent in the first term.

The second term, on the other hand, is due to diagrams where the W-boson is interacting with *internal* (virtual, that is) up-type quarks, for instance, penguin diagrams. Since the exchange of virtual quarks $u \leftrightarrow c \leftrightarrow t$ can only effect the coefficient functions, each quark sector induces the same set of local operators $\vec{Q}_{in}$. However, in case of the top contribution, the quark mass can not be neglected which results in a different Wilson coefficient $\vec{C}_{in}(m_t)$.

If we now exploit the unitarity relation

$$\lambda_t + \lambda_c + \lambda_u \;=\; 0 \tag{2.6}$$

the second term in (2.5) simplifies to

$$\mathcal{H}_{\mathit{eff}} \;=\; \vec{C}^{\,T}_{ex} \cdot \Big\{\lambda_u \vec{Q}^{\,u}_{ex} + \lambda_c \vec{Q}^{\,c}_{ex}\Big\} - \lambda_t \Big\{\vec{C}^{\,T}_{in}(0) - \vec{C}^{\,T}_{in}(m_t)\Big\} \cdot \vec{Q}_{in} \tag{2.7}$$

Furthermore, in the specific case of a $b \to s$ transition, there is a hierarchic structure between the flavour sectors, namely

$$\lambda_u \;\ll\; \lambda_t, \lambda_c \tag{2.8}$$

This then allows to further simplify the structure of the effective Hamiltonian

$$\mathcal{H}_{\mathit{eff}} \;=\; -\lambda_t \Big[\vec{C}^{\,T}_{ex} \cdot \vec{Q}^{\,c}_{ex} + \Big\{\vec{C}^{\,T}_{in}(0) - \vec{C}^{\,T}_{in}(m_t)\Big\} \cdot \vec{Q}_{in}\Big] \;\equiv\; -\lambda_t C_i Q_i \tag{2.9}$$

2.3 Operator Bases

In the following, two different sets of operators, henceforth denoted as $\{\mathcal{O}_i\}$ and $\{\mathcal{Q}_i\}$, are introduced. While, in principle, these two sets represent equally legitimate operator bases for the effective Hamiltonian, one of them is usually better suited for a specific task.

The traditional operator basis $\{\mathcal{O}_i\}$ [10, 11] is in general more transparent and will therefore be employed throughout most of this work. The basis $\{\mathcal{Q}_i\}$, established by the authors of [15, 16, 17, 18, 19], however, is more convenient for higher order calculations which, in the context of this work, only concerns the next-to-next-to-leading order (NNLO) analysis performed in chapter 9. The transfer of results from one basis to another is shortly discussed in appendix D.5.

2.3.1 Conventions

So that operators and Wilson coefficients can unambiguously be defined, let us clarify the conventions that complement the two Hamiltonians (2.20) and (2.16) beforehand:

- It is common practice, to factor out the constant

$$\frac{G_F}{\sqrt{2}} = \frac{g^2}{8M_W^2} \qquad \text{where} \qquad g^2 = \frac{e^2}{\sin^2\theta_W} \tag{2.10}$$

  At this, G_F, g and θ_W are the Fermi constant, the weak coupling constant and the Weinberg angle, respectively.

- For the covariant derivatives of quarks and charged leptons, we take

$$D_\mu = \partial_\mu + ieQ_e A_\mu \qquad \text{and} \qquad D_\mu = \partial_\mu + ieQ_q A_\mu + ig_s T^a A_\mu^a, \tag{2.11}$$

  respectively. Here Q_f denotes the charge quantum number of the fermion in question ($Q_e e = -e$ is the charge of the electron), and the $SU(3)$ generators satisfy

$$\left[T^a, T^b\right] = if^{abc}T^c \qquad T^a_{ij}T^a_{kl} = \frac{1}{2}\delta_{il}\delta_{kj} - \frac{1}{2N}\delta_{ij}\delta_{kl} \tag{2.12}$$

  The specification (2.11) is required for an unambiguous definition of operators containing the field strength tensor of electromagnetic or strong interaction

$$F_{\mu\nu} = \partial_\mu A_\nu - \partial_\nu A_\mu \qquad G^a_{\mu\nu} = \partial_\mu A^a_\nu - \partial_\nu A^a_\mu - g_s f^{abc} A^b_\mu A^c_\nu \tag{2.13}$$

  The conventions chosen here imply negative magnetic Wilson coefficients $C_{7,8}(\mathcal{C}_{7,8})$, which is the prevalent convention in the literature as well.

- It is stressed that by $C_{7,8}(\mathcal{C}_{7,8})$ we always mean the corresponding effective coefficients as defined in (D.12)((D.13)).

- Lastly, regarding the notation of chiral fields, it should be kept in mind that left- and right-handed fields are defined by means of projection operators

$$\bar{q}_{L,R} = \frac{1}{2}\bar{q}(1 \pm \gamma_5) \qquad \text{and} \qquad q_{L,R} = \frac{1}{2}(1 \mp \gamma_5)q \tag{2.14}$$

In contrast to this, the vector and axial vector current are normalized as

$$(\bar{q}q)_V \;=\; (\bar{q}\gamma_\mu q) \qquad\qquad (\bar{q}q)_A \;=\; (\bar{q}\gamma_\mu\gamma_5 q) \tag{2.15}$$

All in all, this introduces a relative factor of two when switching between these two notations.

2.3.2 Traditional Basis

With the effective weak Hamiltonian for $b \to s\ell^+\ell^-\,(\nu\bar{\nu})$ transitions defined as

$$\mathcal{H}_{\mathit{eff}} \;=\; -\frac{G_F}{\sqrt{2}}\lambda_t\left[\sum_{i=1}^{10} C_i(\mu)\mathcal{O}_i(\mu) \;+\; C_\nu(\mu)\mathcal{O}_\nu(\mu)\right] \;+\; \text{h.c.} \tag{2.16}$$

our "standard" operator basis $\{\mathcal{O}_i\}$ reads [10, 11]

$$\begin{aligned}
\mathcal{O}_1 &= (\bar{s}c)_{V-A}(\bar{c}b)_{V-A} & \mathcal{O}_2 &= (\bar{s}_i c_j)_{V-A}(\bar{c}_j b_i)_{V-A} \\
\mathcal{O}_3 &= (\bar{s}b)_{V-A}\textstyle\sum_q(\bar{q}q)_{V-A} & \mathcal{O}_4 &= (\bar{s}_i b_j)_{V-A}\textstyle\sum_q(\bar{q}_j q_i)_{V-A} \\
\mathcal{O}_5 &= (\bar{s}b)_{V-A}\textstyle\sum_q(\bar{q}q)_{V+A} & \mathcal{O}_6 &= (\bar{s}_i b_j)_{V-A}\textstyle\sum_q(\bar{q}_j q_i)_{V+A} \\
\mathcal{O}_7 &= \frac{e}{8\pi^2}\,m_b\,\bar{s}\sigma^{\mu\nu}(1+\gamma_5)b\,F_{\mu\nu} & \mathcal{O}_8 &= \frac{g_s}{8\pi^2}\,m_b\,\bar{s}\sigma^{\mu\nu}(1+\gamma_5)T^a b\,G^a_{\mu\nu} \\
\mathcal{O}_9 &= \frac{\alpha_e}{2\pi}(\bar{s}b)_{V-A}\textstyle\sum_\ell(\bar{\ell}\ell)_V & \mathcal{O}_{10} &= \frac{\alpha_e}{2\pi}(\bar{s}b)_{V-A}\textstyle\sum_\ell(\bar{\ell}\ell)_A \\
\mathcal{O}_\nu &= \frac{\alpha_e}{2\pi}(\bar{s}b)_{V-A}\textstyle\sum_\nu(\bar{\nu}\nu)_{V-A}
\end{aligned} \tag{2.17}$$

Here $\alpha_e = \frac{e^2}{4\pi}$ is the well known fine-structure constant and a summation over repeated colour indices i, j is – as always – implicitly understood.

As explained in the previous section (2.2), there are also contributions of relative order λ_u/λ_t, which can be summarized in the Hamiltonian

$$\mathcal{H}^u_{\mathit{eff}} \;\equiv\; \frac{G_F}{\sqrt{2}}\lambda_u\mathcal{H}_u \;\equiv\; \frac{G_F}{\sqrt{2}}\lambda_u\sum_{i=1,2} C_i(\mathcal{O}^u_i - \mathcal{O}_i) \tag{2.18}$$

where

$$\mathcal{O}^u_1 \;=\; (\bar{s}u)_{V-A}(\bar{u}b)_{V-A} \qquad\qquad \mathcal{O}^u_2 \;=\; (\bar{s}_i u_j)_{V-A}(\bar{u}_j b_i)_{V-A} \tag{2.19}$$

While, in principle, (2.18) should be added to the Hamiltonian (2.16), this is only necessary when considering the variant of a $b \to d\ell^+\ell^- \, (\nu\bar{\nu})$ transition, where no Cabibbo suppression is active.[1]

Lastly, it is worth mentioning that with respect to [10] the labels of the operators $\mathcal{O}_{1,2}$ are interchanged and, furthermore, the semileptonic operators $\mathcal{O}_{9,10}$ in [10] lack the prefactor $\frac{\alpha_e}{2\pi}$ of our operators.

2.3.3 Basis Ensuring γ_5-free Traces

The crucial difference of this basis lies in its different definition of the penguin operators $\mathcal{Q}_{3-6}$. Owing to this, no γ_5 can appear in loop-induced traces to leading order in weak but to all orders in electromagnetic and strong interaction [16]. By adopting this basis, one therefore avoids the technical difficulties that otherwise arise at higher orders when using dimensional regularization in conjunction with a fully anticommuting γ_5.

Following the convention of [15], the effective Hamiltonian is now defined with an additional prefactor of four with respect to (2.16)

$$\tilde{\mathcal{H}}_{\mathit{eff}} \;=\; -\frac{4G_F}{\sqrt{2}}\,\lambda_t \left[\sum_{i=1}^{10} \mathcal{C}_i(\mu)\mathcal{Q}_i(\mu) \;+\; \mathcal{C}_\nu(\mu)\mathcal{Q}_\nu(\mu)\right] \;+\; \text{h.c.} \tag{2.20}$$

In this work, every use of the operator basis $\{\mathcal{Q}_i\}$ implicitly includes the above redefinition of the Hamiltonian. Otherwise retaining the previous conventions, the operator basis $\{\mathcal{Q}_i\}$ is given as

$$\begin{aligned}
\mathcal{Q}_1 &= (\bar{s}_L\gamma^\mu T^a c)(\bar{c}_L\gamma_\mu T^a b) & \mathcal{Q}_2 &= (\bar{s}_L\gamma^\mu c)(\bar{c}_L\gamma_\mu b) \\
\mathcal{Q}_3 &= (\bar{s}_L\gamma^\mu b)\textstyle\sum_q(\bar{q}\gamma_\mu q) & \mathcal{Q}_4 &= (\bar{s}_L\gamma^\mu T^a b)\textstyle\sum_q(\bar{q}\gamma_\mu T^a q) \\
\mathcal{Q}_5 &= (\bar{s}_L\gamma^\mu\gamma^\nu\gamma^\rho b)\textstyle\sum_q(\bar{q}\gamma_\mu\gamma_\nu\gamma_\rho q) & \mathcal{Q}_6 &= (\bar{s}_L\gamma^\mu\gamma^\nu\gamma^\rho T^a b)\textstyle\sum_q(\bar{q}\gamma_\mu\gamma_\nu\gamma_\rho T^a q) \\
\mathcal{Q}_7 &= \frac{e}{16\pi^2}\,m_b(\bar{s}_L\sigma^{\mu\nu}b)F_{\mu\nu} & \mathcal{Q}_8 &= \frac{g_s}{16\pi^2}\,m_b(\bar{s}_L\sigma^{\mu\nu}T^a b)\,G^a_{\mu\nu} \\
\mathcal{Q}_9 &= \frac{\alpha_e}{\alpha_s}(\bar{s}_L\gamma^\mu b)\textstyle\sum_\ell(\bar{\ell}\gamma_\mu\ell) & \mathcal{Q}_{10} &= \frac{\alpha_e}{\alpha_s}(\bar{s}_L\gamma^\mu b)\textstyle\sum_\ell(\bar{\ell}\gamma_\mu\gamma_5\ell) \\
\mathcal{Q}_\nu &= \frac{\alpha_e}{2\pi}(\bar{s}_L\gamma^\mu b)\textstyle\sum_\nu(\bar{\nu}_L\gamma_\mu\nu)
\end{aligned} \tag{2.21}$$

[1] Furthermore, in this case, all explicit strange quarks in the operators (2.17) and (2.19) are to be replaced by down quarks and the λ_p adjusted according to (2.4).

3 Hadronic Matrix Elements

With the effective Hamiltonian at our disposal, it essentially remains to evaluate the matrix elements of the local operators in between the respective meson states

$$\langle \bar{M}\ell^+\ell^- | \mathcal{H}_{\mathit{eff}} | \bar{B} \rangle \quad \propto \quad C_i \cdot \langle \bar{M}\ell^+\ell^- | \mathcal{O}_i | \bar{B} \rangle \tag{3.1}$$

The fundamental difficulty of the task at hand lies in the non-perturbative nature of the long-distance dynamics involved, which refers in particular to the hadronization process, where the typical relative momentum between the constituent quarks is set by the *soft* QCD-scale Λ_{QCD}. But then again, considering the large mass of the initial B meson, there is a scale for *hard* contributions as well. In exploiting the hierarchy between these two scales $m_b \gg \Lambda_{QCD}$ the hadronic matrix element (3.1) can be simplified significantly.

As far as *inclusive* decays, for instance $\bar{B} \to X_s \ell^+\ell^-$, are concerned, the standard practice consists in performing a so-called *heavy quark expansion* (HQE) [6]. As a result, the problem is reduced virtually to the one of free quarks.

For *exclusive* decays, such as $\bar{B} \to \bar{K}^{(*)}\ell^+\ell^-$, however, the situation turns out to be more complicated. While it is at least possible to disentangle short- and long-distance dynamics systematically, predictions still suffer from the large uncertainties in the form factors, containing the hadronic information. Moreover, depending on the energy of the kaon, the theoretical tools to achieve the aforementioned factorization are quite different:

At large kaon recoil $E \gg \Lambda_{QCD}$, exclusive decays are properly described using the established framework of *QCD factorization* (QCDF) [6]. This approach, briefly discussed in the following section, however, is not justified in case of a soft final meson.

Indeed, at low kaon recoil $E \sim m_K$, the hadronic matrix element should be addressed by performing an OPE for the non-leptonic part of the Hamiltonian. More about this formalism, developed and discussed at length in chapter 5, can also be found in [1, 20, 21].

3.1 QCD Factorization

The intuitive reasoning underlying QCDF is known by the name of *colour transparency* [6]. It refers to the decoupling of a small-sized, highly energetic and, in particular, colour neutral meson from soft external gluons. In other words, interactions with the light meson system are dominated by the exchange of hard gluons. The most important implication of this is the factorization of perturbative and non-perturbative dynamics in the limit of a large kaon energy

$$m_B, E \;\gg\; \Lambda_{QCD}, m_K \tag{3.2}$$

With respect to the exclusive $B \to M\ell^+\ell^-$ decays discussed in this work, this circumstance can be represented schematically by means of the *factorization formula*

$$\begin{aligned} \langle \bar{M}\ell^+\ell^- | \mathcal{H}_{\mathit{eff}} | \bar{B} \rangle \;&=\; T^{\mathrm{I}}_\mu \cdot \langle \bar{M} | \bar{s}\Gamma^\mu b | \bar{B} \rangle + \langle \bar{M} | \bar{s}_\beta q_\alpha | 0 \rangle \otimes T^{\mathrm{II}}_{\beta\alpha\rho\eta} \otimes \langle 0 | \bar{q}_\rho b_\eta | \bar{B} \rangle & (3.3) \\ &\equiv\; T^{\mathrm{I}}_\mu(q^2) \cdot F^\mu_{B\to M}(q^2) + \iint du\, d\omega\; \Phi^M_{\beta\alpha}(u)\, T^{\mathrm{II}}_{\beta\alpha\rho\eta}(q^2, u, \omega)\, \Phi^B_{\rho\eta}(\omega) & (3.4) \end{aligned}$$

Here Γ^μ denotes a generic Dirac structure and the variables u,ω parametrize the distribution of the respective meson momentum among the constituent quarks. The neglected soft contributions on the r.h.s. of (3.3) are, in accordance with (3.2), of relative order Λ_{QCD}/m_B. The aforementioned factorization is thereby realized as follows:

- The form factors $F^\mu_{B\to M}$ and distribution amplitudes $\Phi^{B,M}$ describe the long-distance dynamics of the respective process. As of this, they are inherently non-perturbative quantities, which limits their theoretical determination to other methods, such as lattice QCD [8] or QCD sum rules on the light-cone [9]. Fortunately, they are rather universal in the sense that each respective quantity appears in a variety of (related, but different) decays. In fact, this can be exploited by extracting the non-perturbative input needed for the prediction of one decay from the experimental data of another.

- The hard-scattering kernels $T^{\mathrm{I,II}}$, on the other hand, contain exclusively short-distance dynamics and therefore represent perturbative quantities. On the downside, they are specific to a given decay, that is, they must be calculated for every decay separately.

In short, the factorization (3.3) represents a substantial simplification, for the evaluation of the matrix element (3.1) is reduced to the calculation of quantities that are either universal or perturbatively accessible.

3.2 Heavy-to-Light Form Factors

Quite generally, a form factor describes the non-perturbative dynamics contained in the matrix element of a local current in between two meson states. At this, it is common practice to decompose the matrix element into a full set of possible Lorentz structures

$$\langle M(k,\varepsilon) | \bar{s}\Gamma^\mu b | \bar{B}(p) \rangle \;\equiv\; F^\mu_{B\to M}(p,k,\varepsilon) \;=\; \sum_i V^\mu_i(p,k,\varepsilon) f_i(q^2) \tag{3.5}$$

where every such Lorentz structure V_i^μ is associated with different hadronic dynamics and thus comes with its own scalar form factor $f_i(q^2)$.

For the sake of clarity, let us now introduce the shorthand notations

$$S \;=\; \bar{s}b \qquad P \;=\; \bar{s}\gamma_5 b \qquad V^\mu \;=\; \bar{s}\gamma^\mu b \tag{3.6}$$

$$A^\mu \;=\; \bar{s}\gamma^\mu\gamma_5 b \qquad T^{\mu\nu} \;=\; \bar{s}\sigma^{\mu\nu} b \qquad T_5^{\mu\nu} \;=\; \bar{s}\sigma^{\mu\nu}\gamma_5 b \tag{3.7}$$

for scalar, pseudoscalar, vector, axialvector, tensor and pseudotensor current, respectively. Furthermore, the auxiliary momentum $\tilde{q} = p + k$ is assigned. The "standard" heavy-to-light form factors, employed throughout this work, are then defined as [22]

$$\begin{aligned}
\langle \bar{P}(k)|V^\mu|\bar{B}(p)\rangle &= f_+(q^2)\left[\tilde{q}^\mu - \frac{\tilde{q}\cdot q}{q^2}\,q^\mu\right] + f_0(q^2)\,\frac{\tilde{q}\cdot q}{q^2}\,q^\mu \\
&= f_+(q^2)\tilde{q}^\mu + f_-(q^2)q^\mu
\end{aligned} \tag{3.8}$$

$$\langle \bar{P}(k)|T^{\mu\nu}|\bar{B}(p)\rangle = \frac{2if_T(q^2)}{m_B + m_P}\,(p^\mu q^\nu - p^\nu q^\mu) \tag{3.9}$$

$$\langle \bar{V}(k,\varepsilon)|V^\mu|\bar{B}(p)\rangle = \frac{2iV(q^2)}{m_B + m_V}\,\varepsilon^{\mu\nu\alpha\beta}\varepsilon^*_\nu k_\alpha p_\beta \tag{3.10}$$

$$\begin{aligned}
\langle \bar{V}(k,\varepsilon)|A^\mu|\bar{B}(p)\rangle &= 2m_V A_0(q^2)\,\frac{\varepsilon^*\cdot q}{q^2}\,q^\mu \\
&\quad + A_1(q^2)(m_B + m_V)\left[\varepsilon^{*\mu} - \frac{\varepsilon^*\cdot q}{q^2}\,q^\mu\right] \\
&\quad - A_2(q^2)\,\frac{\varepsilon^*\cdot q}{m_B + m_V}\left[\tilde{q}^\mu - \frac{\tilde{q}\cdot q}{q^2}\,q^\mu\right]
\end{aligned} \tag{3.11}$$

$$q_\nu\langle \bar{V}(k,\varepsilon)|T^{\mu\nu}|\bar{B}(p)\rangle = -\,2T_1(q^2)\varepsilon^{\mu\nu\alpha\beta}\varepsilon^*_\nu k_\alpha p_\beta \tag{3.12}$$

$$\begin{aligned}
q_\nu\langle \bar{V}(k,\varepsilon)|T_5^{\mu\nu}|\bar{B}(p)\rangle &= -\,iT_2(q^2)(\tilde{q}\cdot q\,\varepsilon^{*\mu} - \varepsilon^*\cdot q\,\tilde{q}^\mu) \\
&\quad -\,iT_3(q^2)\,\frac{\varepsilon^*\cdot q}{\tilde{q}\cdot q}\,(q\cdot\tilde{q}\,q^\mu - q^2\,\tilde{q}^\mu)
\end{aligned} \tag{3.13}$$

At this, the sign convention for the totally antisymmetric *Levi-Cevita* tensor is $\varepsilon^{0123} = -1$, which, however, is contrary to the convention adopted in [22]. The employed form factors parametrizations, finally, are presented in appendix B.1.

3.3 Form Factor Symmetries

As it turns out, the form factors defined in (3.9) – (3.13) are not completely independent from one another. Not surprisingly, this is related to the large mass of the B meson, which allows for several different hierarchies one may consider. First of all, the hadronic matrix elements can be investigated in the heavy quark limit (HQL)

$$m_B \;\gg\; \Lambda_{QCD}, m_K \tag{3.14}$$

Instead of or in addition to this, one may also assume the limit of a very large

$$E \;\gg\; \Lambda_{QCD}, m_K \tag{3.15}$$

or, alternatively, a very small kaon recoil

$$m_B \;\gg\; E \tag{3.16}$$

By exploiting these hierarchies, it is possible to derive so-called form factor relations, which make connection between the different form factors of the same transition. At this, each kinematic scenario uses different simplifications, and thus obtains slightly different but nevertheless consistent form factor relations.

Before discussing the hierarchies (3.14) – (3.16) in detail, some useful formulas, which hold independently of the concrete kinematics, are presented.

Useful Formulas of General Validity

In any kinematic setting, one may utilize the QCD e.o.m. as well as the translation invariance of QCD. Most notably, they can be combined into the identity

$$\bar{s}_L \not{q} b \;=\; i\partial_\mu(\bar{s}_L\gamma^\mu b) \;=\; i\bar{s}_L\big(\overleftarrow{\not{D}} + \overrightarrow{\not{D}}\big)b \;=\; m_b\bar{s}_L b \tag{3.17}$$

which, however, implicitly assumes a $B \to K^{(*)}$ matrix element in the first step.[1]

With the help of (3.17), a connection between the "scalar" and "vector" matrix elements can already be established:

$$q_\mu\langle P|V^\mu|B\rangle \;=\; m_b\langle P|S|B\rangle \;=\; (m_B^2 - m_K^2)f_+(q^2) + q^2 f_-(q^2) \tag{3.18}$$

$$-q_\mu\langle V|A^\mu|B\rangle \;=\; m_b\langle V|P|B\rangle \;=\; -2m_V(\varepsilon^*\!\cdot q)A_0(q^2) \tag{3.19}$$

Besides, the other "scalar" matrix elements vanish by reason of parity

$$\langle P|P|B\rangle \;=\; 0 \qquad\qquad \langle V|S|B\rangle \;=\; 0 \tag{3.20}$$

Furthermore, we will repeatedly resort to the $B \to V$ matrix elements of tensor currents

[1] More precisely, we require that b and s quark taken together generate a momentum q^μ pointing into the $\bar{s}_L\gamma^\mu b$ vertex.

in their respective uncontracted form [23]

$$\begin{aligned}\langle V|T^{\mu\nu}|B\rangle &= T_1(s)\varepsilon^{\mu\nu\tilde{q}\varepsilon^*} + \Big[T_2(s) - T_1(s)\Big]\frac{\tilde{q}\cdot q}{q^2}\,\varepsilon^{\mu\nu q\varepsilon^*} \\ &\quad + \left[T_2(s) - T_1(s) + T_3(s)\frac{q^2}{\tilde{q}\cdot q}\right]\frac{\varepsilon^{*}\!\cdot q}{q^2}\,\varepsilon^{\mu\nu\tilde{q}q} \end{aligned} \tag{3.21}$$

$$\begin{aligned}\langle V|T_5^{\mu\nu}|B\rangle &= iT_1(s)(\varepsilon^{*\nu}\tilde{q}^{\mu} - \varepsilon^{*\mu}\tilde{q}^{\nu}) + i\Big[T_2(s) - T_1(s)\Big]\frac{\tilde{q}\cdot q}{q^2}(\varepsilon^{*\nu}q^{\mu} - \varepsilon^{*\mu}q^{\nu}) \\ &\quad + i\left[T_2(s) - T_1(s) + T_3(s)\frac{q^2}{\tilde{q}\cdot q}\right]\frac{\varepsilon^{*}\!\cdot q}{q^2}(\tilde{q}^{\mu}q^{\nu} - \tilde{q}^{\nu}q^{\mu}) \end{aligned} \tag{3.22}$$

3.3.1 Heavy Quark Limit $m_b \gg \Lambda_{QCD}$

To start with, the hadronic matrix elements are considered assuming the heavy-quark limit $m_b \gg \Lambda_{QCD}$ [24]. In consequence, the strong interactions of the b quark simplify and are best described using *heavy quark effective theory* (HQET) [6]. In this formalism, the large heavy-quark field Ψ_b is decomposed into two components

$$b_{\pm}(x) \equiv e^{im_b v\cdot x}\,\frac{1 \pm \not{v}}{2}\,\Psi_b(x) \tag{3.23}$$

Exploiting the QCD e.o.m, the "minus" projection is then found to be subleading in the Λ/m_B counting

$$\Psi_b(x) = e^{-im_b v\cdot x}\,b_+(x) + \mathcal{O}(\Lambda/m_b) \tag{3.24}$$

With this piece of information, the effective e.o.m. for the b quark can be directly read off of (3.23):

$$\not{v} b_+ = b_+ \tag{3.25}$$

In order to take full advantage of (3.25), the hadronic matrix elements are contracted with p_ν, which yields

$$\langle P|V^p|B\rangle = m_B\langle P|S|B\rangle \qquad \langle P|T^{\mu p}|B\rangle = i\langle P|(m_B V^{\mu} - p^{\mu}S)|B\rangle \tag{3.26}$$

$$\langle V|V^p|B\rangle = m_B\langle V|S|B\rangle \qquad \langle V|T^{\mu p}|B\rangle = i\langle V|(m_B V^{\mu} - p^{\mu}S)|B\rangle \tag{3.27}$$

$$\langle V|A^p|B\rangle = -m_B\langle V|P|B\rangle \qquad \langle V|T_5^{\mu p}|B\rangle = -i\langle V|(m_B A^{\mu} + p^{\mu}P)|B\rangle \tag{3.28}$$

As a next step, the matrix elements in (3.26) – (3.28) are to be replaced by the explicit parametrizations, given on the right-hand sides of the equations (3.8) – (3.13) and (3.18) – (3.20) respectively. By comparing the terms proportional to $\tilde{q}^{\mu}$, q^{μ} and $\varepsilon^{*\mu}$

separately, one then obtains two independent $B \to P$

$$f_-(s) \;=\; -f_+(s)\frac{1-s+3r}{1-s-r} \tag{3.29}$$

$$\frac{2f_T(s)}{1+\sqrt{r}} \;=\; f_+(s) - f_-(s) \;=\; 2f_+(s)\frac{1-s+r}{1-s-r} \tag{3.30}$$

and four independent $B \to V$ constraints

$$2\sqrt{r}A_0(s) \;=\; A_1(s)(1+\sqrt{r}) - \frac{A_2(s)}{1+\sqrt{r}}\frac{\lambda(s)}{1-s-r} \tag{3.31}$$

$$\frac{2V(s)}{1+\sqrt{r}} \;=\; T_1(s) + \Big[T_1(s) - T_2(s)\Big]\frac{1-r}{s} \tag{3.32}$$

$$2T_1(s) \;=\; A_1(s)(1+\sqrt{r}) + (1+s-r)\frac{V(s)}{1+\sqrt{r}} \tag{3.33}$$

$$\frac{A_2(s)}{1+\sqrt{r}}(1-r) \;=\; \frac{1-s-r}{1-s+r}\left[T_1(s) + T_3(s) - (1+r)\frac{V(s)}{1+\sqrt{r}}\right] \tag{3.34}$$

Finally, it is reminded that, since

$$m_B - m_b \;\sim\; \Lambda \;\to\; 0 \tag{3.35}$$

the heavy-quark limit does not allow to distinguish between the mass of the B meson and the mass of the b quark.

3.3.2 Large Kaon Recoil $E \gg \Lambda_{QCD}, m_K$

Alternatively (or additionally), the hadronic matrix elements can be investigated in the limit of a highly energetic kaon $E \gg \Lambda_{QCD}, m_K$ [22, 25]. This kinematic domain is the application area of *soft-collinear effective theory* (SCET) [26, 27], where now, in analogy to the previous section, two components of the strange quark-field, featuring a distinct scaling behaviour in the high-energy limit, can be identified

$$s_+(x) \;\equiv\; e^{iE\cdot x}\,\frac{\not{n}_+\not{v}}{2}\,\Psi_s(x) \qquad\qquad s_-(x) \;\equiv\; e^{iE\cdot x}\,\frac{\not{v}\not{n}_+}{2}\,\Psi_s(x) \tag{3.36}$$

Since the "minus" projection is (again) power-suppressed with respect to the "plus" projection, the effective e.o.m. for the strange quark reads

$$\bar{s}_+\not{n}_+ \;=\; 0 \tag{3.37}$$

In order to make use of the effective e.o.m (3.37), one should now consider hadronic matrix elements contracted with k_ν:

$$\langle P|V^k|B\rangle = 0 \qquad \langle P|T^{\mu k}|B\rangle = ik^\mu\langle P|S|B\rangle \tag{3.38}$$

$$\langle V|V^k|B\rangle = 0 \qquad \langle V|T^{\mu k}|B\rangle = ik^\mu\langle V|S|B\rangle \tag{3.39}$$

$$\langle V|A^k|B\rangle = 0 \qquad \langle V|T_5^{\mu k}|B\rangle = ik^\mu\langle V|P|B\rangle \tag{3.40}$$

Proceeding as in the previous section, one eventually arrives at two independent $B \to P$

$$f_+(s) = -f_-(s)\frac{1-s-r}{1-s+3r} = \frac{f_T(s)}{1+\sqrt{r}}\frac{m_b}{m_B}\left(1+\frac{4rs}{\lambda(s)}\right) \tag{3.41}$$

and three independent $B \to V$ form factor relations

$$2\sqrt{r}A_0(s) = A_1(s)(1+\sqrt{r}) - \frac{A_2(s)}{1+\sqrt{r}}\frac{\lambda(s)}{1-s-r} \tag{3.42}$$

$$= \frac{1-s-r}{1-r}\frac{m_b}{m_B}\Big[T_1(s) - T_3(s)\Big] \tag{3.43}$$

$$T_2(s) = \frac{1-s-r}{1-r}T_1(s) \tag{3.44}$$

Note that the kaon mass has only been kept here if it represents a "kinematic" correction, that is, if it stems from the form factors definitions (3.8) – (3.13).

3.3.3 Combined Limit $m_B, E \gg \Lambda_{QCD}, m_K$

In the literature, heavy-quark and high-energy limit are usually taken together [22, 25]. Based on this, it can be shown that the $B \to P$ form factors are already completely determined by a single universal function $\zeta(m_B, E)$ according to [22]

$$f_+(s) = -f_-(s) = \frac{f_T(s)}{1+\sqrt{r}} = \frac{1-r}{1-s-r}f_0(s) = \zeta(m_B, E) \tag{3.45}$$

Likewise, the $B \to V$ matrix elements can be reduced to two independent functions, denoted as $\zeta_\perp(m_B, E)$ and $\zeta_\|(m_B, E)$. Expressed in terms of these functions, the standard form factors read [22]

$$V(s) = (1+\sqrt{r})\zeta_\perp(m_B,E) \tag{3.46}$$

$$A_0(s) = \sqrt{r}\,\zeta_\perp(m_B,E) + \frac{1-s-r}{1-s+r}\,\zeta_\parallel(m_B,E) \tag{3.47}$$

$$A_1(s) = \frac{1-s+r}{1+\sqrt{r}}\,\zeta_\perp(m_B,E) \tag{3.48}$$

$$A_2(s) = (1+\sqrt{r})\left[\zeta_\perp(m_B,E) - \frac{2\sqrt{r}}{1-s+r}\,\zeta_\parallel(m_B,E)\right] \tag{3.49}$$

$$T_1(s) = \zeta_\perp(m_B,E) \tag{3.50}$$

$$T_2(s) = \frac{1-s-r}{1-r}\,\zeta_\perp(m_B,E) \tag{3.51}$$

$$T_3(s) = \zeta_\perp(m_B,E) - \frac{2\sqrt{r}\,(1-r)}{1-s+r}\,\zeta_\parallel(m_B,E) \tag{3.52}$$

As required by consistency, these findings are equivalent to the heavy-quark relations (3.29) – (3.34) combined with the large-recoil relations (3.41) – (3.44) up to and including terms of relative order (m_K/m_B).

Furthermore, it is pointed out that all form factor relations presented up to now hold only to leading order in Λ/m_B and, in particular, α_s. The symmetry breaking diagrams (hard vertex correction and hard spectator interactions) have been calculated by the authors of [25]. This issue is discussed in more detail in the context of the NNLO-analysis of $B \to K\ell^+\ell^-$ in chapter 9.

More information about form factor relations at high recoil in general can be found in [28, 29, 30].

3.3.4 Low Kaon Recoil $m_B \gg E, m_K$

Lastly, one may also consider the limit of a very soft kaon $m_B \gg E, m_K$. It is then justified to drop matrix elements that contain a covariant derivative acting on the strange quark

$$\langle \bar{K}^{(*)}|\,\bar{s}_L\overleftarrow{D}^\mu\Gamma b\,|\bar{B}\rangle \;\sim\; \mathcal{O}(E/m_B) \;\to\; 0 \tag{3.53}$$

which are typically encountered when evaluating matrix elements of the tensor currents $T^{\mu\nu}_{(5)}$ contracted with q_ν. In general, matrix elements of the type (3.53) would then require the introduction of additional hadronic form factors, thereby rendering the resulting form factor relations rather useless. However, exploiting (3.53), one now obtains

$$\langle P|T^{\mu q}|B\rangle \;=\; i\langle P|(m_b V^\mu - q^\mu S)|B\rangle \tag{3.54}$$

$$\langle V|T^{\mu q}|B\rangle \;=\; i\langle V|(m_b V^\mu - q^\mu S)|B\rangle \tag{3.55}$$

$$\langle V|T_5^{\mu q}|B\rangle \;=\; -i\langle V|(m_b A^\mu + q^\mu P)|B\rangle \tag{3.56}$$

By comparing once again the terms proportional to $\tilde{q}^\mu$, q^μ and $\varepsilon^{*\mu}$ separately, one then finds (here $s = 1$)

$$f_-(s) \;=\; -f_+(s) \qquad\qquad \frac{f_T(s)}{1+\sqrt{r}} \;=\; \frac{m_b}{m_B}\, f_+(s) \tag{3.57}$$

and

$$T_1(s) \;=\; \frac{V(s)}{1+\sqrt{r}}\frac{m_b}{m_B} \qquad T_2(s) \;=\; \frac{A_1(s)}{1-\sqrt{r}}\frac{m_b}{m_B} \qquad T_3(s) \;=\; \frac{A_2(s)}{1+\sqrt{r}}\frac{m_b}{m_B} \tag{3.58}$$

for pseudoscalar and vector meson, respectively. Note that again only the "kinematic" m_K-dependence has been retained, and furthermore, on account of the scaling $A_1/A_2 \sim \Lambda_{QCD}/m_B$ at low recoil, a term proportional to A_1 has been dropped in the last relation of (3.58).

3.3.5 Universal Relations

In what follows, we investigate the question of universal form factor relations, that is, identities that hold independently of a specific kaon energy. While the heavy-quark relations (3.29) – (3.34) obviously fall into this category, it is the main objective of this section to establish further identities. Following the reasoning initially put forward in [31], we therefor assume that relations that can be derived in both energy-specific limits in fact apply to the entire spectrum. Related discussions can also be found in [28, 29].

Since only the leading-power terms of the three scenarios (3.14) – (3.16) are actually parametrically comparable, we henceforth drop the respective subleading terms of relative order

$$m_K^2/m_B^2 \;\equiv\; 0 \qquad\qquad \text{and} \qquad\qquad m_B - m_b \;\sim\; \Lambda_{QCD} \;\equiv\; 0 \tag{3.59}$$

which does not represent a substantial reduction in accuracy anyway. The "kinematic" m_K-corrections, however, will again be kept.

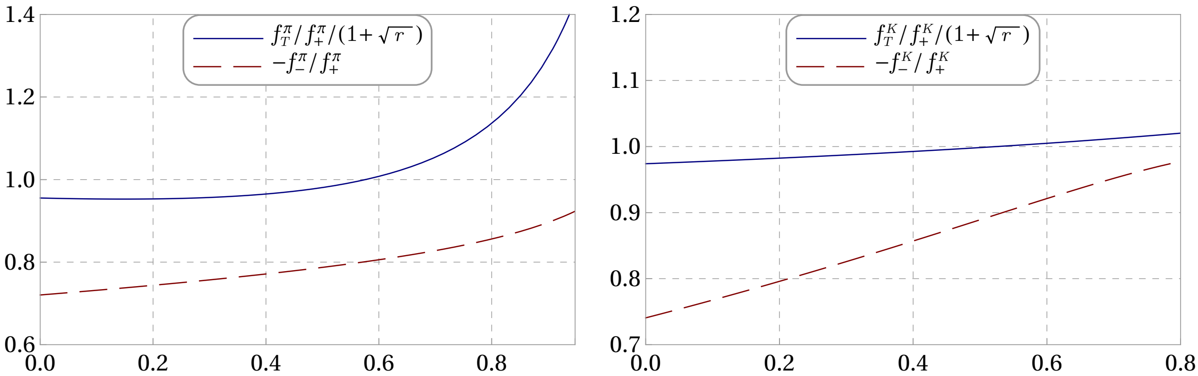

Figure 3.1: $B \to P$ form factor ratios for the pion (left) and kaon (right) as functions of s. For all form factors, the parametrization (B.1), along with the parameter values given in (B.10) – (B.11) (pion) and (B.16) – (B.19) (kaon), is employed. Note that the "f_- / f_+" ratios are not used in this work.

Universal $B \to P$ Relations

As regards the form factors of $B \to P$ transitions, all three limits individually lead to the same relations

$$f_+(s) \;=\; -f_-(s) \;=\; \frac{f_T(s)}{1+\sqrt{r}} \tag{3.60}$$

which puts them on a firm footing indeed.

As can be observed from Fig. 3.1, the relevant relations are, in general, quite well fulfilled. Considering the fact that the contributions from f_- (or f_0) are, in the present context, practically irrelevant and even the f_T-term is generally more of a correction to the dominant f_+ component, the usage of (3.60) in the entire q^2-range seems tenable. Correspondingly, the natural approach would be to express the form factors f_T and f_- in terms of the dominant f_+.

Universal $B \to V$ Relations

In case of the $B \to V$ form factors, it is most convenient to compare the soft kaon identities (3.58) directly with the HQET/ SCET combinations (3.46) – (3.52). In so doing, one obtains the universal relations

$$T_1(s) \;=\; \frac{V(s)}{1+\sqrt{r}} \qquad \frac{T_2(s)}{1+\sqrt{r}} \;=\; A_1(s) \qquad T_3(s) \;=\; \frac{A_2(s)}{1+\sqrt{r}} \tag{3.61}$$

which can be used to eliminate the tensor form factor from theoretical expressions. The fourth universal identity

$$A_1(s)(1+\sqrt{r}) \;=\; \frac{V(s)}{1+\sqrt{r}}(1-s) \tag{3.62}$$

can then be derived by combining the identities (3.61) with the heavy-quark relation (3.32) or (3.33). Note that the middle equation in (3.61) (compare, for instance,

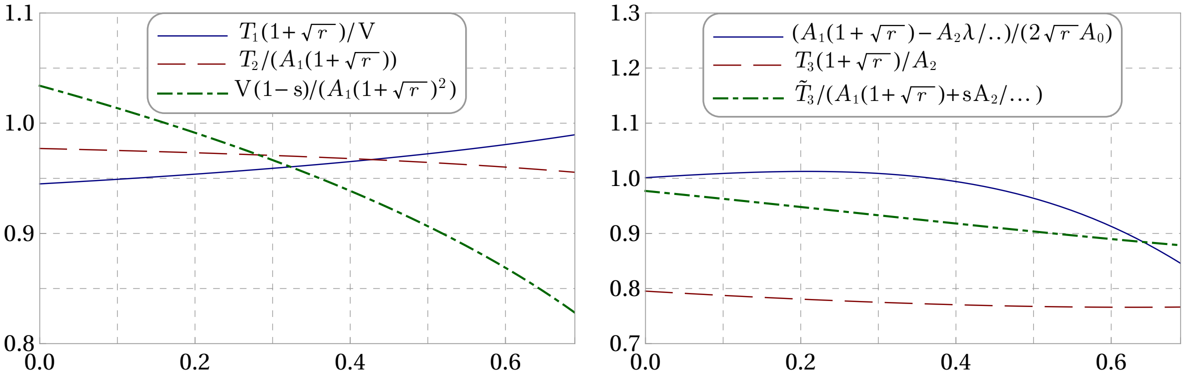

Figure 3.2: $B \to V$ form factor ratios for the K^*-vector meson as functions of s. For all form factors, the parametrization (B.1), along with the parameter values given in Tab. B.1 and (B.34) – (B.37), is employed.

with (3.58)) has been adjusted by a term of $\mathcal{O}(r)$ so that the kinematic condition $T_1(0) = T_2(0)$ is exactly fulfilled.

Lastly, there is the relation (3.31), which is universal and may be used in unchanged form

$$2\sqrt{r}A_0(s) \;=\; A_1(s)(1+\sqrt{r}) - \frac{A_2(s)}{1+\sqrt{r}}\frac{\lambda(s)}{1-s-r} \tag{3.63}$$

for it follows already from the heavy-quark limit alone.

Concerning the actual implementation, it is in general preferable to express the tensor form factors in terms of V (or A_1) and A_2. The form factor $T_3(s)$, however, enters the $B \to K^*\ell^+\ell^-$ decay rate only in the linear combination

$$\tilde{T}_3(s) \;\equiv\; T_2(s) + \frac{s}{1-r}T_3(s) \tag{3.64}$$

In fact, the authors of [23] only provide an explicit parametrization for $\tilde{T}_3(s)$. Numerical values for $T_3(s \neq 0)$ must therefore be obtained through (3.64), which is, in particular for small values of s, rather imprecise.

For instance, using (3.64) together with the provided parametrizations for $\tilde{T}_3(s)$ and $T_2(s)$, one finds $T_3(0) = 0.175$. However, the value directly calculated from light-cone sum rules, which is given in [23] as well, is $T_3(0) = 0.205$.[2] Similarly, the "direct" value of the corresponding form factor ratio is $T_3(0)(1+\sqrt{r})/A_2(0) \approx 0.93$ and not ≈ 0.80, as depicted in Fig. 3.2.

In order to gauge the quality of the form factor relations, it might therefore be more conclusive to examine the relation

$$\tilde{T}_3(s) \;=\; A_1(s)(1+\sqrt{r}) + \frac{s}{1-r}\frac{A_2(s)}{1+\sqrt{r}} \tag{3.65}$$

instead of the $T_3(s)/A_2(s)$ relation in (3.61).

[2] or $T_3(0) = 0.202$ without the Gegenbauer update (see discussion around equation (B.30))

In any case, as can be observed from Fig. 3.2, all relevant ratios are, for our purposes, sufficiently well satisfied.

3.4 Light-Cone Distribution Amplitudes

Light-cone projectors, also known as distribution amplitudes, describe the long-distance dynamics contained in the matrix element of a bilocal current in between a single meson state and the vacuum. Such matrix elements are typically encountered when the spectator quark actively participates in a process. At this point, the interested reader is made aware of the relevant literature [25, 32, 33].

3.4.1 Projections of Light Mesons

The light-cone projector of the kaon or, more generally, of a light meson, is defined in coordinate space through the bilocal matrix element

$$\Phi^{K^{(*)}}_{\beta\alpha}(z)(\delta_{ij}/N) \;\equiv\; \langle \bar{K}^{(*)}(k,\varepsilon)|\, \bar{s}_{i,\beta}(z)P(z,0)d_{j,\alpha}(0)|\,0\,\rangle \tag{3.66}$$

where the color indices i, j as well as the Wilson line $P(z,0)$, ensuring gauge invariance, will be suppressed from now on. It is usually convenient to break down the matrix element (3.66) into the possible Dirac-structures [34, 35, 36]

$$\Phi^{K}_{\beta\alpha}(z) \;=\; \frac{if_K}{4}\int_0^1 du\, e^{iu\,k\cdot z}\left\{\not{k}\gamma_5\phi(u) \,-\, \mu_K\gamma_5\left(\phi_P(u) \,-\, \sigma^{kz}\,\frac{\phi_\sigma(u)}{6}\right)\right\}_{\alpha\beta} \tag{3.67}$$

$$\Phi^{K^*}_{\beta\alpha}(z) \;=\; -\frac{i}{4}\int_0^1 du\, e^{iu\,k\cdot z}\left\{\not{k}\,\frac{\varepsilon^*\cdot z}{k\cdot z}\,f_\parallel\phi_\parallel(u) \,+\, \not{\varepsilon}^*_\perp\not{k} f_\perp\,\phi_\perp(u)\right\}_{\alpha\beta} \tag{3.68}$$

where the total meson momentum k^μ is distributed between quark and antiquark momentum, k_1^μ and k_2^μ, according to $(u = 1 - \bar{u})$

$$k_1^\mu \;=\; uEn_+^\mu + k_\perp^\mu + \frac{\vec{k}_\perp^{\,2}}{4uE}n_-^\mu \qquad\qquad k_2^\mu \;=\; \bar{u}En_+^\mu - k_\perp^\mu + \frac{\vec{k}_\perp^{\,2}}{4\bar{u}E}n_-^\mu \tag{3.69}$$

Further note that the second term in (3.67) is actually a twist-3 contribution, and thus *formally* subleading. This is directly linked to the scaling of

$$\mu_K(\mu) \;\equiv\; \mu_\pi(\mu) \;=\; \frac{m_\pi^2}{m_u(\mu) + m_d(\mu)} \;\sim\; \Lambda_{QCD} \tag{3.70}$$

in the heavy-quark limit. This being said, there is a *chiral* enhancement of μ_K which makes said power suppression *numerically* rather ineffective. For this reason, the contributions $\propto \mu_K$ are occasionally taken into account as well.

The desired momentum space representations of the projectors (3.67) – (3.68) can be derived via Fourier transformation. For this purpose, the spatial coordinate is first replaced by its momentum space representation

$$z^\mu \;\longrightarrow\; -i\partial^\mu_{k_1} \;=\; -i\left(\frac{n_-^\mu}{2E}\,\partial_u \;+\; \partial^\mu_{k_\perp} \;+\; ...\right) \tag{3.71}$$

Next, the derivative with respect to u, which initially acts on the corresponding hard scattering amplitude, can be made to act on the distribution amplitudes via integration by parts. In this way, one finds the following expressions for the momentum space projectors [37]

$$\Phi^K_{\beta\alpha}(u) \;=\; \frac{if_K}{4}\left\{\not{k}\,\gamma_5\,\phi(u) \;-\; \mu_K\,\gamma_5\,\frac{\not{k}_2\not{k}_1}{k_2\cdot k_1}\,\phi_P(u)\right\}_{\alpha\beta} \tag{3.72}$$

$$\Phi^{K^*}_{\beta\alpha}(u) \;=\; -\frac{i}{4}\left\{\not{k}\,\frac{m_K}{2E}\,(\varepsilon^*\!\cdot n_-)\,f_\parallel\,\phi_\parallel(u) \;+\; \not{\varepsilon}^*_\perp\not{k}\,f_\perp\,\phi_\perp(u)\right\}_{\alpha\beta} \tag{3.73}$$

Note that, since the two orientations of the polarization vector scale as $(\varepsilon^*\!\cdot n_-) \sim E/m_K$ and $\varepsilon^*_\perp \sim 1$, respectively, the two terms in (3.73) are indeed of the same order in the E/m_K counting.

Finally, it is mentioned that all kaon distribution amplitudes are normalized to unity $\int du\,\phi \;=\; 1$. This is essentially a consistency requirement, for in the limit $z \to 0$ the projection operators (3.67) – (3.68) must reproduce the definitions of the decay constants

$$\langle \bar{K}(k)\,|\,\bar{s}\,\gamma^\mu\gamma_5\,d\,|\,0\rangle \;=\; -if_K\,k^\mu \tag{3.74}$$

$$\langle \bar{K}^*_\parallel(k,\varepsilon)\,|\,\bar{s}\,\gamma^\mu d\,|\,0\rangle \;=\; -if_\parallel\,m_K\,\varepsilon^{*\mu} \tag{3.75}$$

$$\langle \bar{K}^*_\perp(k,\varepsilon)\,|\,\bar{s}\,\sigma^{\mu\nu}d\,|\,0\rangle \;=\; f_\perp\big(k^\mu\varepsilon^{*\nu} \;-\; k^\nu\varepsilon^{*\mu}\big) \tag{3.76}$$

Explicit parametrizations of the kaon wave functions can be found in appendix B.2.1.

3.4.2 Projection of the B Meson

To start with, the B meson projector is defined in coordinate space by means of the bilocal matrix element

$$\tilde{\Phi}^B_{\beta\alpha}(z)(\delta_{ij}/N) \;\equiv\; \langle 0\,|\,\bar{q}_{i,\beta}(z)P(z,0)b_{j,\alpha}(0)\,|\bar{B}(p)\rangle \tag{3.77}$$

where the hadronic dynamics contained therein are parametrized as [38] ($t \;\equiv\; v\cdot z \;=\; z^0$)

$$\tilde{\Phi}^B_{\beta\alpha}(z) \;=\; -\frac{if_B\,m_B}{4}\left\{\frac{1+\not{v}}{2}\left[2\tilde{\phi}_+(t) \;+\; \frac{\tilde{\phi}_-(t)\;-\;\tilde{\phi}_+(t)}{t}\,\not{z}\right]\gamma_5\right\}_{\alpha\beta} \tag{3.78}$$

In order to proceed, we require a (convenient) representation of the individual B meson momenta, for instance

$$p_b^\mu \;=\; m_b v^\mu + \mathcal{O}(\Lambda/m_B) \qquad\qquad l^\mu \;=\; \frac{l_+}{2} n_+^\mu + \frac{l_-}{2} n_-^\mu + l_\perp^\mu \tag{3.79}$$

Now, as it turns out, the hard scattering amplitude depends only on one of the momentum components $l_\pm$. More precisely, the perturbative part of the relevant diagram is always found to have the structure

$$A(l) \;=\; A^{(0)}(l_x) + l_\perp^\mu A_\mu^{(1)}(l_x) + \mathcal{O}(\Lambda/m_B) \tag{3.80}$$

where $l_x = l_\pm$, depending on the diagram in question. For instance, the hard-spectator scattering processes contributing to $B \to M\ell^+\ell^-$ have $l_x = l_-$ if the virtual photon is emitted from the loop (Fig. 9.3). If, on the other hand, the photon is emitted from one of the mesons' valence quarks (Fig. 9.2) the relevant momentum component is, as in the case of weak annihilation, $l_x = l_+$.

Either way, as a consequence of (3.80), the matrix element $\tilde{\Phi}^B_{\beta\alpha}(z)$ has to be evaluated on the light-cone ($z^2 = 0$) only. This then allows to derive the momentum space representation of the projection operator from

$$\int d^4z\, \tilde{\Phi}^B_{\beta\alpha}(z) A_{\beta\alpha}(z) \;=\; \int \frac{d^4l}{(2\pi)^4} A(l) \int d^4z\, e^{il\cdot z}\, \tilde{\Phi}^B(z) \;\equiv\; \int_0^\infty d\omega\, \Phi^B(\omega) A(l)\Big|_{l=\frac{\omega}{2}n_x} \tag{3.81}$$

Note that the sign in the exponential is in fact positive. The reason being that, on the hard scattering side of the diagram, there is a total momentum flow of $-l$, which points into the z-vertex.

Defining the momentum space representations of the projection amplitudes through

$$\tilde{\phi}_\pm(t) \;\equiv\; \int_0^\infty d\omega\, e^{-i\omega t} \phi_\pm(\omega) \tag{3.82}$$

an explicit calculation yields [25]

$$\Phi^B_{\beta\alpha}(\omega) \;=\; -\frac{if_B m_B}{4} \left\{ \frac{1+\not{v}}{2} \left[\phi_+(\omega) \not{n}_x + \phi_-(\omega) \Big(2\not{v} - \not{n}_x - \omega \gamma_\mu \frac{\partial}{\partial l_{\perp\mu}} \Big) \right] \gamma_5 \right\}_{\alpha\beta} \tag{3.83}$$

The derivative, which acts on the hard scattering amplitude, must of course be performed before the antiquark momentum is set to $l = \frac{\omega}{2} n_x$. Also, just like before, the definition of the B meson decay constant

$$\langle\, 0 \,|\, \bar{d}\gamma^\mu\gamma_5 b \,|\, \bar{B}(p) \rangle \;=\; if_B p^\mu \tag{3.84}$$

imposes the normalization of the momentum wave functions to unity $\int d\omega\, \phi = 1$. Finally, the model functions employed for the B meson projectors can be found in appendix B.2.2.

Part III

Theory of $B \to M\ell^+\ell^-$ at high q^2

4 Current Correlator and Role of Dilepton-Mass

The transition amplitude of exclusive $B \to M\ell^+\ell^-$ decays can be written as

$$\langle \bar{M}\ell^+\ell^- | \mathcal{H}_{\text{eff}} | \bar{B} \rangle \;=\; -\frac{G_F}{\sqrt{2}}\,\frac{\alpha}{2\pi}\,\lambda_t \left[\left(\mathcal{A}_9^\mu(s) + \frac{\lambda_u}{\lambda_t}\,\mathcal{A}_u^\mu(s) \right) \bar{u}\gamma_\mu v + \mathcal{A}_{10}^\mu \bar{u}\gamma_\mu\gamma_5 v \right] \tag{4.1}$$

Employing the operator basis (2.17), the different sub-amplitudes in (4.1) read

$$\begin{aligned} \mathcal{A}_9^\mu(s) \;&=\; C_9 \langle \bar{M} | \bar{s}\gamma^\mu(1-\gamma_5) b | \bar{B} \rangle - C_7 \frac{2im_b}{q^2} \langle \bar{M} | \bar{s}\sigma^{\mu q}(1+\gamma_5) b | \bar{B} \rangle \\ &\quad - \frac{8\pi^2}{q^2}\, i \int d^4x\, e^{iq\cdot x} \langle \bar{M} | T j^\mu(x) \mathcal{H}_h(0) | \bar{B} \rangle \end{aligned} \tag{4.2}$$

$$\mathcal{A}_u^\mu \;=\; \frac{8\pi^2}{q^2}\, i \int d^4x\, e^{iq\cdot x} \langle \bar{M} | T j^\mu(x) \mathcal{H}_u(0) | \bar{B} \rangle \tag{4.3}$$

$$\mathcal{A}_{10}^\mu \;=\; C_{10} \langle \bar{M} | \bar{s}\gamma^\mu(1-\gamma_5) b | \bar{B} \rangle \tag{4.4}$$

where

$$\mathcal{H}_h \;\equiv\; \sum_{i=1}^{6,8} C_i \mathcal{O}_i \qquad \text{and} \qquad j^\mu \;=\; \sum_q Q_q\, (\bar{q}\gamma^\mu q) \tag{4.5}$$

are the hadronic part of the effective weak Hamiltonian and the electromagnetic current of quarks, respectively.

The amplitude $\mathcal{A}_u^\mu$ contains the contributions from the "up" sector of the effective weak Hamiltonian. More specifically, we have

$$\mathcal{H}_u \;=\; \frac{\sqrt{2}}{G_F \lambda_u} \mathcal{H}_{\text{eff}}^u \;=\; \sum_{i=1,2} C_i (\mathcal{O}_i^u - \mathcal{O}_i) \tag{4.6}$$

where the $\mathcal{O}_i^u$ are the operators defined in (2.19). Note that, as far as $b \to s\ell^+\ell^-$ transitions are concerned, the contribution (4.3) is suppressed by the smallness of its relative prefactor λ_u/λ_t and therefore can usually be neglected.

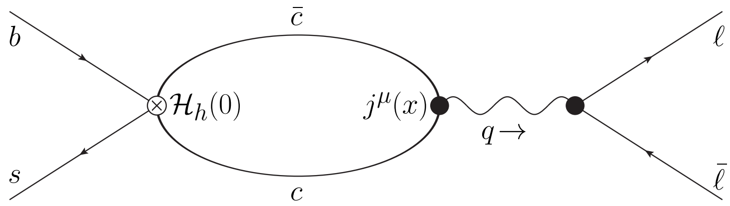

Figure 4.1: Charm correlator (4.7) at leading order in perturbation theory: The two charm quarks, created by one of the 4-quark operators $\mathcal{O}_{1-6}$, annihilate into the outgoing leptons via virtual photon exchange.

Two Types of Contributions

The contributions to the amplitudes $\mathcal{A}^\mu_{9,10,u}$ can be divided into two categories, featuring quite distinct properties:

- On the one hand, there are the matrix elements of the non-hadronic operators $\mathcal{O}_{7,9,10}$ They dominate the spectrum outside the domain of the narrow charmonium resonances owing to the size of the semileptonic Wilson coefficients $C_{9,10}$. These contributions are also rather clean and simple from the theoretical point of view, as short- and long-distance dynamics factorize completely into coefficient functions and standard $B \to M$ form factors, respectively.

- On the other hand, there are the contributions from the hadronic operators, which can be subsumed in the *current correlator*

$$\langle \mathcal{K}^\mu(q) \rangle \;\equiv\; -\frac{8\pi^2}{q^2}\, i \int d^4x\, e^{iq\cdot x}\, \langle \bar{M}(k) \big| T j^\mu(x) \mathcal{H}_h(0) \big| \bar{B}(p) \rangle \tag{4.7}$$

  Although small in comparison to the semileptonic contributions, this term must be taken into account as well in order to obtain an accurate prediction. Unfortunately, however, a straightforward perturbative calculation of this term suffers from two major difficulties.

Role of Dilepton-Mass

One of said obstacles when evaluating the non-local matrix element (4.7) consists in non-factorizable soft contributions.[1] While a systematic calculation of these contributions is in general still possible, the appropriate framework to perform this task differs at low and high kaon recoil.

The other issue is the existence of the charmonium resonances in the middle and upper part of the q^2-spectrum, which gives rise to violations of quark-hadron duality.

[1] In particular, these contributions can not be expressed in terms of form factors or distribution amplitudes.

Since this represents an inherent limitation of the quark model itself, the corresponding theoretical uncertainty is qualitatively different from other uncertainties, usually related to neglected orders in some expansion parameter. In the upper part of the spectrum, where sensible predictions are again possible, a quantitative estimate of duality violating effects is nevertheless mandatory.

On account of the things just mentioned, the properties (and with them the theoretical challenges and the treatment) of the correlator differ significantly depending on the size of the momentum flow through the loop q^2. For this reason, the theory of $B \to M\ell^+\ell^-$ decays recognizes three characteristic kinematic domains:

- $q^2 \lesssim 7\mathrm{GeV}^2$: In the domain below the first charmonium resonance, there are essentially no duality violating effects. This is also where the kaon is highly energetic
$$E \gg \Lambda_{QCD}, m_K \tag{4.8}$$
which allows to address the non-local term in the QCDF framework, using the formalisms of HQET [6, 32, 39] and SCET [22, 26, 27].
For most decays this domain is already well explored. As for $B \to K^{(*)}\ell^+\ell^-$ in particular, this was initially done by the authors of [40] (For a more recent analysis see also [41]). An exhaustive list of references concerning B decays at high recoil can be found in [42].

- $7\mathrm{GeV}^2 \lesssim q^2 \lesssim 15\mathrm{GeV}^2$: This part of the spectrum is governed by the presence of the first, narrow charmonium resonances. Indeed, the decay $B \to K^{(*)}\psi$, followed by $\psi \to \ell^+\ell^-$, gives rise to large violations of duality, which exceed the perturbative contributions by two orders of magnitude [7]. For this reason, the middle domain is frequently removed from experimental data by suitable cuts.

- $15\mathrm{GeV}^2 \lesssim q^2$: With increasing q^2, the resonances continuously broaden, and, as a consequence thereof, duality violation is dampened. When this mechanism finally takes full effect, the kinematics are characterized by the hierarchy
$$m_B, \sqrt{q^2} \gg E, \Lambda_{QCD} \tag{4.9}$$
Historically, little attention has been paid to the domain of low (kaon) recoil (4.9), which suffers mainly from the following two issues:
For one thing, as one approaches the kinematic endpoint, the kaon becomes soft $E \sim m_K$ and the familiar SCET/QCDF framework loses its justification. The appropriate framework to address the non-local term (4.7) is then given by the OPE [1, 20, 21], which is developed and further investigated in the following chapter 5.
For another thing, while duality violations are presumably rather small, they must still be quantified for (precise) theoretical predictions to be meaningful. This issue is thoroughly discussed in section 6.

5 Systematic Framework: OPE for Current Correlator

Towards the kinematic endpoint, the hierarchy (4.9), defining the domain of low kaon recoil, transitions into the OPE limit

$$m_B \;\sim\; \sqrt{q^2} \;\gg\; E, \Lambda_{QCD} \tag{5.1}$$

For the correlator (4.7) this implies that two different types of interactions are involved: On the one hand, perturbative dynamics, governed by the hard scales $m_B, \sqrt{q^2}$ and, on the other hand, non-perturbative dynamics, governed by the soft scales E, Λ_{QCD}.

In the OPE limit (5.1), the short-distance dynamics appear to be local at distances set by E and Λ_{QCD}. This can be exploited by performing an OPE for the non-local matrix element (4.7). In so doing, one obtains a framework in which the $B \to M\ell^+\ell^-$ amplitude can systematically be expanded in powers of $E/\sqrt{q^2}$ (or equivalently Λ_{QCD}/m_B). In particular at the endpoint $E \sim m_K$, where the QCDF framework is not legitimate at all, the OPE allows for reliable theoretical predictions.

5.1 General Structure

In performing the OPE, the non-local interactions contained in the correlator are approximated by a series of local operators with increasing dimension. This instance may formally be written as

$$\mathcal{K}^\mu(q) \;=\; -\frac{8\pi^2}{q^2}\, i\int d^4x\, e^{iq\cdot x}\, T j^\mu(x)\mathcal{H}_h(0) \;=\; \sum_{d,n} C_{d,n}(q)\mathcal{O}^\mu_{d,n} \tag{5.2}$$

whereat the index n labels different operators $\mathcal{O}^\mu_{d,n}$ of the same mass dimension d. Similar to the construction of the weak Hamiltonian, the expansion (5.2) leads to a factorization of physics from distinct scales into Wilson coefficients $(m_B, \sqrt{q^2})$, calculable in perturbation theory, and matrix elements of local operators (E, Λ_{QCD}), which simplifies the calculation of $\langle \mathcal{K}^\mu(q)\rangle$ significantly.

Dimensionality and Scaling

Since the individual terms on the r.h.s. of (5.2) must all have the same dimensionality, each local operator is necessarily accompanied by a Wilson coefficient of complementary dimension:

$$\big[\mathcal{K}^\mu\big] \;=\; \big[C_{d,n}\big] + \big[\mathcal{O}^\mu_{d,n}\big] \;=\; 3 \qquad \Longrightarrow \qquad \big[C_{d,n}\big] \;=\; 3-d \tag{5.3}$$

The coefficients, which may depend on the hard scales only, therefore scale as

$$C_{d,n}(q) \;\sim\; m_B^{3-d} \tag{5.4}$$

in the OPE limit. Consequently the individual matrix elements behave as

$$\langle \bar{K}^{(*)}(k,\varepsilon)\big| C_{d,n}(q)\mathcal{O}^\mu_{d,n}\big|\bar{B}(p)\rangle \;\sim\; \sqrt{\Lambda m_B}\left(\frac{\Lambda}{m_B}\right)^{d-3} \tag{5.5}$$

which also showcases the power suppression of contributions from higher dimensional operators.

General Properties of the Local Operators

On the basis of quite general considerations, the following assertions about the local operators appearing in the OPE can be made:

- The Ward identity, imposed by current conservation, is individually satisfied by each operator
$$q_\mu \mathcal{O}^\mu_{d,n} \;=\; 0 \tag{5.6}$$

- The operators are gauge invariant combinations of quark and gluon fields that reproduce the flavour quantum numbers of $(\bar{s}b)$.

- As shown in appendix E, only covariant derivatives acting on the strange quark generate a soft momentum and thus can increase the operator dimension (in the OPE counting). Since additional derivatives acting on the bottom quark give no independent operators of the same dimension, the generic $(d+3)$-dimensional two-quark operator appearing in the OPE can be written as
$$\bar{s}_L(\overleftarrow{D}^d\Gamma)^\mu b \tag{5.7}$$

Explicit Structure of the Leading Operators

In the following, we discuss the explicit structure of the leading terms in the OPE expansion, which begins with the operators of dimension $d = 3$. Thereby we frequently draw on the results of the (rather technical) analysis presented in appendix E.

- $d \leqslant 4, m_s = 0$: In the chiral limit, a complete basis for the operators up to dimension 4 is given by

$$\mathcal{O}^{\mu}_{3,1} = \left(g^{\mu\nu} - \frac{q^{\mu}q^{\nu}}{q^2}\right)\bar{s}\gamma_{\nu}(1-\gamma_5)b \tag{5.8}$$

$$\mathcal{O}^{\mu}_{3,2} = \frac{im_b}{q^2}\,\bar{s}\sigma^{\mu q}(1+\gamma_5)b \tag{5.9}$$

It is worth mentioning that the two operators $\mathcal{O}^{\mu}_{3,1}$ and $\mathcal{O}^{\mu}_{3,2}$ differ only by a dimension-4 operator. Thus, strictly speaking, there is only one independent operator at leading order in the power counting.

This being said, any operator of dimension $d = 4$ can be expressed in terms of the dimension-3 operators (5.8) – (5.9) multiplied by kinematic prefactors. In case of a dimension-4 operator not proportional to the difference $\mathcal{O}^{\mu}_{3,1} - \mathcal{O}^{\mu}_{3,2}$, the kinematic prefactors must be of $\mathcal{O}(E/m_B)$.

- $d \leqslant 4, m_s \neq 0$: Assuming $\Lambda \sim m_s$ in the OPE limit, there are principally two additional (independent) operators, namely

$$\mathcal{O}^{\mu}_{4,1} = m_s\left(g^{\mu\nu} - \frac{q^{\mu}q^{\nu}}{q^2}\right)\bar{s}\gamma_{\nu}(1+\gamma_5)b \tag{5.10}$$

$$\mathcal{O}^{\mu}_{4,2} = \frac{im_s m_b}{q^2}\,\bar{s}\sigma^{\mu q}(1-\gamma_5)b \tag{5.11}$$

They are counted as operators of dimension-4, for the (admittedly purely kinematic) suppression is closely linked to the chiral structure of the operators and therefore always present. The $\mathcal{O}^{\mu}_{4,n}$ do, however, not emerge at the α_s^0 level, and hence have a relative impact of only $\alpha_s m_s/m_b \approx 0.5\%$. On this account, we will henceforth neglect the $\mathcal{O}^{\mu}_{4,n}$ and perform the OPE in the chiral limit ($m_s = 0$).

In any case, the most important implication of (5.8) – (5.11) is certainly that (independent of the chiral limit) no non-standard form factors are required at the dimension-3 and -4 level.

- $d = 5$: The first power corrections that require the introduction of additional hadronic form factors to describe the corresponding $B \to M\ell^+\ell^-$ matrix elements are encountered at the dimension-5 level. Of course, such corrections can only arise from genuine dimension-5 operators, which contain the gluon field strength tensor $G^a_{\mu\nu}$ (see appendix E) and have the general form

$$\mathcal{O}^{\mu}_{5,n} = g_s\,\bar{s}_L(\Gamma_n G^a T^a)^{\mu} b \tag{5.12}$$

with different Lorentz/Dirac-structures Γ_n.

Note that we give a full treatment of the dimension-5 level. The "non-genuine" second-order power corrections, however, are contained in the coefficient functions of the dimension-3 operators and not mentioned explicitly.

- $d = 6$: As an example for a dimension-6 term, weak annihilation processes will be considered here as well. After all, weak annihilation represents the only remaining α_s^0-contribution and, furthermore, becomes of leading-power at low-q^2.
  The relevant diagrams are shown in Fig. 5.1 (d) and give rise to four-quark operators with the general structure
$$\mathcal{O}^{\mu}_{6a,n} \;=\; (\bar{r}\,\Gamma_n b\,\bar{s}\,\tilde{\Gamma}_n r)^{\mu} \tag{5.13}$$
  where r stands for the light quark in the B meson.

Summarizing the above, the explicit OPE discussion will cover the three terms on the r.h.s. of
$$\mathcal{K}^{\mu}(q) \;\equiv\; \mathcal{K}^{\mu}_3 + \mathcal{K}^{\mu}_5 + \mathcal{K}^{\mu}_{6a} + \mathcal{O}\big((\Lambda/m_B)^3, \alpha_s\big) \tag{5.14}$$
whereat the lower indices indicate the dimension of the local operators contained.

5.2 Coefficient Functions at Leading Order in α_s

In this section, we present analytic expressions for the coefficient functions of the three terms on the r.h.s of (5.14). They are given in the $\overline{MS}$ scheme to leading order in perturbation theory, which is sufficient for a next-to-leading order (NLO) analysis of $B \to M\ell^+\ell^-$ decays.

Leading Power Term $\mathcal{K}^{\mu}_3$ ($d = 3$)

The Feynman diagrams relevant to the dimension-3 term are displayed in Fig. 5.1 (a). One finds $\mathcal{K}^{\mu}_3 = C_{3,1} \cdot \mathcal{O}^{\mu}_{3,1}$, where
$$\begin{aligned} C_{3,1} \;=\; & (C_1 + NC_2)h_c - \frac{1}{2}(C_3 + NC_4)[h_s + h_b] \\ & + (NC_3 + C_4 + NC_5 + C_6)\Big[h_c - \frac{h_b}{2} + \frac{2}{9}\Big] \end{aligned} \tag{5.15}$$

Each row in (5.15) corresponds to all contributions from one of the two Fierz-related variants of diagram Fig. 5.1 (a), and the function $h_q \equiv h(q^2, m_q)$ is given as ($x = 4m_q^2/q^2$)
$$\begin{aligned} h(q^2, m_q) \;=\; & -\frac{8}{9}\ln\frac{m_b}{\mu} - \frac{8}{9}\ln\frac{m_q}{m_b} + \frac{8}{27} + \frac{4}{9}x \\ & - \frac{2}{9}(2+x)\sqrt{|1-x|}\cdot\begin{cases} 2\arctan\frac{1}{\sqrt{x-1}} & x > 1 \\ \ln\frac{1+\sqrt{1-x}}{1-\sqrt{1-x}} - i\pi & x < 1 \end{cases} \end{aligned} \tag{5.16}$$

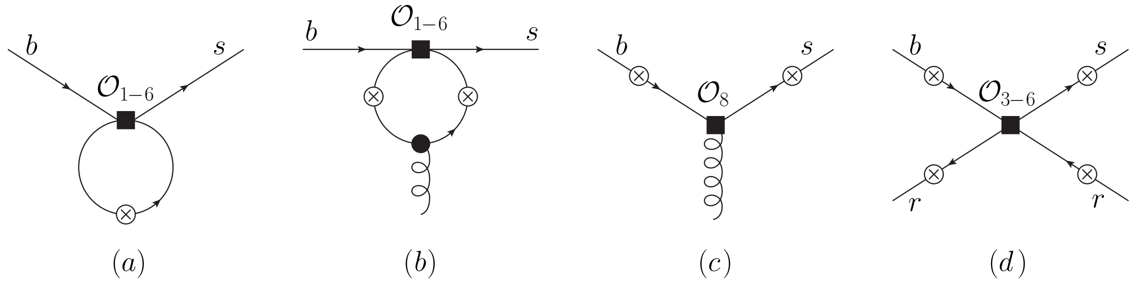

Figure 5.1: OPE for $\mathcal{K}^\mu$ at leading order in α_s: More specifically, diagram (a) gives rise to the leading-power term $\mathcal{K}_3^\mu$, the diagrams (b) and (c) to the gluon term $\mathcal{K}_5^\mu$, and diagram (d) to the weak annihilation term $\mathcal{K}_{6a}^\mu$. The crossed circles $\otimes$ denote possible insertion points for the electromagnetic current operator $j^\mu = \sum_q Q_q(\bar{q}\gamma^\mu q)$.

In the case of a (approximately) massless quark ($q = u, d, s$), the loop function simplifies to

$$h(q^2, 0) \;=\; \frac{8}{27} - \frac{8}{9}\ln\frac{m_b}{\mu} - \frac{4}{9}\ln\frac{q^2}{m_b^2} + \frac{4}{9}i\pi \tag{5.17}$$

If required, the exact position in the complex plane can always be determined by restoring the Feynman prescription $m_q^2 \to m_q^2 - i\epsilon$, which corresponds to the replacement $x \to x - i\epsilon$ in (5.16).

Note that, in keeping the q^2-dependence in the coefficient functions, $\mathcal{K}_3^\mu$ also contains contributions of dimension 4 and higher.

Finally, it is pointed out that (5.15) depends on the chosen scheme for the UV renormalization. This, however, only influences the constant terms, such as the "2/9" in the second row of (5.15), which corresponds to the $\overline{MS}$ scheme, used here. This ambiguity is cancelled by an opposing scheme dependency of the Wilson coefficient C_9, which results in an overall scheme independent amplitude $\mathcal{A}_9^{(*)\mu}$ to the given order.

Second-Order Power Corrections $\mathcal{K}_5^\mu$ ($d = 5$)

At next, we already have the dimension-5 term, which has its origin in the Feynman diagrams shown in Fig. 5.1 (b) and (c). The calculation yields[1] ($\varepsilon^{0123} = -1$)

$$\begin{aligned}\mathcal{K}_5^\mu \;=\; & \frac{2g_s}{q^4}\Big\{Q_c f(q^2, m_c)(C_1 + C_4 - C_6) + Q_b f(q^2, m_b)(C_3 + C_4 - C_6) \\ & + Q_s f(q^2, m_s) C_3\Big\}(\varepsilon^{\alpha q\mu\beta} q^\nu - \varepsilon^{\alpha q\mu\nu} q^\beta)\, G^a_{\alpha\beta}\, \bar{s}_L \gamma_\nu T^a b \\ & + \frac{8g_s}{q^2}\frac{C_8 Q_b}{m_B}(g^{\mu\alpha} q_\nu - g^\mu{}_\nu q^\alpha)\, G^a_{\alpha\beta}\, \bar{s}_L \sigma^{\beta\nu} T^a b\end{aligned} \tag{5.18}$$

[1] At this point, special thanks go to Prof. Jürgen Körner for drawing our attention to the Schouten identity, which allowed for a simplification of our original result.

where $(x = 4m_q^2/q^2)$

$$f(q^2, m_q) \;=\; \frac{-x}{\sqrt{1-x}}\left(\ln\frac{1+\sqrt{1-x}}{1-\sqrt{1-x}} - i\pi\right) - 2 \tag{5.19}$$

which simplifies for a massless quark to $f(q^2, 0) = -2$. The entire loop contribution, i.e. the first two rows of (5.18), can also be extracted from [43].

Further note that this term is, to a large extent, scheme independent. In particular, the expression (5.18) does not depend on the chosen operator basis. This is due to the cancellation of the infinities between the two symmetric diagrams of Fig. 5.1. More details on this and the calculation in general can be found in section 9.2.3, where the more general case of an arbitrary kaon energy is addressed.

Weak Annihilation Term $\mathcal{K}^{\mu}_{6a}$ $(d = 6)$

At last, we have the weak annihilation term, induced by the processes of Fig. 5.1 (d). This completely scheme independent term may be written as

$$\begin{aligned}\mathcal{K}^{\mu}_{6a} \;=\; \frac{16\pi^2}{q^4}\sum_{r=u,d}\Big\{&\big(\delta_{ij}\delta_{kl}C_4 + \delta_{il}\delta_{kj}C_3\big)\Big[\frac{i}{3}\varepsilon^{q\mu\alpha\beta} + Q_r\big(g^{\mu\alpha}q^{\beta} - g^{\mu\beta}q^{\alpha}\big)\Big]\\ &\cdot\; \bar{r}_i\gamma_\alpha(1-\gamma_5)b_j\,\bar{s}_k\gamma_\beta(1-\gamma_5)r_l\\ &+ i\big(\delta_{ij}\delta_{kl}C_6 + \delta_{il}\delta_{kj}C_5\big)\Big[\Big(Q_r - \frac{1}{3}\Big)\bar{r}_i(1-\gamma_5)b_j\,\bar{s}_k\sigma^{\mu q}(1+\gamma_5)r_l\\ &+ \Big(Q_r + \frac{1}{3}\Big)\bar{r}_i\sigma^{\mu q}(1-\gamma_5)b_j\,\bar{s}_k(1+\gamma_5)r_l\Big]\Big\}\end{aligned} \tag{5.20}$$

Of course, only the component of $\mathcal{K}^{\mu}_{6a}$ for which r coincides with the respective spectator quark contributes to a given decay.

5.3 Impact of $\mathcal{O}(\alpha_s)$ Corrections

The Feynman diagrams responsible for the non-factorizable $\mathcal{O}(\alpha_s)$ corrections to the leading-power term $\mathcal{K}^{\mu}_3$ are shown in Fig. 5.2. Owing to the smallness of the penguin coefficients, the contributions from the operators $\mathcal{O}_{3-6}$ will be neglected.

Beforehand, attention is drawn to the peculiar colour structure of the LO term (Fig. 5.1 (a)). In combination with the numerical size of the Wilson coefficients $C_{1,2}$ at $\mu \sim m_b$, this entails a suppression of this term. The NLO term, on the other hand, allows for a $c\bar{c}$ pair in the colour-octet state and, due to this, has no such suppression.

Figure 5.2: OPE for $\mathcal{K}^\mu$: Diagrams responsible for the $\mathcal{O}(\alpha_s)$ corrections to the leading-power term $\mathcal{K}_3^\mu$. The crossed circles $\otimes$ denote possible insertion points for the electromagnetic current operator $j^\mu = \sum_q Q_q(\bar{q}\gamma^\mu q)$. Diagrams related to (b) by symmetry are not shown.

Schematically, this instance reads

$$\text{LO} \;\propto\; C_1 + NC_2 \;\approx\; 1.137 + 3\cdot(-0.303) \;=\; 0.23 \tag{5.21}$$

$$\text{NLO} \;\propto\; C_F C_1 \;\approx\; \frac{4}{3}\cdot(1.137) \;=\; 1.52 \tag{5.22}$$

In consequence, the LO charm-loop (Fig. 5.1 (a)) and the corresponding $\mathcal{O}(\alpha_s)$ corrections (Fig. 5.2) are comparable in size and, as it turns out, compensate each other to a large extent. It is stressed that even higher order contributions $\sim \mathcal{O}(\alpha_s^n)$ with $n \geqslant 2$ do not come with enhanced colour structures and thus should indeed be small.

For $m_c = 0$, the q^2-dependency of the charm-loop correction was first presented in analytic form in [44]. Later, a Taylor series in the small parameter $z = m_c^2/m_b^2$ was presented in [45]. The authors of [45] also affirm a good convergence behaviour for $\hat{s} = q^2/m_b^2 \geqslant 0.6$, which corresponds to $q^2 \geqslant 10.5\,\text{GeV}^2$ and thus applies to the OPE domain. Consequently, the MATHEMATICA input files attached to [45] may be used to compute the $\mathcal{O}(\alpha_s)$ corrections to $\mathcal{K}_3^\mu$.

Now, as for the actual results, real and imaginary part of the correction term are both found to be negative and roughly of the same size. Adding the $\mathcal{O}(\alpha_s)$ corrections to the amplitude $\mathcal{A}_9^\mu$, the real part and hence the absolute value of $\mathcal{A}_9^\mu$ are reduced by $7-14\%$, whereat, however, a strong dependence of the impact on the chosen scheme for the charm mass can be observed. While the imaginary part of $\mathcal{A}_9^\mu$ is changed drastically, this has virtually no impact on $|\mathcal{A}_9^\mu|$ (and consequently the branching fractions), for $\mathcal{A}_9^\mu$ is and remains almost completely real.

The above findings qualitatively agree with the corresponding results for the high-q^2 region of the inclusive $B \to X_s\ell^+\ell^-$ decay rate, discussed in [45]. Furthermore, the effect found for exclusive $B \to M\ell^+\ell^-$ decays at low-q^2 is similar [46].

5.4 Impact of $\mathcal{O}(E/m_B)$ Corrections

In principle, the OPE allows for a systematic expansion of $B \to M\ell^+\ell^-$ decay amplitudes in powers of E/m_B. This being said, at low recoil, the matrix elements of higher-dimensional operators can not be expressed in terms of the "standard" form factors (3.8) – (3.13). Instead they require the introduction of new, presently unknown,

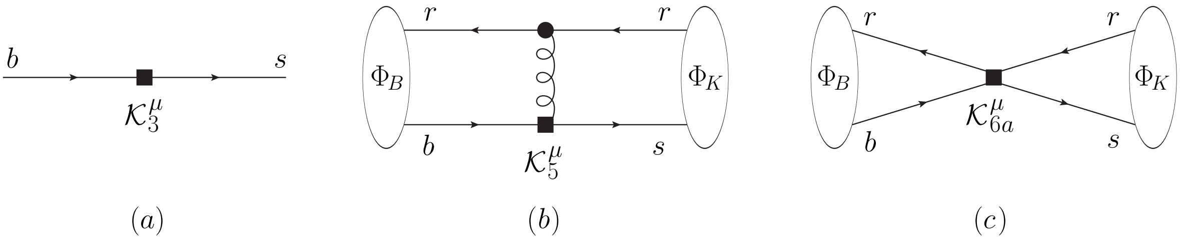

Figure 5.3: In the OPE framework, the leading-power contributions to the $\bar{B} \to \bar{K}^{(*)}\ell^+\ell^-$ amplitude are obtained from the matrix elements of the local operators $\mathcal{K}_3^\mu$, $\mathcal{K}_5^\mu$ and $\mathcal{K}_{6a}^\mu$.

form factors, which renders the actual (numerical) calculation of power corrections at high-q^2 currently unfeasible.

While power-counting arguments indicate the smallness of these contributions, it is certainly preferable to quantify the possible impact of power corrections more concretely. To this end, we henceforth assume the kinematic setting

$$\sqrt{q^2} \;\gg\; E \;\gg\; \Lambda_{QCD}, m_K \tag{5.23}$$

for this allows to a the matrix elements of the local operators, shown in Fig. 5.3, within the framework of QCDF. Admittedly, towards the kinematic endpoint $q^2 \sim m_B^2$, the results obtained in this way can only serve as very rough estimates. Nevertheless, drawing qualitative conclusions should still be justified. A discussion similar to the one below was given in [1].

5.4.1 Evaluation of $B \to P$ Matrix Elements

Approaching the pseudoscalar matrix elements as outlined above, one finds

$$\langle \bar{K}(k)|\mathcal{K}_3^\mu|\bar{B}(p)\rangle \;=\; 2f_+(q^2)C_{3,1}(q^2)\Big[k^\mu \;-\; \frac{k\cdot q}{q^2}q^\mu\Big] \tag{5.24}$$

$$\langle \bar{K}(k)|\mathcal{K}_5^\mu|\bar{B}(p)\rangle \;=\; -\frac{\pi\alpha_s(E)C_F}{N}C_1Q_c f(q^2,m_c)\frac{m_B f_B f_K}{q^2\lambda_+}\Big[k^\mu \;-\; \frac{k\cdot q}{q^2}q^\mu\Big] \tag{5.25}$$

$$\langle \bar{K}(k)|\mathcal{K}_{6a}^\mu|\bar{B}(p)\rangle \;=\; -16\pi^2 Q_r\Big(\frac{C_3}{N} \;+\; C_4\Big)\frac{f_B f_K}{q^2}\Big[k^\mu \;-\; \frac{k\cdot q}{q^2}q^\mu\Big] \tag{5.26}$$

where, in (5.25), the penguin coefficients have been neglected and the function λ_+^{-1}, specified in appendix B.2.2, is the first inverse moment of the B meson. Furthermore, in the dimension-6 term (5.26), Q_r denotes the charge quantum number of the spectator quark, which is the light quark in the B meson.

Note that the contributions from the matrix elements (5.24) and (5.26) to the decay rate coincide with the results from “naive” QCDF (that is, if no OPE is performed first). The contribution due to the dimension-5 term (5.25), on the other hand,

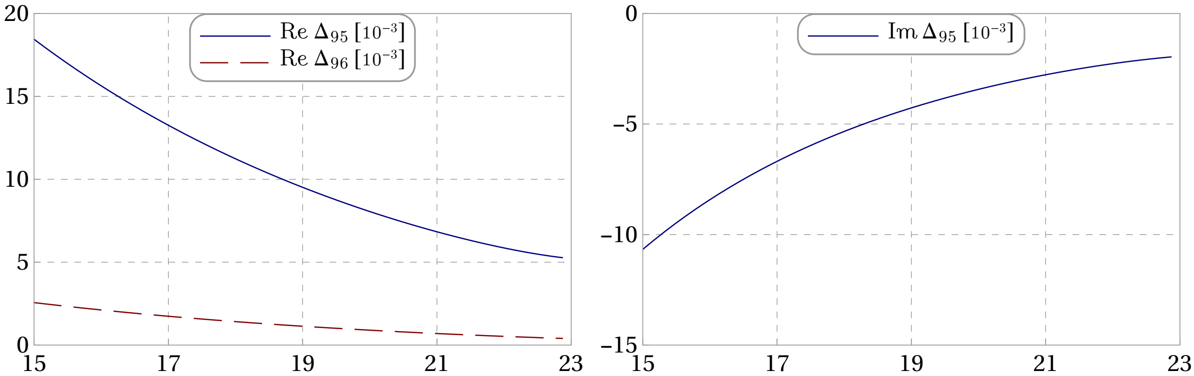

Figure 5.4: Power-suppressed contributions to $B \to K\ell^+\ell^-$: Correction terms Δ_{9i}, normalized to the amplitude coefficient $C_9^{\text{eff}} \approx 4$, as functions of $q^2[\text{GeV}^2]$. The weak annihilation term corresponds to $Q_r = Q_u$. Only Δ_{95} develops an imaginary part, namely for $q^2 > 4m_c^2$.

differs slightly from its QCDF-based counterpart, which is discussed at length in section (5.5).

Finally, it is pointed out that the matrix element of the C_8 term in (5.18) is heavily constrained by its three antisymmetries and Lorentz invariance (in particular the limited number of independent momenta available). In consequence, this matrix element vanishes completely in the pseudoscalar case

$$(g^{\mu\alpha}q_\nu - g^\mu{}_\nu q^\alpha)\langle \bar{K}(k)|\, G^a_{\alpha\beta}\,\bar{s}_L\sigma^{\beta\nu}T^a b\,|\bar{B}(p)\rangle \;=\; 0 \tag{5.27}$$

Numerical Impact: Effective Coefficient and Correction Terms

In order to investigate the relative size of the higher-dimensional contributions, the matrix elements (5.24) – (5.26) are expressed as corrections to the effective coefficient C_9^{eff}, which multiplies the local operator $\dfrac{2\pi}{\alpha_e}\mathcal{O}_9 = (\bar{s}b)_{V-A}\sum_\ell(\bar{\ell}\ell)_V$. More specifically, the amplitude (4.2) is expressed as (omitting terms $\propto q^\mu$)

$$\mathcal{A}_9^\mu(s) \;\equiv\; C_9^{\text{eff}}(s)\langle\bar{K}|\,\bar{s}\gamma^\mu(1-\gamma_5)b\,|\bar{B}\rangle \;=\; 2C_9^{\text{eff}}(s)\,f_+(s)k^\mu \tag{5.28}$$

The effective coefficient is then given as

$$C_9^{\text{eff}} \;=\; C_9 + \frac{2m_b}{m_B + m_K}\,\frac{f_T(s)}{f_+(s)}\,C_7 + \Delta_{93} + \Delta_{95} + \Delta_{96a} + \;\ldots \tag{5.29}$$

where the correction terms Δ_{9i} are obtained from the expressions (5.24) – (5.26) via normalization to the matrix element of the local operator $(\bar{s}b)_{V-A}$ according to

$$\Delta_{9i} \;\equiv\; \frac{\langle\bar{K}(k)|\,\mathcal{K}_i^\mu\,|\bar{B}(p)\rangle}{\langle\bar{K}|\,\bar{s}\gamma^\mu(1-\gamma_5)b\,|\bar{B}\rangle} \tag{5.30}$$

The Δ_{9i} can essentially read off of (5.24) – (5.26), but are nevertheless given explicitly

	Δ_{95}	$\Delta_{95\|}$	$\Delta_{95\perp}$	$\Delta^{(u)}_{96a}$	$\Delta^{(u)}_{96a\|}$	$\Delta^{(u)}_{96a\perp}$	$\Delta^{(d)}_{96a}$	$\Delta^{(d)}_{96a\|}$	$\Delta^{(d)}_{96a\perp}$
$[10^{-3}]$	$18-11i$	$20-11i$	$14-9i$	2.6	2.8	3.1	-1.3	-1.4	-6.1

Table 5.1: Maximum values of the corrections terms Δ_{9i}, attained at $q^2 = 15\,\text{GeV}^2$.

for the sake of completeness:

$$\Delta_{93} = C_{3,1}(q^2) \tag{5.31}$$

$$\Delta_{95} = -\frac{\pi\alpha_s(E)C_F}{2N}\,C_1 Q_c\, f(q^2,m_c)\,\frac{m_B f_B f_K}{f_+(q^2)\,q^2\lambda_+} \tag{5.32}$$

$$\Delta_{96a} = -8\pi^2 Q_r\left(\frac{C_3}{N}+C_4\right)\frac{f_B f_K}{f_+(q^2)\,q^2} \tag{5.33}$$

The two subleading terms, Δ_{95} and Δ_{96a}, are displayed in Fig. 5.4, where a continuous decrease with increasing q^2 can be observed. This behaviour is in line with the power-suppression of these terms in the OPE limit and implies that the maximum values, given in Tab. 5.1, are attained at our lower bound $q^2 = 15\,\text{GeV}^2$.

Comparing the maximum values with the leading-power coefficient $C_9^{\text{eff}} \approx 4.1 + 0.8i$ (using NNLO Wilson coefficients and $q^2 = 15\,\text{GeV}^2$), one finds for the dimension-5 term an impact to real and imaginary part of 0.5% and 1.4%, respectively. However, since $\text{Im}[C_9^{\text{eff}}]$ is strongly order and scheme dependent, the impact on the imaginary component can potentially go up to 5%. This being said, the real component of C_9^{eff} is much larger than the imaginary, and therefore the total impact of Δ_{95} to the decay rate is only about 0.5% and stems, in any case, almost exclusively from $\text{Re}[\Delta_{95}]$.

As far as the weak annihilation term is concerned, the large numerical prefactor "$8\pi^2$" is, for the most part, compensated by the smallness of the penguin coefficients. The overall impact of this contribution to the decay rate stays well below 0.1% and thus is completely negligible.

Again, these results are based on QCDF, which loses its validity if the kaon becomes soft. Nevertheless, qualitatively these results should hold even towards the kinematic endpoint $q^2 \sim m_B^2$, particularly in view of the fact that the power suppression becomes fully effective there. In other words, the impact of the power-suppressed terms should be the largest where the QCDF-based estimates presented here are most reliable.

5.4.2 Evaluation of $B \to V$ Matrix Elements

It is convenient to consider the decay into a longitudinally and transversely polarized vector meson separately. Once again, the kinematic setting (5.23) is assumed. Fur-

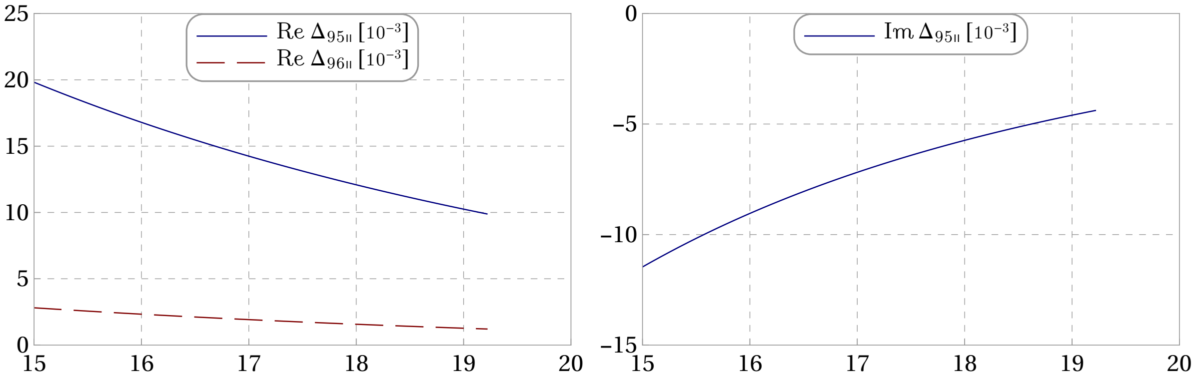

Figure 5.5: Power-suppressed contributions to $B \to K_\parallel^* \ell^+\ell^-$: Correction terms $\Delta_{9i\parallel}$, normalized to the amplitude coefficient $C_{9\parallel}^{eff} \approx 4$, as functions of $q^2[\mathrm{GeV}^2]$. The weak annihilation term corresponds to $Q_r = Q_u$. Only $\Delta_{95\parallel}$ develops an imaginary part, namely for $q^2 > 4m_c^2$.

thermore, the universal form factor relations (3.61) – (3.63) are utilized to simplify the matrix elements of the leading operator $\mathcal{O}_9$ to (dropping terms of relative order m_K^2/m_B^2 or proportional to q^μ)

$$\langle \bar{K}_\parallel^* | \bar{s}\gamma^\mu(1-\gamma_5)b|\bar{B}\rangle = \frac{2\varepsilon_\parallel^* \cdot q}{m_B + m_K} A_2(q^2)k^\mu - A_1(q^2)(m_B + m_K)\varepsilon_\parallel^{*\mu} \tag{5.34}$$

$$= -2A_0(q^2)k^\mu \tag{5.35}$$

$$\langle \bar{K}_\perp^* | \bar{s}\gamma^\mu(1-\gamma_5)b|\bar{B}\rangle = \frac{2iV(q^2)}{m_B + m_K}\varepsilon^{\mu kp\varepsilon_\perp^*} - A_1(q^2)(m_B + m_K)\varepsilon_\perp^{*\mu} \tag{5.36}$$

$$= \frac{-2V(q^2)}{m_B + m_K}\left[i\varepsilon^{\mu qk\varepsilon_\perp^*} + k\cdot q\,\varepsilon_\perp^{*\mu}\right] \tag{5.37}$$

The decay into a longitudinal vector meson is (then) very similar to the preceding pseudoscalar case. In the calculations, one simply has to replace

$$f_+(q^2) \to -A_0(q^2) \qquad \text{and} \qquad f_K \to -f_\parallel \tag{5.38}$$

and, consequently, the longitudinal matrix elements are found to be

$$\langle \bar{K}_\parallel^*(k,\varepsilon)|\mathcal{K}_3^\mu|\bar{B}(p)\rangle = -2C_{3,1}(q^2)A_0(q^2)\left[k^\mu - \frac{k\cdot q}{q^2}q^\mu\right] \tag{5.39}$$

$$\langle \bar{K}_\parallel^*(k,\varepsilon)|\mathcal{K}_5^\mu|\bar{B}(p)\rangle = \frac{\pi\alpha_s(E)C_F}{N}C_1 Q_c f(q^2,m_c)\frac{m_B f_B f_\parallel}{q^2\lambda_+}\left[k^\mu - \frac{k\cdot q}{q^2}q^\mu\right] \tag{5.40}$$

$$\langle \bar{K}_\parallel^*(k,\varepsilon)|\mathcal{K}_{6a}^\mu|\bar{B}(p)\rangle = 16\pi^2 Q_r\left(\frac{C_3}{N} + C_4\right)\frac{f_B f_\parallel}{q^2}\left[k^\mu - \frac{k\cdot q}{q^2}q^\mu\right] \tag{5.41}$$

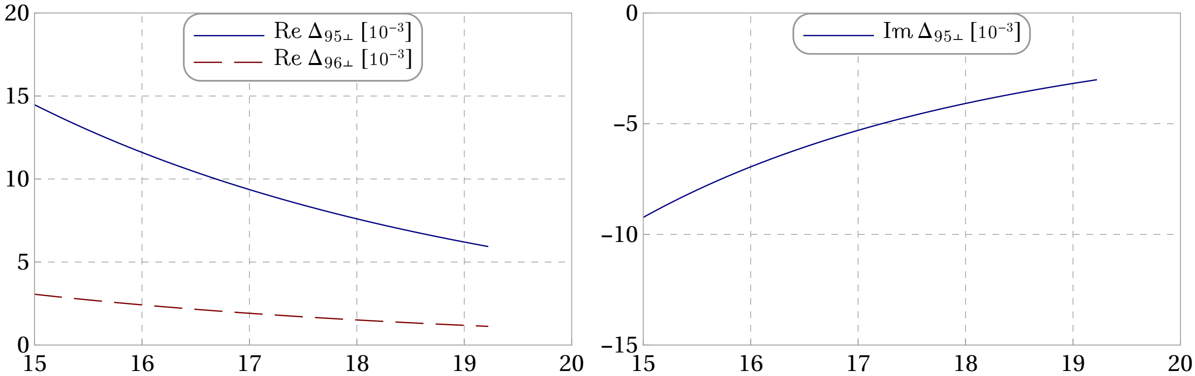

Figure 5.6: Power-suppressed contributions to $B \to K^*_\perp \ell^+\ell^-$: Correction terms $\Delta_{9i\perp}$, normalized to the amplitude coefficient $C^{\mathit{eff}}_{9\perp} \approx 4$, as functions of $q^2[\mathrm{GeV}^2]$. The weak annihilation term corresponds to $Q_r = Q_u$. Only $\Delta_{95\perp}$ develops an imaginary part, namely for $q^2 > 4m_c^2$.

The transverse polarizations, on the other hand, presents itself somewhat different, and one obtains

$$\langle \bar{K}^*_\perp | \mathcal{K}^\mu_3 | \bar{B} \rangle \;=\; 2C_{3,1}(q^2)\frac{V(q^2)}{m_B}\left[i\varepsilon^{\mu q k \varepsilon^*_\perp} + k\cdot q\,\varepsilon^{*\mu}_\perp\right] \tag{5.42}$$

$$\langle \bar{K}^*_\perp | \mathcal{K}^\mu_5 | \bar{B} \rangle \;=\; \frac{\pi\alpha_s(E)C_F}{2N}\left[C_1 Q_c \frac{f(q^2,m_c)}{s} + 8C_8 Q_b\right]\frac{f_B f_\perp}{q^2\lambda_+}\left[i\varepsilon^{\mu q k \varepsilon^*_\perp} + k\cdot q\,\varepsilon^{*\mu}_\perp\right] \tag{5.43}$$

$$\langle \bar{K}^*_\perp | \mathcal{K}^\mu_{6a} | \bar{B} \rangle \;=\; 16\pi^2\left(Q_r - \tfrac{1}{3}\right)\left(\frac{C_5}{N} + C_6\right)\frac{m_B f_B f_\perp}{q^4}\left[i\varepsilon^{\mu q k \varepsilon^*_\perp} + k\cdot q\,\varepsilon^{*\mu}_\perp\right] \tag{5.44}$$

As before, penguin suppressed contributions have been neglected in (5.40) and (5.43), and the Q_r in (5.41) and (5.44) refers to the charge quantum number of the respective spectator quark.

Numerical Impact: Effective Coefficients and Correction Terms

The effective coefficients, one for each polarization, are now defined as

$$\mathcal{A}^\mu_{9\|}(s) \;\equiv\; C^{\mathit{eff}}_{9\|}(s)\langle \bar{K}^*_\| | \bar{s}\gamma^\mu(1-\gamma_5)b | \bar{B}\rangle \;=\; -2C^{\mathit{eff}}_{9\|}A_0(s)k^\mu \tag{5.45}$$

$$\mathcal{A}^\mu_{9\perp}(s) \;\equiv\; C^{\mathit{eff}}_{9\perp}(s)\langle \bar{K}^*_\perp | \bar{s}\gamma^\mu(1-\gamma_5)b | \bar{B}\rangle \;=\; \frac{-2C^{\mathit{eff}}_{9\perp}V(s)}{m_B + m_K}\left[i\varepsilon^{\mu q k \varepsilon^*_\perp} + k\cdot q\,\varepsilon^{*\mu}_\perp\right] \tag{5.46}$$

which results in power expansions of the form

$$C^{\mathit{eff}}_{9\|}(s) \;=\; C_9 + 2C_7\frac{m_b}{m_B} + \Delta_{93\|} + \Delta_{95\|} + \Delta_{96a\|} + \;\ldots \tag{5.47}$$

$$C^{\mathit{eff}}_{9\perp}(s) \;=\; C_9 + \frac{2C_7}{s}\frac{m_b}{m_B} + \Delta_{93\perp} + \Delta_{95\perp} + \Delta_{96a\perp} + \;\ldots \tag{5.48}$$

Defined analogous to (5.30), the correction terms appearing in (5.47) and (5.48) read

$$\Delta_{95\parallel} \;=\; -\frac{\pi\alpha_s(E)C_F}{2N}\,C_1Q_c\,f(q^2,m_c)\,\frac{m_Bf_Bf_\parallel}{A_0(q^2)q^2\lambda_+} \tag{5.49}$$

$$\Delta_{95\perp} \;=\; -\frac{\pi\alpha_s(E)C_F}{4N}\left[\frac{C_1Q_c}{s}f(q^2,m_c)+8C_8Q_b\right]\frac{m_Bf_Bf_\perp}{V(q^2)q^2\lambda_+} \tag{5.50}$$

$$\Delta_{96\parallel} \;=\; -8\pi^2\,Q_r\left(\frac{C_3}{N}+C_4\right)\frac{f_Bf_\parallel}{A_0(q^2)q^2} \tag{5.51}$$

$$\Delta_{96\perp} \;=\; -8\pi^2\left(Q_r-\tfrac{1}{3}\right)\left(\frac{C_5}{N}+C_6\right)\frac{m_B^2f_Bf_\perp}{V(q^2)q^4} \tag{5.52}$$

They are displayed as functions of q^2 in Fig. 5.5 and 5.6; the respective maximum values, attained at $q^2 = 15\,\mathrm{GeV}^2$, are given in Tab. 5.1. The numerical situation is for both directions of polarization quantitatively and, in particular, qualitatively similar to the pseudoscalar case, and thus we refrain here from an explicit discussion.

5.4.3 Scaling and Power Suppression

Individual Components

First of all, the scaling behaviour in the heavy-quark limit of the individual scale-dependent components is listed separately. Let us begin with the quantities where the scaling does not depend on the size of q^2, which are

$$f_B \sim (\Lambda^3/m_B)^{1/2} \qquad\qquad f_K \sim f_\parallel \sim f_\perp \sim \Lambda \qquad\qquad \lambda_+ \sim \Lambda \tag{5.53}$$

As for the remaining quantities, the size (or the scaling) of q^2 is decisive. For the form factors, we have

$$f_\pm(q^2\simeq m_B^2) \sim (\Lambda/m_B)^{-1/2} \qquad \text{and} \qquad f_{+,0}(q^2\simeq 0) \sim (\Lambda/m_B)^{3/2} \tag{5.54}$$

where the relation on the l.h.s. can be derived from the Isgur-Wise scaling law [47]; the relation on the r.h.s. from QCD sum rules [48] or, alternatively, SCET [22]. The corresponding form factors of the vector meson behave similarly in the heavy-quark limit $f_+(q^2) \sim A_0(q^2) \sim V(q^2)$. Finally, we have the scaling

$$\lambda_-(q^2\simeq m_B^2) \sim m_B \qquad \text{and} \qquad \lambda_-(q^2\simeq m_B\omega_0) \sim \Lambda \tag{5.55}$$

However, note that

$$\lambda_-^{-1}(q^2 \ll m_B \omega_0) \;=\; \frac{1}{\omega_0}\Big[i\pi - \gamma - \ln\frac{s m_B}{\omega_0} + \mathcal{O}\Big(\frac{s m_B}{\omega_0}\Big)\Big] \tag{5.56}$$

is divergent in the limit $q^2 \to 0$.

Correction Terms

In avoidance of repetition, only the scalar case is discussed explicitly; both polarized cases are analogous to and can easily be obtained from the scalar case by performing the appropriate replacements (e.g. via (5.38) in the case of a $K^*_\parallel$).

Putting everything together, the proper scaling behaviour of the correction terms in the OPE limit ($m_B \sim \sqrt{q^2} \gg \Lambda$)

$$\Delta_{95} \sim \frac{m_B f_B f_K}{f_+(q^2)q^2\lambda_+} \sim (\Lambda/m_B)^2 \qquad\qquad \Delta_{96a} \sim \frac{f_B f_K}{f_+(q^2)q^2} \sim (\Lambda/m_B)^3 \tag{5.57}$$

can easily be verified. Moreover, as a direct consequence of the different scaling of $f_+(q^2)$ and $\lambda_-^{-1}(q^2)$ at high- and low-q^2, it can be shown that Δ_{95} and Δ_{96a} are leading-power contributions at low-q^2. For this, however, the λ_-^{-1} in the weak annihilation term needs to be recovered first (e.g. by undoing the replacement (B.45), or by resorting directly to a QCDF-based expression, such as (9.4)).

5.5 Transition Domain: OPE vs. QCD Factorization

Transition Domain

It is instructive to compare the OPE-based results with those obtained in the framework of QCDF. Admittedly, these two theoretical approaches address, in principle, the opposing endpoints of the spectrum. This being said, what OPE and QCDF require are, strictly speaking, only the hierarchies

$$\sqrt{q^2} \;\gg\; E, \Lambda_{QCD} \qquad\text{and}\qquad E \;\gg\; \Lambda_{QCD}, m_K \tag{5.58}$$

respectively. However, the two kinematic limits (5.58) are not mutually exclusive. As a matter of fact, they can be combined, which formally defines a transition region

$$\sqrt{q^2} \;\gg\; E \;\gg\; \Lambda_{QCD}, m_K \tag{5.59}$$

where both theoretical frameworks are equally well justified. Not surprisingly, (5.59) coincides with the setting (5.23), assumed above to calculate the matrix elements of the local operators with the help of QCDF. In other words, in the transition domain (5.59), “naive” (pure) QCDF is just as justified as the “mixed” approach of the previous sections, and it is the relation between these two we want to investigate in this section.

Now let us continue to determine the range in q^2 where the hierarchies (5.59) are at least roughly realized. For obvious reasons constraining the search to our default OPE domain, the lowest point that comes into question is $q^2 = 15\,\mathrm{GeV}^2$. At this value of q^2, (5.59) numerically reads (kaon)

$$3.87\,\mathrm{GeV} \;\gg\; 1.24\,\mathrm{GeV} \;\gg\; 0.5\,\mathrm{GeV} \tag{5.60}$$

which can be considered halfway decent hierarchies. From here the transition region stretches a few GeV^2 upwards until *both* QCDF-based approaches eventually lose their remaining validity.

For definiteness, the following discussion will be restricted to the case of a pseudoscalar kaon (which is equivalent to a longitudinal vector meson). Also, in order to keep the following discussion as simple as possible, the small penguin coefficients are dropped.

OPE and QCDF Expressions for Leading Correction Terms

In both theoretical frameworks, the result obtained for the leading contribution to the charm loop, given by the diagram in Fig. 5.1 (a), is identical.[2] Consequently, we will focus our attention on the respective first correction term, which arises from the spectator processes shown in Fig. 5.1 (b) and (c).

The required QCDF expression may be extracted from [40], where it is decomposed into two components $\Delta_{9\|\pm}$, each proportional to one of the B meson projectors.[3] The minus component is given as $(m_K = 0)$

$$\Delta_{9\|-} \;=\; -\frac{\pi\alpha_s(E)C_F}{2N}\,Q_r\,\frac{f_B f_K}{f_+(q^2)}\,\frac{m_b}{m_B}\int\frac{d\omega\,\phi_-(\omega)}{\omega m_B \,-\, q^2 \,-\, i\epsilon}$$

$$\cdot\int_0^1 du\,\phi_K(u)\left[\frac{8C_8}{\bar{u}\,+\,us} \,+\, \frac{6m_B}{m_b}\,C_1\,h(q^2,m_q)\Big|_{q^2\to\bar{u}m_B^2+\,uq^2}\right] \tag{5.61}$$

where $h(q^2, m_q)$ is the function defined in (5.16) and Q_r refers to the charge quantum number of the spectator quark.

Actually, related to the scaling of λ_-^{-1} in this kinematic region (see (5.55)), the contribution (5.61) is subleading in the OPE limit $\Delta_{9\|-} \sim 1/m_B^3$. Using Wilson coefficients in leading logarithmic approximation (LLA), this term amounts to $(Q_r = Q_u)$

$$\Delta_{9\|-}(q^2 = 15\,\mathrm{GeV}^2) \;=\; (0.091 \,+\, 3.90i)\cdot 10^{-3} \tag{5.62}$$

from where it further diminishes continuously with increasing q^2. Noteworthy, using

[2] As an aside, the same holds for the weak annihilation term Fig. 5.1 (d).

[3] The notation for the lower indices is adopted from [40], which only discusses the vector meson explicitly.

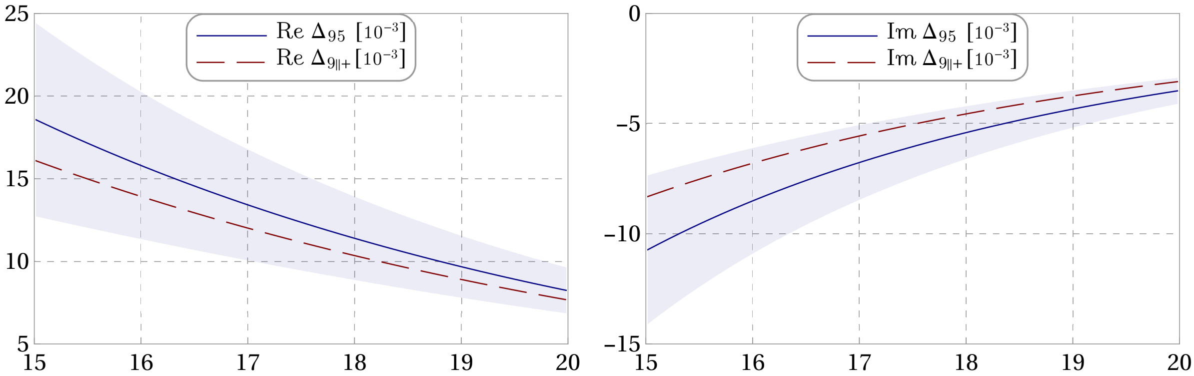

Figure 5.7: Comparison of OPE - and QCDF-based result as given in (5.63) and (5.64), respectively. The shaded areas illustrate the expected deviation between the two curves due to the "missing" terms of relative order $E/\sqrt{q^2}$.

NLLA coefficients, almost halves the result to $\Delta_{9\|-} = (0.048 + 3.77i) \cdot 10^{-3}$. In any case, at high-$q^2$, the minus component is negligible for sure, which is in perfect agreement with the absence of such a term in the OPE expression Δ_{95}.[4]

Turning our attention now to the plus component, the corresponding OPE expression is given as well (or rather once again) to allow for a direct comparison. The two correction terms read

$$\Delta_{95} = -\frac{\pi\alpha_s(E)C_F}{2N} C_1 Q_c \frac{f_B f_K}{f_+(q^2)} \int \frac{d\omega}{\omega m_B} \phi_+(\omega) \cdot f(q^2, m_c) \frac{m_B^2}{q^2} \tag{5.63}$$

$$\Delta_{9\|+} = -\frac{\pi\alpha_s(E)C_F}{2N} C_1 Q_c \frac{f_B f_K}{f_+(q^2)} \int \frac{d\omega}{\omega m_B} \phi_+(\omega) \cdot \int_0^1 du\, \phi(u)\, t_\|(q^2, m_c, u) \tag{5.64}$$

where ($t \equiv m_q^2/m_B^2, \bar{u} = 1 - u$)

$$t_\|(s,t,u) = \frac{4t}{\bar{u}^2(1-s)^2}\left[F^2\left(\frac{4t}{\bar{u}+us}\right) - F^2\left(\frac{4t}{s}\right)\right] - \frac{4}{s} \tag{5.65}$$

$$F(x) = \ln\frac{1+\sqrt{1-x}}{1-\sqrt{1-x}} - \frac{\bar{u}+us}{2t}\sqrt{1-x} - i\pi \tag{5.66}$$

It is to be stressed that, even though our definitions for $\Delta_{9\|+}$, i.e. the equations (5.64) – (5.66), look significantly simpler than the ones used in [40], they are nevertheless equivalent (most notably, the functions $\Delta_{9\|+}$ and $t_\|$ are identical). In this context, further note that the imaginary part has been made explicit for high values of $q^2 > 4m_c^2$.

[4]In particular, the OPE result is proportional to λ_+^{-1} and lacks a C_8 term.

Numerical Comparison

Comparing the OPE result (5.63) with the QCDF result (5.64), the close resemblance is easy to recognize. The two expressions differ just by the replacement

$$\int_0^1 du\, \phi(u)\, t_\parallel(q^2, m_c, u) \;=\; -5.04 + 2.61i \quad\to\quad \frac{f(q^2, m_c)}{s} \;=\; -5.81 + 3.36i \qquad (5.67)$$

where the numerical values correspond, once again, to our reference point $q^2 = 15\,\mathrm{GeV}^2$. The shift in (5.67) represents a change of real and imaginary part by 16% and 30%, respectively. This corresponds to the expected size, for the expansion parameter that separates the two is $E/\sqrt{q^2} \approx 0.3$. In accordance therewith, the absolute and relative difference between the two expressions in (5.67) decreases from here with the kaon energy. All of this can also be observed in Fig. 5.7.

Analytical Comparison

In order to complement the picture, the relation between OPE and QCDF is investigated with analytical methods as well. To this end, the energy relation of the kaon is utilized in the form $s = 1 - 2E/m_B$ to rewrite $t_\parallel(q^2, m_q, u)$ as a function of E/m_B, thereby eliminating q^2 completely. An expansion in E/m_B, subsequently performed, then reveals that

$$s \cdot t_\parallel(q^2, m_c, u) \;=\; f(q^2, m_c) + \mathcal{O}(E/m_B) \qquad (5.68)$$

In particular, the square bracket in (5.65) is proportional to $(\bar{u}E/m_B)^2$ in the OPE limit. Also note that, apart from subleading terms, both sides of (5.68) depend solely on the ratio $t/s = m_c^2/q^2$, and this is how the remaining q^2-dependence is to be understood. Furthermore, the finding (5.68) immediately clarifies the parametric situation in (5.67); OPE and QCDF differ indeed just by terms of $\mathcal{O}(E/m_B)$.

Conclusions and Implications

On the basis of the above findings, it can be concluded that, even at values of q^2 as low as $15\,\mathrm{GeV}^2$, the OPE still gives sensible results. As a matter of fact, the numerical difference between OPE and QCDF is virtually negligible, as it concerns only the second order correction, which is fairly small to begin with.

This applies to $B \to M\ell^+\ell^-$ decays in general, for the difference between OPE and QCDF lies in the treatment of the charm-loop and therefore is independent from the outer (hadronic) dynamics. For instance, in the case of a transversely polarized vector meson, we have[5] $t_\perp = t_\parallel + \mathcal{O}(E/m_B)$, implying that an equation of the form (5.68) can be derived for $t_\perp$ as well.

[5] The function $t_\perp$, which is given in [40] as well, plays a similar role in $\Delta_{9\perp+}$ as $t_\parallel$ in $\Delta_{9\parallel+}$.

5.6 Comments on the Literature

A similar OPE framework for the study of $B \to M\ell^+\ell^-$ decays at high-q^2 to the one presented in this work has been established by the authors of [21]. It has already been put to use for the calculation of the low recoil domain of $B \to K^*\ell^+\ell^-$ [49].

The two approaches, however, also differ in several respects. Apart from some minor differences and the additional content provided here, there are two major differences in the conceptual implementation of the OPE formalism. These points are now discussed in turn.

Additional Content and Smaller Differences

To begin with, the present discussion includes an extensive investigation of quark-hadron duality and its connection to the OPE. The issue of duality violation is of particular importance, since the charmonium resonances are located in the relevant high-q^2 part of the spectrum.

Moreover, we go one full step further in the OPE by calculating the coefficient functions of the dimension-5 term and partly the dimension-6 term as well (weak annihilation only). In addition, the $B \to K^{(*)}$ matrix elements of these subleading terms are estimated quantitatively.

Finally, it should be mentioned that, whereas the coefficient functions in [21] are presented in expanded form around $q^2 = m_b^2$, they are given here with their full (kinematic) q^2-dependence.

Treatment of Bottom Quark

The local operators in this work are composed of b quark fields in full QCD. As a consequence, one finds a simpler operator basis, and the leading-power matrix element is given in terms of the known standard $B \to K^{(*)}$ form factors. While this makes the OPE, in particular the evaluation of higher dimensional matrix elements, more transparent, the m_b-dependence is not fully explicit. However, power corrections can still be included consistently and this is what matters in practice. The present approach has already been adopted for an OPE of the inclusive mode to calculate the lifetime difference of B_s mesons, including power [50] and $\mathcal{O}(\alpha_s)$ corrections [51].

The local operators in [21], on the other hand, are build from effective heavy-quark fields. Due to this, the OPE yields a multitude of local operators, the matrix elements of which can not be expressed just by the standard form factors. In [21], the matching onto HQET fields is therefore partly undone back to full QCD fields in order to simplify the obtained expressions.

Treatment of Charm Quark

We here assume the hierarchy $m_b \sim m_c \gg \Lambda_{QCD}$ and integrate out the charm along with the bottom quark at the scale $m_b \approx \sqrt{q^2}$, thereby absorbing all charm quark effects into the coefficient functions.

In contrast to this, the authors of [21] assume the hierarchy $m_b \gg m_c$, resulting in a charm quark field that remains an active degree of freedom below the expansion scale m_b. The coefficients functions are then evaluated at $m_c = 0$, and local operators, containing the charm quark field, such as ($\Gamma_\alpha = \gamma_\alpha(1-\gamma_5)$)

$$\mathcal{K}^{\mu}_{6c} \;=\; \frac{16\pi^2}{q^4}\, Q_c \big(\delta_{ij}\delta_{kl} C_1 + \delta_{il}\delta_{kj} C_2\big)\big(g^{\alpha\mu}q^\beta - g^{\beta\mu}q^\alpha\big)\, \bar{c}_i \Gamma_\alpha b_j\, \bar{s}_k \Gamma_\beta c_l \tag{5.69}$$

appear additionally in the OPE at operator dimension 6 or higher. Assuming further the hierarchy $m_c \gg \Lambda_{QCD}$, the charm quark is then integrated out in a separate step, performed at the scale $\mu \sim m_c$, as well.

The main advantage that arises from an active charm below $\mu \sim m_b$ is that it allows, in case of a strong hierarchy $m_c \ll m_b$, the resummation of large logarithms $\ln m_b/m_c$. In reality, however, this is hardly necessary, for the logarithms are not large at all $\ln m_b/m_c \approx 1.2$ and appear earliest at order $1/m_b^3$ in the power counting. Therefore, it seems preferable to opt for the simpler operator basis that is offered by an OPE performed in a single step at $\mu \sim m_b$.

6 Quark-Hadron Duality

Quark-hadron duality refers to a correspondence between partonic and hadronic world [52]: Perturbative calculations implicitly rely on duality, they are performed in terms of quarks and gluons. The actual world, however, consists of hadrons.

More precisely, in order to speak of duality, the difference between theory and experiment should not significantly exceed the neglected orders in α_s or $\Lambda_{QCD}/\sqrt{q^2}$. Conversely, discrepancies larger than the ones naively expected qualify as violations of quark-hadron duality.

As far as $b \to s\ell^+\ell^-$ transitions are concerned, in particular the matrix element of the non-local term ($j^\mu = \sum_q Q_q\,(\bar{q}\gamma^\mu q)$)

$$\langle \mathcal{K}^\mu(q)\rangle \;\equiv\; -\frac{8\pi^2}{q^2}\, i\int d^4x\, e^{iq\cdot x}\,\langle \bar{M}(k)|\,T j^\mu(x)\,\mathcal{H}_h(0)|\bar{B}(p)\rangle \tag{6.1}$$

is susceptible to such duality violating effects. Of course, this is related to the existence of the charmonium resonances and thus concerns primarily the charm correlator in the upper part of the q^2-spectrum. It is no coincidence either that, in this kinematic domain, theoretical calculations are justified by the OPE.

In order to shed some light on this relation between OPE and the violation of duality, let us consider the coordinate formulation of the OPE

$$j^\mu(x)\,\mathcal{H}_h(0) \;=\; \sum_d C_d(x)\mathcal{O}_d(0) \tag{6.2}$$

Clearly, the approximation in terms of local operators is most fitting in the limit of a small current separation $x \to 0$. In momentum space, this is mirrored by the well known fact that coefficient of higher dimensional operators are power suppressed, in this case as $C_d(q) \sim (q^2)^{(3-d)/2}$. However, due to the presence of the charmonium resonances, a perturbative calculation of the Wilson coefficients is not justified at large *timelike* momenta $q^2 > 0$. In fact, the calculation should be performed far off any intermediate states, that is, in the deep *Euclidean* domain [2], at large *spacelike* momenta $q^2 \to -\infty$. The results obtained in this way can then analytically be continued to the *Minkowski* domain, where the experiments take place.

Of course, for practical reasons alone, both the OPE series as well as the perturbative expansions of the individual coefficients have to be truncated eventually. But this translates only to a similar polynomial uncertainty in the Minkowski domain and therefore does not cause a violation of duality.

Indeed, the origin of duality violation lies in the existence of terms exponentially suppressed in the $q^2 \to -\infty$ limit. The OPE, which is performed in this limit, is oblivious to their existence, as they are beyond (i.e. parametrically smaller than) any order in the $1/q^2$ expansion. However, as long as q^2 remains finite, at some order the missing, exponentially suppressed terms become numerically more relevant than the next term in the $1/q^2$ series. Mathematically speaking, the OPE yields a non-convergent *asymptotic series*, which must, to obtain the best approximation, be truncated when the individual terms start to rise again. In principle, already this sets a limit to the theoretical (OPE-based) accuracy.

The main issue, however, is the transition from the Euclidean to the Minkowski domain. Thereby, the exponential suppression is converted into a characteristic oscillatory behaviour and thus, to a large extent, lost. Although some damping still remains, the enhancement is in many cases large enough to cause a serious violation of quark-hadron duality.

The existence of duality violation implies an uncertainty in theoretical predictions, which must – as any other uncertainty – be quantified, so that effects from new physics can reliably be identified. With this in mind, the following chapter, based on [1], investigates the issue of duality, with particular emphasis on $B \to K^{(*)}\ell^+\ell^-$ decays in the kinematic domain of large $q^2 \geqslant 15\,\mathrm{GeV}^2$.

Meanwhile, quark-hadron duality is already known to fail for semileptonic decays in the regime of the narrow charmonium resonances $7\,\mathrm{GeV}^2 \leqslant q^2 \leqslant 15\,\mathrm{GeV}^2$ by over two orders of magnitude [7]. A theoretical explanation for this is given by the approximate form of the correlator in the vicinity of the J/ψ resonance [7]

$$|\Pi(M_\psi^2)| \;=\; |\mathrm{Im}\,\Pi(M_\psi^2)| \;=\; f_\psi^2/(M_\psi\,\Gamma_\psi) \qquad (6.3)$$

For a narrow resonance, the resonant contribution (6.3) exceeds the partonic result, which remains a quantity of $\mathcal{O}(1)$, locally by a factor of $|\Pi(M_\psi^2)| \approx 560$. This leads to a violation of global duality of similar size if an observable is quadratic in the correlator.[1]

6.1 Shifman's Resonance-Based Model

For the theoretical study of duality, it seems to be almost essential to have a hadronic expression for the correlator. The corresponding partonic expression is then easily obtained – it is just the power series of the hadronic expression obtained in the $q^2 \to -\infty$ limit. Based on this, the mechanisms of duality can be investigated and even the typical size of violating effects can, at least qualitatively, be estimated.

To this end, we will adopt Shifman's resonance-based model of the (charm) correlator [52] ($j_q^\mu = \bar{q}\gamma^\mu q$)

$$\Pi^{\mu\nu}(q^2) \;=\; i\int d^4x\, e^{iq\cdot x}\,\langle 0\,|\,T j_q^\mu(x)\, j_q^\nu(0)\,|\,0\rangle \;\equiv\; (q^\mu q^\nu - q^2 g^{\mu\nu})\Pi(q^2) \qquad (6.4)$$

[1]Indeed, if an observable is only linear in the correlator, global duality in general still holds. This happens, for instance, in the case of the R-ratio [7].

which has already been utilized to study the violation of duality in the R-ratio [52, 53, 54] and τ decays [55].

Intended as an introduction to the conceptual aspects, a simplified version of Shifman's model is presented first. It is then gradually refined in the subsequent sections to be closer to the real world.

6.1.1 Zero-Width Approximation

Shifman's model [52] understands the correlator (6.4) as an infinite series of resonances, describing the individual resonance by means of the *Breit-Wigner formula*

$$\frac{f_n^2}{q^2 - M_n^2 + i\Gamma_n M_n} \tag{6.5}$$

The other basic assumption underlying Shifman's model is a resonance spectrum that follows a so-called linear *Regge trajectory*, meaning that the squared masses are assumed to be equidistant

$$M_n^2 \;=\; M_0^2 + n\lambda^2 \qquad\qquad n \;=\; 0, 1, 2, ... \tag{6.6}$$

On the theoretical side, (6.6) represents the asymptotic high-energy behaviour predicted by confinement [56, 57]. Since duality violation is governed by the resonances at infinitely high n's [58], the present context allows to use (6.6) freely for the entire mass spectrum. Apart from that, the pattern (6.6) can, in many cases, be observed experimentally already at low energies. This applies, for instance, to the case of light mesons [59, 60] as well as charmonia [61].

Finally, for the time being, let us assume resonances of zero width, which, according to the scaling of the resonance widths $\Gamma_n \sim \mathcal{O}(1/N)$ [53, 62], corresponds to the large colour limit $N \to \infty$.

Putting everything together, Shifman's zero-width correlator then reads

$$\Pi^{\text{had}}_{\text{Shif}}(q^2) \;\equiv\; -\frac{N\lambda^2}{12\pi^2}\sum_{n=0}^{\infty}\frac{1}{q^2 - \lambda^2 n - M_0^2} \;=\; \frac{N}{12\pi^2}\sum_{n=0}^{\infty}\frac{1}{z+n} \tag{6.7}$$

where

$$z \;=\; \frac{M_0^2 - q^2 - i\epsilon}{\lambda^2} \tag{6.8}$$

As a matter of fact, the sum in (6.7) is, up to an infinite constant, a common series expression of the *digamma function* $\psi(z)$. In exploiting this, Shifman's correlator can be written as

$$\Pi^{\text{had}}_{\text{Shif}}(q^2) \;=\; -\frac{N}{12\pi^2}\left[\psi(z) + \gamma - \sum_{n=1}^{\infty}\frac{1}{n}\right] \;\widehat{=}\; -\frac{N}{12\pi^2}\,\psi(z) \tag{6.9}$$

Note that constant terms, such as the *Euler-Mascheroni* constant

$$\gamma \;=\; -\psi(1) \;=\; 0.5772\ldots \tag{6.10}$$

and the (divergent) harmonic series in the square bracket of (6.9), are at this point meaningless, for a renormalization scheme has not yet been specified.

Since there is a close relation between Shifman's correlator and the *digamma function*, the most relevant properties of this important mathematical function are recapitulated below. Thereafter, the properties of Shifman's hadronic correlator (6.9) and its partonic counterpart are discussed in turn.

Digamma Function $\psi(z)$

The *digamma function* $\psi(z)$ is usually defined as

$$\psi(z) \;\equiv\; \frac{d}{dz}\ln\Gamma(z) \;=\; \frac{\Gamma'(z)}{\Gamma(z)} \tag{6.11}$$

At this, $\Gamma(z)$ is the *gamma function*, which is for $\mathrm{Re}[z] > 0$ identical with Euler's integral of the second kind

$$\Gamma(z) \;\equiv\; \int_0^\infty dt\, t^{z-1}e^{-t} \tag{6.12}$$

By means of analytic continuation, the definition (6.12) can then be extended unambiguously to the entire complex plane, except for $z \in \mathbb{N}_0^-$, where the simple poles of $\Gamma(z)$ are located.

Furthermore, the two meromorphic functions satisfy the (related) recurrence relations

$$\Gamma(z+1) \;=\; z\Gamma(z) \qquad \Rightarrow \qquad \psi(z+1) \;=\; \psi(z) + \frac{1}{z} \tag{6.13}$$

which are particularly useful in combination with the "starting values" $\Gamma(1) = 1$ and $\psi(1) = -\gamma$. Finally, since both functions are real valued on the real axis, they satisfy the analytic identities

$$\Gamma(z) \;=\; \overline{\Gamma}(\overline{z}) \qquad \text{and} \qquad \psi(z) \;=\; \overline{\psi}(\overline{z}) \tag{6.14}$$

Hadronic Zero-Width Correlator $\Pi^{\mathrm{had}}_{\mathrm{Shif}}(q^2)$

Drawing on the existing knowledge about $\psi(z)$, the following analytic properties of Shifman's hadronic (zero-width) correlator (6.9) are easily inferred:

- The zero-width correlator is a meromorphic function with (isolated) singularities on the positive real axis, located at

$$q^2 \;=\; M_0^2 + n\lambda^2 \qquad\qquad n \;=\; 0, 1, 2, \ldots \tag{6.15}$$

- Furthermore, the correlator (6.9) is a single-valued function and, consequently, there is no branch cut.

- The analytic identities (6.14) transfer directly to Shifman's correlator

$$\Pi^{\text{had}}_{\text{Shif}}(q^2) \;=\; \overline{\Pi^{\text{had}}_{\text{Shif}}}(\overline{q^2}) \tag{6.16}$$

  Actually, this represents an important (known) property of the correlator, which Shifman's model is able to reproduce. In the SM, it derives from the optical theorem and assures that $\Pi^{\text{had}}_{\text{Shif}}(q^2)$ is real valued for $q^2 < M_0^2$ [2].

- From (6.16) we infer that $\Pi^{\text{had}}_{\text{Shif}}$ is, in general, real valued and continuous on the real axis. Near a singular point z_0, however, the correlator behaves as

$$\Pi^{\text{had}}_{\text{Shif}}(z_0 + dz) \;=\; 1/(4\pi^2 dz) + \mathcal{O}(dz^0) \tag{6.17}$$

  Thus, the correlator has a non-zero imaginary part close to the poles, at $z = z_0 \pm i\epsilon$, which, in accordance with (6.16), changes its sign when crossing the real axis. As in the SM, this allows to derive the *dispersion relation*

$$\Pi(q^2) \;=\; \frac{1}{\pi}\int_0^\infty dt\,\frac{\operatorname{Im}\Pi(t)}{t - q^2 - i\epsilon} \tag{6.18}$$

Partonic Zero-Width Correlator $\Pi^{\text{OPE}}_{\text{Shif}}(q^2)$

The OPE expression corresponding to the correlator (6.9) (the hypothetical result of an OPE performed in Shifman's (model) "world") is given as the asymptotic expansion of $\psi(z)$ in the deep Euclidean domain

$$\underset{z\to\infty}{\text{series}}\{\psi(z)\} \;=\; \ln z - \frac{1}{2z} - \sum_{n=1}^{\infty}\frac{B_{2n}}{2n}\,z^{-2n} \;\equiv\; -\frac{12\pi^2}{N}\,\Pi^{\text{OPE}}_{\text{Shif}}(q^2) \tag{6.19}$$

whereat the B_{2n} are known as *Bernoulli numbers*. The series expression in (6.19) reveals the following properties of the partonic correlator:

- In the asymptotic limit $q^2 \to \infty$, Shifman's OPE expression (as well as the hadronic correlator (6.9), for that matter) coincides with the corresponding QCD expression, given in (6.51)

$$\Pi^{\text{OPE}}_{\text{Shif}}(q^2) \;\overset{q^2\to\infty}{\sim}\; -\frac{N}{12\pi^2}\ln\frac{-q^2 - i\epsilon}{\lambda^2} \;\overset{q^2\to\infty}{\sim}\; \Pi^{\text{OPE}}_{\text{SM}}(q^2) \tag{6.20}$$

  Note that this is exactly what motivates the choice of normalization in (6.7).

- Applying *Stirling's approximation* to the Bernoulli numbers

$$B_{2n} \;=\; (-1)^{n+1}\,\frac{2(2n)!}{(2\pi)^{2n}}\,\zeta(2n) \;\overset{n\to\infty}{\sim}\; 4(-1)^{n+1}\sqrt{\pi n}\left(\frac{n}{\pi e}\right)^{2n} \tag{6.21}$$

one finds the following high-n behaviour for the individual summands of the asymptotic series in (6.19)

$$\frac{2}{\sqrt{ez}}\sum_{n\gg 1}^{\infty}(-1)^n\left(\frac{n}{\pi e z}\right)^{2n-1/2} \tag{6.22}$$

which makes the factorial divergence of the series coefficients easy to recognize. In consequence, the series must be truncated eventually. Since, in the present context (alternating series, factorial divergence), the deviation from the true value is always smaller than the first neglected term, the highest precision is achieved just before the smallest summand, which can be determined via

$$\partial_n\left(\frac{n}{\pi e z}\right)^{(2n-1/2)} \overset{!}{=} 0 \qquad \Rightarrow \qquad \ln\frac{n}{\pi z} - \frac{1}{4n} \;=\; 0 \tag{6.23}$$

The turning point is thus reached around $n_{max} \simeq \pi z$, which sets the minimal OPE uncertainty in Shifman's model to the extremely small value of (using $z = 3$)

$$\Delta^{\text{OPE}}_{min} \;=\; \pm\frac{N}{6\pi^2\sqrt{|z|}}\,e^{-2\pi z} \;\approx\; 2\cdot 10^{-10} \tag{6.24}$$

- In the Minkowski domain $q^2 > 0$, the OPE result for the correlator has a constant imaginary part:

$$\text{Im}\big[\Pi^{\text{OPE}}_{\text{Shif}}(q^2)\big] \;=\; -\frac{N}{12\pi^2}\,\text{Im}[\ln z] \;=\; \frac{N}{12\pi} \tag{6.25}$$

Since the imaginary part of the hadronic correlator (6.9) is actually an infinite sum of δ-functions, this may be seen as the largest violation of local duality possible [52]. More importantly, the zero-width model fails to reproduce the damping of duality violation at high energies, observed in experiments. Considering the dispersion relation (6.18), this concerns the real part as well.

6.1.2 Finite Resonance Width

So far we have assumed resonances of zero width, leading us to a model that already reproduces many important properties the correlator is known to have. This being said, the zero-width model also has its shortcomings, which became apparent at the end of the last section.

What makes the zero-width assumption problematic is ultimately the fact that the resonances at infinitely large n's (and exactly these determine duality violation) do actually not have a small width at all. This is a direct consequence of the asymptotically constant width to mass ratio [53, 62]

$$b \;\equiv\; \lim_{n\to\infty} \frac{\Gamma_n}{M_n} \;=\; \mathcal{O}(1/N) \qquad \Longleftrightarrow \qquad \Gamma_n \;\overset{n\to\infty}{\sim}\; M_n\, b \;=\; \sqrt{n}\lambda b \tag{6.26}$$

Thus, as long as the number of colours remains finite (their actual number is only $N = 3$), the resonance widths will become arbitrarily large. Eventually, the initially separated resonances will start to overlap, which should lead to the desired improvement of local quark-hadron duality at high energies [52].

To incorporate a finite resonance width into the model, let us insert the width to mass relation (6.26) into the Breit-Wigner formula

$$\frac{f_n^2}{q^2 - M_n^2 + i\Gamma_n M_n} \;=\; \frac{f_n^2}{q^2 - M_n^2(1 - ib)} \;\xrightarrow{q^2 = M_n^2 + i\epsilon}\; \frac{f_n^2}{ibM_n^2} \tag{6.27}$$

The Breit-Wigner description (6.27), however, is only accurate in the proximity of the respective excitation, that is, close to the corresponding pole, at $q^2 = M_n^2 + i\epsilon$. It fails far off the pole, which is reflected in singularities on the physical sheet, at $q^2 = (1 - ib)M_n^2$. This would carry over to the correlator, resulting in a wrong analytic behaviour.

In order to obtain a correlator without poles on the physical sheet, the resonance description (6.27) is modified to [52]

$$\frac{-\tilde{f}_n^2}{-q^2\left(-q^2/\lambda^2\right)^{-b/\pi} + \tilde{M}_n^2} \;\xrightarrow{q^2 = M_n^2 + i\epsilon}\; \frac{f_n^2}{ibM_n^2} \tag{6.28}$$

where the shifted quantities

$$\tilde{f}_n^2 \;=\; f_n^2\left(M_n^2/\lambda^2\right)^{-b/\pi} \frac{\sin b}{b} \qquad \text{and} \qquad \tilde{M}_n^2 \;=\; M_n^2\left(M_n^2/\lambda^2\right)^{-b/\pi} \cos b \tag{6.29}$$

are determined by the fact that the two expressions (6.27) and (6.28) must coincide in the vicinity of the pole. This property is exactly what justifies to use the above modification, for it shows that (6.28) is an equivalent representation of a "Breit-Wigner resonance".

So that Shifman's resonance summation can still be carried out, some conceptually unimportant (small) shifts of $\mathcal{O}(b)$ have to be neglected. The finite-width correlator then reads

$$\Pi^{\text{had}}_{\text{Shif}}(q^2) \;\equiv\; \frac{N}{12\pi^2}\, \frac{1}{1 - b/\pi} \sum_{n=0}^{\infty} \frac{1}{\left((M_0^2 - q^2)/\lambda^2\right)^{1-b/\pi} + n} \tag{6.30}$$

$$= \; -\frac{N}{12\pi^2}\, \frac{1}{1 - b/\pi} \Big[\psi(z) + \text{const.}\Big] \tag{6.31}$$

with the modified variable

$$z \;=\; (-r - i\epsilon)^{1-b/\pi} \qquad\qquad r \;=\; (q^2 - M_0^2)/\lambda^2 \tag{6.32}$$

Note that the sole purpose of the different normalization in (6.31) is to maintain the asymptotic behaviour (6.20) in view of the modified variable (6.32). Furthermore, it is worth mentioning that, since $z(\overline{q^2}) = \bar{z}(q^2)$, the dispersion relation is still satisfied. This being said, let us turn to the changes in the finite-width model.

Finite-Width Model - Notable Changes

The crucial difference of the finite-width model lies in its definition of the variable z in (6.32), which results in the following changes for the correlator:

- There is a branch cut on the positive real q^2-axis, starting at $q^2 = M_0^2$. The singularities, however, are shifted away from the real axis to unphysical sheets. To demonstrate this, polar coordinates are most convenient

$$z \;=\; |r|^{1-b/\pi} e^{i\cdot\arg(-r)(1-b/\pi)} \tag{6.33}$$

  According to (6.32), we have $\arg(-r) \in [-\pi, \pi[$ on the physical sheet, and thus

$$|\arg(z)| \;=\; |\arg(-r)|(1 - b/\pi) \;<\; \pi \tag{6.34}$$

  which shows that $z \notin \mathbb{R}^-$. Admittedly, the $z = 0$, that is, the first ($n = 0$) singularity remains on the physical sheet. While this is, in principle, immaterial for duality violation at high q^2, the $n = 0$ pole may as well be removed by redefining $M_0^2 \to M_0^2 - \lambda^2$ and shifting the starting point of the summation to $n = 1$. This results in a correlator $\Pi \propto \psi(z' + 1)$, which differs from $\Pi \propto \psi(z)$ by terms of $\mathcal{O}(b)$, which are not consistently kept track of anyway.

- At this point, we only state that the finite-width model reproduces the softening of local duality violation at high energies in the form of an exponential suppression $e^{-2\pi b z}$. In section 6.2.4, we shall return to this issue in more detail.

6.1.3 Model Fit on BES Data of R-ratio

Based on Shifman's model, a suitable fit ansatz for the BES data of the R-ratio [63, 64, 65] is developed. In this way, realistic parameter values for a model description of the charm correlator can be determined. Furthermore, this allows to convince oneself of the quality of Shifman's model.

BES Data

The provided data represents a measurement of the R-ratio

$$R \;\equiv\; \frac{\sigma(e^+e^- \;\to\; \text{hadrons})}{\sigma(e^+e^- \;\to\; \mu^+\mu^-)} \;=\; R_{\text{light}} + 12\pi Q_c^2 \, \mathrm{Im}\,\Pi_c(q^2) \tag{6.35}$$

Charmonium Resonances [66]				
n^3S_1	$J/\psi(1S)$	$\psi(2S)$	$\psi(4040)$	$\psi(4415)$
m[MeV]	3096.916 ± 0.011	$3686.109^{+0.012}_{-0.014}$	4039 ± 1	4421 ± 4
Γ [MeV]	0.0929 ± 0.0028	0.299 ± 0.008	80 ± 10	62 ± 20
n^3D_1	$\psi(3770)$	$\psi(4160)$	–	–
m[MeV]	3773.15 ± 0.33	4191 ± 5	–	–
Γ [MeV]	27.2 ± 1.0	70 ± 10	–	–

Table 6.1: Charmonium states with quantum numbers $I^G(J^{PC}) = 0^-(1^{--})$.

at a center of mass energy between 2 and 5 GeV. Since this is the kinematic domain of the $c\bar{c}$ resonances, the R-ratio is – up to a constant R_{light}, which stems from the continuum of light quarks (u,d,s) – essentially the imaginary part of the charm correlator. As is evident from the dispersion relation (6.18), the information contained in the R-ratio is to completely determine the real part of the correlator up to a scheme dependent subtraction constant as well.

Fit Ansatz

Taking a closer look at the BES data, displayed in Fig. 6.1, as well as the relevant $J^{PC} = 1^{--}$ charmonia, summarized in Tab. 6.1, the following observations can be made:

- The masses of the first n^3S_1 states already exhibit the general pattern assumed in the derivation of Shifman's model

$$M_n^2 = 4m_c^2 + n\lambda^2 \qquad n = 1, 2, ... \tag{6.36}$$

- This being said, the first two n^3S_1 resonances, $\psi(3097)$ and $\psi(3686)$, are extremely narrow and can not decay into open charm. Thus, in general, they must be described separately using explicit Breit-Wigner terms.

  In the present context, however, this is not advisable, for these two resonances are actually not visible in the BES data. Therefore, only the starting point of Shifman's resonance summation will be shifted from $n = 1$ to $n = 3$.

- There is a second trajectory, consisting of the n^3D_1 states. To keep the fit ansatz simple, we will exploit that the n^3D_1 are rather close to the $(n+1)^3S_1$ excitations and subsume each of these pairs into a single peak.

- The $\psi(3770)$ resonance is still too narrow to be captured by Shifman's model.[2]

[2] As can be seen in Fig. 6.1, the $\psi(3770)$ peak is completely "ignored" when fitting Shifman's model onto the BES data. Using $n = 2$ does not change this.

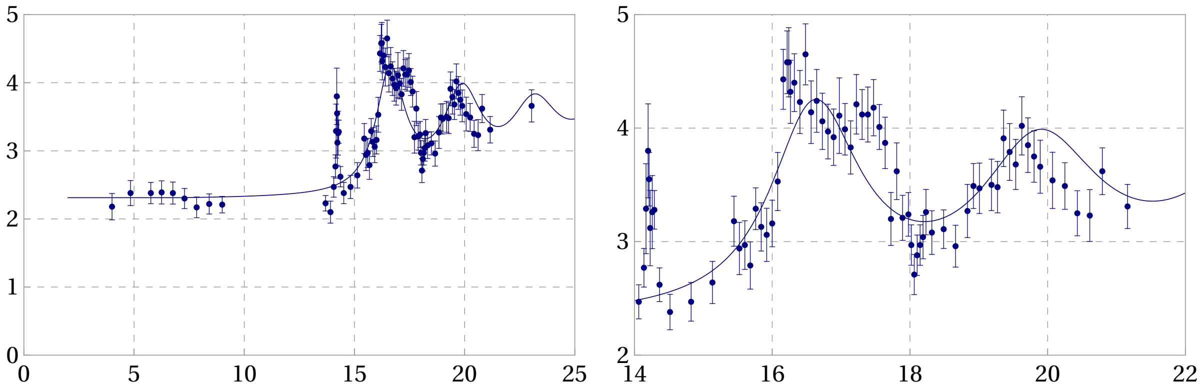

Figure 6.1: BES data and model description of the R-ratio, plotted against q^2[GeV^2]. The right hand side shows an enlarged view of the resonance region.

Therefore, the starting point of the resonance summation will be kept at $n = 3$.

- However, unlike the narrow n^3S_1 resonances, the $\psi(3770)$ state can decay into open charm and the BES date clearly exhibits a peak at the corresponding position. Since a single resonance should, in principle, not affect duality (violation), our first ansatz will ignore the existence of $\psi(3770)$ completely. In order to demonstrate the stability of the continuum parameters, we then consider a second, more refined ansatz, which has an explicit $\psi(3770)$ term.

Everything combined, we thus employ the following fit ansatz for the BES data

$$R = R_{\text{light}} - \frac{4}{3(\pi - b)}\,\mathrm{Im}\Big[\psi(3+z)\Big] \qquad z = \left(\frac{-q^2 + 4m_c^2 - i\epsilon}{\lambda^2}\right)^{1-b/\pi} \tag{6.37}$$

where R_{light}, b, m_c and λ^2 are treated as fit parameters.

Simple Model - Fit Results

Performing a numerical fit on the ansatz (6.37), one finds

$$R_{\text{light}} = 2.312 \qquad b = 0.0818 \tag{6.38}$$

$$m_c = 1.333\,\text{GeV} \qquad \lambda^2 = 3.080\,\text{GeV}^2 \tag{6.39}$$

which corresponds to a $\chi^2/\text{d.o.f.} \simeq 2.47$.The quality of this fit, (6.37) – (6.39), can be surveyed on the basis of Fig. 6.1 as well.

Besides, the fit value for R_{light} is in agreement with the experimental measurement of the R-ratio below charm threshold $R_{\text{uds}} = 2.141 \pm 0.09$ [64] and the theoretical prediction $R_{\text{uds}} = 2.15 \pm 0.03$ [65, 67, 68]. Furthermore, the values found for the parameters of the mass trajectory are consistent with the findings $m_c = 1.3\text{GeV}$ and $\lambda^2 = 3.2\text{GeV}^2$, presented in [61].

Refined Model - Explicit $\psi(3770)$ Resonance

For the explicit description of the $\psi(3770)$ excitations, we resort to Shifman's modification of the Breit-Wigner formula (6.28) and shift the variable in order to reproduce the analytic behaviour introduced by the $D\bar{D}$-threshold

$$\Delta R_{\psi(3770)} = -f_\psi \, \mathrm{Im}\Big[\big(-q^2 + 4m_D^2 - i\epsilon\big)^{1-b_\psi/\pi} + \big(m_\psi^2 - 4m_D^2\big)^{1-b_\psi/\pi} \cos b_\psi\Big]^{-1} \quad (6.40)$$

Adding the above term to the original ansatz (6.37) improves the quality of the fit significantly $\chi^2/\mathrm{d.o.f.} \to 1.78$.Thereby, the fit parameters describing the $\psi(3770)$ resonance are found to be

$$m_\psi = 3.771\,\mathrm{GeV}\ (3.773\ [66]) \qquad m_D = 1.872\,\mathrm{GeV}\ (1.865\ [66]) \quad (6.41)$$

$$f_\psi = 0.0819 \qquad b_\psi = 0.3207 \quad (6.42)$$

Note that the fit values for the mass parameters in (6.41) almost exactly coincide with the corresponding experimental measurements, given in the parentheses. Calculating the resonance width from the fit values, however, gives only the right order of magnitude:

$$\Gamma_\psi = \sin b_\psi (m_\psi^2 - 4m_D^2)/m_\psi \approx 17\,\mathrm{MeV} \quad (6.43)$$

Meanwhile, the impact on the original parameters, which are the ones relevant to the violation of duality, is rather small

$$R_{\text{light}} = 2.259 \qquad b = 0.0793 \quad (6.44)$$

$$m_c = 1.349\,\mathrm{GeV} \qquad \lambda^2 = 3.030\,\mathrm{GeV}^2 \quad (6.45)$$

This is to be expected, for the continuum parameters reflect the asymptotic high-energy behaviour and thus, in theory, are independent from the treatment of a particular resonance (or any finite number, for that matter). Furthermore, the $\psi(3770)$ resonance is below our – admittedly somewhat arbitrary – lower limit of the high-q^2 region, $q^2 = 15\,\mathrm{GeV}^2$. In consequence, the model description based on the original, simple ansatz (6.37) will be employed in the $B \to K\ell^+\ell^-$ analysis.

6.2 Mechanism of Duality Violation in a Toy Model

The toy model suggested in [7] provides a simpler framework for an analysis of duality violation in the charm-loop than the standard model decay $B \to K^{(*)}\ell^+\ell^-$. At the same time, the characteristic features of quark-hadron duality are maintained and therefore can be discussed in a more transparent way.

6.2.1 Description of the Model

In order to remove the disturbance caused by external hadronic dynamics, two leptons $\ell_{1,2}$, which will take the role of bottom and strange quark, respectively, are introduced. In more specific terms, we assign the lepton masses $m_{1,2} = m_{b,s}$ and impose the effective weak Hamiltonian

$$\mathcal{H}_{\mathit{eff}} \;=\; \frac{G_F}{\sqrt{2}}\Big[(\bar{\ell}_2\ell_1)_{V-A}(\bar{c}c)_{V-A} \;-\; (\bar{\ell}_2\ell_1)_{V-A}(\bar{t}t)_{V-A}\Big] \tag{6.46}$$

inducing the model process $\ell_1 \to \ell_2\, e^+e^-$ via penguin-type diagrams. Apart from the above adjustment, all particles, in particular the *leptons* $\ell_{1,2}$, are subject to the Standard model electromagnetic and strong interactions.

Further note the destructive interference between charm and top sector in (6.46), which intends to mimic the *GIM mechanism* of the SM. This is particularly convenient, for it avoids some issues related to scheme dependency and renormalization in the following discussion.

Then, by construction, the entire hadronic dynamics of the model decay $\ell_1 \to \ell_2\, e^+e^-$ are contained in the familiar two-point functions ($j_q^\mu = \bar{q}\gamma^\mu q$)

$$\Pi_q^{\mu\nu}(q^2) \;=\; i\int d^4x\, e^{iq\cdot x}\,\langle\, 0\,|\, T j_q^\mu(x)\, j_q^\nu(0)\,|\, 0\,\rangle \;\equiv\; (q^\mu q^\nu \,-\, q^2 g^{\mu\nu})\,\Pi_q(q^2) \tag{6.47}$$

Defining the scheme independent quantity $\Pi \equiv \Pi_c - \Pi_t$, the decay amplitude can be written as

$$\mathcal{A}(\ell_1 \to \ell_2\, e^+e^-) \;=\; -\frac{G_F}{\sqrt{2}}\, Q_c\, e^2\, \Pi(q^2)\, \bar{\ell}_2\gamma^\mu(1 - \gamma_5)\ell_1\, \bar{e}\gamma_\mu e \tag{6.48}$$

This general form holds to leading order in the weak but to any order in the strong and electromagnetic interaction. The corresponding differential decay rate is then easily derived as ($s = q^2/m_1^2$, $m_2 = m_s = 0$)

$$\frac{d\Gamma}{ds}(\ell_1 \to \ell_2\, e^+e^-) \;=\; \frac{G_F^2\,\alpha_e^2\, m_1^5}{27\pi}\, g(s)\big|\Pi(q^2)\big|^2 \tag{6.49}$$

whereat

$$g(s) \;=\; (1 - s)^2(1 + 2s) \tag{6.50}$$

is a purely kinematic, phase-space related quantity.

6.2.2 Charm Correlator in Standard Model

Using the OPE framework developed in section 5, the correlator (6.47) can be calculated in perturbation theory, which yields (one-loop level)

$$\Pi_{\mathrm{SM},q}^{\mathrm{OPE}}(q^2) \;=\; \frac{3N}{16\pi^2}\, h(q^2, m_q) \tag{6.51}$$

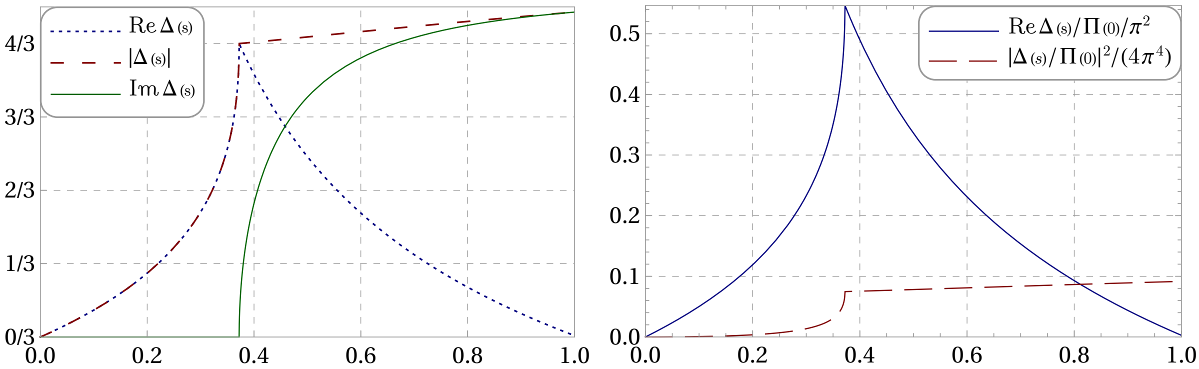

Figure 6.2: Hierarchic structure of the Standard model correlator $\Pi_{\rm SM}^{\rm OPE}(s)$. Left: Real and imaginary part of $\Delta_{\rm SM}^{\rm OPE}$, which are added to the short-distance quantity $\ln(m_t/m_c) = 4.88$. Right: Relative impact of the subleading terms in (6.55) on the squared correlator.

where $h(q^2, m_q)$ is the function defined in (5.16). Using the decomposition[3]

$$\Pi_{\rm SM}^{\rm OPE}(q^2) \;=\; \Pi_{\rm SM}^{\rm OPE}(0) + \Delta_{\rm SM}^{\rm OPE}(q^2)/(2\pi^2) \tag{6.52}$$

we explicitly have

$$\Pi_{\rm SM}^{\rm OPE}(0) \;\equiv\; \Pi_{{\rm SM},c}^{\rm OPE}(0) - \Pi_{{\rm SM},t}^{\rm OPE} \;=\; \frac{N}{6\pi^2}\ln\frac{m_t}{m_c} \;=\; 0.242 \tag{6.53}$$

and $(x = 4m_c^2/q^2)$

$$\Delta_{\rm SM}^{\rm OPE}(q^2) \;=\; \frac{5}{6} + \frac{x}{2} - \frac{1}{4}(2+x)\sqrt{|1-x|}\cdot\begin{cases} 2\arctan\frac{1}{\sqrt{x-1}} & x \;>\; 1 \\ \ln\frac{1+\sqrt{1-x}}{1-\sqrt{1-x}} - i\pi & x \;<\; 1 \end{cases} \tag{6.54}$$

Hierarchic Structure of $\Pi_{\rm SM}^{\rm OPE}(q^2)$

Using the above decomposition, the squared correlator breaks down into three parts of distinct hierarchy

$$4\pi^4\left|\Pi_{\rm SM}^{\rm OPE}\right|^2 \;=\; \ln^2\frac{m_t}{m_c} + 2\ln\frac{m_t}{m_c}\,{\rm Re}\big[\Delta_{\rm SM}^{\rm OPE}(q^2)\big] + \left|\Delta_{\rm SM}^{\rm OPE}(q^2)\right|^2 \tag{6.55}$$

The term of first order in the small quark-level quantity $\Delta_{\rm SM}^{\rm OPE}(q^2)$ reaches its peak at $q^2 = 4m_c^2$, corresponding to a relative impact of 55% (Fig. 6.2). Meanwhile, the impact of the second order term grows monotonically, but stays below 10%.

In short, just as the SM decay $B \to K\ell^+\ell^-$, the model decay $\ell_1 \to \ell_2 e^+e^-$ is dominated numerically and parametrically by its short-distance component.

[3]This is in contrast to the decomposition (6.59): Since the corresponding hadronic expression $\Pi(0)$ is unknown, we have set $\Delta^{\rm OPE}(0) = 0$ (instead of $\Delta(0) = 0$).

6.2.3 Shifman Model for Charm Correlator

In order to proceed with the toy model analysis of duality, Shifman's model (6.31) is now employed for the charm correlator. For the sake of transparency, we will drop the charm mass $M_0^2 = 4m_c^2 = 0$ and set the starting point of the resonance summation to $n = 1$, which corresponds to a shift $\psi(z) \to \psi(z+1)$. Meanwhile, the top quark contribution does not violate duality and is most accurately described by the SM/OPE result (6.51).

That is, everything combined we take

$$\Pi_c(q^2) \;=\; -\frac{N}{12\pi^2}\,\frac{1}{1-b/\pi}\,\psi(z+1) + C_c(\mu) \tag{6.56}$$

$$\Pi_t \;=\; \frac{3N}{16\pi^2}\,h(0,m_t) + C_t(\mu) \tag{6.57}$$

where the renormalization constants $C_{c,t}(\mu)$ are yet to be determined.

Decomposition of $\Pi(q^2)$

For the subsequent analysis, it will be convenient to define the quantities

$$\Delta(q^2) \;\equiv\; 2\pi^2\left[\Pi(q^2) - \Pi(0)\right] \tag{6.58}$$

$$\Delta^{\mathrm{OPE}}(q^2) \;\equiv\; 2\pi^2\left[\Pi^{\mathrm{OPE}}(q^2) - \Pi(0)\right] \tag{6.59}$$

Roughly speaking, they represent the long-distance components of the hadronic correlator and OPE approximation, respectively. The difference of the two contains all duality violation:

$$\Delta^{\mathrm{DV}}(q^2) \;\equiv\; \Delta(q^2) - \Delta^{\mathrm{OPE}}(q^2) \;=\; 2\pi^2\,\Pi^{\mathrm{DV}}(q^2) \tag{6.60}$$

While each of the above quantities is, a priori, composed of a charm and a top contribution, the hierarchy $0 \leqslant q^2 \leqslant m_1^2 \ll m_t^2$ implies that the entire top sector consists just of a (real) constant

$$\Pi_t(q^2) \;=\; \Pi_t^{\mathrm{OPE}}(q^2) \;=\; \Pi_t(0) \;\equiv\; \Pi_t \tag{6.61}$$

Consequently, all "Δ" quantities, in particular $\Delta^{\mathrm{DV}}(q^2)$, are determined by the charm correlator alone.

Explicit Hadronic Expressions

Since $\Delta(0) = 0$, the long-distance component is independent from the renormalization scheme and can immediately be specified as

$$\Delta(q^2) \;=\; -\frac{N}{6}\,\frac{1}{1-b/\pi}\left[\psi(z+1) + \gamma\right] \tag{6.62}$$

where

$$z \;=\; (-us - i\epsilon)^{1-b/\pi} \qquad\qquad u \;=\; \frac{m_1^2}{\lambda^2} \qquad\qquad s \;=\; \frac{q^2}{m_1^2} \tag{6.63}$$

The short-distance component

$$\Pi(0) \;=\; \Pi_c(0) \,-\, \Pi_t \tag{6.64}$$

on the other hand, is not so easily obtained. First, we must impose the same renormalization scheme on the two terms on the r.h.s of (6.64). To this end, both terms are expressed by means of the dispersion relation (6.18) regularized by a cutoff (using $b = 0$)

$$\frac{6\pi^2}{N}\,\Pi_t \;=\; \int_{2m_t}^{\mu} \frac{dq}{q^4}\,(q^2 + 2m_t^2)\sqrt{q^2 - 4m_t^2} \;=\; \ln\frac{\mu}{m_t} \,-\, \frac{5}{6} \,+\, \mathcal{O}(m_t/\mu) \tag{6.65}$$

$$\frac{6\pi^2}{N}\,\Pi_c(0) \;=\; \frac{1}{2}\int_0^{\mu^2} dt \sum_{n=1}^{\infty} \frac{\delta(n-t)}{t} \;=\; \frac{1}{2}\sum_{n=1}^{\lfloor \mu^2/\lambda^2 \rfloor} \frac{1}{n} \;\overset{\mu/\lambda\to\infty}{=}\; \ln\frac{\mu}{\lambda} \,+\, \frac{\gamma}{2} \tag{6.66}$$

Since the short-distance component, which is given as the difference between the above two expressions (using $\lambda^2 = 2.3\,\mathrm{GeV}^2$)

$$\Pi(0) \;=\; \frac{N}{6\pi^2}\left[\ln\frac{m_t}{\lambda} \,+\, \frac{\gamma}{2} \,+\, \frac{5}{6}\right] \;=\; 0.295 \tag{6.67}$$

is finite, the limit $\mu \to \infty$ may then formally be taken to send the neglected contributions in (6.67) to zero.

Numerically, the zero-width approximation (6.67) is only 0.277% smaller than the result of a numerical integration using $b = 1/6$. Furthermore, it is of similar size as the partonic SM/OPE finding $\Pi_{\mathrm{SM}}^{\mathrm{OPE}}(0) = 0.242$, presented in the last section.

Decomposition into OPE and Duality Violating Component

The decomposition of Shifman's correlator into an OPE and a duality violating component is now performed explicitly. To this end, one best starts in the deep Euclidean domain, where the partonic expression is given as the asymptotic series of the hadronic correlator. One then continues with an analytic continuation of the series – term by term – to the Minkowski domain:

$$\frac{-6}{N}\,\Delta^{\mathrm{OPE}}_{\mathrm{Shif}}(q^2) - \gamma \;=\; \underset{\substack{|z|\to\infty \\ \arg(z)\neq\pm i\pi}}{\mathrm{series}}\Big\{\psi(z+1)\Big\} \;=\; \ln z - \frac{1}{2z} - \sum_{n=1}^{\infty}\frac{B_{2n}}{2n}\,z^{-2n} + \frac{1}{z} \tag{6.68}$$

$$\overset{\mathrm{Im}[z]<0}{=} \ln(-z) - i\pi + \frac{1}{2z} - \sum_{n=1}^{\infty}\frac{B_{2n}}{2n}\,(-z)^{-2n} \tag{6.69}$$

$$= \underset{\substack{|z|\to\infty \\ \arg(z)\neq 0}}{\mathrm{series}}\Big\{\psi(-z) - i\pi\Big\} \tag{6.70}$$

Here "series" denotes the asymptotic series of the expression in the respective curly bracket in the specified limit. According to (6.68) – (6.70), the two functions $\psi(z+1)$ and $\psi(-z) - i\pi$ have the same asymptotic series if $\mathrm{Im}[z] < 0$, which happens for physical values of q^2. Alternatively, this can be derived from Euler's reflection formula

$$\psi(z+1) \;=\; \psi(-z) + \pi\cot(-\pi z) \tag{6.71}$$

in conjunction with the fact that an asymptotic series – which is exactly what the OPE represents – is oblivious to exponentially suppressed terms. Therefore, the second term on the r.h.s. of (6.71) is seen as

$$\pi\cot(-\pi z) \;=\; (i\pi)\,\frac{1+e^{2i\pi z}}{1-e^{2i\pi z}} \;\overset{\mathrm{Im}[z]\to-\infty}{=}\; -i\pi \tag{6.72}$$

At finite values of $z > 1$, the truncated OPE series gives an excellent numerical approximation[4] for $\psi(-z) - i\pi$ (not so for $\psi(z+1)$) and thus is henceforth identified with it.[5] Consequently, we will decompose Shifman's correlator in the Minkowski domain according to the two square brackets on the r.h.s of

$$\Big[\psi(z+1) + \gamma\Big]_{\mathrm{had}} \;=\; \Big[\psi(-z) + \gamma - i\pi\Big]_{\mathrm{OPE}} + \Big[\pi\cot(-\pi z) + i\pi\Big]_{\mathrm{DV}} \tag{6.73}$$

6.2.4 Parametric Dependencies in Duality Violation

In order to clarify the parametric dependencies of the duality violating effects in the integrated $\ell_1 \to \ell_2\, e^+e^-$ decay rate, the duality violating component

$$\Delta^{\mathrm{DV}}_{\mathrm{Shif}}(q^2) \;=\; \frac{N}{6}\,\frac{\pi}{1-b/\pi}\Big[\cot(\pi z) - i\Big] \;=\; \frac{Ni}{3}\,\frac{\pi}{1-b/\pi}\,\frac{e^{-2i\pi z}}{1-e^{-2i\pi z}} \tag{6.74}$$

is simplified using the approximation

$$z \;=\; -e^{ib}(us)^{1-b/\pi} \;=\; -(1+ib)us + \mathcal{O}(b^2, b\ln(us)/\pi) \tag{6.75}$$

[4] At $z = -2$, for instance, just the first two terms of the series already give $\ln 2 - \frac{1}{4} \approx 1.05\,\psi(2)$.

[5] This is mainly a matter of convenience. Strictly speaking, the OPE result is the series expression.

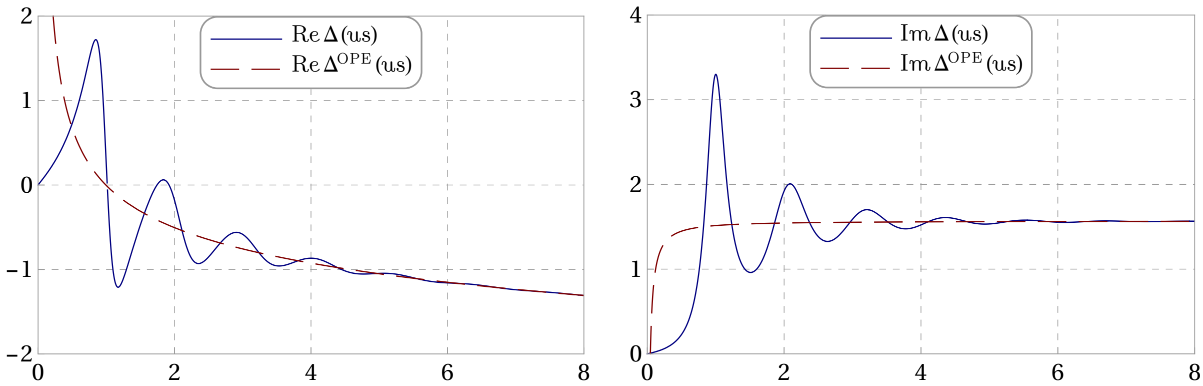

Figure 6.3: Shifman model for charm correlator, using $b = 1/6$: Real (left) and imaginary part of $\Delta(us)$ (right) as functions of $us = q^2/\lambda^2$. The hadronic correlator (6.62) (oscillating) is compared with the corresponding OPE expression, obtained from the decomposition (6.73).

In this way, one finds

$$\Delta^{\mathrm{DV}}_{\mathrm{Shif}}(q^2) \;=\; \frac{Ni}{3}\,\frac{\pi}{1-b/\pi}\,e^{2\pi us(i-b)} + \mathcal{O}(e^{-4\pi bus}) \tag{6.76}$$

First of all, (6.76) showcases that both characteristic features of duality violation, oscillation and exponential suppression at high-q^2, are reproduced by Shifman's model of the charm correlator. The exponential suppression becomes effective around $2\pi bus \approx us \simeq 1$, corresponding to $q^2 \simeq \lambda^2$. Though there is a slight numerical enhancement from the prefactor, local duality can in general be expected to set in already after a few resonances. All of this can also be observed in Fig. 6.3.

For the discussion of global duality in the toy model, we will consider the $\ell_1 \to \ell_2\, e^+e^-$ decay rate integrated over a variable upper part of the spectrum $s \in [s_0, 1]$. Since the duality violating component enters schematically as

$$\Gamma \;\propto\; \left|2\pi^2\Pi(0) + \Delta^{\mathrm{OPE}}_{\mathrm{Shif}}\right|^2 + 2\mathrm{Re}\Big[\big(2\pi^2\Pi(0) + \Delta^{\mathrm{OPE}}_{\mathrm{Shif}}\big)^*\Delta^{\mathrm{DV}}_{\mathrm{Shif}}\Big] + \left|\Delta^{\mathrm{DV}}_{\mathrm{Shif}}\right|^2 \tag{6.77}$$

there are three different duality violating terms, investigated in turn now.

Linear Term $\propto \Pi(0)\mathrm{Re}\big[\Delta^{\mathrm{DV}}_{\mathrm{Shif}}(q^2)\big]$

The first duality violating term in (6.77) is linear in $\Delta^{\mathrm{DV}}_{\mathrm{Shif}}(q^2)$ and gives a contribution to the integrated decay rate proportional to

$$\frac{\Delta_{\mathrm{DV},1}}{4\pi^2\,\Pi(0)} \;=\; \int_{s_0}^{1} ds\, g(s)\mathrm{Re}\big[\Delta^{\mathrm{DV}}_{\mathrm{Shif}}(s)\big] \;\approx\; -\frac{N\pi}{3}\int_{s_0}^{1} ds\, g(s)\sin(2\pi us)\,e^{-2\pi bus} \tag{6.78}$$

$$\;=\; -\frac{N}{6u}\,g(s_0)\cos(2\pi us_0)\,e^{-2\pi bus_0} + \mathcal{O}\big(b/u, 1/u^2\big) \tag{6.79}$$

where, in the last step, we have used integration by parts and the vanishing of the phase space at the endpoint $g(1) = 0$. By inspecting Fig. 6.4 one can convince oneself that

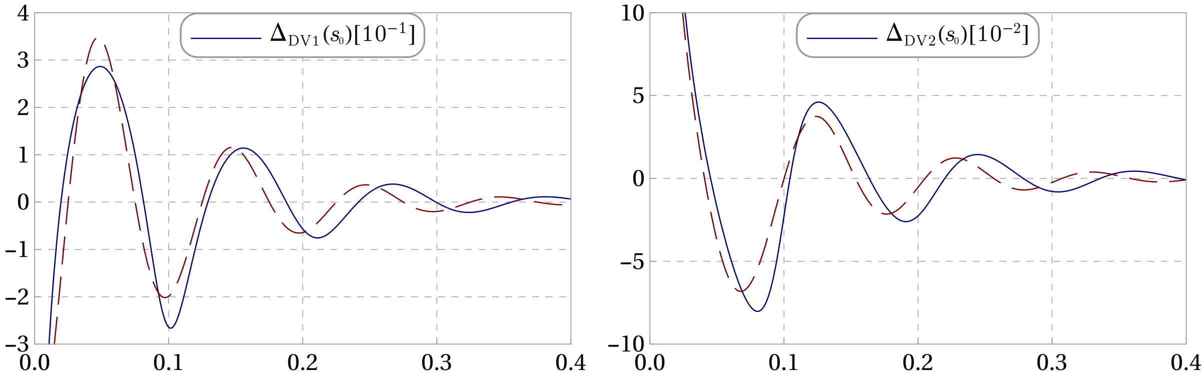

Figure 6.4: Shifman model for charm correlator, using $b = 1/6$ and $u = 10$: Duality violating terms $\Delta_{\mathrm{DV},1}$ (left, solid) and $\Delta_{\mathrm{DV},2}$ (right, solid) and the corresponding approximations, (6.79) and (6.81) (both dashed), all as functions of the lower limit of integration s_0.

the approximate expression (6.79) gives qualitatively the right picture. The following aspects of (6.79) are to be emphasized:

- The exponential suppression carries over from the local expression (6.74). Its effectiveness is now determined by the size of the exponent $2\pi bus_0$, and thus the lower limit of integration should be at least $q_0^2 \gtrsim \lambda^2/(2\pi b) \approx \lambda^2$. In practise, this usually does not represent a severe restriction as the OPE requires a not to small q^2 anyway.

- In addition, there is a power suppression in $1/u = \lambda^2/m_1^2$. It is independent from the lower limit of integration s_0, for it stems from the cancellation caused by the oscillatory behaviour of the integrand: In the integral (6.78), effectively only some fraction of the first period contributes.[6] Hence, in a first approximation, the integral is proportional to “value of the integrand at s_0” × “period length $T = 1/u$” × “oscillating function of s_0”.

- The impact of $\Delta_{\mathrm{DV},1}$ on the decay rate is suppressed numerically and parametrically by one power of $1/(2\pi^2\Pi(0))$.

Linear Term $\propto \mathrm{Re}\big[\Delta^{\mathrm{DV}}_{\mathrm{Shif}}(q^2)\Delta^{\mathrm{OPE}\,*}_{\mathrm{Shif}}(q^2)\big]$

The second duality violating term (see r.h.s. of Fig. 6.4)

$$\frac{\Delta_{\mathrm{DV},2}}{2} = \int_{s_0}^{1} ds\, g(s)\mathrm{Re}\big[\Delta^{\mathrm{DV}}_{\mathrm{Shif}}\,\Delta^{\mathrm{OPE}*}_{\mathrm{Shif}}\big] \approx \frac{-N\pi}{3}\int_{s_0}^{1} ds\, g(s)\mathrm{Im}\big[e^{2\pi us(i-b)}\Delta^{\mathrm{OPE}\,*}_{\mathrm{Shif}}(s)\big] \quad (6.80)$$

$$= \frac{-N}{6u}\, g(s_0)\mathrm{Re}\big[e^{2\pi u(i-b)s_0}\Delta^{\mathrm{OPE}\,*}_{\mathrm{Shif}}(s_0)\big] + \mathcal{O}\big(b/u, 1/u^2, 1/bu^3\big) \quad (6.81)$$

[6]This is related to the fact that the value of an alternating series with decreasing summands lies between the first and second partial sum (in fact, between any two successive partial sums).

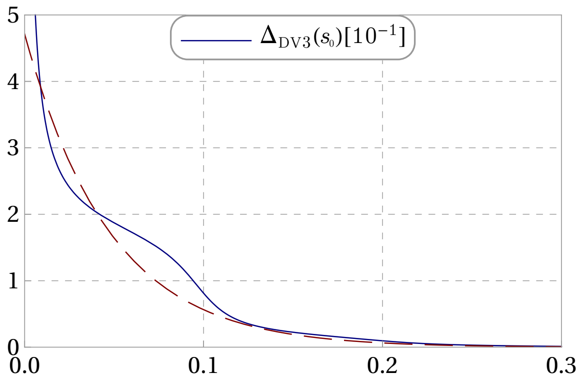

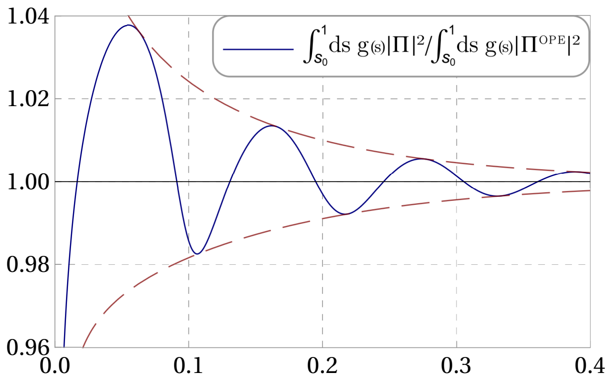

Figure 6.5: Shifman model for charm correlator, using $b = 1/6$ and $u = 10$. Left: $\Delta_{\mathrm{DV},3}$ (solid) and corresponding approximation (6.83) (dashed) as functions of s_0. Right: Relative uncertainty of the OPE-based prediction for the partially integrated $b \to s\ell^+\ell^-$ decay rate again as a function of s_0.

is linear in the duality violating component as well. With respect to b and u, it has the same parametric behaviour as $\Delta_{\mathrm{DV},1}$: An exponential suppression, governed by $2\pi b u s_0$, and a power suppression in $1/u$. In contrast to $\Delta_{\mathrm{DV},1}$, however, the contribution of $\Delta_{\mathrm{DV},2}$ to the decay rate is suppressed as $1/(2\pi^2\Pi(0))^2$.

Quadratic Term $\propto |\Delta^{\mathrm{DV}}_{\mathrm{Shif}}(q^2)|^2$

The term quadratic in the duality violating component can be simplified as

$$\Delta_{\mathrm{DV},3} \;=\; \int_{s_0}^{1} ds\, g(s) |\Delta^{\mathrm{DV}}_{\mathrm{Shif}}(q^2)|^2 \;\approx\; \left(\frac{N\pi}{3}\right)^2 \int_{s_0}^{1} ds\, g(s)\, e^{-4\pi b u s} \tag{6.82}$$

$$= \frac{\pi N^2}{36 b u}\, g(s_0)\, e^{-4\pi b u s_0} \;+\; \mathcal{O}(1/b^2u^2) \tag{6.83}$$

which has the following implications:

- There is a strong exponential suppression, governed by the exponent $4\pi b u s_0$.
- An oscillatory cancellation in the integrand, and consequently a pure $1/u$ suppression, is absent. Closely related to this, the quadratic term always causes a positive deviations from the OPE-based expectation.
- The expression (6.83) is obtained via repeated integration by parts, which yields a formal expansion in powers of $1/(bu)$, ending at $1/(bu)^4$. Admittedly, since the $1/u$ power suppression and the $1/b$ enhancement usually compensate each other, the quantity $1/(bu) = \mathcal{O}(1)$ is, in itself, a poor expansion parameter. The actual expansion parameter, however, is $1/(4\pi bu)$, which makes (6.83) in most cases a reasonable numerical approximation (see l.h.s. of Fig. 6.5).

- The quadratic term is qualitatively different from the linear terms. It features a particular susceptibility to small values of b, which may cause large violations of duality. This finding is in general agreement with [7], where the impact of a single narrow resonance on the squared correlator $|\Pi(q^2)|^2$ is investigated.

- Finally, the contribution of the quadratic term to the decay rate is of second order in the $1/(2\pi^2\Pi(0))$ counting.

6.2.5 Numerical Example

The toy model analysis concludes with a short numerical example of duality violation in the integrated $\ell_1 \to \ell_2 e^+e^-$ decay rate. For this, we use the parameter values

$$b = 1/6 \qquad \text{and} \qquad u = 10 \tag{6.84}$$

where the latter could, for instance, be the result of the semi-realistic setting

$$\lambda^2 = 2.3\,\mathrm{GeV}^2 \qquad m_1 = 4.8\,\mathrm{GeV} \tag{6.85}$$

When estimating the potential size of duality violation, it is important to keep in mind that all three duality violating terms are, to some extent, oscillating. In first approximation, the dominant term $\Delta_{\mathrm{DV},1}$ can be maximized by starting the numerical integration at one of the zero points of $\mathrm{Re}\big[\Delta^{\mathrm{DV}}_{\mathrm{Shif}}(q^2)\big]$, located at $(n \in \mathbb{N}_+)$

$$us = \left[\frac{n}{2\cos b}\right]^{\frac{\pi}{\pi-b}} \approx 0.488, 1.015, 1.557, 2.110... \tag{6.86}$$

Besides, for even n, (6.86) describes the resonance spectrum in units of λ^2. It deviates somewhat from an ideal *Regge trajectory* $q^2/\lambda^2 = 1, 2, ..,$ since the mass shift (6.29) is not counteracted in our model. Taking a conservative approach, the lower limit of integration is chosen to be the first resonance $s_0 = 0.1015$, which gives

$$4\pi^4 \int_{s_0}^{1} ds\, g(s)\, |\Pi^{\mathrm{OPE}}(s)|^2 = 11.21\,{}^{+0.27}_{\mathbf{-0.27}}\,{}^{\mathbf{+0.02}}_{-0.02}\,{}^{\mathbf{+0.08}}_{-0.00} \tag{6.87}$$

where the bold errors correspond to the $\Delta_{\mathrm{DV,i}}$, and the plain errors assume a symmetric oscillation. The result (6.87) is composed of the contributions

$$4\pi^4\,|\Pi(0)|^2 \int_{s_0}^{1} ds\, g(s) = 13.55 \tag{6.88}$$

$$4\pi^2\,\Pi(0) \int_{s_0}^{1} ds\, g(s)\, \mathrm{Re}\big[\Delta^{\mathrm{OPE}}_{\mathrm{Shif}}(s)\big] = -3.59 \qquad [-0.266] \tag{6.89}$$

$$\int_{s_0}^{1} ds\, g(s)\, |\Delta^{\mathrm{OPE}}_{\mathrm{Shif}}(s)|^2 = 1.24 \qquad [+0.015][+0.077] \tag{6.90}$$

At this, the central values correspond to Shifman's OPE; the square brackets to the shift caused by the replacement $\Delta^{\rm OPE}_{\rm Shif}(s) \to \Delta^{\rm OPE}_{\rm Shif}(s) + \Delta^{\rm DV}_{\rm Shif}(s)$ in the integrands on the left hand side.

However, only the dominating term $\Delta_{\rm DV,1}$ is maximized; the duality violating terms $\Delta_{\rm DV,2\text{-}3}$ potentially exceed the values given in (6.90) significantly. This issue may be addressed by replacing $z \to z + \varphi$ in (6.74) and finding the "optimal phase" $\varphi_\pm(s_0)$, which maximizes (minimizes) the integrals. In this way, the dashed lines on the r.h.s. of Fig. 6.5, which illustrate the actual total uncertainty in the integrated decay rate due to violations of duality, are obtained.

At $s_0 = 0.1015$, this procedure numerically yields $11.21^{+0.189}_{-0.269}{}^{+0.065}_{-0.061}{}^{+0.086}_{-0.054}$ for the individual (separate optimization) and $^{+0.267}_{-0.204}$, or $^{+2.4\%}_{-1.8\%}$, for the total "uncertainty". Note that the oscillation of $\Delta^{\rm DV}_{\rm Shif}$ is not symmetric, that is, the positive amplitude of $\mathrm{Re}\big[\Delta^{\rm DV}_{\rm Shif}\big]$ is smaller than the negative, i.e. $|0.189| < |-0.269|$. In consequence, the total positive uncertainty maximized is only 0.267, which significantly smaller than what one might naively expect from (6.89) – (6.90) (say $0.27 + 0.08 = 0.35$).

6.3 Duality Violation in $B \to K\ell^+\ell^-$

The general principles of duality violation discussed in the previous sections certainly apply to $B \to K\ell^+\ell^-$ as well. However, even qualitative statements about the size of duality violating effects are better based on an investigation of $B \to K\ell^+\ell^-$ itself.

6.3.1 Simplifications

The charm-loop enters the decay rates of $b \to s\,\ell^+\ell^-$ transitions via the matrix element of the correlator between the respective initial and final hadron state

$$\langle \mathcal{K}^\mu(q)\rangle \;\equiv\; -\frac{8\pi^2}{q^2}\, i\int d^4x\, e^{iq\cdot x}\,\langle \bar{K}(k)\big|T j^\mu(x)\mathcal{H}^c(0)\big|\bar{B}(p)\rangle \tag{6.91}$$

Without reducing the overall accuracy, the duality violations caused by the non-local term (6.91) will be investigated using the following simplifications:

- The penguin operators are dropped on account of their small coefficients, leaving the effective weak Hamiltonian

  $$\mathcal{H}^c \;=\; C_1\mathcal{O}^c_1 + C_2\mathcal{O}^c_2 \;\equiv\; a_2(\bar{s}b)_{V-A}(\bar{c}c)_{V-A} \tag{6.92}$$

  In the following, the coefficient a_2 is assumed to be real and treated as a phenomenological parameter. Its numerical value may then be extracted from measurements of the $B \to K\psi$ decay rate, which gives $a_2 = 0.3$.

  It should be noted that this is significantly larger than the perturbative value $a_2^{\rm th} = C_1/N + C_2$, which corresponds to $a_2^{\rm LO} = 0.10$ and $a_2^{\rm NLO} = 0.17$ at leading and next-to-leading order, respectively.

- The charm fields from $\mathcal{H}^c$ are always contracted with those in the electromagnetic current. In other words, we neglect annihilation processes of the charm pair into gluons, which are of higher order in α_s. As a consequence, only the charm component of the electromagnetic current may contribute, and hence we effectively have

$$j^\mu \;\equiv\; Q_c\,\bar{c}\,\gamma^\mu c \tag{6.93}$$

- Finally, a factorization of the charm-loop and the $\bar{B} \to \bar{K}$ system is assumed. The neglected contributions are, again, of higher perturbative order and, according to the OPE, atleast power-suppressed as $1/q^2$.

6.3.2 Analytic Structure

In order to discuss its analytic properties, the matrix element (6.91) is rewritten using the completeness relation $\hat{1} = \sum_X |X\rangle\langle X|$:

$$-\frac{q^2}{8\pi^2}\langle\bar{K}|\mathcal{K}^\mu|\bar{B}\rangle \;=\; i\int d^4x\, e^{iq\cdot x}\,\langle\bar{K}(k)|T\,j^\mu(x)\mathcal{H}^c(0)|\bar{B}(p)\rangle \tag{6.94}$$

$$\begin{aligned} &= \sum_X \frac{(2\pi)^3\delta(\vec{q}+\vec{k}-\vec{p}_X)}{p_{X0}-q_0-k_0-i\epsilon}\,\langle\bar{K}(k)|\,j^\mu(0)|X\rangle\langle X|\mathcal{H}^c(0)|\bar{B}(p)\rangle \\ &+ \sum_X \frac{(2\pi)^3\delta(\vec{q}+\vec{p}_X-\vec{p})}{p_{X0}+q_0-p_0-i\epsilon}\,\langle\bar{K}(k)|\mathcal{H}^c(0)|X\rangle\langle X|\,j^\mu(0)|\bar{B}(p)\rangle \end{aligned} \tag{6.95}$$

So that k_0 and p_0 can be treated as fixed at their physical values, a spurion 4-momentum [69] $r = (r_0, 0, 0, 0)$ is injected into the H^c vertex $p + r = q + k$. The matrix element (6.94) can then be treated as a function of q_0, and the physical kinematics are recovered for $r = 0$.

Assuming the simplifications specified in the previous section, the intermediate states of the first term in (6.95) always contain a $c\bar{c}$ pair and a strange quark, and consequently we have $p_{X0} - k_0 \gtrsim 2m_c$. Since the denominator corresponds to a delta function which switches its sign upon crossing the real axis (to be explicit, a denominator with "$\mp i\epsilon$" corresponds to a $\pm i\pi\delta(p_{X0} - q_0 - k_0)$), the first term has a branch cut on the positive real axis at $2m_c \lesssim q_0 < \infty$.

Likewise, in the second term, the intermediate state always contain a $c\bar{c}$ pair and a b quark, and thus we have $p_{X0} - p_0 \gtrsim 2m_c$. Again, the sign of the delta function from the denominator $\pm i\pi\delta(p_{X0} + q_0 - p_0)$ depends on the exact position in the complex plane "$\mp i\epsilon$", which now implies a branch cut on the negative real axis at $-\infty < q_0 < -2m_c$.

If we allow for intermediate states without a $c\bar{c}$ pair, the cuts would simply extend to lower values of $|q_0|$.

Relation OPE - Duality Violation

It follows from the above that the OPE is justified for q_0 on the imaginary axis far away from the resonances, that is, in the deep Euclidean domain $-iq_0 \equiv q_{0E} \gg \Lambda_{QCD}$. Predictions for large $q_0 \gg \Lambda_{QCD}$ can then be obtained via analytic continuation of the *individual* OPE terms. However, through this transfer to the Minkowskian domain, terms exponentially suppressed in Λ_{QCD}/q_{0E} partially lose their suppression and acquire a characteristic oscillatory behaviour [69]. As these terms are invisible at any finite order in the OPE, they can be identified as those responsible for the violation of duality.

6.3.3 Charm-Loop Contribution

Using the above simplifications and further neglecting the longitudinal component $\sim q^\mu$, the matrix element (6.94) assumes the form

$$\langle \bar{K} | \mathcal{K}^\mu | \bar{B} \rangle \;=\; 8\pi^2 Q_c a_2 \langle \bar{K} | \bar{s}\gamma^\mu (1-\gamma_5) b | \bar{B} \rangle \Pi_c(q^2) \tag{6.96}$$

In order to quantitatively estimate the duality violating component of the charm correlator Π_c, we now make use of the modified version of Shifman's model developed in section 6.1.3. Expressed as a correction to the effective coefficient C_9^{eff}, the contribution of the charm-loop to the $B \to K\ell^+\ell^-$ amplitude then reads

$$\Delta_{\text{charm}}(q^2) \;\equiv\; \frac{16\pi^2}{3} a_2 \Pi_c(q^2) \;=\; -\frac{4}{3}\frac{a_2}{1-b/\pi}\psi(z+3) \tag{6.97}$$

where

$$z \;=\; (-r - i\epsilon)^{1-b/\pi} \qquad r \;=\; \frac{q^2 - 4m_c^2}{\lambda^2} \;\equiv\; u(s-s_c) \qquad u \;=\; \frac{m_B^2}{\lambda^2} \tag{6.98}$$

For the numerical values of the parameters, we take the fit results (6.38) – (6.39)

$$b \;=\; 0.0818 \qquad m_c \;=\; 1.333\,\text{GeV} \qquad \lambda^2 \;=\; 3.080\,\text{GeV}^2 \tag{6.99}$$

which brings with it $u = 9.05$ and $s_c = 0.255$.

In analogy to the discussion around equation (6.73), the charm contribution (6.97) is decomposed into an OPE and a duality violating component according to

$$\Big[\psi(z+3)\Big]_{\text{had}} \;\equiv\; \Big[\psi(-z-2) - i\pi\Big]_{\text{OPE}} + \Big[-\pi\cot(\pi z) + i\pi\Big]_{\text{DV}} \tag{6.100}$$

The duality violating component thus explicitly reads

$$\Delta^{\text{DV}}(q^2) \;=\; \frac{4\pi}{3}\frac{a_2}{1-b/\pi}\Big[\cot(\pi z) - i\Big] \;\approx\; \frac{8\pi i}{3} a_2 e^{2\pi u(s-s_c)(i-b)} \tag{6.101}$$

where, in the second step, the hierarchy $\pi \gg b\ln q^2/\lambda^2$ was assumed.

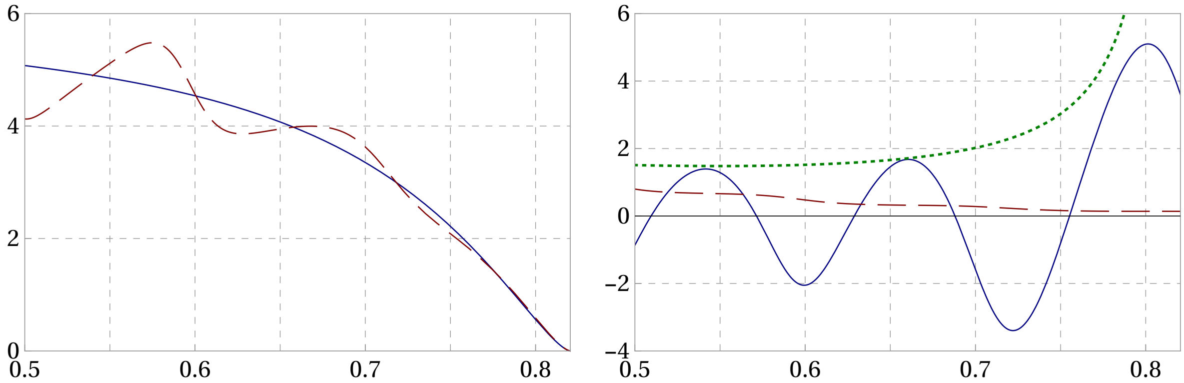

Figure 6.6: Duality violation in $B^+ \to K^+\ell^+\ell^-$: Local duality (l.h.s.): OPE-based (solid) and hadronic (dashed) dilepton-mass spectrum, that is, (6.102) with and without $\Delta^{\mathrm{DV}}(s)$, in units of $[10^{-7}]$. Global duality (r.h.s.): $R_{\mathrm{DV},1}$ (solid), the corresponding approximation (6.105) (dotted), and $R_{\mathrm{DV},2}$ (dashed) as functions of s_0 and in units of $[10^{-2}]$.

Finally, it is pointed out that the perturbative contribution of the charm-loop is described more accurately by the actual Standard model OPE result (6.53) – (6.54), and thus Shifman's OPE expression, defined through (6.100), will not be used to describe the charm-loop contributions contained in $C_9^{\mathit{eff}}(s)$.

6.3.4 Quantitative Estimate

The general structure of the $\bar{B} \to \bar{K}\ell^+\ell^-$ decay spectrum with respect to the duality violating component $\Delta^{\mathrm{DV}}(s)$ can schematically be written as

$$\frac{d\Gamma}{ds}(\bar{B} \to \bar{K}\ell^+\ell^-) = \mathit{const.} \times \left\{|C_9^{\mathit{eff}}(s) + \Delta^{\mathrm{DV}}(s)|^2 + |C_{10}|^2\right\} \lambda^{3/2}(s) f_+^2(s) \quad (6.102)$$

One may discern two duality violating terms - one being linear, the other quadratic in $\Delta^{\mathrm{DV}}(s)$. The relative impact of these terms on the partially integrated decay rate is now discussed in turn.

Term Linear in Δ^{DV}

When integrating the branching fraction from some lower limit $s_0 = q_0^2/m_B^2$ to the endpoint of the spectrum $s_m = (m_B - m_K)^2/m_B^2$, the relative size of the linear term is given as

$$R_{\mathrm{DV},1} \approx \frac{2\int_{s_0}^{s_m} ds\, \lambda^{3/2}(s) f_+^2(s)\, \mathrm{Re}\left[C_9^{\mathit{eff}*}(s)\, \Delta^{\mathrm{DV}}(s)\right]}{\int_{s_0}^{s_m} ds \left(|C_9^{\mathit{eff}}(s)|^2 + C_{10}^2\right) \lambda^{3/2}(s) f_+^2(s)} \quad (6.103)$$

To clarify the parametric situation, this term may be approximated as

$$R_{\mathrm{DV},1} \approx \frac{-16\pi}{3} \frac{a_2 C_9}{C_9^2 + C_{10}^2} \frac{\int_{s_0}^{s_m} ds\, \lambda^{3/2}(s) f_+^2(s)\, e^{-2\pi b u(s-s_c)} \sin(2\pi u(s - s_c))}{\int_{s_0}^{s_m} ds\, \lambda^{3/2}(s) f_+^2(s)} \tag{6.104}$$

$$\lesssim \frac{8}{3u} \frac{a_2 C_9}{C_9^2 + C_{10}^2} \frac{\lambda^{3/2}(s_0) f_+^2(s_0)}{\int_{s_0}^{s_m} ds\, \lambda^{3/2}(s) f_+^2(s)}\, e^{-2\pi b u(s_0-s_c)} \tag{6.105}$$

At this, the first steps assumes $C_9^{\mathit{eff}}(s) \equiv C_9$ along with the simplification (6.101), the second step an integration by parts, similar to (6.79).

We note an $1/u = \lambda^2/m_B^2$ power suppression due to the oscillating integrand as well as an exponential suppression for sufficiently large $2\pi b u_0$. This being said, the potential impact of $R_{\mathrm{DV},1}$ grows, as can be observed in Fig. 6.6, with increasing s_0, reaching 5.1% towards the end of the spectrum. This is ultimately a consequence of the fact that, towards the kinematic endpoint $s_0 \to s_m$, the integral over a single period (length $T = 1/u$) represents a larger fraction of the integral over the entire interval $[s_0, s_m]$. For a lower limit of integration between $0.5 \leqslant s_0 \leqslant 0.6$, however, the impact of the linear term stays below 2.1%.

Term Quadratic in $\boldsymbol{\Delta}^{\mathrm{DV}}$

For the relative impact of the quadratic term we have

$$R_{\mathrm{DV},2} = \frac{\int_{s_0}^{s_m} ds\, \lambda^{3/2}(s) f_+^2(s)\, |\Delta^{\mathrm{DV}}(s)|^2}{\int_{s_0}^{s_m} ds \left(|C_9^{\mathit{eff}}(s)|^2 + C_{10}^2\right) \lambda^{3/2}(s) f_+^2(s)} \tag{6.106}$$

$$\approx \frac{64\pi^2}{9} \frac{a_2^2}{C_9^2 + C_{10}^2} \frac{\int_{s_0}^{s_m} ds\, \lambda^{3/2}(s) f_+^2(s)\, e^{-4\pi b u(s-s_c)}}{\int_{s_0}^{s_m} ds\, \lambda^{3/2}(s) f_+^2(s)} \tag{6.107}$$

$$\lesssim \frac{16\pi}{9bu} \frac{a_2^2}{C_9^2 + C_{10}^2} \frac{\lambda^{3/2}(s_0) f_+^2(s_0)}{\int_{s_0}^{s_m} ds\, \lambda^{3/2}(s) f_+^2(s)}\, e^{-4\pi b u(s_0-s_c)} \tag{6.108}$$

As already discussed in section 6.2.4, the quadratic term differs qualitatively from the linear: There is (practically) no oscillation in the integrand, and, related to this, $R_{\mathrm{DV},2}$ is a strictly positive, monotonously decreasing function of s_0 (see r.h.s. of Fig. 6.6). Furthermore, while there is still an exponential $2\pi b u_0$ suppression, the power suppression in $1/u$ is counteracted by an $1/b$ enhancement. In practice, the second order term is kept in check by the size of the ratio $|a_2/C_{9,10}|^2$.

Numerically, one finds $R_{\mathrm{DV},2} = 0.67\%$ at our reference value $s_0 = 15\,\mathrm{GeV}^2/m_B^2 \approx 0.55$, and thus $R_{\mathrm{DV},2}$ is completely negligible.

Part IV

Phenomenology

7 Precision Flavour Physics with $\bar{B}^0 \to \pi^+\ell^-\bar{\nu}$ and $B^\pm \to \pi^\pm\mu^+\mu^-$

Theoretical predictions for the decay rates of $\bar{B}^0 \to \pi^+\ell^-\bar{\nu}$ and $B^\pm \to \pi^\pm\mu^+\mu^-$ suffer from large uncertainties in the relevant form factors. Since both decays share similar hadronic dynamics, this problem may be addressed by considering ratios of the corresponding branching fractions. To investigate the quality of such (precision) observables is the main objective of the following chapter.

On a related note, a precise (NNLO) prediction of the $B^\pm \to \pi^\pm\mu^+\mu^-$ branching fraction, using measurements of $\bar{B}^0 \to \pi^+\ell^-\bar{\nu}$ as input, can be found in [70].

7.1 Dilepton-Mass Spectra

From a theoretical point of view, the decay $B^+ \to \pi^+\mu^+\mu^-$ is in many respects analogous to the already discussed $B \to K\ell^+\ell^-$. There is, however, a non-trivial difference, which stems from the non-hierarchic flavour structure of $b \to d$ transitions. More specifically, the relevant CKM-entries

$$\lambda_p = V_{pd}^* V_{pb} \qquad \text{with} \qquad p = u, c, t \tag{7.1}$$

are all of the same order of magnitude. Thus, the so far neglected component of the effective Hamiltonian $\mathcal{H}_{\mathit{eff}}^u$, defined in (2.18), must now be taken into account as well. Apart from said inclusion of $\mathcal{H}_{\mathit{eff}}^u$, the effective Hamiltonian for $b \to d$ transitions only differs by the replacement of all (explicit) strange quarks in the operators (2.17) (and (2.19)) by down quarks.

As regards the decay $\bar{B}^0 \to \pi^+\ell^-\bar{\nu}$, the theoretical picture is extremely simple and clean. The decay is induced by the tree-level process shown in Fig. 7.1 (a) at the weak scale. As a consequence, all strong interactions are contained in the standard form factor $f_+^\pi(s)$. In particular, there are no perturbative corrections.

The two differential decay rates read [9, 70, 71] ($\ell = e$ or μ)

$$\frac{d\Gamma}{ds}(\bar{B}^0 \to \pi^+\ell^-\bar{\nu}) = \frac{G_F^2 m_B^5}{192\pi^3}\left|V_{ub}\right|^2 \lambda^{3/2}(s)\left|f_+^\pi(s)\right|^2 \tag{7.2}$$

$$\frac{d\Gamma}{ds}(B^\pm \to \pi^\pm\mu^+\mu^-) = \frac{G_F^2 \alpha_e^2 m_B^5}{1536\pi^5}\lambda^{3/2}(s)\left|f_+^\pi(s)\right|^2\left(\left|\lambda_t C_{10}\right|^2 + \left|C_9^{\mathit{eff}}(s)\right|^2\right) \tag{7.3}$$

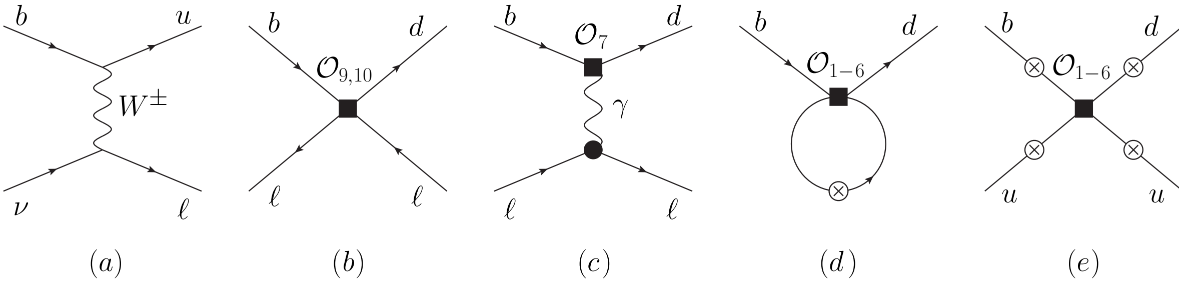

Figure 7.1: The Feynman diagrams responsible for the semileptonic decays $\bar{B}^0 \to \pi^+\ell^-\bar{\nu}$ and $B^\pm \to \pi^\pm\mu^+\mu^-$ are shown of Fig. (a) and $(b) - (e)$, respectively. The crossed circles $\otimes$ in (d) and (e) denote the possible insertion points for the electromagnetic current operator $j^\mu = \sum_q Q_q(\bar{q}\gamma^\mu q)$.

where

$$\begin{aligned} C_9^{eff}(s) \;=\; & \lambda_t\Big\{C_9 + (C_1 + NC_2)h_c - \frac{1}{2}(C_3 + NC_4)[h_s + h_b] \\ & + (NC_3 + C_4 + NC_5 + C_6)\Big[h_c - \frac{h_b}{2} + \frac{2}{9}\Big] \\ & + \frac{2m_b}{m_B + m_{\pi^\pm}}\frac{f_T^\pi(s)}{f_+^\pi(s)}C_7 + \big[C_3 + NC_4 - \frac{2\mu_\pi}{m_B}(C_5 + NC_6)\big]\Delta_{\mathrm{WA}}(s)\Big\} \\ & + \lambda_u\Big\{(C_1 + NC_2)[h_c - h_u] - (NC_1 + C_2)\Delta_{\mathrm{WA}}(s)\Big\} \end{aligned} \tag{7.4}$$

The function $h_q \equiv h(q^2, m_q)$ coincides with the one defined in (5.16), and

$$\Delta_{\mathrm{WA}}(s) \;=\; \frac{8Q_u}{m_B}\frac{f_B f_\pi}{f_+^\pi(s)}\frac{\pi^2}{N}\lambda_-^{-1}(s) \tag{7.5}$$

describes the contributions from the weak annihilation diagrams in Fig. 7.1 (e). At this point, a few remarks on weak annihilation seem necessary:

- The proper scale to renormalize the weak annihilation term (including the Wilson coefficients) is not $\mu = \mathcal{O}(m_b)$, but rather the *hard-collinear scale* $\mu_h = \sqrt{\mu\Lambda_h}$, where $\Lambda_h = 0.5\,\mathrm{GeV}$ [33].

- Admittedly, the term proportional to $\mu_\pi = m_\pi^2/(m_u + m_d) \sim \Lambda_{QCD}$ is formally power-suppressed in the heavy-quark limit. Since, however, the actual size of $2\mu_\pi/m_B \approx 0.75$ is close to unity, it is nevertheless taken into account.

- As discussed in the context of the OPE, $\Delta_{\mathrm{WA}}(s)$ develops a power-suppression at large invariant mass q^2. Even though there are now contributions with the

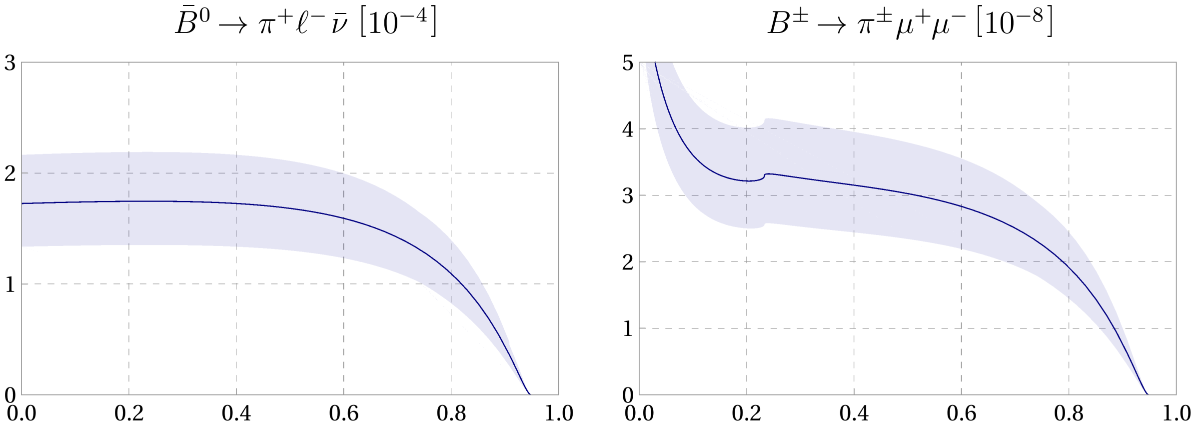

Figure 7.2: Differential branching fractions $(d\mathcal{B}/ds)(s)$ of $\bar{B}^0 \to \pi^+\ell^-\bar{\nu}$ and $B^\pm \to \pi^\pm\mu^+\mu^-$ as functions of s: The shaded areas correspond to a separate variation of the form factor parameters in the intervals specified in (B.10).

dominant coefficients $C_{1,2}$ as well, the impact of weak annihilation is already below 0.5% at $q^2 = 15\,\mathrm{GeV}$, and thus remains negligible at high-q^2.

- For $s \to 0$, on the other hand, $\Delta_{\mathrm{WA}}(s)$ becomes singular (though still integrable). This can be observed in Fig. 7.2 and follows from the asymptotic behaviour of

$$\lambda_-^{-1}(s) \quad \xrightarrow{s \ll 1} \quad \frac{1}{\omega_0}\left[i\pi - \gamma - \ln\frac{s m_B}{\omega_0} + \ldots\right] \tag{7.6}$$

- Finally, attention is drawn to the fact that, in the case of $B^\pm \to \pi^\pm\mu^+\mu^-$, weak annihilation actually generates a relevant contribution to the integrated decay rate (roughly 7%). This is in contrast to similar kaon decays, e.g. $B^{0,+} \to K^{0,+}\mu^+\mu^-$, where the contributions from weak annihilation are suppressed by the smallness of the penguin coefficients ($K^{0,+}$) or the off-diagonal elements of the CKM matrix (K^+) [29].

7.2 Numerical Results

Before investigating the matter of precision observables, the numerical results for the individual decays are presented first. To allow for comparison, for each integrated branching fraction, both the SM prediction as well the current experimental status are presented.

For the theoretical predictions, the form factor relation (3.60) is used to eliminate $f_T^\pi(s)$ in favor of $f_+^\pi(s)$. The parametrization employed for the latter can be found in appendix (B.1.2).

In order to estimate the form factor uncertainties, the form factor parameters are varied separately in their default ranges, given in (B.10). The individual parameter errors obtained in this way are, however, not independent from one another. Thus, adding them naively severely overestimates the total uncertainty.

7.2.1 Integrated $\bar{B}^0 \to \pi^+\ell^-\bar{\nu}$ Branching Fraction

For our tree-level process, we have

$$\mathcal{B}(\bar{B}^0 \to \pi^+\ell^-\bar{\nu})_{exp} = (1.45 \pm 0.05) \cdot 10^{-4} \qquad ([66]) \tag{7.7}$$

$$\mathcal{B}(\bar{B}^0 \to \pi^+\ell^-\bar{\nu})_{th} = (1.40^{+0.36}_{-0.32}[f_+(0)]\,^{+0.19}_{-0.17}[a_0]\,^{+0.06}_{-0.08}[b_1]) \cdot 10^{-4} \tag{7.8}$$

where, to be explicit, the "ℓ" stands for either an e or a μ. There is a good agreement between theoretical prediction and experiment, albeit – as anticipated – at a rather large form factor uncertainty.

7.2.2 Integrated $B^\pm \to \pi^\pm\mu^+\mu^-$ Branching Fraction

Taking the lower limit of integration $q_0^2 = 4m_\mu^2$, we find for the rare mode

$$\mathcal{B}(B^\pm \to \pi^\pm\mu^+\mu^-)_{exp} = (2.3 \pm 0.6(\text{stat.}) \pm 0.1(\text{syst.})) \cdot 10^{-8} \qquad ([72]) \tag{7.9}$$

$$\mathcal{B}(B^\pm \to \pi^\pm\mu^+\mu^-)_{th} = (2.69^{+0.13}_{-0.08}[\mu]\,^{+0.65}_{-0.58}[f_+(0)]\,^{+0.34}_{-0.31}[a_0]\,^{+0.11}_{-0.13}[b_1]) \cdot 10^{-8} \tag{7.10}$$

where, in accordance with standard practice, the perturbative uncertainty is estimated by varying the renormalization scale in the interval $m_b/2 \leqslant \mu \leqslant 2m_b$. Note that the $B^\pm \to \pi^\pm\mu^+\mu^-$ branching ratio has been measured only recently, and, in consequence, there is a sizeable uncertainty on the experimental side as well.

For the sake of comparison, we also quote the following theoretical predictions from the literature

$$\mathcal{B}(B^\pm \to \pi^\pm\mu^+\mu^-)_{th} = (1.88^{+0.32}_{-0.21}) \cdot 10^{-8} \qquad ([70]) \tag{7.11}$$

$$\mathcal{B}(B^\pm \to \pi^\pm\mu^+\mu^-)_{th} = (2.03 \pm 0.23) \cdot 10^{-8} \qquad ([73]) \tag{7.12}$$

The numerical discrepancy between the two results (7.8) and (7.12) can be accounted for by the following different input parameters[1], used in [73],

$$\lambda_t = 0.00827\,(-13\%) \qquad \alpha_e = 1/137 \quad (-11\%) \tag{7.13}$$

$$\sin^2\theta_W^{\overline{MS}}(M_Z) = 0.22306\,(+7.4\%) \qquad m_{t,pole} = 174.2\,\text{GeV}\,(-3\%) \tag{7.14}$$

[1]The percentages in the parentheses refer to the change in the $B^\pm \to \pi^\pm\mu^+\mu^-$ branching fraction when using the respective value in place of the one given in appendix A.

$q^2[(\mathrm{GeV}/c^2)^2]$	$4m_\mu^2 - 2.00$	$2.00 - 4.30$	$4.30 - 8.68$	$10.09 - 12.86$
$\mathcal{B}(\bar{B}^0 \to \pi^+\ell^-\bar{\nu})_{th}$	$1.21^{+0.00}_{-0.00}{}^{+0.31}_{-0.27}$	$1.44^{+0.00}_{-0.00}{}^{+0.37}_{-0.33}$	$2.74^{+0.00}_{-0.00}{}^{+0.73}_{-0.65}$	$1.71^{+0.00}_{-0.00}{}^{+0.49}_{-0.44}$
$\mathcal{B}(B^\pm \to \pi^\pm\mu^+\mu^-)_{th}$	$0.35^{+0.01}_{-0.00}{}^{+0.07}_{-0.06}$	$0.29^{+0.01}_{-0.00}{}^{+0.07}_{-0.06}$	$0.51^{+0.03}_{-0.03}{}^{+0.13}_{-0.12}$	$0.31^{+0.02}_{-0.02}{}^{+0.09}_{-0.08}$
$\mathcal{R}^\pi_{th}$	$3490^{+2}_{-75}{}^{+194}_{-230}$	$4919^{+13}_{-122}{}^{+90}_{-113}$	$5347^{+274}_{-320}{}^{+18}_{-23}$	$5485^{+300}_{-348}{}^{+3}_{-3}$
$q^2[(\mathrm{GeV}/c^2)^2]$	$14.18 - 16.00$	> 16.00	$1.00 - 6.00$	$0.00 - max$
$\mathcal{B}(\bar{B}^0 \to \pi^+\ell^-\bar{\nu})_{th}$	$1.08^{+0.00}_{-0.00}{}^{+0.34}_{-0.31}$	$4.11^{+0.00}_{-0.00}{}^{+1.54}_{-1.41}$	$3.12^{+0.00}_{-0.00}{}^{+0.80}_{-0.71}$	$13.97^{+0.00}_{-0.00}{}^{+4.09}_{-3.69}$
$\mathcal{B}(B^\pm \to \pi^\pm\mu^+\mu^-)_{th}$	$0.19^{+0.01}_{-0.01}{}^{+0.06}_{-0.05}$	$0.72^{+0.03}_{-0.02}{}^{+0.26}_{-0.23}$	$0.64^{+0.02}_{-0.00}{}^{+0.15}_{-0.13}$	$2.69^{+0.13}_{-0.08}{}^{+0.74}_{-0.66}$
$\mathcal{R}^\pi_{th}$	$5587^{+219}_{-302}{}^{+1}_{-2}$	$5674^{+146}_{-257}{}^{+3}_{-3}$	$4848^{+25}_{-130}{}^{+95}_{-120}$	$5196^{+151}_{-239}{}^{+69}_{-85}$

Table 7.1: Results for the individual standard bins: Standard model predictions for the partial branching fractions of $\bar{B}^0 \to \pi^+\ell^-\bar{\nu}$ and $B^\pm \to \pi^\pm\mu^+\mu^-$ in units of 10^{-4} and 10^{-5}, respectively; ratio $\mathcal{R}^\pi$ in units of 10^0. The uncertainties correspond to the perturbative (first) and the combined form factor uncertainty (second), respectively.

in combination with the complete neglect of weak annihilation (-7%). Through these adjustments alone, our SM predictions would become $\mathcal{B}(B^\pm \to \pi^\pm\mu^+\mu^-)_{th} = 2.01 \cdot 10^{-8}$, which is already in good agreement with (7.12).

As far as the NNLO prediction (7.11) is concerned, we only remark that a contribution from weak annihilation is missing in [70] as well.

7.2.3 Precision Observables

In the present context, the obvious candidates for precision observables are ratios of the form

$$\mathcal{R}^\pi \equiv \frac{\mathcal{B}(\bar{B}^0 \to \pi^+\ell^-\bar{\nu})}{\mathcal{B}(B^\pm \to \pi^\pm\mu^+\mu^-)} = \frac{8\pi^2\tau_{B^0}}{\alpha_e^2\tau_{B^+}} \frac{|V_{ub}|^2 \int \lambda^{3/2}(s) f_+^2(s)}{\int \lambda^{3/2}(s) f_+^2(s)\big(|\lambda_t C_{10}|^2 + |C_9^{\mathit{eff}}(s)|^2\big)} \tag{7.15}$$

In general, the cancellation of the hadronic uncertainties in (7.15) is most effective if the two branching fractions are integrated over the same domain. Then, the only thing that prevents a complete elimination is the s-dependence of $C_9^{\mathit{eff}}(s)$, which is dominated by the weak annihilation term.

Numerically, an integration over the entire spectrum $4m_\mu^2 \leqslant q^2 \leqslant (m_B - m_{\pi^\pm})^2$ yields

$$\mathcal{R}^\pi_{th} = 5196^{+151}_{-239}[\mu]^{+50}_{-65}[f_+(0)]^{+44}_{-51}[a_0]^{+18}_{-23}[b_1] = (5.20^{+0.17}_{-0.25}) \cdot 10^3 \tag{7.16}$$

which is to be compared with the experimental value

$$\mathcal{R}^\pi_{exp} = (6.3 \pm 1.7) \cdot 10^3 \tag{7.17}$$

The total theoretical uncertainty in the precision observable (7.16) is roughly 5% and dominated by the perturbative error, which can be reduced systematically. Correspondingly, the remaining hadronic uncertainties are found to be rather small $\sim 1.6\%$.

The cancellation of form factor uncertainties, though still effective, is, however, not as complete as in similar kaon decays [29]. In particular, the variation of $f_+(0)$ has a substantial impact on the ratio (7.16). This mainly harks back to the lack of a strong suppression of the weak annihilation term in $B^\pm \to \pi^\pm\mu^+\mu^-$ decays.

In order to avoid the domain of the narrow charmonium resonances, one may opt to exclude the middle part $0.25 \leqslant s \leqslant 0.6$ from the integration. For this modified observable, one finds

$$\mathcal{R}^{\pi}_{th,cut} \;=\; 5006\,^{+62}_{-170}[\mu]\,^{+79}_{-101}[f_+(0)]\,^{+69}_{-77}[a_0]\,^{+34}_{-42}[b_1] \;=\; (5.01\,^{+0.13}_{-0.22})\cdot 10^3 \qquad (7.18)$$

which is qualitatively similar to the result (7.16). The moderate increase of the form factor uncertainties in (7.18) can be attributed to the higher weighting of the low-q^2 region $s \lesssim 0.2$, where the impact of weak annihilation is felt the most. This can also be inferred from the numerical results obtained for the individual standard bins, displayed in Tab. 7.1.

8 Precision Flavour Physics with $B \to K^*\nu\bar{\nu}$ and $B \to K^*\ell^+\ell^-$

In the spirit of the previous chapter, a combined analysis of the decays $B \to K^*\nu\bar{\nu}$ and $B \to K^*\ell^+\ell^-$ is performed. While the underlying concept remains the same, the multitude of different form factors involved requires a somewhat more elaborate implementation.

8.1 Dilepton-Mass Spectra

The dilepton mass spectra of the two rare decays $B \to K^*\nu\bar{\nu}$ and $B \to K^*\ell^+\ell^-$ can be written as [74]

$$\frac{d\Gamma}{ds}(B \to K^*\nu\bar{\nu}) = \frac{G_F^2\alpha_e^2 m_B^5}{1024\pi^5}\left|V_{ts}^* V_{tb}\right|^2 \lambda^{1/2}(s)\left|\mathcal{C}_\nu\right|^2 R_9(s) \tag{8.1}$$

$$\begin{aligned}\frac{d\Gamma}{ds}(B \to K^*\ell^+\ell^-) = {} & \frac{G_F^2\alpha_e^2 m_B^5}{6144\pi^5}\left|V_{ts}^* V_{tb}\right|^2 \lambda^{1/2}(s)\Big\{\Big(\left|C_9^{\mathit{eff}}(s)\right|^2 + \left|C_{10}\right|^2\Big)R_9(s) \\ & + R_7(s)\frac{m_b^2}{m_B^2}\left|C_7\right|^2 + R_{97}(s)\frac{m_b}{m_B}\,\mathrm{Re}\Big[C_9^{\mathit{eff}}(s)C_7^*\Big]\Big\}\end{aligned} \tag{8.2}$$

At this, for reasons of experimental feasibility, all three families are counted in the neutrino mode (8.1). In the formula for the charged mode (8.2), on the other hand, the "ℓ" stands for either an e or a μ.

The effective coefficient in (8.2) reads

$$\begin{aligned}C_9^{\mathit{eff}}(s) = {} & C_9 + (C_1 + NC_2)h_c - \frac{1}{2}(C_3 + NC_4)[h_s + h_b] \\ & + (NC_3 + C_4 + NC_5 + C_6)\Big[h_c - \frac{h_b}{2} + \frac{2}{9}\Big]\end{aligned} \tag{8.3}$$

where $h_q \equiv h(q^2, m_q)$ is the function defined in (5.16).

Note that the weak annihilation contribution to $B \to K^*\ell^+\ell^-$, which is proportional to the small penguin coefficients, would require the introduction of two effective coefficients $C_{9\parallel,\perp}^{\mathit{eff}}$ and has therefore been neglected for the sake of simplicity.

Finally, we have [74]

$$R_9(s) = \frac{1}{r}\left[\frac{A_2(s)}{1+\sqrt{r}}\,\lambda(s) - A_1(s)(1+\sqrt{r})(1-s-r)\right]^2 + 8s\left[\frac{V^2(s)}{(1+\sqrt{r})^2}\,\lambda(s) + A_1^2(s)(1+\sqrt{r})^2\right] \tag{8.4}$$

$$R_7(s) = \frac{4}{rs^2}\left[\tilde{T}_3(s)\lambda(s) - T_2(s)(1-r)(1-s-r)\right]^2 + \frac{32}{s}\left[T_1^2(s)\lambda(s) + T_2^2(s)(1-r)^2\right] \tag{8.5}$$

$$R_{97}(s) = \frac{4}{rs}\left[\frac{A_2(s)}{1+\sqrt{r}}\,\lambda(s) - A_1(s)(1+\sqrt{r})(1-s-r)\right] \cdot \left[\tilde{T}_3(s)\lambda(s) - T_2(s)(1-r)(1-s-r)\right] + \frac{32V(s)}{1+\sqrt{r}}\,T_1(s)\lambda(s) + 32A_1(s)T_2(s)(1-r)(1+\sqrt{r}) \tag{8.6}$$

where

$$\tilde{T}_3(s) \equiv T_2(s) + \frac{s}{1-r}\,T_3(s) \tag{8.7}$$

It is worth mentioning that the respective first term in (8.4) – (8.6) corresponds to a longitudinally, the second to a transversely polarized vector meson.

8.2 Variation of Form Factors

In order to estimate the hadronic uncertainties in observables, the different form factors are to be varied. The effective number of independent form factor parameters can be reduced significantly by exploiting the form factor symmetries (3.61) – (3.62). While this course of action is certainly preferable in terms of convenience and transparency, it is most of all necessary to avoid a severe overestimation of the hadronic uncertainties.

Now, in principle, the decision which of the six form factors appearing in (8.4) – (8.6) to eliminate is arbitrary. This being said, the tensor form factors T_i have (at least in the largest part of the spectrum $q^2 \gtrsim 1\,\mathrm{GeV}^2$) a comparatively small numerical impact. Since the form factor relations are not exact identities, and thus introduce an error of

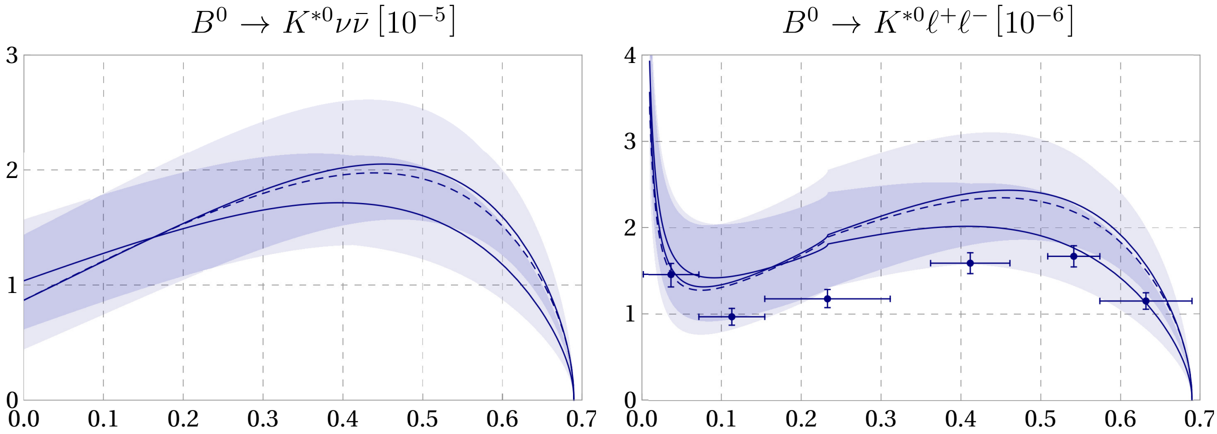

Figure 8.1: Differential branching fractions $(d\mathcal{B}/ds)(s)$ of the rare decays $B \to K^*\nu\bar{\nu}$ and $B \to K^*\ell^+\ell^-$ as functions of s: The dashed curves show the default predictions; the solid curves correspond to the two "form factor scenarios" as explained in the text. The form factor uncertainties (shaded areas) are obtained from a separate parameter variation; darker shaded areas (essentially overlaps) belong to both scenarios. The data points represent the averaged measurements provided by the HFAG [75] (also given in Tab. 8.1).

their own, it therefore seems more natural to remove the T_i in favour of the dominant form factors V, A_1 and A_2.

In this spirit, the tensor form factors are always eliminated using the relations

$$T_1(s) = \frac{V(s)}{1+\sqrt{r}} \qquad T_2(s) = \frac{V(s)}{1+\sqrt{r}}(1-s) \qquad T_3(s) = \frac{A_2(s)}{1+\sqrt{r}} \tag{8.8}$$

In addition, this ensures that the kinematic constraints

$$T_2(0) = T_1(0) = \tilde{T}_3(0) \tag{8.9}$$

are always exactly maintained, in particular also when the individual form factor parameters are varied.

There is one further relation we may exploit, namely

$$A_1(s)(1+\sqrt{r})^2 = V(s)(1-s) \tag{8.10}$$

which can be used to eliminate either $A_1(s)$ or $V(s)$ from theoretical expressions. Both variants will be considered here – mostly to get an impression of the error introduced by the relations themselves: Just by imposing the form factor symmetries in one way or another, theoretical predictions are shifted differently. The difference between the two implementations of (8.10), for instance, can be observed in Fig. 8.1.

Thus, in summary, we are in both cases left with two independent form factors; in the first scenario with (V, A_2), and in the second with (A_1, A_2). Using the form factor parametrizations (B.31) – (B.33), this corresponds to 6 and 5 independent parameters, respectively, which will be varied separately within the boundaries specified in (B.34) – (B.35).

8.3 Numerical Results

The numerical results for the integrated branching fractions and precision observables are presented and compared with the current experimental findings. At this, for each observable, up to three different theoretical predictions are given. One, usually the first, forgoes the form factor relation entirely and may be seen as the default value. The other two results, carrying a subscript $i = 1, 2$, have the relations implemented (differently) as discussed in the previous section (8.2), which allows to estimate the hadronic uncertainties in a sensible way.

8.3.1 Integrated $B \to K^*\nu\bar{\nu}$ Branching Fraction

As far as the neutrino mode is concerned, experimental measurements still only allow to specify upper bounds for the total branching fractions [75]

$$\mathcal{B}(B \to K^*\nu\bar{\nu})_{exp} < 76 \cdot 10^{-6} \tag{8.11}$$

$$\mathcal{B}(B^0 \to K^{*0}\nu\bar{\nu})_{exp} < 55 \cdot 10^{-6} \tag{8.12}$$

$$\mathcal{B}(B^+ \to K^{*+}\nu\bar{\nu})_{exp} < 40 \cdot 10^{-6} \tag{8.13}$$

For the corresponding SM prediction, we employ the NLO approximation of the Wilson coefficient C_ν, given in (D.17). Not yet exploiting any form factor symmetries, one then obtains for the fully (starting at $q_0^2 = 0$) integrated $B \to K^*\nu\bar{\nu}$ branching fraction

$$\mathcal{B}(B^0 \to K^{*0}\nu\bar{\nu})_{th} = 10.6 \cdot 10^{-6} \tag{8.14}$$

While this result is virtually free of perturbative uncertainties, it comes with a quite substantial hadronic uncertainty of about 40%: Imposing now the form factor relations as described in the previous section, a separate variation of the remaining form factor parameters yields

$$\mathcal{B}(B^0 \to K^{*0}\nu\bar{\nu})_1 = (96^{+28}_{-24}[V_0]^{+19}_{-17}[a_V]^{+8}_{-10}[b_V]^{+12}_{-10}[A_{20}]^{+5}_{-4}[a_{A2}]^{+4}_{-3}[b_{A2}]) \cdot 10^{-7} \tag{8.15}$$

$$= (96^{+37}_{-33}) \cdot 10^{-7} \tag{8.16}$$

$$\mathcal{B}(B^0 \to K^{*0}\nu\bar{\nu})_2 = (109^{+36}_{-30}[A_{10}]^{+16}_{-13}[b_{A1}]^{+12}_{-10}[A_{20}]^{+5}_{-5}[a_{A2}]^{+4}_{-3}[b_{A2}]) \cdot 10^{-7} \tag{8.17}$$

$$= (109^{+41}_{-35}) \cdot 10^{-7} \tag{8.18}$$

$q^2[(\mathrm{GeV}/c^2)^2]$	$0.00 - 2.00$	$2.00 - 4.30$	$4.30 - 8.68$	$10.09 - 12.86$
HFAG [75]	$1.02^{+0.09}_{-0.10}$	0.80 ± 0.08	$1.85^{+0.17}_{-0.16}$	1.58 ± 0.12
$\mathcal{B}_{th1}$	$1.77^{+0.27}_{-0.17}{}^{+0.70}_{-0.58}$	$1.20^{+0.06}_{-0.04}{}^{+0.62}_{-0.52}$	$2.76^{+0.29}_{-0.24}{}^{+1.17}_{-1.02}$	$2.00^{+0.17}_{-0.14}{}^{+0.74}_{-0.69}$
$\mathcal{B}_{th2}$	$1.61^{+0.25}_{-0.16}{}^{+0.74}_{-0.59}$	$1.14^{+0.06}_{-0.03}{}^{+0.68}_{-0.54}$	$2.93^{+0.30}_{-0.26}{}^{+1.31}_{-1.10}$	$2.38^{+0.21}_{-0.17}{}^{+0.82}_{-0.71}$
$q^2[(\mathrm{GeV}/c^2)^2]$	$14.18 - 16.00$	> 16.00	$1.00 - 6.00$	$0.00 - max$
HFAG [75]	1.09 ± 0.08	1.33 ± 0.11	1.90 ± 0.18	10.5 ± 1.0
$\mathcal{B}_{th1}$	$1.15^{+0.08}_{-0.06}{}^{+0.45}_{-0.43}$	$1.22^{+0.08}_{-0.05}{}^{+0.53}_{-0.49}$	$2.73^{+0.14}_{-0.08}{}^{+1.36}_{-1.14}$	$12.00^{+0.68}_{-0.40}{}^{+4.59}_{-4.09}$
$\mathcal{B}_{th2}$	$1.49^{+0.10}_{-0.08}{}^{+0.50}_{-0.42}$	$1.68^{+0.11}_{-0.07}{}^{+0.60}_{-0.48}$	$2.64^{+0.14}_{-0.08}{}^{+1.49}_{-1.20}$	$13.50^{+0.82}_{-0.52}{}^{+5.20}_{-4.36}$

Table 8.1: Partial branching fractions of $B \to K^*\ell^+\ell^-$ in units of 10^{-7}. The theoretical uncertainties correspond to the perturbative (first) and the combined form factor uncertainty (second), respectively.

8.3.2 Integrated $B \to K^*\ell^+\ell^-$ Branching Fraction

As for the charged mode, the total branching fractions, extrapolated from the measured non-resonant part of the spectrum, are measured to be [75]

$$\mathcal{B}(B \to K^*\ell^+\ell^-)_{exp} = (1.05 \pm 0.10) \cdot 10^{-6} \tag{8.19}$$

$$\mathcal{B}(B^0 \to K^{*0}\ell^+\ell^-)_{exp} = (0.99^{+0.13}_{-0.11}) \cdot 10^{-6} \tag{8.20}$$

$$\mathcal{B}(B^+ \to K^{*+}\ell^+\ell^-)_{exp} = (1.29^{+0.22}_{-0.21}) \cdot 10^{-6} \tag{8.21}$$

In contrast to the neutral mode, the charged mode has a (non-integrable) $1/s$ divergence, related to the increasing difficulty to experimentally distinguish between $B \to K^*\ell^+\ell^-$ and $B \to K^{*0}\gamma$. Therefore, the q^2-integration is cut at $q_0^2 = 0.05\,\mathrm{GeV}^2$, which yields

$$\mathcal{B}(B^0 \to K^{*0}\ell^+\ell^-)_{th} = (1.31^{+0.08}_{-0.05}[\mu]) \cdot 10^{-6} \tag{8.22}$$

This corresponds to a moderate perturbative error of 6%, which is significantly exceeded by the large (about 40%) hadronic uncertainties, in detail estimated to be

$$\mathcal{B}(B^0 \to K^{*0}\ell^+\ell^-)_1 \cdot 10^8 = 120^{+7}_{-4}[\mu]^{+35}_{-30}[V_0]^{+23}_{-21}[a_V]^{+10}_{-12}[b_V]^{+15}_{-13}[A_{20}]^{+6}_{-6}[a_{A2}]^{+5}_{-4}[b_{A2}] \tag{8.23}$$

$$= 120^{+7}_{-4}(\mathrm{scale})\ ^{+46}_{-41}(\mathrm{hadronic}) \tag{8.24}$$

$$\mathcal{B}(B^0 \to K^{*0}\ell^+\ell^-)_2 \cdot 10^8 = 135^{+8}_{-5}[\mu]^{+45}_{-38}[A_{10}]^{+19}_{-15}[b_{A1}]^{+15}_{-13}[A_{20}]^{+6}_{-6}[a_{A2}]^{+5}_{-4}[b_{A2}] \tag{8.25}$$

$$= 135\ ^{+8}_{-5}(\mathrm{scale})\ ^{+52}_{-44}(\mathrm{hadronic}) \tag{8.26}$$

A comparison between the theoretical predictions and the experimental measurements of the individual standard bins, as given in Tab. 8.1, shows qualitatively the same

$q^2[(\mathrm{GeV}/c^2)^2]$	$0.00 - 2.00$	$2.00 - 4.30$	$4.30 - 8.68$	$10.09 - 12.86$
$\mathcal{R}^{K^*}_{th1}[10^{-2}]$	$444^{+47}_{-58}{}^{+68}_{-86}$	$899^{+27}_{-45}{}^{+48}_{-34}$	$878^{+85}_{-82}{}^{+32}_{-27}$	$849^{+65}_{-68}{}^{+10}_{-9}$
$\mathcal{R}^{K^*}_{th2}[10^{-2}]$	$432^{+48}_{-59}{}^{+77}_{-100}$	$902^{+27}_{-45}{}^{+55}_{-36}$	$874^{+85}_{-82}{}^{+32}_{-26}$	$846^{+64}_{-68}{}^{+9}_{-8}$
$q^2[(\mathrm{GeV}/c^2)^2]$	$14.18 - 16.00$	> 16.00	$1.00 - 6.00$	$0.00 - max$
$\mathcal{R}^{K^*}_{th1}[10^{-2}]$	$836^{+45}_{-55}{}^{+3}_{-3}$	$829^{+37}_{-49}{}^{+1}_{-1}$	$873^{+26}_{-43}{}^{+35}_{-25}$	$797^{+28}_{-43}{}^{+7}_{-8}$
$\mathcal{R}^{K^*}_{th2}[10^{-2}]$	$835^{+45}_{-55}{}^{+3}_{-3}$	$828^{+37}_{-49}{}^{+1}_{-1}$	$875^{+27}_{-44}{}^{+40}_{-28}$	$804^{+32}_{-46}{}^{+6}_{-6}$

Table 8.2: Precision observable $\mathcal{R}^{K^*}$ for the individual standard bins. The first error represents the perturbative; the second error the combined form factor uncertainty.

picture (general agreement of theory and experiment, small perturbative, large hadronic uncertainty).

8.3.3 Precision Observables

For our precision observables we will consider ratios of the form

$$\mathcal{R}^{K^*} \equiv \frac{\displaystyle\int_a^b ds\, d\mathcal{B}(B \to K^*\nu\bar{\nu})/ds}{\displaystyle\int_a^b ds\, d\mathcal{B}(B \to K^*\ell^+\ell^-)/ds} \tag{8.27}$$

where, to ensure an efficient cancellation of the hadronic uncertainties, the two branching fractions are always integrated over the same part of the q^2-spectrum.

Again, the numerical findings for the entire spectrum $0.05\,\mathrm{GeV}^2 \leqslant q^2 \leqslant (m_B - m_{K^*})^2$ are presented in detail first. For the current experimental status and our theoretical default value, we have

$$\mathcal{R}^{K^*}_{exp} \cdot 10^2 \;<\; 3101^{+603}_{-452} \qquad\qquad \mathcal{R}^{K^*}_{th} \cdot 10^2 \;=\; 809^{+34}_{-47}(\text{scale}) \tag{8.28}$$

While the perturbative uncertainty is unchanged at 6%, the hadronic uncertainties are now estimated to be

$$\mathcal{R}^{K^*}_{th1} \cdot 10^2 = 797^{+28}_{-43}[\mu]^{+2}_{-2}[V_0]^{+5}_{-6}[a_V]^{+2}_{-4}[b_V]^{+3}_{-3}[A_{20}]^{+1}_{-1}[a_{A2}]^{+1}_{-1}[b_{A2}] = 797^{+28}_{-43}{}^{+7}_{-8} \tag{8.29}$$

$$\mathcal{R}^{K^*}_{th2} \cdot 10^8 = 804^{+32}_{-46}[\mu]^{+3}_{-3}[A_{10}]^{+3}_{-3}[b_{A1}]^{+3}_{-3}[A_{20}]^{+2}_{-2}[a_{A2}]^{+1}_{-1}[b_{A2}] = 804^{+32}_{-46}{}^{+6}_{-6} \tag{8.30}$$

which represents a significant reduction down to the 1% level.

The results for the individual bins, presented in Tab. 8.2, reveal that at low-q^2 the cancellation of hadronic uncertainties is less effective, though still quite significant. This is mainly a consequence of the divergent $1/s$ component in the C_7 term of the $B \to K^*\ell^+\ell^-$ branching fraction.

9 Precision Flavour Physics with $B \to K\nu\bar{\nu}$ and $B \to K\ell^+\ell^-$

For our last precision observable, we simultaneously consider the integrated branching fractions of $\bar{B} \to \bar{K}\nu\bar{\nu}$ and $\bar{B} \to \bar{K}\ell^+\ell^-$. The two decay rates are presented at NNLO accuracy, using the more suitable operator basis (2.21). We then proceed to investigate the residual hadronic uncertainty in the corresponding ratios. A similar analysis, though only at NLO, was given in [29].

9.1 Dilepton-Mass Spectra

The differential branching fractions of the decays $\bar{B} \to \bar{K}\nu\bar{\nu}$ and $\bar{B} \to \bar{K}\ell^+\ell^-$ can, to any order in α_s, be written as

$$\frac{d\Gamma}{ds}(\bar{B} \to \bar{K}\nu\bar{\nu}) = \frac{G_F^2\alpha_e^2 m_B^5}{256\pi^5}|\lambda_t|^2\lambda^{3/2}(s)f_+^2(s)|\mathcal{C}_\nu|^2 \tag{9.1}$$

$$\frac{d\Gamma}{ds}(\bar{B} \to \bar{K}\ell^+\ell^-) = \frac{G_F^2\alpha_e^2 m_B^5}{1536\pi^5}|\lambda_t|^2\lambda^{3/2}(s)f_+^2(s)\left\{\left|\frac{4\pi}{\alpha_s}\mathcal{C}_{10}\right|^2 + \left|\mathcal{C}_9^{\mathit{eff}}(s)\right|^2\right\} \tag{9.2}$$

At this, the Wilson coefficients $\mathcal{C}_{10}$ and $\mathcal{C}_\nu$ are simple short-distance quantities, induced at the weak scale, and consequently are known very precisely.

The effective coefficient $\mathcal{C}_9^{\mathit{eff}}$, on the other hand, is more complicated: Next to the contributions from $\mathcal{Q}_{7,9}$, it also contains the non-local matrix element of $\mathcal{Q}_{1-6}$, which requires a virtual photon to create the outgoing lepton pair. At NLO, one finds [10, 76, 77] ($\hat{\mu}_K \equiv \mu_K/m_B$)

$$\begin{aligned}
\mathcal{C}_{9,\mathrm{NLO}}^{\mathit{eff}} = {} & \frac{4\pi}{\alpha_s}\mathcal{C}_9 + \frac{2m_b}{m_K + m_B}\frac{f_T(s)}{f_+(s)}\mathcal{C}_7 + (C_F\mathcal{C}_1 + \mathcal{C}_2)h_c + 2N\mathcal{C}_3\left[h_c - \frac{h_b}{2} + \frac{2}{9}\right] \\
& - (\mathcal{C}_3 + C_F\mathcal{C}_4)\left[\frac{h_s}{2} + \frac{h_b}{2} + (2\hat{\mu}_K - 1)\Delta_{\mathrm{WA}}\right] + 20N\mathcal{C}_5\left[h_c - \frac{h_b}{2} + \frac{4}{45}\right] \\
& - 8(\mathcal{C}_5 + C_F\mathcal{C}_6)\left[h_s + h_b - \frac{2}{9} + (\hat{\mu}_K - 2)\Delta_{\mathrm{WA}}\right]
\end{aligned} \tag{9.3}$$

where the penguin contributions from the four-quark operators (Fig. 9.1 (c)) are described by the function $h_q = h(q^2, m_q)$, defined in (5.16).

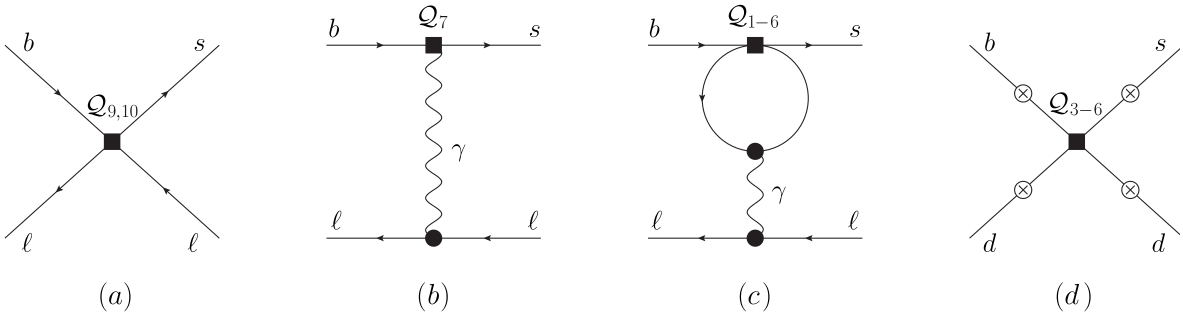

Figure 9.1: Feynman diagrams responsible for the leading and next-to-leading order contributions to the $\bar{B} \to \bar{K}\ell^+\ell^-$ amplitude.

Weak Annihilation (NLO)

The effective coefficient $\mathcal{C}_9^{\mathit{eff}}$ receives contributions from the weak annihilation diagrams in Fig. 9.1 (d). They are here expressed in terms of the function

$$\Delta_{\mathrm{WA}}(s) \;=\; \frac{8Q_r}{m_B}\,\frac{f_B f_K}{f_+(s)}\,\frac{\pi^2}{N}\,\lambda_-^{-1}(s) \tag{9.4}$$

where Q_r denotes the charge quantum number of the spectator quark. In contrast to the other terms in the effective coefficient (9.3), the weak annihilation term (9.4) should not be evaluated at $\mu \sim m_b$, but rather the hard-collinear scale $\mu_h = \sqrt{\mu/2}$.

While power suppressed $\sim (\Lambda_{QCD}/m_B)^3$ at high-q^2 (as already discussed in the context of the OPE), the expression (9.4) becomes of leading power at low-q^2. Even then, however, weak annihilation is still penguin-suppressed and, as a consequence, remains negligibly small (below 1%) in the entire spectrum [29]. This being said, for reasons of principle alone, the (NLO) weak annihilation term (9.4) should certainly be included at the NNLO level.

9.2 $\mathcal{C}_9^{\mathit{eff}}$ at Next-to-Next-to Leading Order

In order to obtain the NNLO decay rate of $\bar{B} \to \bar{K}\ell^+\ell^-$, two different types of corrections have to be included.

Firstly, the Wilson coefficients are now required with next-to-leading logarithmic (NLL) accuracy, except for $\mathcal{C}_9$, which is now required with next-to-next-to-leading logarithmic (NNLL) accuracy. This rather technical procedure is explained in appendix D.

Secondly, the NNLO matrix elements of the local operators give rise to additional contributions, in the following written as corrections to the effective coefficient

$$\mathcal{C}_{9,\mathrm{NNLO}}^{\mathit{eff}} \;=\; \mathcal{C}_{9,\mathrm{NLO}}^{\mathit{eff}} + \Delta_-^{\mathrm{spec}} + \Delta_+^{\mathrm{spec}} + \Delta^{\text{2-loop}} + \Delta_8 \tag{9.5}$$

The different correction terms Δ_i are now discussed in turn.

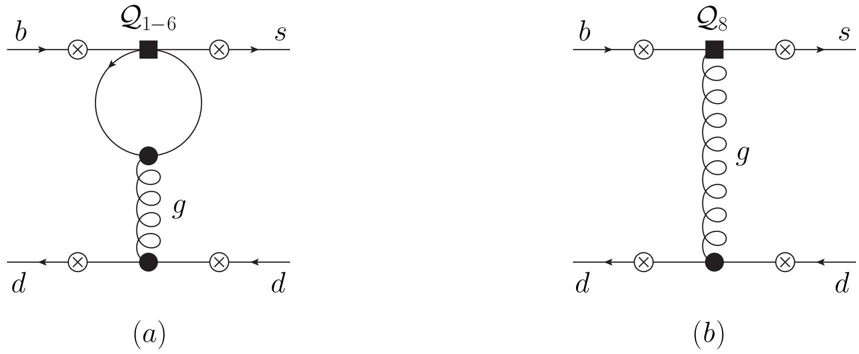

Figure 9.2: $\bar{B} \to \bar{K}\ell^+\ell^-$ at NNLO: Hard spectator scattering $\propto \phi_-(\omega)$. The crossed circles $\otimes$ denote possible insertion points for the electromagnetic current operator $j^\mu = \sum_q Q_q\,(\bar{q}\gamma^\mu q)$.

9.2.1 Weak Annihilation (NNLO)

At NNLO, weak annihilation receives additional contributions due to "vertex corrections", which can be obtained from Fig. 9.1 (d) by attaching a virtual gluon.

However, as stated above, already the leading contribution of weak annihilation, which ranges at the 1% level, is very small. Thus, the perturbative corrections to weak annihilation, further suppressed in α_s, are numerically completely insignificant and therefore can safely be neglected.

9.2.2 Hard Spectator Scattering $\propto \phi_-(\omega)$

As far as processes involving the spectator quark are concerned, the diagrams where the virtual photon is emitted from an external quark line (Fig. 9.2) are considered first. Since the calculation essentially factorizes into "loop function" $\times$ "weak annihilation structure", this contribution is proportional to the minus projector of the B meson $\phi_-(\omega)$.

The corresponding correction to the effective coefficient $\mathcal{C}_9^{\text{eff}}$ is given by [40]

$$\begin{aligned}
\Delta_-^{\text{spec}} \;=\;& -\pi\alpha_s(\mu)\frac{3Q_r}{m_B}\,\frac{C_F}{N}\,\frac{f_B f_K}{f_+(s)}\,\lambda_-^{-1}(s)\int du\,\phi(u)\bigg\{\frac{4m_b}{3m_B}\,\frac{\mathcal{C}_8}{\bar{u}+us} + \Big(\mathcal{C}_2 - \frac{\mathcal{C}_1}{2N}\Big)h_c \\
& + \Big(\mathcal{C}_3 - \frac{\mathcal{C}_4}{2N}\Big)[h_b + h_0] + 16\Big(\mathcal{C}_5 - \frac{\mathcal{C}_6}{2N}\Big)\Big[h_b + h_0 - \frac{2}{9}\Big] \\
& + \mathcal{C}_4\Big[h_c + h_b + 3h_0 + \frac{20}{9}\Big] + 10\mathcal{C}_6\Big[h_c + h_b + 3h_0 + \frac{8}{9}\Big]\bigg\}
\end{aligned} \tag{9.6}$$

where, for this contribution, $h_q \equiv h(\bar{u}m_B^2 + uq^2, m_q)$ and Q_r denotes the charge quantum number of the respective spectator quark. The proper scale to renormalize this contribution is $\mu_h = \sqrt{\mu\Lambda_h}$.

As already known from the discussion in section (5.5), this contribution is power-suppressed $\sim (\Lambda/m_B)^3$ and, as a consequence, negligible at high-q^2.

9.2.3 Hard Spectator Scattering $\propto \phi_+(\omega)$

The spectator processes where the virtual photon is emitted from the loop (see Fig. 9.3) is responsible for the corrections proportional to the light-cone distribution amplitude $\phi_+(\omega)$ [40]. The result presented in [40] has been checked by an independent calculation as a part of this work, the individual steps of which are outlined below.

General Structure

Inserting the generic four-quark operator $\mathcal{Q} = (\bar{s}_i\Gamma^1)_{\tilde{\nu}}(b_i)_{\tilde{\mu}}(\bar{q}_j\Gamma^2)_{\tilde{\alpha}}(q_j)_{\tilde{\beta}}$, the diagrams shown in Fig. 9.3 give rise to an amplitude of the form

$$i\mathcal{M} = \frac{e^2 g_s^2 Q_q}{Eq^2}\frac{C_F}{2N}\bar{v}\gamma_\mu u \iint \frac{du\,d\omega}{\bar{u}\,\omega}\,(L^{\eta\mu}\Gamma^2)_{\tilde{\beta}\tilde{\alpha}}(\Phi^B\gamma_\eta\Phi^K\Gamma^1)_{\tilde{\mu}\tilde{\nu}} \tag{9.7}$$

At this, $\{\tilde{\alpha},\tilde{\beta},\tilde{\nu},\tilde{\mu}\}$ denote spinor, $\{i,j\}$ colour, and $\{\eta,\mu\}$ Lorentz indices. Furthermore, Q_q is the charge quantum number of the quark in the loop, and $\Phi^K(u)$ and $\Phi^B(\omega)$ are the momentum space projectors, defined in (3.72) and (3.83), respectively. Note that, in the present context, the projector $\phi_+(\omega)$ in Φ^B multiplies $\not{n}_-$: The amplitude depends (only) on the "minus" component of the spectator quark momentum p_s, namely via the denominator of the gluon propagator $k'^2 = -2\bar{u}k\cdot p_s = -2\bar{u}\omega E$.

Feynman Parameters

Since the two diagrams in Fig. 9.3 are related by symmetry, it is advantageous to treat them together. Then, regardless of the concrete operator $\mathcal{Q}$, the loop contribution $L^{\eta\mu}$ can always be written as ($\gamma_\alpha m_q^\alpha \equiv m_q, \int_{p_i} = \int d^D p_i/(2\pi)^D$)

$$i\left[\gamma^\alpha\gamma^\eta\gamma^\beta\gamma^\mu\gamma^\gamma - \gamma^\gamma\gamma^\mu\gamma^\beta\gamma^\eta\gamma^\alpha\right]\int_{p'}\frac{(p'+m_q)_\alpha}{p'^2-m_q^2}\,\frac{(p'+k'+m_q)_\beta}{(p'+k')^2-m_q^2}\,\frac{(p'+k'+q+m_q)_\gamma}{(p'+k'+q)^2-m_q^2} \tag{9.8}$$

where each Dirac structure corresponds to one of the two diagrams in Fig. 9.3. As for the second diagram (b), this requires a substitution, e.g. $p' = -p'' - q - k$ (afterwards p'' is relabeled as p') and exploits the fact that m_q enters the amplitude only quadratically (this becomes apparent in (9.18)), for this allows to replace $m_q \to -m_q$.

Using the Feynman parametrization

$$\frac{1}{ABC} = \int_0^1\!\!\int_0^1 \frac{2x\,dx\,dy}{\left[(Axy + B(1-y)x + C(1-x)\right]^3} \tag{9.9}$$

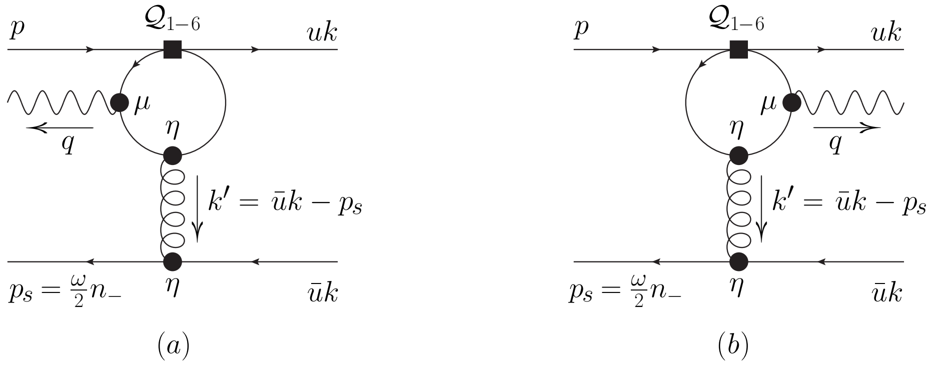

Figure 9.3: $\bar{B} \to \bar{K}\ell^+\ell^-$ at NNLO: Hard spectator scattering $\propto \phi_+(\omega)$.

the loop contribution $L^{\eta\mu} = (9.8)$ assumes the form

$$L^{\eta\mu} \;=\; i\big[\gamma^\alpha\gamma^\eta\gamma^\beta\gamma^\mu\gamma^\gamma - \gamma^\gamma\gamma^\mu\gamma^\beta\gamma^\eta\gamma^\alpha\big]\int_0^1\!\!\int_0^1\!\!\int_l \frac{2x\,dx\,dy}{\big(l^2 - a^2\big)^3}\,(\bar{\Lambda} - k')^\alpha\bar{\Lambda}^\beta(\bar{\Lambda} + q)^\gamma \tag{9.10}$$

where ($s = q^2/m_B^2,\, t = m_q^2/m_B^2,\, \bar{u} = 1 - u$)

$$l \;=\; p' + k'(1 - xy) + q(1 - x) \tag{9.11}$$

$$a^2 \;=\; m_B^2\big[t - x(1 - x)(s + y\bar{u}(1 - s))\big] \tag{9.12}$$

$$\Lambda \;\equiv\; \bar{\Lambda} - l - m_q \;=\; k'xy - q(1 - x) \tag{9.13}$$

Performing the momentum integration is now straight forward ($D = 4 - 2\epsilon$)

$$\int_l \frac{l^2}{\big(l^2 - a^2\big)^3} \;=\; \frac{i\Gamma(\epsilon)}{(4\pi)^{2-\epsilon}}\big(1 - \tfrac{\epsilon}{2}\big)a^{-2\epsilon} \qquad\qquad \int_l \frac{1}{\big(l^2 - a^2\big)^3} \;=\; \frac{-i}{(4\pi)^2}\frac{1}{2a^2} \tag{9.14}$$

Divergent Term

After exploiting the symmetry constraint $l^\alpha l^\beta \to l^2 g^{\alpha\beta}/D$, the (potentially) divergent part of $L^{\eta\mu}$ consists of the terms proportional to l^2. Collecting these terms and performing the momentum integration, one finds

$$\big(1 - \tfrac{\epsilon}{2}\big)\big[\gamma^\alpha\gamma^\mu\gamma^\eta - \gamma^\eta\gamma^\mu\gamma^\alpha\big]\int_0^1\!\!\int_0^1\!\!\int_l \frac{x\,dx\,dy\,l^2}{\big(l^2 - a^2\big)^3}\big[(3 + 2\epsilon)\Lambda - k' + q\big]^\alpha \tag{9.15}$$

$$= \;\frac{i\Gamma(\epsilon)}{(4\pi)^{2-\epsilon}}\big[\gamma^\alpha ...\big](1 - \epsilon)\int_0^1\!\!\int_0^1 \frac{dx\,dy}{a^{2\epsilon}}\big[(3x^2y - x)k' + (3x^2 - 2x)q + 2\epsilon\Lambda x\big]^\alpha \tag{9.16}$$

$$= \;\frac{i}{(4\pi)^2}\big[\gamma^\alpha ...\big]\int_0^1\!\!\int_0^1 dx\,dy\Big[\ln a^{-2}\big[(3x^2y - x)k' + (3x^2 - 2x)q\big] + 2\Lambda x\Big]^\alpha \tag{9.17}$$

As expected by gauge invariance, the divergences of the two diagrams, that is to say, the $1/\epsilon$ terms in (9.17), cancel each other out, resulting in the finite expression (9.17). In consequence, the remaining part of the calculation can be done in $D = 4$ dimensions, which in turn implies that the two diagrams combined are independent of the chosen operator basis.

Dirac Structure

Assuming for now that the generic operator $\mathcal{Q} = (\bar{s}_i b_j)_{V-A}(\bar{q}_j q_i)_{V\pm A}$ is inserted in (9.7), the two Dirac structures stay separate, each of them becoming a trace. Exploiting the invariance of the trace under cyclic permutations in combination with the reverse identity $\mathrm{tr}[\gamma^\alpha\gamma^\beta\gamma^\gamma...] = \mathrm{tr}[...\gamma^\gamma\gamma^\beta\gamma^\alpha]$, the loop trace simplifies to

$$\mathrm{tr}\Big[(\gamma^\alpha\gamma^\eta\gamma^\beta\gamma^\mu\gamma^\gamma - \gamma^\gamma\gamma^\mu\gamma^\beta\gamma^\eta\gamma^\alpha)\gamma^\nu(1\pm\gamma_5)\Big] \;=\; \mp 2\,\mathrm{tr}\Big[\gamma^\nu\gamma^\alpha\gamma^\eta\gamma^\beta\gamma^\mu\gamma^\gamma\gamma_5\Big] \tag{9.18}$$

It now becomes crucial that the number of γ matrices in (9.18) can always be reduced to four: In the nontrivial case where all three indices $\alpha\beta\gamma$ are contracted with momenta q, k', this can be achieved by using identities of the general form $..\not{q}\gamma^\eta\not{q}.. = ..(q^\eta\not{q} - q^2\gamma^\eta)...$ The trace (9.18) thus always gives a tensor $\varepsilon^{\nu\eta\mu p_x}$, which can only result in a non-zero contribution to the amplitude when contracted with another ε-tensor. Since this second tensor must come from the other trace, we may thus replace

$$\mathrm{tr}\Big[\Phi^B\gamma_\eta\Phi^K\gamma_\nu(1-\gamma_5)\Big] \;\overset{\rightarrow}{=}\; -\frac{i}{4}\,\phi(u)\phi_+(\omega)f_B f_K\,\varepsilon^{qk\nu\eta} \tag{9.19}$$

Contracting (9.18) with $(\bar{\Lambda} - k')^\alpha\bar{\Lambda}^\beta(\bar{\Lambda}+q)^\gamma$, one then finds (omitting terms $\propto q^\mu$)

$$\begin{aligned}\mathrm{tr}\Big[\gamma^\nu\gamma^\alpha\gamma^\eta\gamma^\beta\gamma^\mu\gamma^\gamma\gamma_5\Big]\varepsilon^{qk\nu\eta}(\bar{\Lambda}-k')^\alpha\bar{\Lambda}^\beta(\bar{\Lambda}+q)^\gamma \;=\; -8i\Big\{\frac{l^2}{2}\Big[(3+2\epsilon)\Lambda + q - k'\Big]\cdot q \\ - m_q^2\Big[\Lambda + q - k'\Big]\cdot q + \Lambda^{qqq}q^4 + \Big[\Lambda^{qkq}+\Lambda^{qqk}+\Lambda^{kqq}\Big]q^2(k\cdot q) + 2(k\cdot q)^2\Lambda^{qkk}\Big\}k^\mu\end{aligned} \tag{9.20}$$

where, in the l^2-term, the "ϵ" has only been kept if it actually leads to a finite contribution (in other words, terms $\propto \epsilon l^2(3\Lambda + q - k')$ have been dropped) and, for instance, Λ^{qkq} is the coefficient multiplying $q^\alpha k^\beta q^\gamma$ in $(\Lambda - k')^\alpha\Lambda^\beta(\Lambda+q)^\gamma \equiv \sum \Lambda^{p_ip_jp_k}p_i^\alpha p_j^\beta p_k^\gamma$. The coefficients $\Lambda^{p_ip_jp_k}$ appearing in (9.20) are explicitly given as

$$\Lambda^{qqq} \;=\; x(1-x)^2 \qquad\qquad \Lambda^{qqk} \;=\; (1-x)^2xy\bar{u} \tag{9.21}$$

$$\Lambda^{qkq} \;=\; -(1-x)x^2y\bar{u} \qquad\qquad \Lambda^{kqq} \;=\; (1-x)x(1-xy)\bar{u} \tag{9.22}$$

$$\Lambda^{qkk} \;=\; (x-1)x^2y^2\bar{u}^2 \tag{9.23}$$

Important Steps in the Calculation

Putting everything together, the most important steps leading to the Feynman amplitude of the operator $\mathcal{Q} = (\bar{s}_i b_j)_{V-A}(\bar{q}_j q_i)_{V\pm A}$ read ($\hat{u} = \bar{u}(1-s)$, omitting terms $\propto q^\mu$)

$$\frac{8\pi^2}{m_B^2}\int\frac{d\omega}{\omega}\,(L^{\eta\mu}\Gamma^2)_{\tilde{\alpha}\tilde{\alpha}}\,(\Phi^B\gamma_\eta\Phi^K\Gamma^1)_{\tilde{\nu}\tilde{\nu}} \;=\; \mp\frac{8\pi^2 f_B f_K}{m_B^2\,\lambda_+}\,\phi(u)\int_0^1\!\!\int_0^1\!\!\int_l\frac{x\,dx\,dy}{\left(l^2-a^2\right)^3}\cdot(9.20) \tag{9.24}$$

$$\begin{aligned}
&= \mp\frac{f_B f_K}{\lambda_+}\,k^\mu\phi(u)\int_0^1\!\!\int_0^1 dx\,dy\,x\left\{\frac{4\Lambda\cdot q}{m_B^2} - \frac{2\ln a^2}{m_B^2}\Big[3\Lambda+q-k'\Big]\cdot q + \frac{2t}{a^2}\Big[\Lambda+q-k'\Big]\cdot q\right.\\
&\qquad\left. - \frac{m_B^2}{a^2}\Big[2\Lambda^{qqq}s^2 + \big(\Lambda^{qkq}+\Lambda^{qqk}+\Lambda^{kqq}\big)\hat{u}s + \hat{u}^2\Lambda^{qkk}\Big]\right\}
\end{aligned}\tag{9.25}$$

$$\begin{aligned}
&= \mp\frac{f_B f_K}{\lambda_+}\,k^\mu\phi(u)\left\{\frac{\hat{u}-2s}{3} - 3\hat{u}\tilde{Y}^1_{2,0} + 6s\tilde{Y}^0_{1,1} + (\hat{u}-2s)\tilde{Y}^0_{1,0}\right.\\
&\qquad\left. + \Big[\hat{u}Y^1_{2,0} - \hat{u}Y^0_{1,0} + 2sY^0_{2,0}\Big] - \frac{1}{t}\Big[2s^2Y^0_{2,2} + 2s\hat{u}Y^0_{2,1} - 3s\hat{u}Y^1_{3,1} - \hat{u}^2Y^2_{3,1}\Big]\right\}
\end{aligned}\tag{9.26}$$

$$\begin{aligned}
&= \mp\frac{f_B f_K}{\lambda_+}\,k^\mu\phi(u)\left\{\frac{\hat{u}-5s}{6} + \frac{s}{2\hat{u}}(\hat{u}+s)X^{10}_{0,0} + \frac{t}{\hat{u}}\Big[2\hat{u}X^1_{0,0} - (\hat{u}+s)X^{10}_{-1,0}\Big]\right.\\
&\qquad\left. + \frac{t}{\hat{u}}\Big[(\hat{u}-s)X^{10}_{-1,0} - \hat{u}X^1_{0,0}\Big] + \left[\frac{s}{2\hat{u}}(\hat{u}+s)X^{10}_{0,0} - tX^1_{0,0} - \frac{\hat{u}+s}{6}\right]\right\}
\end{aligned}\tag{9.27}$$

$$= \pm\frac{f_B f_K}{\lambda_+}\,k^\mu\phi(u)\,\frac{s\hat{u}}{4}\,t_\parallel(s,t,u) \tag{9.28}$$

The integration over Feynman parameters (last 2 steps) as well as the functions appearing in (9.26) – (9.27) are discussed in appendix F. The corresponding matrix element is then found to be

$$\big\langle\bar{M}\ell^+\ell^-\big|(\bar{s}_i b_j)_{V-A}(\bar{q}_j q_i)_{V\pm A}\big|\bar{B}\big\rangle \;=\; \pm\alpha\alpha_s Q_q\,\frac{C_F}{2N}\,\frac{f_B f_K}{m_B\,\lambda_+}\,\bar{v}\not{k}u\int du\,\phi(u)t_\parallel(s,t,u) \tag{9.29}$$

where

$$t_\parallel(s,t,u) \;=\; \frac{4t}{\bar{u}^2(1-s)^2}\left[F^2\Big(\frac{4t}{\bar{u}+us}\Big) - F^2\Big(\frac{4t}{s}\Big)\right] - \frac{4}{s} \tag{9.30}$$

$$F(x) \;=\; \ln\frac{1+\sqrt{1-x}}{1-\sqrt{1-x}} - \frac{\bar{u}+us}{2t}\sqrt{1-x} - i\pi \tag{9.31}$$

Contribution to the effective coefficient $\mathcal{C}_9^{\mathit{eff}}$

If we would use the operator basis $\{\mathcal{O}_i\}$, the structure of Wilson coefficients C_{1-6} would be identical with the one in the OPE term $\mathcal{K}_5^{\mu}$, given in (5.18). Since Δ_+^{spec} is independent from the chosen operator basis, just by using the transformation matrix (D.65) the correct expression corresponding to the operator basis $\{\mathcal{Q}_i\}$ can be obtained ($t_q \equiv t_{\|}(q^2, m_q, u)$)

$$\Delta_+^{\text{spec}} = \frac{-\pi\alpha_s(\mu)C_F}{2N}\frac{f_B f_K}{f_+(q^2)\lambda_+ m_B}\int du\,\phi(u)\Big\{Q_u t_c(\mathcal{C}_2 - \frac{\mathcal{C}_1}{2N})$$

$$+ Q_d(t_b + t_0)(\mathcal{C}_3 - \frac{\mathcal{C}_4}{2N} + 16\mathcal{C}_5 - \frac{8}{N}\mathcal{C}_6) + 6\mathcal{C}_6(Q_d t_b + Q_u t_c)\Big\} \tag{9.32}$$

As with the other spectator term, Δ_+^{spec} has to be evaluated at $\mu_h = \sqrt{\mu/2}$ and becomes power-suppressed at high-q^2. Finally, note that (9.32) is in agreement with the result presented in [40].

9.2.4 Two-Loop Contributions

The two-loop diagrams contributing to the NNLO decay rate of $\bar{B} \to \bar{K}\ell^+\ell^-$ are displayed in Fig. 9.4 (a)-(b). The corresponding matrix elements are usually expressed as

$$\langle s\,\ell^+\ell^-|\,\mathcal{Q}_i\,|b\rangle_{\text{2-loop}} = -\Big(\frac{\alpha_s}{4\pi}\Big)^1 F_i^{(7)}\langle\mathcal{Q}_7\rangle_{\text{tree}} - \Big(\frac{\alpha_s}{4\pi}\Big)^2 F_i^{(9)}\langle\mathcal{Q}_9\rangle_{\text{tree}} \tag{9.33}$$

Neglecting the penguin contributions on account of the small coefficients $\mathcal{C}_{3-6}$, the correction to the effective coefficient $\mathcal{C}_9^{\mathit{eff}}$ is then given as

$$\Delta^{\text{2-loop}} = -\frac{\alpha_s(\mu)}{4\pi}\left[\frac{2m_b}{m_B}(\mathcal{C}_1 - 2N\mathcal{C}_2)F_1^{(7)} + \mathcal{C}_1 F_1^{(9)} + \mathcal{C}_2 F_2^{(9)}\right] \tag{9.34}$$

The functions $F_{1-2}^{(7,9)}$ have been presented as expansions in $\hat{s} = q^2/m_b^2$, $z = m_c^2/m_b^2$ and $\hat{s}/(4z)$ in [78, 79, 80, 81]. Consequently, these expansions are valid in the domain of high recoil or, more precisely, in the energetic range $0.05 \leqslant \hat{s} \leqslant 0.25$. In the domain of low recoil, on the other hand, we will rely on the results presented in [45]. The provided expansions in m_c^2/m_b^2, which go up to the tenth order, show a good convergence behaviour for $\hat{s} > 0.6$ [45], and thus can be used in our entire high-q^2 region $s \geqslant 15\text{GeV}/m_B^2$. In short, the MATHEMATICA input files attached to [45], which contain the low as well as the high recoil results just mentioned, are employed for the numerical analysis.

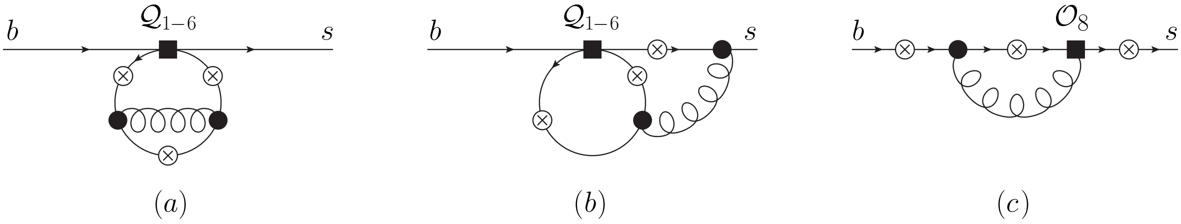

Figure 9.4: $\bar{B} \to \bar{K}\ell^+\ell^-$ at NNLO: Diagrams related by symmetry to (b) and (c) are not shown. The crossed circles $\otimes$ denote possible insertion points for the electromagnetic current operator $j^\mu = \sum_q Q_q\,(\bar{q}\gamma^\mu q)$.

Dependence on Scheme of Charm Mass

The authors of [45] provide functions $F_{1,2}^{(9)}$, which correspond to the pole scheme of the charm mass, along with functions $\triangle_{1,2}^{(9)}$, which have to be added to the pole functions in order to obtain the corresponding $\overline{MS}$ functions $\bar{F}_{1,2}^{(9)}$. The $\triangle_{1,2}^{(9)}$ can also be calculated from the relation between pole and $\overline{MS}$ mass

$$\bar{m}_c(\mu_c) \;=\; m_c\Big(1 + \frac{\alpha_s(\mu_c)}{4\pi}\,C_F\Big[3\ln\frac{m_c^2}{\mu_c^2} - 4\Big] + \mathcal{O}(\alpha_s^2)\Big) \tag{9.35}$$

and the fact that the effective coefficient $\mathcal{C}_9^{\text{eff}}$ must be scheme independent to the given order in α_s: $(x = 4m_q^2/q^2, \partial_x h(x,\mu) = -f(x)/3)$

$$\triangle_1^{(9)}(\bar{m}_c) \;\equiv\; \bar{F}_1^{(9)}(\bar{m}_c) - F_1^{(9)}(m_c) \;=\; \frac{4\pi}{\alpha_s(\mu_b)}\,C_F\Big[h_c(\bar{m}_c) - h_c(m_c)\Big] \tag{9.36}$$

$$= \frac{4\pi}{\alpha_s(\mu_b)}\,C_F\,\frac{\partial h(q^2,m_c)}{\partial m_c}\Big[\bar{m}_c(\mu_c) - m_c\Big] \tag{9.37}$$

$$= -\frac{2}{3}\,C_F^2\,x f(x)\,\frac{\alpha_s(\mu_c)}{\alpha_s(\mu_b)}\Big[3\ln\frac{m_c^2}{\mu_c^2} - 4\Big] \tag{9.38}$$

where $h(q^2, m_q)$ and $f(q^2, m_q)$ are the functions defined in (5.16) and (5.19), respectively. In addition, it is evident from the above that $\triangle_2^{(9)} = \triangle_1^{(9)}/C_F$.

9.2.5 Chromomagnetic Contributions

The 1-loop contributions of the operator $\mathcal{Q}_8$, shown in Fig. 9.4 (c), can be written as

$$\langle\, s\,\ell^+\ell^-\,|\,\mathcal{Q}_8\,|\,b\,\rangle_{\text{1-loop}} \;=\; -\Big(\frac{\alpha_s}{4\pi}\Big)^1 F_8^{(7)}\langle\mathcal{Q}_7\rangle_{\text{tree}} - \Big(\frac{\alpha_s}{4\pi}\Big)^2 F_8^{(9)}\langle\mathcal{Q}_9\rangle_{\text{tree}} \tag{9.39}$$

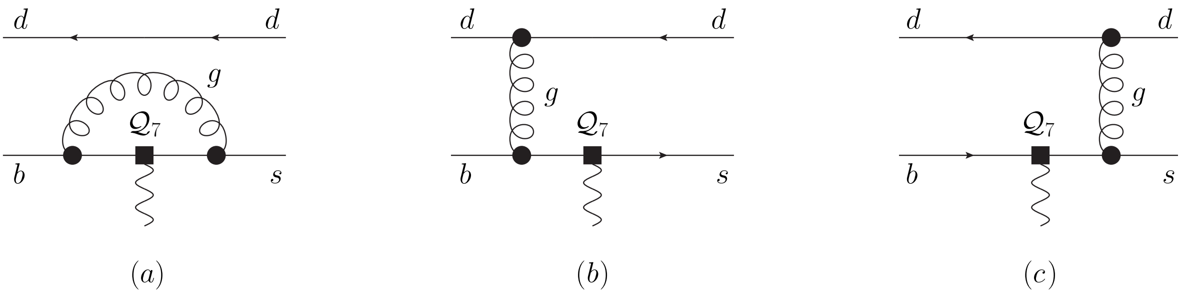

Figure 9.5: $\bar{B} \to \bar{K}\ell^+\ell^-$ at NNLO: Symmetry-breaking corrections to the $B \to K$ form factor relations. Diagram (a) displays the vertex correction; the diagrams (b) and (c) the corrections due to hard spectator scattering.

Similar to before, the corresponding correction to the effective coefficient $\mathcal{C}_9^{\text{eff}}$ reads

$$\Delta_8 \;=\; -\frac{\alpha_s(\mu)}{4\pi}\,\mathcal{C}_8\left[\frac{2m_b}{m_B}\,F_2^{(7)} \;+\; F_8^{(9)}\right] \tag{9.40}$$

The analytic expressions for the $F_8^{(7,9)}$ presented in [45] are fairly simple and hence can be given explicitly:

$$\begin{aligned} F_8^{(7)} \;=\;& \frac{4\pi^2}{27}\,\frac{2+\hat{s}}{(1-\hat{s})^4} - \frac{4}{9}\,\frac{11-16\hat{s}+8\hat{s}^2}{(1-\hat{s})^2} - \frac{8}{9}\,\frac{\sqrt{\hat{s}}\,\sqrt{4-\hat{s}}}{(1-\hat{s})^3}(9-5\hat{s}+2\hat{s}^2)\arcsin\left(\frac{\sqrt{\hat{s}}}{2}\right) \\ & - \frac{16}{3}\,\frac{2+\hat{s}}{(1-\hat{s})^4}\arcsin^2\left(\frac{\sqrt{\hat{s}}}{2}\right) - \frac{8\hat{s}}{9(1-\hat{s})}\ln\hat{s} - \frac{32}{9}\ln\frac{\mu}{m_b} - \frac{8}{9}\pi i \end{aligned} \tag{9.41}$$

$$\begin{aligned} F_8^{(9)} \;=\;& -\frac{8\pi^2}{27}\,\frac{4-\hat{s}}{(1-\hat{s})^4} + \frac{8}{9}\,\frac{5-2\hat{s}}{(1-\hat{s})^2} + \frac{16}{9}\,\frac{\sqrt{4-\hat{s}}}{\sqrt{\hat{s}}\,(1-\hat{s})^3}(4+3\hat{s}-\hat{s}^2)\arcsin\left(\frac{\sqrt{\hat{s}}}{2}\right) \\ & + \frac{32}{3}\,\frac{4-\hat{s}}{(1-\hat{s})^4}\arcsin^2\left(\frac{\sqrt{\hat{s}}}{2}\right) + \frac{16}{9(1-\hat{s})}\ln\hat{s} \end{aligned} \tag{9.42}$$

These findings are valid for arbitrary $\hat{s} = q^2/m_b^2$. In particular, both functions are finite at and holomorphically extendable over $\hat{s} = 1$.

9.2.6 Corrections to Form Factor Ratio f_T/f_+

Though the contribution from $\mathcal{Q}_7$ itself remains unchanged at NNLO, the form factor relation (3.60) (which we intend to use), describing the ratio $f_T(q^2)/f_+(q^2)$, receives $\mathcal{O}(\alpha_s)$ corrections from the diagrams in Fig. 9.5. The calculation yields [25]

$$\frac{f_T(s)}{f_+(s)} \;=\; (1+\sqrt{r})\left(1 + \frac{\alpha_s(\mu)C_F}{4\pi}\left[\ln\frac{m_b^2}{\mu^2} + 2L\right] - \frac{\alpha_s(\mu_H)C_F}{4\pi}\,\frac{m_B}{2E}\,\frac{\Delta F_K}{\zeta_K}\right) \tag{9.43}$$

where

$$\zeta_K(m_B, E) = \left(\frac{m_B}{2E}\right)^2 f_+^K(0) \qquad\qquad L \equiv \frac{s-1}{s}\ln(1-s) \tag{9.44}$$

and ($\bar{u} = 1 - u$)

$$\Delta F_K = \frac{8\pi^2 f_B f_K}{N m_B}\lambda_+^{-1}\int du\,\frac{\phi(u)}{\bar{u}} \tag{9.45}$$

Note that the vertex diagram gives rise to the first; the hard spectator diagrams to the second correction term in (9.43). In consequence, the first term has to be evaluated at the usual renormalization scale $\mu \sim m_b$, whereas the second at the hard scattering scale $\mu_H = 1.47\text{GeV}$ [25]. Furthermore, only the second term is power suppressed at high-q^2.

9.3 Numerical Results

First, the $B \to K\nu\bar{\nu}$ and $B \to K\ell^+\ell^-$ branching fraction are considered separately. This includes a short review of the current experimental situation and the presentation of the corresponding Standard Model predictions. We then proceed to discuss the numerical results for the precision observables.

9.3.1 Integrated $B \to K\nu\bar{\nu}$ Branching Fraction

In case of the neutrino mode, the current experimental results only allow for the specification of upper bounds [75, 82]

$$\mathcal{B}(B \to K\nu\bar{\nu})_{exp} < 17\cdot 10^{-6} \tag{9.46}$$

$$\mathcal{B}(B^0 \to K^0\nu\bar{\nu})_{exp} < 49\cdot 10^{-6} \tag{9.47}$$

$$\mathcal{B}(B^+ \to K^+\nu\bar{\nu})_{exp} < 16\cdot 10^{-6} \tag{9.48}$$

Assuming the Standard Model, the fully integrated $B^+ \to K^+\nu\bar{\nu}$ branching fraction is expected to be

$$\mathcal{B}(B^+ \to K^+\nu\bar{\nu})_{th} = (4.83^{+1.43}_{-1.24}[f_+(0)]^{+0.55}_{-0.51}[a_0]^{+0.15}_{-0.19}[b_1])\cdot 10^{-6} \tag{9.49}$$

$$= (4.8^{+1.5}_{-1.4})\cdot 10^{-6} \tag{9.50}$$

It is noteworthy that the prediction for the neutrino mode is essentially free of perturbative uncertainties. The overall form factor uncertainty of $\pm 31\%$, on the other hand, is quite substantial.

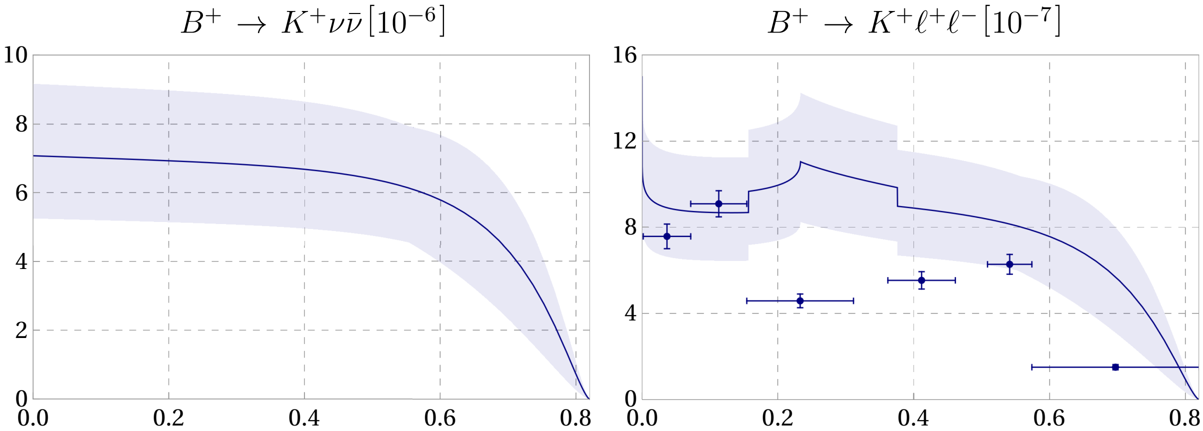

Figure 9.6: NNLO differential branching fractions $(d\mathcal{B}/ds)(s)$ of the rare decays $B^+ \to K^+\nu\bar{\nu}$ (left) and $B^+ \to K^+\ell^+\ell^-$ (right) as functions of s: The shaded areas correspond to a separate variation of the form factor parameters in the intervals specified in (B.16) and (B.18); the data points represent the experimental data provided by the HFAG [75, 82]. The discontinuity in the $B \to K\ell^+\ell^-$ branching fraction stems from switching off the 2-loop functions in the interval $0.25 \leqslant \hat{s} \leqslant 0.6$.

9.3.2 Integrated $B \to K\ell^+\ell^-$ Branching Fraction

At present, the different $B \to K\ell^+\ell^-$ branching fractions are measured to be [75, 82]

$$\mathcal{B}(B \to K\ell^+\ell^-)_{exp} = (0.48 \pm 0.04) \cdot 10^{-6} \tag{9.51}$$

$$\mathcal{B}(B^0 \to K^0\ell^+\ell^-)_{exp} = (0.31\,^{+0.08}_{-0.07}) \cdot 10^{-6} \tag{9.52}$$

$$\mathcal{B}(B^+ \to K^+\ell^+\ell^-)_{exp} = (0.51 \pm 0.05) \cdot 10^{-6} \tag{9.53}$$

With respect to theoretical predictions for $B \to K\ell^+\ell^-$, it is reminded that the two-loop functions $F_{1-2}^{(7,9)}$ are only known in expanded form. As mentioned before, there is a middle domain, specified in [45] as $0.25 \leqslant \hat{s} \leqslant 0.6$, where neither of the two available expansions should be used. If not explicitly mentioned otherwise, the two-loop functions are therefore set to zero in this domain. Fortunately, this domain largely coincides with the part of the spectrum dominated by the narrow charmonium resonances, roughly $0.25 \leqslant s \leqslant 0.6$ [29], which is frequently cut from the spectrum anyway. It is, however, stressed that both these kinematic regions are not precisely defined and, to some extent, arbitrary.

This being said, our SM prediction for the entire branching fraction reads

$$\mathcal{B}(B^+ \to K^+\ell^+\ell^-)_0^{s_{max}} \cdot 10^8 = 65.6^{+2.9}_{-1.8}[\mu]^{+19.2}_{-16.8}[f_+(0)]^{+7.4}_{-6.8}[a_0]^{+2.0}_{-2.5}[b_1] \tag{9.54}$$

$$= 65.6^{+2.9}_{-1.8}(\text{scale})\,^{+20.7}_{-18.3}(\text{hadronic}) \tag{9.55}$$

where, as expected, the perturbative uncertainty of 4% is small in comparison to the

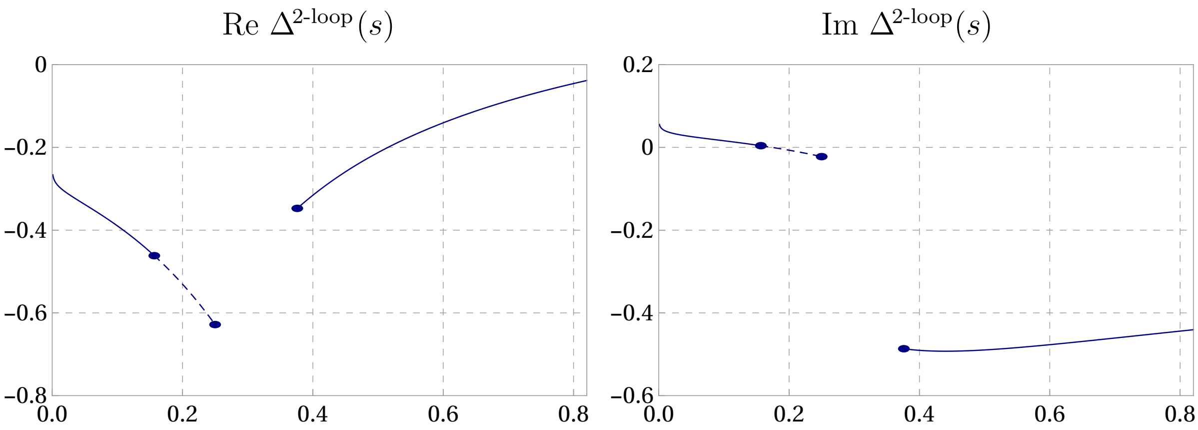

Figure 9.7: Real (left) and imaginary part (right) of $\Delta^{\text{2-loop}}$ as functions of s: The dots mark the points $\hat{s} = 1/4$, $s = 1/4$ and $\hat{s} = 3/5$. In the dashed segments, the low-q^2 expansions of the two-loop functions $F_{1-2}^{(7,9)}$ are less reliable, which motivates the comparison (9.57) – (9.58).

hadronic uncertainty of 32%.

The numerical results for the individual standard bins are collected in Tab. 9.1. While the hadronic uncertainty is consistently found at the 30% level, with respect to the perturbative uncertainty, the picture is more diverse: In observables where the two-loop functions can fully be used the scale dependency is reduced to $2-3\%$, or even below 1% (first bin). In particular the third bin (which should be considered a NLO prediction), however, suffers from a large perturbative uncertainty of 11%.

Impact of Two-Loop Term

In order to investigate the impact of the two-loop term $\Delta^{\text{2-loop}}$, the cut point

$$s_c \;=\; (m_b/m_B)^2/4 \;\approx\; 0.16 \tag{9.56}$$

is introduced. It is then instructive to compare the two results

$$\mathcal{B}(B^+ \to K^+\ell^+\ell^-)_{s_c}^{0.25} \;=\; (9.47^{+0.99}_{-0.90}[\mu]\,^{+2.78}_{-2.43}[f_+(0)]\,^{+0.52}_{-0.51}[a_0]\,^{+0.03}_{-0.05}[b_1])\cdot 10^{-8} \tag{9.57}$$

$$\tilde{\mathcal{B}}(B^+ \to K^+\ell^+\ell^-)_{s_c}^{0.25} \;=\; (8.36^{+0.26}_{-0.24}[\mu]\,^{+2.46}_{-2.14}[f_+(0)]\,^{+0.46}_{-0.45}[a_0]\,^{+0.03}_{-0.04}[b_1])\cdot 10^{-8} \tag{9.58}$$

where $\tilde{\mathcal{B}}$ continues to use the low-q^2 expansions of the two-loop functions $F_{1-2}^{(7,9)}$ up to the endpoint $s = 0.25$.

In consequence, the partial branching fraction $\tilde{\mathcal{B}}$ is decreased by roughly 10%, and, formally, the perturbative uncertainty is reduced from 10% down to 3%. Since, however, the expansions used for the functions $F_{1-2}^{(7,9)}$ are not as reliable between $s_c \leqslant s \leqslant 0.25$, the actual perturbative uncertainty of (9.58) is larger for sure.

$q^2[(\text{GeV}/c^2)^2]$	$0.00 - 2.00$	$2.00 - 4.30$	$4.30 - 8.68$	$10.09 - 12.86$
$\mathcal{B}(B^+ \to K^+\ell\ell)_{exp}$	5.3 ± 0.4	7.5 ± 0.5	7.2 ± 0.5	5.5 ± 0.4
$\mathcal{B}(B^+ \to K^+\ell\ell)_{th}$	$6.49^{+0.05}_{-0.00}{}^{+1.89}_{-1.65}$	$7.17^{+0.14}_{-0.10}{}^{+2.13}_{-1.86}$	$16.17^{+1.73}_{-1.58}{}^{+4.85}_{-4.25}$	$8.91^{+0.27}_{-0.09}{}^{+2.83}_{-2.51}$
$\mathcal{R}_{th}$	$778^{+0}_{-6}{}^{+3}_{-4}$	$804^{+11}_{-15}{}^{+0.5}_{-0.4}$	$670^{+72}_{-65}{}^{+1.4}_{-1.8}$	$741^{+8}_{-22}{}^{+2}_{-2}$
$q^2[(\text{GeV}/c^2)^2]$	$14.18 - 16.00$	> 16.00	$1.00 - 6.00$	$0.00 - max$
$\mathcal{B}(B^+ \to K^+\ell\ell)_{exp}$	4.1 ± 0.3	3.7 ± 0.3	$12.6^{+0.9}_{-0.8}$	48 ± 4
$\mathcal{B}(B^+ \to K^+\ell\ell)_{th}$	$5.31^{+0.09}_{-0.00}{}^{+1.83}_{-1.64}$	$12.38^{+0.27}_{-0.01}{}^{+4.85}_{-4.38}$	$16.31^{+0.75}_{-0.62}{}^{+4.85}_{-4.23}$	$65.58^{+2.86}_{-1.82}{}^{+20.68}_{-18.25}$
$\mathcal{R}_{th}$	$761^{+0}_{-12}{}^{+1}_{-2}$	$768^{+1}_{-16}{}^{+1}_{-1}$	$768^{+31}_{-34}{}^{+0.9}_{-0.8}$	$736^{+21}_{-31}{}^{+1.7}_{-2.1}$

Table 9.1: Results for the individual standard bins: Experimental measurements [75, 82] (HFAG) and SM predictions for the partial branching fractions of $B^+ \to K^+\ell^+\ell^-$ in units of 10^{-6}; precision observables (9.59) in units of 10^{-2}. The theoretical uncertainties correspond to the perturbative (first) and the combined form factor uncertainty (second), respectively.

9.3.3 Precision Observables

As precision observables we take ratios of the two branching fractions both integrated over the same range in s

$$\mathcal{R}_a^b \equiv \frac{\int_a^b ds\, d\mathcal{B}(B \to K\nu\bar{\nu})/ds}{\int_a^b ds\, d\mathcal{B}(B \to K\ell^+\ell^-)/ds} \tag{9.59}$$

An integration over the entire spectrum $0 \leqslant q^2 \leqslant (m_B - m_K)^2$ yields

$$\mathcal{R}_0^{s_{max}} = 7.36^{+0.21}_{-0.31}[\mu]^{+0.013}_{-0.018}[f_+(0)]^{+0.007}_{-0.007}[a_0]^{+0.007}_{-0.008}[b_1] \tag{9.60}$$

$$= 7.36^{+0.21}_{-0.31}(\text{scale})^{+0.017}_{-0.021}(\text{hadronic}) \tag{9.61}$$

corresponding to a perturbative and hadronic uncertainty of 4% and 0.3%, respectively.

Results for the individual standard bins can be found in table (9.1), where, most notably, all ratios are found to be virtually free of form factor uncertainties. Since the perturbative uncertainty of the ratios is solely due to the $B^+ \to K^+\ell^+\ell^-$ branching fractions, it ranges in the same way between 1% and 10%.

Part V

Conclusions

Theory of $B \to M\ell^+\ell^-$ at high q^2

The amplitude of $\bar{B} \to \bar{M}\ell^+\ell^-$ decays, given in (4.1), contains the non-local term

$$\langle \mathcal{K}^\mu(q)\rangle \;\equiv\; -\frac{8\pi^2}{q^2}\, i\int d^4x\, e^{iq\cdot x}\,\langle \bar{M}(k)\big|T j^\mu(x)\mathcal{H}_h(0)\big|\bar{B}(p)\rangle \tag{9.62}$$

which stems from the hadronic part of the effective weak Hamiltonian $\mathcal{H}_h$. Although small in comparison to the semileptonic contributions (about 10%), precise theoretical predictions require reliable results for the matrix element (9.62) as well.

Operator Product Expansion

The OPE framework established in this work offers a systematic expansion of the decay amplitude in powers of $E/\sqrt{q^2}$ (or equivalently Λ_{QCD}/m_B). It thus allows for a theoretical computation of the correlator (9.62) in the low-recoil domain, where the QCDF formalism is no longer justified (somewhere above $q^2 \gtrsim 15\,\mathrm{GeV}^2$). The following aspects and findings of the OPE formalism presented in this work are most relevant:

- The OPE yields a series of local operators multiplied by coefficient functions, calculable in perturbation theory. The local operators are of increasing mass dimension $d \geqslant 3$ and composed of b quark fields in full QCD; the entire dependence on m_b, m_c and q^2, factorized into the coefficient functions, is retained.

- In the chiral limit $m_s = 0$ and up to operator dimension 4, a basis for the operators possibly appearing in the OPE is given by two dimension-3 operators of the form $\bar{s}_L\gamma^\mu b$ and $\bar{s}_L\sigma^{\mu q}b$. However, these two operators are equivalent at $d = 3$, and the second operator does not arise at $\mathcal{O}(\alpha_s^0)$.

- For $m_s \neq 0$, the operator basis has to be extended by two right-handed operators of the form $m_s\bar{s}_R\gamma^\mu b$ and $m_s\bar{s}_R\sigma^{\mu q}b$, formally counted as of dimension 4. Such operators, however, do not arise at α_s^0 and therefore can safely be neglected, as their impact is suppressed by a relative factor of $\alpha_s m_s/m_b \sim 0.5\%$.

- The above implies that the matrix element of any local operator of dimension $d \leqslant 4$ appearing in the OPE can be expressed in terms of the standard $B \to M$ form factors. This statement holds to any order in α_s and independently of whether the chiral limit is assumed.

- The OPE is explicitly performed up to operator dimension $d = 5$. Moreover, the coefficient functions of the weak annihilation term, a dimension-6 effect, are presented.

- In the chiral limit $m_s = 0$, the first genuine power corrections are due to dimension-5 operators of the general form $g_s \bar{s}_L (\Gamma_n G^a T^a)^\mu b$. They contain the gluon field strength tensor, and thus their matrix elements require, in general, the introduction of new, currently unknown, form factors.

- In the transition domain $\sqrt{q^2} \gg E \gg \Lambda$, however, the matrix element of the dimension-5 term can be calculated explicitly, or rather estimated, within the QCDF framework. The result differs (numerically and parametrically) from the direct QCDF approach by terms of order $E/\sqrt{q^2} \approx 0.3$ and has an an impact of 0.5% on the amplitude $\mathcal{A}_9^\mu$. Considering the power suppression $\sim 1/q^2$, this should hold qualitatively also towards the kinematic endpoint $E \sim \Lambda$.

- In the same way, the weak annihilation term is investigated and found to be completely negligible $< 0.1\%$.

Duality Violation

The other main obstacle to the precise theoretical prediction of the correlator (9.62) at high q^2 is the violation of quark-hadron duality, caused by the presence of charmonium resonances. Using Shifman's model [52], which understands the correlator as an infinite series of equidistant excitations, our investigation of global duality violation reveals:

- In order to clarify the analytic structure of the correlator, we have formally defined the OPE with the help of a spurion momentum, injected into the H^c vertex. Defined thus, q^2 can be varied while keeping E and m_B fixed at their physical values. It then becomes clear that the OPE is to be defined in the deep Euclidean domain and that duality violation is linked to the existence of the OPE through the terms exponentially suppressed for large imaginary q^2.

- The term linear and quadratic in the duality violating component are qualitatively different in their sensitivity to duality violation. The quadratic term is particularly susceptible to a small resonance width but represents an effect of second order in the charm-loop and, on this account, features a strong numerical suppression.

- The duality violation related uncertainty of the $B \to K\ell^+\ell^-$ decay rate integrated over the high-q^2 region is estimated at roughly $\pm 2\%$. This estimate is rather conservative, for it is based on the global use of the phenomenological value for the parameter $a_2 = 3$, which is substantially larger than the perturbative value. We thus assume a simplified analytic structure, where the different (oscillating) duality violating contributions add up coherently.

Conclusion

In conclusion, the high-q^2 region of $B \to M\ell^+\ell^-$ decays is theoretically well under control: The only non-perturbative quantities required for accurate predictions are the standard form factors; the impact of power-corrections and violations of quark-hadron duality is at the level of a few percent and thus negligible.

Phenomenology - Precision Observables

Theoretical predictions for exclusive $B \to M\ell^+\ell^-$ decays still suffer from large uncertainties in the relevant form factors. This problem is addressed in the second, phenomenological part of this work by investigating the quality of precision observables constructed from pairs of related decay channels.

In detail, we consider here the three decay pairs $B^+ \to \pi^+\mu^+\mu^-$ and $\bar{B}^0 \to \pi^+\ell^-\bar{\nu}$, $\bar{B} \to \bar{K}^*\ell^+\ell^-$ and $\bar{B} \to \bar{K}^*\nu\bar{\nu}$, as well as $\bar{B} \to \bar{K}\ell^+\ell^-$ and $\bar{B} \to \bar{K}\nu\bar{\nu}$, finding a reduction of the form factor uncertainties to 1.6%, 1% and 0.3% in the fully integrated π, K^* and K ratio, respectively. The corresponding perturbative uncertainties amount to 5%, 6% and 4%, respectively, and hence are significantly larger. On the other hand, these can still be reduced systematically.

Conclusion

The main conclusion is that the considered ratios are essentially free of hadronic uncertainties and, consequently, excellent probes for the search of NP. While, admittedly, the sensitivity to some NP is lost in the ratios, going to higher perturbative orders will ultimately allow for precision tests at the percent level.

Appendix

A Numerical Input

Apart from the CKM matrix, discussed below, the numerical values of the phenomenological input parameters are summarized in Tab. A.1.

CKM Matrix - Wolfenstein Parametrization and Global Fit

As far as the entries of the CKM matrix $V \equiv V_{\mathrm{CKM}}$ are concerned, it is reminded that, assuming the SM, there are just four independent observable parameters. This circumstance finds its expression in the well-known *Wolfenstein parametrization*

$$V = \begin{pmatrix} V_{ud} & V_{us} & V_{ub} \\ V_{cd} & V_{cs} & V_{cb} \\ V_{td} & V_{ts} & V_{tb} \end{pmatrix} = \begin{pmatrix} 1-\lambda^2/2 & \lambda & A\lambda^3(\rho - i\eta) \\ -\lambda & 1-\lambda^2/2 & A\lambda^2 \\ A\lambda^3(1-\rho-i\eta) & -A\lambda^2 & 1 \end{pmatrix} \tag{A.1}$$

which also showcases the hierarchic structure of the individual entries, known from experiments, through an expansion in the small quantity λ.

The *Wolfenstein parameters* can be determined most precisely by combining all available data in a global fit, whereby unitarity is imposed on the matrix. In this way, one finds [66]

$$\lambda = 0.22537 \pm 0.00061 \qquad A = 0.814 \pm^{0.023}_{0.024} \tag{A.2}$$

$$\bar{\rho} = 0.117 \pm 0.021 \qquad \bar{\eta} = 0.353 \pm 0.013 \tag{A.3}$$

where $(\bar{\rho} - i\bar{\eta}) = (\rho - i\eta)(1 - \lambda^2/2 + \ldots)$.

Unless explicitly stated otherwise, the numerical results presented in this work are based on the CKM matrix defined through (A.1) – (A.3) and not (A.4) – (A.5).

CKM Matrix - Individual Entries

For most semileptonic decays, only the magnitudes of the respective CKM-entries are relevant. At present, the individual entries are experimentally constraint as [66]

$$|V| = \begin{pmatrix} 0.97425 \pm 0.00022 & 0.2244 \pm 0.0024 & 0.00422 \pm 0.00042 \\ 0.225 \pm 0.008 & 0.986 \pm 0.016 & 0.0411 \pm 0.0013 \\ 0.0084 \pm 0.0006 & 0.0400 \pm 0.0027 & 1.021 \pm 0.032 \end{pmatrix} \tag{A.4}$$

Quark masses in MeV [66]					
$m_u^{\overline{MS}}(2\,\mathrm{GeV})$	$m_d^{\overline{MS}}(2\,\mathrm{GeV})$	$m_s^{\overline{MS}}(2\,\mathrm{GeV})$	$m_c^{\overline{MS}}(m_c)$	$m_b^{\overline{MS}}(m_b)$	$m_t^{\overline{MS}}(m_t)$
$2.3^{+0.7}_{-0.5}$	$4.8^{+0.5}_{-0.3}$	95(5)	1275(25)	4180(30)	$(167.2^{+3.8}_{-3.3})\cdot 10^3$

Masses of light mesons in MeV [66]					
m_{π^0}	$m_{\pi^\pm}$	$m_{K^\pm}$	m_{K^0}	$m_{K^{*\pm}}$	$m_{K^{*0}}$
134.9766(6)	139.57018(35)	493.677(16)	497.614(24)	891.66(26)	895.81(19)

Masses of B mesons in MeV [66]				
$m_{B^\pm}$	m_{B^0}	m_{B^*}	$m_{B_s^0}$	$m_{B_s^*}$
5279.26(17)	5279.58(17)	5325.2(4)	5366.77(24)	$5415.4^{+2.4}_{-2.1}$

Electroweak parameters [66]				
α_e	$G_F^2\,[\mathrm{GeV}^{-5}\,ps^{-1}]$	$M_W\,[\mathrm{GeV}]$	$M_Z\,[\mathrm{GeV}]$	$\sin^2\theta_W^{\overline{MS}}(M_Z)$
1/129	206.687	80.385(15)	91.1876(21)	0.23126(5)

Other phenomenological parameters [66]			
$\alpha_s(M_Z)$	$\Lambda_{\overline{MS},5}[\mathrm{MeV}]$	$(m_u + m_d)/2\,(2\,\mathrm{GeV})$	$\mu_\pi\,(2\,\mathrm{GeV})$
0.1185(6)	214^{+8}_{-7}	$3.5^{+0.7}_{-0.2}\,\mathrm{MeV}$	$2.8^{+0.2}_{-0.5}\,\mathrm{GeV}$

Table A.1: Numerical values of the different input parameters. The given values for u-, d-, and s-quark mass correspond to the "current quark" mass, the values for c-, b- and t-quark mass to the "running" mass of the respective quark.

The complex information contained in the CKM-matrix is then expressed in terms of the unitary triangle angles [66]

$$\alpha = (85.4^{+3.9}_{-3.8})^\circ \qquad \sin 2\beta = 0.682 \pm 0.019 \qquad \gamma = (68.0^{+8.0}_{-8.5})^\circ \tag{A.5}$$

which are determined, for example, from CP-violating processes. In the context of this work, however, we only require the angle α, which enters the $B^+ \to \pi^+\mu^+\mu^-$ branching fraction in form of the ratio

$$\frac{\lambda_u}{\lambda_t} = \left|\frac{V_{ud}^* V_{ub}}{V_{td}^* V_{tb}}\right| e^{i\pi(1+\alpha/180^\circ)} \tag{A.6}$$

B Hadronic Input

In this part of the appendix, the parametrizations employed for the form factors and distribution amplitudes are presented. While most of the input given in the previous section is purely phenomenological, the hadronic information that is required for the parametrizations can either be extracted from experimental data or, alternatively, determined by means of theoretical, albeit non-perturbative methods.

B.1 Form Factors

Since the form factor parametrization employed in this work are essentially rewritten versions of the ones presented in [9, 23], the two-step process in which the latter were obtained is briefly outlined below.

To begin with, the form factors are numerically determined using QCD sum rules on the light-cone. This step comes with a total uncertainty of $10 - 13\%$ at $q^2 = 0$, of which 7% are considered irreducible, that is intrinsic to the sum rule approach. With respect to the $K^{(*)}$, there is an additional uncertainty, introduced by the Gegenbauer coefficient $\alpha_1(K)$ (presently about 3%).

However, the numerical results obtained in this way are reliable only in the domain of high recoil $q^2 \lesssim 14\text{GeV}^2$. Also, this procedure does not yield simple expressions, which could be varied in a straightforward way. These issues can be addressed by fitting the sum rule data on parametrizations that are consistent with physical constraints, such as scaling laws [22, 47, 48] or the position of a physical pole.

It is then postulated that the fits correctly extrapolate the sum rule data to the entire spectrum. This expectation is based, firstly, on the proper analytic behaviour of the parametrizations, and, secondly, the stability of the fit parameters. The latter refers to the fact that the parameters are found to be rather insensitive to the particular choice of $q^2_{\max}$, which is the – somewhat arbitrary – point up to which the sum rule results are used as input. In concrete terms, the variation of $q^2_{\max}$ from 7GeV^2 to 14GeV^2 changes the form factor value at 20GeV^2 by 8% in the case of $T_2(q^2)$ and by $1-2\%$ in all other cases [9, 23].

The fits themselves are rather accurate, that is, the deviation of the employed parametrizations from the directly calculated values in the regime of low-q^2 stays below 2.5% for $T_2(q^2)$ and 1.2% for all other form factors. Thus, the overall uncertainty of the parametrizations taken from [9, 23] is roughly 15%.

B.1.1 Different Types of Parametrizations

In this work, form factors are in general parametrized as [29, 30]

$$f_i(s) \;=\; f_i(0)\,\frac{1-(b_{0i}+b_i-a_i b_{0i})s}{(1-b_{0i}s)(1-b_i s)} \;=\; f_i(0)\big(1+a_i b_{0i}s\big)+\mathcal{O}(s^2) \tag{B.1}$$

The main advantage of the form (B.1) over the parametrizations (B.2) and (B.4), employed in [9, 23], is that the parameters $f_i(0)$ and a_i have a clear graphical interpretation as normalization and gradient at $q^2=0$, respectively. This makes the behaviour of the precision observables (ratios of branching fractions) under variation of the form factor parameters, in particular $f_i(0)$, more transparent. Moreover, the ansatz (B.1) is more flexible, meaning it contains the other parametrizations, presented below, as special cases.

Apart from (B.1), we have the following parametrizations: The two-pole parametrization ($b_{0i}>b_i$, (B.2)), the double-pole parametrization ($b_{0i}=b_i$, (B.4)) and, lastly, the single-pole parametrization ($b_{0i}=0$). Note that, in case of the two-pole parametrization, the parameter b_{0i} always represents a physical pole and therefore is treated as fixed. Thus, in any case, there is one independent (variable, that is) pole parameter only.

Becirevic/Kaidalov: Two-Pole Parametrization $b_{0i} > b_i$

This parametrization, originally put forward by Becirevic and Kaidalov, reads [71]

$$f_+(x) \;=\; c_B\left(\frac{1}{1-x}-\frac{\alpha}{1-x/\gamma}\right) \qquad \text{where} \qquad x \;=\; \frac{q^2}{m^2_{B^*_{(s)}}} \tag{B.2}$$

It is used in the situation where the first pole of the form factor is known to stem from a particular meson and therefore treated as fixed. The second pole, an effective fit pole, then serves to subsume the contributions from the higher lying states ($\gamma > 1$).

The parameters of the parametrizations (B.1) and (B.2) are related by

$$f_i(0) \;=\; c_B(1-\alpha) \qquad a_i \;=\; \frac{1-\alpha/\gamma}{1-\alpha} \qquad b_{0i}/b_i \;=\; \gamma \tag{B.3}$$

It is pointed out that for $b_{0i}=b_i$ (B.1) becomes a double-pole parametrization, which is discussed next. The parametrization (B.2), on the other hand, collapses for $\gamma=1$ to a single pole.

Double-Pole Parametrization $b_{0i} = b_i$

In addition to the parametrization (B.2), the authors of [9, 23] also employ

$$f(q^2) \;=\; \frac{r_1}{1-q^2/m_1^2}+\frac{r_2}{(1-q^2/m_1^2)^2} \tag{B.4}$$

from which the parameters for the parametrization (B.1) can be obtained via the relations

$$f_i(0) = r_1 + r_2 \qquad a_i = \frac{r_1 + 2r_2}{r_1 + r_2} \qquad b_{0i} = m_B^2/m_1^2 \tag{B.5}$$

B.1.2 Parametrizations of $B \to \pi$ Form Factors

The $B \to \pi$ form factor parametrizations provided in [9] read

$$f_+^\pi(q^2) = \frac{0.744}{1 - q^2/m_{B^*}^2} - \frac{0.486}{1 - q^2/40.73\,\mathrm{GeV}^2} \tag{B.6}$$

$$f_0^\pi(q^2) = \frac{0.258}{1 - q^2/33.81\,\mathrm{GeV}^2} \tag{B.7}$$

$$f_T^\pi(q^2) = \frac{1.387}{1 - q^2/m_{B^*}^2} - \frac{1.134}{1 - q^2/32.22\,\mathrm{GeV}^2} \tag{B.8}$$

Employed Parametrizations and Parameter Space

For the semileptonic decays $\bar{B}^0 \to \pi^+ \ell^- \bar{\nu}$ and $B^\pm \to \pi^\pm \mu^+ \mu^-$ we only require the form factors $f_+^\pi(s)$ and $f_T^\pi(s)$, which are now rewritten as

$$f_{+,T}^\pi(s) = f_{+,T}^\pi(0)\, \frac{1 - s b_{+,T} - s m_B^2 (1 - a_{+,T})/m_{B^*}^2}{(1 - s m_B^2/m_{B^*}^2)(1 - b_{+,T}\, s)} \tag{B.9}$$

The two form factors have a single pole at $s = m_{B^*}^2/m_B^2 \approx 0.98$, which is treated as fixed by reason of its clear physical interpretation as the pole introduced by the B^* vector meson. Since the original parametrizations (B.6) and (B.8) are of the two-pole type (B.2), the parameters in (B.9) can be obtained using the parameter relations (B.3), which gives

$$f_+^\pi(0) = 0.258 \pm 0.031 \qquad a_+ = 1.572 \pm 0.15 \qquad b_+ = 0.684\,^{+0.075}_{-0.125} \tag{B.10}$$

$$f_T^\pi(0) = 0.253 \pm 0.028 \qquad a_T = 1.537 \pm 0.11 \qquad b_T = 0.865\,^{+0.032}_{-0.049} \tag{B.11}$$

At this, the individual parameter uncertainties were determined as follows: The error margins of $f_{+,T}^\pi(0)$ are explicitly specified in [9], and Furthermore, for the parameters $a_{+,T}$ and $b_{+,T}$, we take the maximum range consistent with a form factor uncertainty of 15% (separate variation of $a_{+,T}$ and $b_{+,T}$).

B.1.3 Parametrizations of $B \to K$ Form Factors

As before, we first quote the form factor parametrizations presented in [9]:

$$f_+^K(q^2) = \frac{0.162}{1 - q^2/m_{B_s^*}^2} + \frac{0.173}{(1 - q^2/m_{B_s^*}^2)^2} \tag{B.12}$$

$$f_0^K(q^2) = \frac{0.330}{1 - q^2/37.46\,\mathrm{GeV}^2} \tag{B.13}$$

$$f_T^K(q^2) = \frac{0.161}{1 - q^2/m_{B_s^*}^2} + \frac{0.198}{(1 - q^2/m_{B_s^*}^2)^2} \tag{B.14}$$

Employed Parametrizations and Parameter Space

Again, we only require the form factors $f_{+,T}^K(s)$ in the rewritten form

$$f_{+,T}^K(s) = f_{+,T}^K(0)\,\frac{1 - sb_{+,T} - sm_B^2(1 - a_{+,T})/m_{B_s^*}^2}{(1 - sm_B^2/m_{B_s^*}^2)(1 - b_{+,T}s)} \tag{B.15}$$

In this case, the original descriptions (B.12) and (B.14) correspond to the double-pole parametrization (B.4). However, instead of using the first relation in (B.5), the normalization parameters $f_{+,T}^K(0)$ will be determined using a formula, provided in [9], as this allows for an update with a more recent value of the Gegenbauer coefficient α_1:

$$f_+^K(0) = 0.331 \pm 0.041 + 0.25(\alpha_1(K) - 0.17) = 0.304 \pm 0.042 \tag{B.16}$$

$$f_T^K(0) = 0.358 \pm 0.037 + 0.31(\alpha_1(K) - 0.17) = 0.324 \pm 0.038 \tag{B.17}$$

While the single pole at $s = 1/b_{0+,T} = m_{B_s^*}^2/m_B^2 \approx 0.95$ is treated as fixed, the remaining parameters are determined through the relation (B.5)

$$a_+ = 1.569 \pm 0.128 \qquad b_+ = b_{0+}{}^{+0.049}_{-0.078} \tag{B.18}$$

$$a_T = 1.611 \pm 0.134 \qquad b_T = b_{0T}{}^{+0.048}_{-0.075} \tag{B.19}$$

where, again, the parameter ranges correspond to a form factor uncertainty of 15%. Note that the variation of $b_{+,T}$ generalizes the original double poles to effective fit poles.

As an aside, it is finally pointed out that the pseudoscalar form factors are subject to the important kinematic constraint

$$f_-(q^2) \equiv \Big[f_0(q^2) - f_+(q^2)\Big]\frac{1 - r}{s} \qquad \Longrightarrow \qquad f_0(0) = f_+(0) \tag{B.20}$$

which is not exactly fulfilled by the kaon parametrizations (B.12) – (B.13). Since, however, the (light) lepton masses are in the context of this work consistently neglected, this is inconsequential to us.

B.1.4 Parametrizations of $B \to K^*$ Form Factors

The (slightly adjusted, see below) $B \to K^*$ form factor parametrizations provided in [23] read

$$V(q^2) = \frac{0.923}{1 - q^2/m_{B^*}^2} - \frac{0.511}{1 - q^2/49.40\,\mathrm{GeV}^2} \tag{B.21}$$

$$A_0(q^2) = \frac{1.364}{1 - q^2/m_B^2} - \frac{0.990}{1 - q^2/36.78\,\mathrm{GeV}^2} \tag{B.22}$$

$$A_1(q^2) = \frac{0.290}{1 - q^2/40.38\,\mathrm{GeV}^2} \tag{B.23}$$

$$A_2(q^2) = \frac{-0.084}{1 - q^2/52.00\,\mathrm{GeV}^2} + \frac{0.342}{(1 - q^2/52.00\,\mathrm{GeV}^2)^2} \tag{B.24}$$

$$T_1(q^2) = \frac{0.823}{1 - q^2/m_{B^*}^2} - \frac{0.490}{1 - q^2/46.31\,\mathrm{GeV}^2} \tag{B.25}$$

$$T_2(q^2) = \frac{0.333}{1 - q^2/41.41\,\mathrm{GeV}^2} \tag{B.26}$$

$$\tilde{T}_3(q^2) = \frac{-0.036}{1 - q^2/48.10\,\mathrm{GeV}^2} + \frac{0.369}{(1 - q^2/48.10\,\mathrm{GeV}^2)^2} \tag{B.27}$$

where

$$\tilde{T}_3(s) = T_2(s) + \frac{s}{1-r}\, T_3(s) \tag{B.28}$$

At this point, it is reminded that the tensor form factors should satisfy [23]

$$T_1(0) = T_2(0) = \tilde{T}_3(0) \tag{B.29}$$

Unfortunately, the original parametrizations, specified in [23], exhibit slight deviations ± 0.001 from (B.29).[1] It is, however, important that the kinematic constraints (B.29) are exactly fulfilled, for otherwise, the $B \to K^* \ell^+ \ell^-$ decay rate develops an artificial $1/s^2$ divergence in the longitudinal component. For this reason, the parametrizations above have already been adjusted accordingly.

[1] This is presumably caused by rounding errors or the fit on the parametrizations.

	F^L	F^{L,α_1}	F^T	F^{T,α_1}	Old Value [23]	New Value
V_0	0.1415	0.0060	0.2234	0.0403	$0.411 \pm 0.033 \pm 0.44\delta_{\alpha_1}$	0.406(36)
A_{00}	0.2071	0.0403	0.1269	−0.0001	$0.374 \pm 0.034 \pm 0.39\delta_{\alpha_1}$	0.360(35)
A_{10}	0.1034	0.0059	0.1545	0.0281	$0.292 \pm 0.028 \pm 0.33\delta_{\alpha_1}$	0.287(30)
A_{20}	0.0614	−0.0080	0.1658	0.0395	$0.259 \pm 0.027 \pm 0.31\delta_{\alpha_1}$	0.257(29)
T_{10}	0.1301	0.0059	0.1665	0.0303	$0.333 \pm 0.028 \pm 0.34\delta_{\alpha_1}$	0.328(30)
T_{30}	0.0436	−0.0103	0.1386	0.0299	$0.202 \pm 0.018 \pm 0.18\delta_{\alpha_1}$	0.205(19)

Table B.1: Update of normalization parameters, using Tab. B.2 as input. Note: Owing to the kinematic constraint $T_1(0) = T_2(0)$, the parameters T_{10} and T_{20} (which is therefore not given) are identical.

Employed Parametrizations and Parameter-Space

The authors of [23] present their results at $q^2 = 0$ also in the form

$$F_i^{B\to K^*}(0) \;=\; \frac{f_\parallel}{217\,\mathrm{MeV}}\left[F_i^L + F_i^{L,\alpha_1}\alpha_1^\parallel\right] + \frac{f_\perp}{170\,\mathrm{MeV}}\left[F_i^T + F_i^{T,\alpha_1}\alpha_1^\perp\right] \tag{B.30}$$

to allow for an update with more recent values of $f_{\parallel,\perp}$ and $\alpha_1^{\parallel,\perp}$. The updated normalization parameters are summarized along with the coefficients $F_i^{(..)}$ in Tab. B.1.

As explained in detail in section (8.2), only the form factors V, A_1 and A_2 will be varied. In accordance with (B.21) – (B.27), they are now parametrized as

$$V(s) \;=\; V_0\frac{1 - sb_V - sm_B^2(1 - a_V)/m_{B^*}^2}{(1 - sm_B^2/m_{B^*}^2)(1 - sb_V)} \tag{B.31}$$

$$A_1(s) \;=\; \frac{A_{10}}{1 - sb_{A1}} \tag{B.32}$$

$$A_2(s) \;=\; A_{20}\frac{1 - sb_{A2}(2 - a_{A2})}{(1 - sb_{A2})^2} \tag{B.33}$$

The numerical values of the remaining parameters are obtained from the parametrizations (B.21) – (B.27) via the relations (B.3) and (B.5):

$$a_V \;=\; 1.528 \pm 0.214 \qquad\qquad a_{A2} \;=\; 2.326 \pm 0.455 \tag{B.34}$$

$$b_V \;=\; 0.564^{+0.256}_{-0.606} \qquad b_{A1} \;=\; 0.690^{+0.099}_{-0.134} \qquad b_{A2} \;=\; 0.536^{+0.057}_{-0.070} \tag{B.35}$$

The uncertainties correspond – as usual – to the maximum range consistent with a 15% form factor uncertainty (separate variation).

As far as the other form factors are concerned, only the central values of the parameters are required. The parameters not given in Tab. B.1 read (using (B.3) and (B.5))

$$a_{A0} = 1.641 \qquad a_{T1} = 1.570 \qquad a_{\tilde{T}3} = 2.108 \tag{B.36}$$

$$b_{A0} = 0.758 \qquad b_{T1} = 0.602 \qquad b_{T2} = 0.673 \qquad b_{\tilde{T}3} = 0.580 \tag{B.37}$$

B.2 Distribution Amplitudes

B.2.1 Kaon

The distribution amplitudes of light mesons are usually expanded in terms of the *Gegenbauer polynomials* $C_n^{(3/2)}(x)$ as follows [33, 83] ($\bar{u} = 1 - u$)

$$\phi(u,\mu) = 6u\bar{u}\left\{1 + \sum_{n=1}^{\infty} \alpha_n(\mu) C_n^{(3/2)}(2u-1)\right\} \tag{B.38}$$

This ansatz is physically motivated by the asymptotic form $\phi(u) \sim 6u\bar{u}$ of the leading-twist amplitudes in the $\mu \to \infty$ limit. Consequently, the *Gegenbauer coefficients* $\alpha_n(\mu)$ are scale-dependent quantities and vanish in this limit.

Most of the time, it is sufficient to keep just the first two terms of the series in (B.38). The corresponding polynomials read

$$C_1^{(3/2)}(x) = 3x \qquad C_2^{(3/2)}(x) = \frac{3}{2}(5x^2 - 1) \tag{B.39}$$

and hence the light-cone wave functions will be described as

$$\phi(u,\mu) = 6u\bar{u}\left\{1 + 3\alpha_1(\mu)(u - \bar{u}) + 6\alpha_2(\mu)(1 - 5u\bar{u})\right\} \tag{B.40}$$

The numerical values for the Gegenbauer coefficients of K, K^* and π meson are given in Tab. B.2.

B.2.2 B Meson

The light-cone wave functions of the B meson may be modeled as [38, 40]

$$\phi_+(\omega) = \frac{\omega}{\omega_0^2}\, e^{-\omega/\omega_0} \qquad \phi_-(\omega) = \frac{1}{\omega_0}\, e^{-\omega/\omega_0} \tag{B.41}$$

where $\omega_0 = (460 \pm 110)\,\mathrm{MeV}$ at $\mu = 1\,\mathrm{GeV}$ [92, 93, 94]. In the context of the semileptonic decays discussed in this work, however, the distribution amplitudes appear only

B meson mean lifetimes [66]		
$\tau_{B^+}[fs]$	$\tau_{B^0}[fs]$	$\tau_{B_s^0}[fs]$
1638(4)	1519(5)	1512(7)

Decay constants in MeV				
f_B[84]	f_K[9, 85]	f_π[9, 85]	$f_\parallel$[42, 86]	$f_\perp(1\mathrm{GeV})$[42, 86]
194(10)	160	131	220(5)	185(10)

Gegenbauer coefficients of the K^* vector meson ($\mu = 1\mathrm{GeV}$)			
$\alpha_1^\parallel(K^*)$[42, 87, 88]	$\alpha_2^\parallel(K^*)$[89, 90]	$\alpha_1^\perp(K^*)$[42, 87, 88]	$\alpha_2^\perp(K^*)$[89, 90]
0.03 ± 0.02	0.11 ± 0.09	0.04 ± 0.03	0.10 ± 0.08

Gegenbauer coefficients of pseudoscalar mesons ($\mu = 1\mathrm{GeV}$)			
$\alpha_1(K)$[42, 87, 88]	$\alpha_2(K)$[42, 87, 91]	$\alpha_1(\pi)$	$\alpha_2(\pi)$[42, 87, 91]
0.06 ± 0.03	$0.27^{+0.37}_{-0.12}$	0	$0.26^{+0.21}_{-0.09}$

Table B.2: B meson lifetimes, Decay constants and Gegenbauer coefficients.

in the form of the two “moments” [40]

$$\lambda_+^{-1} = \int_0^\infty d\omega\, \frac{\phi_+(\omega)}{\omega} = \frac{1}{\omega_0} \tag{B.42}$$

$$\lambda_-^{-1}(q^2) = \int_0^\infty d\omega\, \frac{\phi_-(\omega)}{\omega - q^2/m_B - i\epsilon} = \frac{e^{-q^2/(m_B\,\omega_0)}}{\omega_0}\Big[i\pi - \mathrm{Ei}\big(q^2/(m_B\,\omega_0)\big)\Big] \tag{B.43}$$

where $\mathrm{Ei}(z)$ is the *exponential integral*

$$\mathrm{Ei}(z) = \int_{-\infty}^{z} dt\, \frac{e^t}{t} \tag{B.44}$$

Note that at high-q^2 (and consequently in the context of the OPE), the second moment simplifies to

$$\lambda_-^{-1}(q^2 \gg m_B\,\omega_0) = -\frac{m_B}{q^2} \tag{B.45}$$

C Running Coupling and Three-loop β-Function

In order to remove the divergences that arise at higher orders in perturbation theory, every component of the (bare) Lagrangian must be renormalized at an, in principle, arbitrary scale μ [10]. To this end, the divergences are first parametrized, usually by means of *dimensional regularization*, and subsequently absorbed into the renormalization constants.

As far as the strong coupling constant is concerned, the renormalization is usually realized through

$$g_s^{(0)} \;=\; Z_{g_s}(\mu)\, g_s(\mu)\, \mu^{\epsilon} \tag{C.1}$$

At this, the last factor serves to keep the physical coupling $g_s(\mu)$ dimensionless, even in arbitrary space-time dimension $D = 4 - 2\epsilon$. Also, as already indicated by the notation, the bare coupling $g_s^{(0)}$ is scale-independent; the renormalization constant $Z_{g_s}(\mu)$ and the running coupling $g_s(\mu)$, on the other hand, depend on the renormalization scale μ.

The shift in the strong coupling that comes with a change of the renormalization scale is formally governed by the RGE [10, 11, 95]

$$\frac{d}{d\ln\mu}\left(\frac{\alpha_s(\mu)}{4\pi}\right) \;=\; 2\beta(\epsilon, \alpha_s(\mu)) \tag{C.2}$$

which at the same time is also the defining equation for the *β-function*. With the help of (C.1), the β-function can immediately be related to the renormalization constant

$$\beta(\alpha_s(\mu)) \;\equiv\; \beta(\epsilon, \alpha_s(\mu)) + \frac{\alpha_s(\mu)}{4\pi}\epsilon \;=\; -\frac{\alpha_s(\mu)}{4\pi}\, Z_{g_s}^{-1}(\mu)\, \frac{dZ_{g_s}(\mu)}{d\ln\mu} \tag{C.3}$$

which allows for a calculation in perturbation theory. Consequently, it is convenient to express the β-function in terms of powers in α_s

$$\beta(\alpha_s(\mu)) \;=\; -\sum_{i=0}^{\infty} \beta_i \left(\frac{\alpha_s(\mu)}{4\pi}\right)^{i+2} \tag{C.4}$$

and present the solution of the differential equation (C.2) in terms of the expansion coefficients β_i.

To three-loop accuracy, the solution to the RGE can then be written as

$$\frac{\alpha_s(\mu)}{4\pi} = \frac{1}{\beta_0 \ln \frac{\mu^2}{\Lambda^2}} \left[1 - \frac{\beta_1}{\beta_0^2} \frac{\ln\ln \frac{\mu^2}{\Lambda^2}}{\ln \frac{\mu^2}{\Lambda^2}} + \frac{\beta_1^2}{\beta_0^4 \ln^2 \frac{\mu^2}{\Lambda^2}} \left(\left(\ln\ln \frac{\mu^2}{\Lambda^2} - \frac{1}{2} \right)^2 + \frac{\beta_0 \beta_2}{\beta_1^2} - \frac{5}{4} \right) \right] \tag{C.5}$$

The integration constant Λ is the scale that formally determines the breakdown of perturbative QCD and can only be obtained from experiment. Though related and of similar size, it should not be confused with the conceptually somewhat different QCD scale Λ_{QCD}. For $f = 5$ active quark flavours, the numerical value of Λ is found to be [66]

$$\Lambda_{\overline{MS},5} = 0.214(7)\,\mathrm{GeV} \tag{C.6}$$

The coefficients of the β-function, finally, have been calculated independently by the authors of [95] and [96]. Employing the $\overline{MS}$ scheme, they are given as ($N = 3$, $f = 5$)

$$\beta_0 = \frac{11N - 2f}{3} = \frac{23}{3} \tag{C.7}$$

$$\beta_1 = \frac{34}{3}N^2 - 2C_F f - \frac{10}{3}Nf = \frac{116}{3} \tag{C.8}$$

$$\beta_2 = \frac{2857}{54}N^3 + C_F^2 f - \frac{205}{18}C_F N f - \frac{1415}{54}N^2 f + \frac{11}{9}C_F f^2 + \frac{79}{54}N f^2 = \frac{9769}{54} \tag{C.9}$$

$$C_F = \frac{N^2 - 1}{2N} = \frac{4}{3} \tag{C.10}$$

D Wilson Coefficients

D.1 Renormalization Group Equation

In constructing the weak Hamiltonian, the heavy particles are removed as active degrees of freedom from the full theory, which gives rise to new local interactions. The removed particles, however, are crucial to control the high-energy behaviour of the loop diagrams now involving the aforementioned low-energy effective interactions. As a consequence, the effective theory suffers from new ultraviolet divergences and requires an additional renormalization, the *operator renormalization* [10, 11]

$$\vec{\mathcal{O}}^{(0)} = \hat{Z}(\mu)\vec{\mathcal{O}}(\mu) \qquad \Longleftrightarrow \qquad \vec{C}^{(0)T} = \vec{C}^{T}(\mu)\hat{Z}^{-1}(\mu) \tag{D.1}$$

Of course, for the most part, this is analogous to the renormalization of the strong coupling constant (C.1). There is one difference, though, namely the occurrence of *operator mixing* which requires the introduction of a renormalization matrix $\hat{Z}(\mu)$.

Now, the most important consequence of (D.1) is certainly that the Wilson coefficients, so to say the coupling constants of the local operators, become scale dependent quantities. As the Wilson coefficients can be calculated in perturbation theory only at the weak scale $\mu_0 \sim M_W$ but are actually needed at the much lower scale of the B meson $\mu \sim m_b$, they have to be evolved down in an evolution process, governed by the RGE

$$\frac{d}{d\ln\mu}\vec{C}(\mu) = \frac{d}{d\ln\mu}\hat{Z}^{T}(\mu)\vec{C}^{(0)} \equiv \hat{\gamma}^{T}(\mu)\vec{C}(\mu) \tag{D.2}$$

Exploiting the μ-independency of the bare coefficients $\vec{C}^{(0)}$, the matrix of *anomalous dimensions* $\hat{\gamma}$ can be obtained from

$$\hat{\gamma}(\mu) \equiv \sum_{n=0}^{\infty}\hat{\gamma}^{(n)}\left(\frac{\alpha_s(\mu)}{4\pi}\right)^{n+1} = \hat{Z}^{-1}(\mu)\frac{d}{d\ln\mu}\hat{Z}(\mu) \tag{D.3}$$

Besides, if only the divergences are subtracted during the renormalization (MS scheme), that is to say, if

$$\hat{Z}(\mu) = \hat{1} + \sum_{k=1}^{\infty}\frac{1}{\epsilon^k}\hat{Z}_k(\alpha_{s(\mu)}) \qquad \hat{Z}_k = \sum_{n=k}^{\infty}\hat{Z}_k^{(n)}\left(\frac{\alpha_s(\mu)}{4\pi}\right)^{n} \tag{D.4}$$

the anomalous dimensions are already completely determined by the $1/\epsilon$ - divergences according to [10]

$$\hat{\gamma}^{(n)} = -2(n+1)\hat{Z}_1^{(n+1)} \tag{D.5}$$

This is related to the fact that the $\hat{\gamma}$ matrix is, in any case (thus, in particular, in the MS ($\overline{MS}$) scheme), a finite quantity, implying that the higher pole terms $\sim \hat{Z}^{(n)}_{k\geqslant 2}$ must cancel on the r.h.s. of (D.3). This circumstance can be exploited to simplify the perturbative calculations at higher orders significantly [10].

NNLO Evolution Matrix

The solution to the RGE (D.2) is usually presented in terms of the *evolution matrix* $\hat{U}(\mu, \mu_0)$ defined through

$$\vec{C}(\mu) \;\equiv\; \hat{U}(\mu,\mu_0)\vec{C}(\mu_0) \tag{D.6}$$

The evolution matrix is actually subject to the same differential equation as the coefficients (D.2), but with the more convenient boundary condition $\hat{U}(\mu_0,\mu_0) = \hat{1}$. Its general form can be written as [10, 40]

$$\hat{U}(\mu,\mu_0) \;=\; \hat{V}\hat{M}(\mu)\left(\left[\frac{\alpha_s(\mu_0)}{\alpha_s(\mu)}\right]^{\frac{\vec{\gamma}^{(0)}}{2\beta_0}}\right)_{diag} \hat{M}^{-1}(\mu_0)\hat{V}^{-1} \tag{D.7}$$

where the matrix $\hat{V}$ diagonalizes $\hat{\gamma}^{(0)T}$ according to

$$\left(\hat{V}^{-1}\hat{\gamma}^{(0)T}\hat{V}\right)_{ij} \;=\; \gamma_i^{(0)}\delta_{ij} \;\equiv\; \vec{\gamma}_i^{(0)}\delta_{ij} \tag{D.8}$$

If the matrix $\hat{M}$ is then expanded in powers of α_s

$$\hat{M}(\mu) \;=\; \hat{1} + \sum_{n=1}^{\infty}\hat{M}^{(n)}\left(\frac{\alpha_s(\mu)}{4\pi}\right)^n \tag{D.9}$$

the first two coefficients read [40]

$$\hat{M}^{(1)}_{ij} \;=\; \frac{\beta_1}{2\beta_0^2}\gamma_i^{(0)} \;-\; \frac{\left(\hat{V}^{-1}\hat{\gamma}^{(1)T}\hat{V}\right)_{ij}}{2\beta_0 \,+\, \gamma_i^{(0)} \,-\, \gamma_j^{(0)}} \tag{D.10}$$

$$\begin{aligned}\hat{M}^{(2)}_{ij} \;=&\; \frac{\beta_2}{4\beta_0^2}\gamma_i^{(0)} \;-\; \frac{\left(\hat{V}^{-1}\hat{\gamma}^{(2)T}\hat{V}\right)_{ij}}{4\beta_0 \,+\, \gamma_i^{(0)} \,-\, \gamma_j^{(0)}}\\ &+\sum_k \frac{2\beta_0 \,+\, \gamma_i^{(0)} \,-\, \gamma_k^{(0)}}{4\beta_0 \,+\, \gamma_i^{(0)} \,-\, \gamma_j^{(0)}}\left[\hat{M}^{(1)}_{ik}\hat{M}^{(1)}_{kj} \;-\; \frac{\beta_1}{\beta_0}\hat{M}^{(1)}_{ij}\delta_{jk}\right]\end{aligned} \tag{D.11}$$

D.2 Coefficient Functions at the Weak Scale

The initial values for the RGE evolution, that is, the perturbative expressions for the Wilson coefficients at the weak scale ($\overline{MS}$ scheme), are given below. Some general remarks beforehand:

- The Wilson coefficients of both basis can be expressed – up to trivial constants – as linear combinations of the same functions. Thus, in avoidance of repetition, the analytic expressions for these functions are explicitly stated once only, namely in section D.2.3.

- Throughout this work, we employ the *effective coefficients*

$$C_{7,8}^{\mathit{eff}} \equiv \sum_{j=1}^{8} y_j^{(7,8)} C_j \quad \text{where} \quad \begin{cases} y^{(7)} = (0,0,0,0,-\frac{1}{3},-1,1,0) \\ y^{(8)} = (0,0,0,0,1,0,0,1) \end{cases} \tag{D.12}$$

$$\mathcal{C}_{7,8}^{\mathit{eff}} \equiv \sum_{j=1}^{8} y_j^{(7,8)} \mathcal{C}_j \quad \text{where} \quad \begin{cases} y^{(7)} = (0,0,-\frac{1}{3},-\frac{4}{9},-\frac{20}{3},-\frac{80}{9},1,0) \\ y^{(8)} = (0,0,1,-\frac{1}{6},20,-\frac{10}{3},0,1) \end{cases} \tag{D.13}$$

  in place of the "standard" coefficients of the magnetic-penguin operators [97]. This always applies – even if there is no explicit superscript "*eff*".

- The initial conditions for C_9 refer to the rescaled operator

$$\mathcal{O}_9' = \frac{2\pi}{\alpha_s(\mu)} \mathcal{O}_9 = 2\mathcal{Q}_9 = \frac{\alpha}{\alpha_s} (\bar{s}b)_{V-A} \sum\nolimits_\ell (\bar{\ell}\ell)_V \tag{D.14}$$

- We use the short-hand notations

$$x_t \equiv \left(\frac{m_t^{\overline{MS}}(\mu_0)}{M_W} \right)^2 \qquad\qquad L \equiv \ln \frac{\mu_0^2}{M_W^2} \tag{D.15}$$

- The Wilson coefficients are given through the coefficients of the expansion

$$C_i(\mu_0) = \sum_{n=0}^{\infty} \left(\frac{\alpha_s(\mu_0)}{4\pi} \right)^n C_i^{(n)}(\mu_0) \tag{D.16}$$

  The only exception to this is the scale-independent coefficient $(\mathcal{O}_\nu = 4\mathcal{Q}_\nu)$

$$C_\nu = \mathcal{C}_\nu = -\frac{X_0(x_t)}{\sin^2\theta_W} \eta_X \tag{D.17}$$

  where the $\mathcal{O}(\alpha_s)$ corrections are contained in the factor $\eta_X = 0.994$, which is almost completely independent from $m_t \equiv \bar{m}_t(m_t)$ [98, 99, 100].

D.2.1 Traditional Basis

As far as the operator basis $\{\mathcal{O}_i\}$ is concerned, the matching results required for a NLO-treatment of semileptonic decays, read [10]

$$C_i^{(0)}(\mu_0 = M_W) \;=\; \begin{cases} 1 & \text{for } i \,=\, 1 \\ -\frac{1}{2}D_0'(x_t) & \text{for } i \,=\, 7 \\ -\frac{1}{2}E_0'(x_t) & \text{for } i \,=\, 8 \\ -\frac{Y_0(x_t)}{\sin^2\theta_W} & \text{for } i \,=\, 10 \\ 0 & \text{else} \end{cases} \tag{D.18}$$

$$C_i^{(1)}(\mu_0 = M_W) \;=\; \begin{cases} -\frac{11}{6} & \text{for } i \,=\, 1 \\ \frac{11}{2} & \text{for } i \,=\, 2 \\ \frac{\tilde{E}_0(x_t)}{6} & \text{for } i \,=\, 3,5 \\ \frac{\tilde{E}_0(x_t)}{2} & \text{for } i \,=\, 4,6 \\ \frac{Y_0(x_t)}{\sin^2\theta_W} \,-\, 4Z_0(x_t) \,+\, \frac{4}{9} & \text{for } i \,=\, 9 \end{cases} \tag{D.19}$$

D.2.2 γ_5-free Basis

Since the NNLO analysis of $B \to K\ell^+\ell^-$ is performed in this basis, each coefficient is now required to one higher order in α_s. The relevant initial conditions are given as [18, 19]

$$\mathcal{C}_i^{(0)}(\mu_0) \;=\; \begin{cases} 1 & \text{for } i \,=\, 2 \\ -\frac{1}{2}A_0^t(x_t) \,-\, \frac{23}{36} & \text{for } i \,=\, 7 \\ -\frac{1}{2}F_0^t(x_t) \,-\, \frac{1}{3} & \text{for } i \,=\, 8 \\ 0 & \text{else} \end{cases} \tag{D.20}$$

$$\mathcal{C}_i^{(1)}(\mu_0) = \begin{cases} 15 + 6L & \text{for } i = 1 \\ -\frac{7}{9} + \frac{2}{3}L + E_0^t(x_t) & \text{for } i = 4 \\ \frac{713}{243} + \frac{4}{81}L - \frac{1}{2}A_1^t(x_t) - \frac{4}{9}\mathcal{C}_4^{(1)}(\mu_0) & \text{for } i = 7 \\ \frac{91}{324} - \frac{4}{27}L - \frac{1}{2}F_1^t(x_t) - \frac{1}{6}\mathcal{C}_4^{(1)}(\mu_0) & \text{for } i = 8 \\ \frac{38}{27} - \frac{4}{9}L - 4C_0^t(x_t) - D_0^t(x_t) + \frac{4C_0^t(x_t) - 4B_0^t(x_t) + 1}{4\sin^2\theta_W} & \text{for } i = 9 \\ \frac{4B_0^t(x_t) - 4C_0^t(x_t) - 1}{4\sin^2\theta_W} & \text{for } i = 10 \\ 0 & \text{else} \end{cases} \quad \text{(D.21)}$$

and

$$\mathcal{C}_1^{(2)}(\mu_0) = \frac{7091}{72} + \frac{17}{3}\pi^2 + (16x_t + 8)\sqrt{4x_t - 1}\ \mathrm{Cl}_2\left(2\arcsin\frac{1}{2\sqrt{x_t}}\right)$$
$$- \left(16x_t + \frac{20}{3}\right)\ln x_t - 32x_t + \frac{475}{6}L + 17L^2 \quad \text{(D.22)}$$

$$\mathcal{C}_2^{(2)}(\mu_0) = \frac{127}{18} + \frac{4}{3}\pi^2 + \frac{46}{3}L + 4L^2 \quad \text{(D.23)}$$

$$\mathcal{C}_3^{(2)}(\mu_0) = G_1^t(x_t) - \frac{680}{243} - \frac{20}{81}\pi^2 - \frac{68}{81}L - \frac{20}{27}L^2 \quad \text{(D.24)}$$

$$\mathcal{C}_4^{(2)}(\mu_0) = E_1^t(x_t) + \frac{950}{243} + \frac{10}{81}\pi^2 + \frac{124}{27}L + \frac{10}{27}L^2 \quad \text{(D.25)}$$

$$\mathcal{C}_5^{(2)}(\mu_0) = \frac{2}{15}E_0^t(x_t) - \frac{1}{10}G_1^t(x_t) + \frac{68}{243} + \frac{2}{81}\pi^2 + \frac{14}{81}L + \frac{2}{27}L^2 \quad \text{(D.26)}$$

$$\mathcal{C}_6^{(2)}(\mu_0) = \frac{1}{4}E_0^t(x_t) - \frac{3}{16}G_1^t(x_t) + \frac{85}{162} + \frac{5}{108}\pi^2 + \frac{35}{108}L + \frac{5}{36}L^2 \quad \text{(D.27)}$$

$$\mathcal{C}_9^{(2)}(\mu_0) = \frac{1}{\sin^2\theta_W}\left[C_1^t(x_t) - B_1^t(x_t, -\tfrac{1}{2}) + 1\right] - 4C_1^t(x_t) - D_1^t(x_t)$$
$$+ \frac{524}{729} - \frac{128}{243}\pi^2 - \frac{16}{3}L - \frac{128}{81}L^2 \quad \text{(D.28)}$$

$$\mathcal{C}_{10}^{(2)}(\mu_0) = \frac{B_1^t(x_t, -\frac{1}{2}) - C_1^t(x_t) - 1}{\sin^2\theta_W} \quad \text{(D.29)}$$

It is pointed out that the constants in the coefficients $\mathcal{C}_{3-10}^{(0-2)}$ represent the sector of light quarks, the functions (with the upper index t) the top sector according to

$$\mathcal{C}_{3-10}^{(0-2)} \propto \lambda_u E(0) + \lambda_c E(0) + \lambda_t E(m_t) = \lambda_t \big[E(m_t) - E(0)\big] \tag{D.30}$$

$$= \lambda_t \big[E^t(x_t) - E(0)\big] \tag{D.31}$$

D.2.3 Functions

The functions just used to describe the matching conditions at the weak scale are specified below.

NLO Functions - Semileptonic Coefficients

While the individual contributions from box and penguin diagrams are gauge dependent, the Wilson coefficients themselves, and therefore the following linear combinations, are gauge independent [10, 18, 98]

$$X_0(x) = C_0^t(x) - 4B_0^t(x) + 1 = \frac{x}{8}\left[\frac{x+2}{x-1} + \frac{3x-6}{(x-1)^2}\ln x\right] \tag{D.32}$$

$$Y_0(x) = C_0^t(x) - B_0^t(x) + \frac{1}{4} = \frac{x}{8}\left[\frac{4-x}{1-x} + \frac{3x}{(x-1)^2}\ln x\right] \tag{D.33}$$

$$Z_0(x) = C_0^t(x) + \frac{1}{4} D_0^t(x) - \frac{13}{54} \tag{D.34}$$

$$= \frac{18x^4 - 163x^3 + 259x^2 - 108x}{144(x-1)^3} + \frac{24x^4 - 6x^3 - 63x^2 + 50x - 8}{72(x-1)^4}\ln x \tag{D.35}$$

NLO Functions - Magnetic and QCD Penguin Coefficients

The remaining functions required at the NLO level read [10, 18]

$$D_0^{'}(x) = A_0^t(x) + \frac{23}{18} = \frac{-3x^3 + 2x^2}{2(x-1)^4}\ln x + \frac{8x^3 + 5x^2 - 7x}{12(x-1)^3} \tag{D.36}$$

$$E_0^{'}(x) = F_0^t(x) + \frac{2}{3} = \frac{3x^2}{2(x-1)^4}\ln x + \frac{x^3 - 5x^2 - 2x}{4(x-1)^3} \tag{D.37}$$

$$\tilde{E}_0(x) = E_0^t(x) - \frac{7}{9} = \frac{x^3 + 11x^2 - 18x}{12(x-1)^3} + \frac{-9x^2 + 16x - 4}{6(x-1)^4}\ln x - \frac{2}{3} \tag{D.38}$$

NNLO Functions

The functions required for a NNLO analysis of rare B decays decays are given as [18]

$$
\begin{aligned}
A_1^t(x) \;=\;& \frac{32x^4+244x^3-160x^2+16x}{9(x-1)^4}\,\mathrm{Li}_2\Big(1-\frac{1}{x}\Big)+\frac{774x^4+2826x^3-1994x^2+130x-8}{81(x-1)^5}\ln x \\
&+\frac{-94x^4-18665x^3+20682x^2-9113x+2006}{243(x-1)^4}+\Bigg[\frac{12x^4+92x^3-56x^2}{3(x-1)^5}\ln x \\
&+\frac{-68x^4-202x^3-804x^2+794x-152}{27(x-1)^4}\Bigg]\ln\frac{\mu_0^2}{m_t^2}
\end{aligned}
\tag{D.39}
$$

$$
\begin{aligned}
B_1^t(x,-\tfrac{1}{2}) \;=\;& \frac{-2x}{(x-1)^2}\,\mathrm{Li}_2\Big(1-\frac{1}{x}\Big)+\frac{x^2-17x}{3(x-1)^3}\ln x+\frac{13x+3}{3(x-1)^2} \\
&+\Bigg[\frac{-2x^2-2x}{(x-1)^3}\ln x+\frac{4x}{(x-1)^2}\Bigg]\ln\frac{\mu_0^2}{m_t^2}
\end{aligned}
\tag{D.40}
$$

$$
\begin{aligned}
C_1^t(x) \;=\;& \frac{-x^3-4x}{(x-1)^2}\,\mathrm{Li}_2\Big(1-\frac{1}{x}\Big)+\frac{-3x^3-14x^2-23x}{3(x-1)^3}\ln x+\frac{4x^3+7x^2+29x}{3(x-1)^2} \\
&+\Bigg[\frac{-8x^2-2x}{(x-1)^3}\ln x+\frac{x^3+x^2+8x}{(x-1)^2}\Bigg]\ln\frac{\mu_0^2}{m_t^2}
\end{aligned}
\tag{D.41}
$$

$$
\begin{aligned}
D_1^t(x) \;=\;& \frac{380x^4-1352x^3+1656x^2-784x+256}{81(x-1)^4}\,\mathrm{Li}_2\Big(1-\frac{1}{x}\Big) \\
&+\frac{-304x^4-1716x^3+4644x^2-2768x+720}{81(x-1)^5}\ln x \\
&+\frac{-6175x^4+41608x^3-66723x^2+33106x-7000}{729(x-1)^4} \\
&-\Bigg[\frac{648x^4-720x^3-232x^2-160x+32}{81(x-1)^5}\ln x \\
&+\frac{352x^4-4912x^3+8280x^2-3304x+880}{243(x-1)^4}\Bigg]\ln\frac{\mu_0^2}{m_t^2}
\end{aligned}
\tag{D.42}
$$

$$\begin{aligned}
E_1^t(x) &= \frac{515x^4 - 614x^3 - 81x^2 - 190x + 40}{54(x-1)^4}\,\mathrm{Li}_2\Big(1 - \frac{1}{x}\Big) \\
&+ \frac{1030x^4 - 435x^3 - 1373x^2 - 1950x + 424}{108(x-1)^5}\ln x \\
&+ \frac{-29467x^4 + 45604x^3 - 30237x^2 + 66532x - 10960}{1944(x-1)^4} \\
&+ \Bigg[\frac{1125x^3 - 1685x^2 - 380x + 76}{54(x-1)^5}\ln x \\
&+ \frac{133x^4 - 2758x^3 - 2061x^2 + 11522x - 1652}{324(x-1)^4}\Bigg]\ln\frac{\mu_0^2}{m_t^2}
\end{aligned} \tag{D.43}$$

$$\begin{aligned}
F_1^t(x) &= \frac{4x^4 - 40x^3 - 41x^2 - x}{3(x-1)^4}\,\mathrm{Li}_2\Big(1 - \frac{1}{x}\Big) + \frac{144x^4 - 3177x^3 - 3661x^2 - 250x + 32}{108(x-1)^5}\ln x \\
&+ \frac{-247x^4 + 11890x^3 + 31779x^2 - 2966x + 1016}{648(x-1)^4} \\
&- \Bigg[\frac{17x^3 + 31x^2}{(x-1)^5}\ln x + \frac{35x^4 - 170x^3 - 447x^2 - 338x + 56}{18(x-1)^4}\Bigg]\ln\frac{\mu_0^2}{m_t^2}
\end{aligned} \tag{D.44}$$

$$\begin{aligned}
G_1^t(x) &= \frac{10x^4 - 100x^3 + 30x^2 + 160x - 40}{27(x-1)^4}\,\mathrm{Li}_2\Big(1 - \frac{1}{x}\Big) \\
&+ \frac{30x^3 - 42x^2 - 332x + 68}{81(x-1)^4}\ln x + \frac{6x^3 + 293x^2 - 161x - 42}{81(x-1)^3} \\
&+ \Bigg[\frac{90x^2 - 160x + 40}{27(x-1)^4}\ln x + \frac{-35x^3 - 105x^2 + 210x + 20}{81(x-1)^3}\Bigg]\ln\frac{\mu_0^2}{m_t^2}
\end{aligned} \tag{D.45}$$

For the sake of completeness, integral representations for the *Clausen function* $\mathrm{Cl}_2(x)$, used in (D.22), and the related *dilogarithm* $\mathrm{Li}_2(z)$ are provided here as well:

$$\mathrm{Cl}_2(x) = \mathrm{Im}\big[\mathrm{Li}_2(e^{ix})\big] = -\int_0^x d\theta\, \ln|2\sin(\theta/2)| \tag{D.46}$$

$$\mathrm{Li}_2(z) = -\int_0^z \frac{\ln(1-t)}{t}\,dt \tag{D.47}$$

D.3 Anomalous Dimension Matrix

The anomalous dimensions of the two operator bases are now presented in turn, employing the perturbative expansion

$$\hat{\gamma}(\mu) \;\equiv\; \sum_{n=0}^{\infty} \hat{\gamma}^{(n)} \left(\frac{\alpha_s(\mu)}{4\pi}\right)^{n+1} \tag{D.48}$$

It is pointed out that, in accordance with the previous section, the given matrices describe the evolution of the effective coefficients, defined in (D.12) and (D.13), respectively, as well as $C_9' = \frac{\alpha_s(\mu)}{2\pi} C_9 = 2\mathcal{C}_9$ in case of the basis (2.17). Finally, note that the Wilson coefficients $C_{10,\nu}$, to be renormalized at $\mu_0 = m_t$, are scale-independent, and also that the entries $\hat{\gamma}^{(\prime)(n)}_{i>6,j<7} \equiv 0$ are omitted below.

D.3.1 Traditional Basis

Starting with our "standard" basis $\{\mathcal{O}_i\}$, the non-zero entries of $\hat{\gamma}^{(0)}$, relevant to the leading logarithmic approximation (LLA) of the coefficients, read [10] ($C_F = \frac{N^2-1}{2N}$)

$$\hat{\gamma}^{(0)}_{i\leqslant 6, j\leqslant 6} = \begin{pmatrix} \frac{-6}{N} & 6 & \frac{-2}{3N} & \frac{2}{3} & \frac{-2}{3N} & \frac{2}{3} \\ 6 & \frac{-6}{N} & 0 & 0 & 0 & 0 \\ 0 & 0 & \frac{-22}{3N} & \frac{22}{3} & \frac{-4}{3N} & \frac{4}{3} \\ 0 & 0 & 6 - \frac{2f}{3N} & \frac{2f}{3} - \frac{6}{N} & \frac{-2f}{3N} & \frac{2f}{3} \\ 0 & 0 & 0 & 0 & \frac{6}{N} & -6 \\ 0 & 0 & \frac{-2f}{3N} & \frac{2f}{3} & \frac{-2f}{3N} & \frac{2f}{3} - 12C_F \end{pmatrix} \tag{D.49}$$

$$\hat{\gamma}^{(0)}_{i,j\geqslant 7} = \begin{pmatrix} \frac{104}{27}C_F & \frac{11}{9}N - \frac{29}{9N} & -\frac{16}{9} \\ 0 & 3 & -\frac{16}{9}N \\ -\frac{116}{27}C_F & \frac{22}{9}N - \frac{58}{9N} + 3f & \frac{16}{9}N(\frac{1}{N} + \frac{d}{2} - u) \\ (\frac{104}{27}u - \frac{58}{27}d)C_F & (11N - \frac{29}{N})\frac{f}{9} + 6 & \frac{16}{9}(N + \frac{d}{2} - u) \\ \frac{8}{3}C_F & \frac{4}{N} - 2N - 3f & \frac{16}{9}N(\frac{d}{2} - u) \\ (\frac{50}{27}d - \frac{112}{27}u)C_F & (\frac{25}{N} - 16N)\frac{f}{9} - 4 & \frac{16}{9}(\frac{d}{2} - u) \\ 8C_F & 0 & 0 \\ -\frac{8}{3}C_F & 16C_F - 4N & 0 \\ 0 & 0 & -2\beta_0 \end{pmatrix} \tag{D.50}$$

where $f = u + d$ denotes the sum of active up- and down-type quarks. The coefficients of the β-function are specified in (C.7) – (C.9).

Furthermore, the entries of $\hat{\gamma}^{(1)}$ required for the next-to-leading logarithmic approximation (NLLA) of C_9 are found to be [10]

$$\hat{\gamma}^{(1)}_{i\leqslant 6, j\leqslant 6} = \begin{pmatrix} -\frac{21}{2}-\frac{2f}{9} & \frac{7}{2}+\frac{2f}{3} & -\frac{202}{243} & \frac{1354}{81} & -\frac{1192}{243} & \frac{904}{81} \\ \frac{7}{2}+\frac{2f}{3} & -\frac{21}{2}-\frac{2f}{9} & \frac{79}{9} & -\frac{7}{3} & -\frac{65}{9} & -\frac{7}{3} \\ 0 & 0 & \frac{71f}{9}-\frac{5911}{486} & \frac{5983}{162}+\frac{f}{3} & -\frac{2384}{243}-\frac{71f}{9} & \frac{1808}{81}-\frac{f}{3} \\ 0 & 0 & \frac{56f}{243}+\frac{379}{18} & \frac{808f}{81}-\frac{91}{6} & -\frac{130}{9}-\frac{502f}{243} & \frac{646f}{81}-\frac{14}{3} \\ 0 & 0 & -\frac{61f}{9} & -\frac{11f}{3} & \frac{71}{3}+\frac{61f}{9} & \frac{11f}{3}-99 \\ 0 & 0 & -\frac{682f}{243} & \frac{106f}{81} & \frac{1676f}{243}-\frac{225}{2} & \frac{1348f}{81}-\frac{1343}{6} \end{pmatrix} \tag{D.51}$$

and

$$\hat{\gamma}^{(1)}_{i, j\geqslant 7} = \begin{pmatrix} ? & ? & \frac{400}{81}C_F \\ ? & ? & -\frac{16}{3}NC_F \\ ? & ? & \frac{16}{3}C_F(N\frac{d}{2}-Nu-\frac{58}{27}) \\ ? & ? & \frac{16}{3}C_F(N-\frac{35}{27}u-\frac{8}{27}d) \\ ? & ? & \frac{16}{3}C_FN(\frac{d}{2}-u) \\ ? & ? & \frac{16}{81}C_F(55u-53d) \\ 4C_F(\frac{137}{9}N-4C_F-\frac{14}{9}f) & 0 & 0 \\ \frac{4}{3}C_F(8C_F-\frac{101}{9}N+\frac{14}{9}f) & \frac{214}{9}N^2+\frac{56f}{9N}-\frac{458}{9}-\frac{12}{N^2}-\frac{13}{9}fN & 0 \\ 0 & 0 & -2\beta_1 \end{pmatrix} \tag{D.52}$$

D.3.2 "γ_5-free" Basis

Let us continue with the $\hat{\gamma}'$-matrix, which governs the evolution in the $\{\mathcal{Q}_i\}$ basis. At the LLA level, we have [16, 17]

$$\hat{\gamma}'^{(0)}_{i\leqslant 6, j\leqslant 6} = \begin{pmatrix} -4 & \frac{8}{3} & 0 & -\frac{2}{9} & 0 & 0 \\ 12 & 0 & 0 & \frac{4}{3} & 0 & 0 \\ 0 & 0 & 0 & -\frac{52}{3} & 0 & 2 \\ 0 & 0 & -\frac{40}{9} & \frac{4}{3}f - \frac{160}{9} & \frac{4}{9} & \frac{5}{6} \\ 0 & 0 & 0 & -\frac{256}{3} & 0 & 20 \\ 0 & 0 & \frac{-256}{9} & \frac{40}{3}f - \frac{544}{9} & \frac{40}{9} & -\frac{2}{3} \end{pmatrix} \tag{D.53}$$

and [18]

$$\hat{\gamma}'^{(0)}_{i,j\geqslant 7} = \begin{pmatrix} -\frac{208}{243} & \frac{173}{162} & -\frac{32}{27} \\ \frac{416}{81} & \frac{70}{27} & -\frac{8}{9} \\ -\frac{176}{81} & \frac{14}{27} & -\frac{16}{9} \\ -\frac{152}{243} & -\frac{587}{162} & \frac{32}{27} \\ -\frac{6272}{81} & \frac{6596}{27} & -\frac{112}{9} \\ \frac{4624}{243} & \frac{4772}{81} & \frac{512}{27} \\ \frac{32}{3} & 0 & 0 \\ -\frac{32}{9} & \frac{28}{3} & 0 \\ 0 & 0 & -2\beta_0 \end{pmatrix} \tag{D.54}$$

Next, at NLLA, one finds [16, 17]

$$\hat{\gamma}'^{(1)}_{i\leqslant 6, j\leqslant 6} = \begin{pmatrix} \frac{16}{9}f - \frac{145}{3} & \frac{40}{27}f - 26 & -\frac{1412}{243} & -\frac{1369}{243} & \frac{134}{243} & -\frac{35}{162} \\ \frac{20}{3}f - 45 & -\frac{28}{3} & -\frac{416}{81} & \frac{1280}{81} & \frac{56}{81} & \frac{35}{27} \\ 0 & 0 & -\frac{4468}{81} & -\frac{29129}{81} - \frac{52}{9}f & \frac{400}{81} & \frac{3493}{108} - \frac{2}{9}f \\ 0 & 0 & \frac{368}{81}f - \frac{13678}{243} & \frac{1334}{81}f - \frac{79409}{243} & \frac{509}{486} - \frac{8}{81}f & \frac{13499}{648} - \frac{5}{27}f \\ 0 & 0 & -\frac{244480}{81} - \frac{160}{9}f & -\frac{29648}{81} - \frac{2200}{9}f & \frac{23116}{81} + \frac{16}{9}f & \frac{3886}{27} + \frac{148}{9}f \\ 0 & 0 & \frac{77600}{243} - \frac{1264}{81}f & \frac{164}{81}f - \frac{28808}{243} & \frac{400}{81}f - \frac{20324}{243} & \frac{622}{27}f - \frac{21211}{162} \end{pmatrix} \tag{D.55}$$

and [18]

$$\hat{\gamma}'^{(1)}_{i,j\geqslant 7} = \begin{pmatrix} -\frac{818}{243} & \frac{3779}{324} & -\frac{2272}{729} \\ \frac{508}{81} & \frac{1841}{108} & \frac{1952}{243} \\ \frac{22348}{243} & \frac{10178}{81} & -\frac{6752}{243} \\ -\frac{17584}{243} & -\frac{172471}{648} & -\frac{2192}{729} \\ \frac{1183696}{729} & \frac{2901296}{243} & -\frac{84032}{243} \\ \frac{2480344}{2187} & -\frac{3296257}{729} & -\frac{37856}{729} \\ \frac{4688}{27} & 0 & 0 \\ -\frac{2192}{81} & \frac{4063}{27} & 0 \\ 0 & 0 & -2\beta_1 \end{pmatrix} \quad \text{(D.56)}$$

Finally, we also require the entries of $\hat{\gamma}'^{(2)}$ relevant to the NNLO evolution of $\mathcal{C}_9$. They depend on the *Riemann zeta function*

$$\zeta(s) = \sum_{n=1}^{\infty} \frac{1}{n^s} \quad \text{(D.57)}$$

and are given as [15] ($\zeta_3 \equiv \zeta(3) = 1.2020569...$)

$$\hat{\gamma}'^{(2)}_{i,j\geqslant 9} = \begin{pmatrix} -\frac{1359190}{19683} + \frac{6976}{243}\zeta_3 \\ -\frac{229696}{6561} - \frac{3584}{81}\zeta_3 \\ -\frac{1290092}{6561} + \frac{3200}{81}\zeta_3 \\ -\frac{819971}{19683} - \frac{19936}{243}\zeta_3 \\ -\frac{16821944}{6561} + \frac{30464}{81}\zeta_3 \\ -\frac{17787368}{19683} - \frac{286720}{243}\zeta_3 \\ 0 \\ 0 \\ -2\beta_2 \end{pmatrix}$$

and [17]

$$\hat{\gamma}'^{(2)}_{i,j\leqslant 6} = \left(\begin{array}{cccccc}
-\tfrac{1927}{2}+\tfrac{257}{9}f+\tfrac{40}{9}f^2+(224+\tfrac{160}{3}f)\zeta_3 & \tfrac{475}{9}+\tfrac{362}{27}f-\tfrac{40}{27}f^2-(\tfrac{896}{3}+\tfrac{320}{9}f)\zeta_3 & \tfrac{269107}{13122}-\tfrac{2288}{729}f-\tfrac{1360}{81}\zeta_3 & -\tfrac{2425817}{13122}+\tfrac{30815}{4374}f-\tfrac{776}{81}\zeta_3 & -\tfrac{343783}{52488}+\tfrac{392}{729}f+\tfrac{124}{81}\zeta_3 & -\tfrac{37573}{69984}+\tfrac{35}{972}f+\tfrac{100}{27}\zeta_3 \\
\tfrac{307}{2}+\tfrac{361}{3}f-\tfrac{20}{3}f^2-(1344+160f)\zeta_3 & \tfrac{1298}{3}-\tfrac{76}{3}f-224\zeta_3 & \tfrac{69797}{2187}+\tfrac{904}{243}f+\tfrac{2720}{27}\zeta_3 & \tfrac{1457549}{8748}-\tfrac{22067}{729}f-\tfrac{2768}{27}\zeta_3 & -\tfrac{37889}{8748}-\tfrac{28}{243}f-\tfrac{248}{27}\zeta_3 & \tfrac{366919}{11664}-\tfrac{35}{162}f-\tfrac{110}{9}\zeta_3 \\
0 & 0 & -\tfrac{4203068}{2187}+\tfrac{14012}{243}f-\tfrac{608}{27}\zeta_3 & -\tfrac{18422762}{2187}+\tfrac{888605}{2916}f+\tfrac{272}{27}f^2+(\tfrac{39824}{27}+160f)\zeta_3 & \tfrac{674281}{4374}-\tfrac{1352}{243}f-\tfrac{496}{27}\zeta_3 & \tfrac{9284531}{11664}-\tfrac{2798}{81}f-\tfrac{26}{27}f^2-(\tfrac{1921}{9}+20f)\zeta_3 \\
0 & 0 & -\tfrac{5875184}{6561}+\tfrac{217892}{2187}f+\tfrac{472}{81}f^2+(\tfrac{27520}{81}+\tfrac{1360}{9}f)\zeta_3 & -\tfrac{70274587}{13122}+\tfrac{8860733}{17496}f-\tfrac{4010}{729}f^2+(\tfrac{16592}{81}+\tfrac{2512}{27}f)\zeta_3 & \tfrac{2951809}{52488}-\tfrac{31175}{8748}f-\tfrac{52}{81}f^2-(\tfrac{3154}{81}+\tfrac{136}{9}f)\zeta_3 & \tfrac{3227801}{8748}-\tfrac{105293}{11664}f-\tfrac{65}{54}f^2+(\tfrac{200}{27}-\tfrac{220}{9}f)\zeta_3 \\
0 & 0 & -\tfrac{194951552}{2187}+\tfrac{358672}{81}f-\tfrac{2144}{81}f^2+\tfrac{87040}{27}\zeta_3 & -\tfrac{130500332}{2187}-\tfrac{2949616}{729}f+\tfrac{3088}{27}f^2+(\tfrac{238016}{27}+640f)\zeta_3 & \tfrac{14732222}{2187}-\tfrac{27428}{81}f+\tfrac{272}{81}f^2-\tfrac{13984}{27}\zeta_3 & \tfrac{16521659}{2916}+\tfrac{8081}{54}f-\tfrac{316}{27}f^2-(\tfrac{22420}{9}+200f)\zeta_3 \\
0 & 0 & \tfrac{162733912}{6561}-\tfrac{2535466}{2187}f+\tfrac{17920}{243}f^2+(\tfrac{174208}{81}+\tfrac{12160}{9}f)\zeta_3 & \tfrac{13286236}{6561}-\tfrac{1826023}{4374}f-\tfrac{159548}{729}f^2-(\tfrac{24832}{81}+\tfrac{9440}{27}f)\zeta_3 & -\tfrac{22191107}{13122}+\tfrac{395783}{4374}f-\tfrac{1720}{243}f^2-(\tfrac{33832}{81}+\tfrac{1360}{9}f)\zeta_3 & -\tfrac{32043361}{8748}+\tfrac{3353393}{5832}f-\tfrac{533}{81}f^2+(\tfrac{9248}{27}-\tfrac{1120}{9}f)\zeta_3
\end{array}\right) \tag{D.58}$$

Traditional coefficients at $\mu = m_b = 4.18\text{GeV}$						
	C_1	C_2	C_3	C_4	C_5	C_6
LLA	1.1178	−0.2684	0.0121	−0.0274	0.0080	−0.0342
NLLA	1.0814	−0.1905	0.0137	−0.0358	0.0087	−0.0420
	C_7^{eff}	C_8^{eff}	C_9	C_{10}	C_ν	
LLA	−0.3184	−0.1510	2.0473	0	0	
NLLA	–	–	4.1764	−4.2473	−6.6080	

"γ_5-free" coefficients at $\mu = m_b = 4.18\text{GeV}$						
	$\mathcal{C}_1$	$\mathcal{C}_2$	$\mathcal{C}_3$	$\mathcal{C}_4$	$\mathcal{C}_5$	$\mathcal{C}_6$
LLA	−0.5368	1.0283	−0.0056	−0.0730	0.0005	0.0011
NLLA	−0.3232	1.0093	−0.0053	−0.0881	0.0004	0.0010
NNLLA	−0.3058	1.0118	−0.0062	−0.0722	0.0006	−0.0002
	$\mathcal{C}_7^{\text{eff}}$	$\mathcal{C}_8^{\text{eff}}$	$\mathcal{C}_9$	$\mathcal{C}_{10}$	$\mathcal{C}_\nu$	
LLA	−0.3184	−0.1510	0.0368	0	0	
NLLA	−0.3065	−0.1693	0.0751	−0.0764	−6.6080	
NNLLA	–	–	0.0754	−0.0772	−6.5683	

Table D.1: Wilson coefficients at the scale $\mu = 4.18\text{GeV}$. The relevant input parameters are $\Lambda_{\overline{MS},5} = 214\text{MeV}$, $m_t = 167.2\text{GeV}$, $M_W = 80.385$ and $\sin^2\theta_W = 0.23126$. 3-loop running is continuously used for α_s.

D.4 Wilson Coefficients at $\mu = \mathcal{O}(m_b)$

Utilizing the procedure outlined in the preceding sections, the Wilson coefficients are evolved from the initial scale $\mu_0 = \mathcal{O}(M_W)$ down to the scale $\mu = \mathcal{O}(m_b)$. The numerical results are summarized in Tab. D.1.

As an aside, the (independently calculated) C_i and $\mathcal{C}_i$ coefficients given in Tab. D.1 indeed satisfy the basis transformation (D.62), explained in the following section.

D.5 Change of Basis

In general, the *Fierz-identities* [101, 102, 103] allow to express the operators of two different bases as linear combinations of one another. At LO, this also applies to the Wilson coefficients – they are scheme and basis independent.

At higher orders, however, the Wilson coefficients are basis dependent: Using dimensional regularization, calculations are performed in $D = 4 - 2\epsilon$ dimensions and require the definition of so-called *evanescent operators* [104]. While these operators vanish in $D = 4$ dimensions, they still give relevant (even divergent) contributions, responsible for the basis dependence of the result. Strictly speaking, however, this represents a scheme dependence which is not introduced by the operator basis per se, but rather the associated (often implicit, but in principle arbitrary) choice of evanescent operators.

Of course, a transfer of results from one basis to another is still feasible. In [16], the corresponding procedure is explained and explicitly performed step by step for a transition from the (2.21) to the (2.17) basis. The overall transformation is presented below, thereby we refer to the effective coefficients of the magnetic-penguin operators, as defined in (D.12) – (D.13).

To begin with, the semileptonic coefficients $C_\nu = \mathcal{C}_\nu$ and C_{10} are scheme independent quantities, given by their perturbative expressions at the weak scale. Furthermore, since the coefficient

$$\mathcal{C}_{10}(\mu) = \frac{\alpha_s(\mu)}{4\pi} C_{10} \tag{D.59}$$

is merely rescaled, it is scheme independent as well and its scale dependency is only due the running of the strong coupling.

Before proceeding with the remaining operators, it is reminded that there is a relative factor of 4 in the definition of the two Hamiltonians which implies

$$4\vec{\mathcal{C}}^T(\mu)\vec{\mathcal{Q}}(\mu) = \vec{C}^T(\mu)\vec{\mathcal{O}}(\mu) \tag{D.60}$$

and leads to an "asymmetric" transformation of coefficients and operators. At LO, for instance, we have

$$\vec{C}(\mu) = \hat{M}(\mu)\vec{\mathcal{C}}(\mu) \qquad 4\vec{\mathcal{Q}}(\mu) = \hat{M}^T(\mu)\vec{\mathcal{O}}(\mu) \tag{D.61}$$

This being said, the NLO transformations for the Wilson coefficients and corresponding anomalous dimensions are given as [16] ($\hat{\gamma}'$ corresponds to the $\mathcal{Q}_i$ basis)

$$\vec{C}(\mu) = \left[\hat{1} + \frac{\alpha_s(\mu)}{4\pi}\hat{Z}(\mu)\right]\hat{M}(\mu)\vec{\mathcal{C}}(\mu) \tag{D.62}$$

$$\hat{\gamma}^{(0)} = \hat{M}^{-1T}\hat{\gamma}'^{(0)}\hat{M}^T \tag{D.63}$$

$$\hat{\gamma}^{(1)} = \hat{M}^{-1T}\hat{\gamma}'^{(1)}\hat{M}^T + \left[\hat{\gamma}^{(0)}, \hat{Z}^T\right] - 2\beta_0\hat{Z}^T \tag{D.64}$$

where [16, 40]

$$\hat{M}(\mu) = \begin{pmatrix} \frac{-1}{2N} & 1 & 0 & 0 & 0 & 0 & 0 & 0 & 0 \\ \frac{1}{2} & 0 & 0 & 0 & 0 & 0 & 0 & 0 & 0 \\ 0 & 0 & 1 & \frac{-1}{2N} & 16 & \frac{-8}{N} & 0 & 0 & 0 \\ 0 & 0 & 0 & \frac{1}{2} & 0 & 8 & 0 & 0 & 0 \\ 0 & 0 & 1 & \frac{-1}{2N} & 4 & \frac{-2}{N} & 0 & 0 & 0 \\ 0 & 0 & 0 & \frac{1}{2} & 0 & 2 & 0 & 0 & 0 \\ 0 & 0 & 0 & 0 & 0 & 0 & 1 & 0 & 0 \\ 0 & 0 & 0 & 0 & 0 & 0 & 0 & 1 & 0 \\ 0 & 0 & 0 & 0 & 0 & 0 & 0 & 0 & \frac{4\pi}{\alpha_s(\mu)} \end{pmatrix} \tag{D.65}$$

and

$$\hat{Z}(\mu) = \begin{pmatrix} \frac{2}{3} & -1 & 0 & 0 & 0 & 0 & 0 & 0 & 0 \\ -2 & -\frac{7}{3} & 0 & 0 & 0 & 0 & 0 & 0 & 0 \\ 0 & 0 & \frac{178}{27} & \frac{4}{9} & \frac{-160}{27} & \frac{-13}{9} & 0 & 0 & 0 \\ 0 & 0 & \frac{-34}{9} & \frac{-20}{3} & \frac{16}{9} & \frac{13}{3} & 0 & 0 & 0 \\ 0 & 0 & \frac{-164}{27} & \frac{-23}{9} & \frac{146}{27} & \frac{32}{9} & 0 & 0 & 0 \\ 0 & 0 & \frac{20}{9} & \frac{23}{3} & \frac{-2}{9} & \frac{-16}{3} & 0 & 0 & 0 \\ ? & ? & ? & ? & ? & ? & 0 & 0 & 0 \\ ? & ? & ? & ? & ? & ? & 0 & 0 & 0 \\ 0 & 0 & \frac{-56\pi}{27\alpha_s(\mu)} & \frac{8\pi}{9\alpha_s(\mu)} & \frac{56\pi}{27\alpha_s(\mu)} & \frac{-8\pi}{9\alpha_s(\mu)} & 0 & 0 & 0 \end{pmatrix} \tag{D.66}$$

Finally, it is pointed out that in the evolution process of the $\{\mathcal{O}_i\}$ basis (section D.2 and D.3) the rescaled operator $\mathcal{O}_9' = 2\pi\mathcal{O}_9/\alpha_s(\mu)$ is used instead of $\mathcal{O}_9$. This corresponds to the replacement $\alpha_s(\mu) \to 2\pi$ in the matrices $\hat{M}(\mu)$ and $\hat{Z}(\mu)$.

E Operator Basis for the OPE up to Dimension 5

In this part of the appendix, we show that

$$\mathcal{O}^{\mu}_{3,1} = \left(g^{\mu\nu} - \frac{q^\mu q^\nu}{q^2}\right)\bar{s}\gamma_\nu(1-\gamma_5)b \qquad \mathcal{O}^{\mu}_{3,2} = \frac{im_b}{q^2}\,\bar{s}\sigma^{\mu q}(1+\gamma_5)b \tag{E.1}$$

$$\mathcal{O}^{\mu}_{4,1} = m_s\left(g^{\mu\nu} - \frac{q^\mu q^\nu}{q^2}\right)\bar{s}\gamma_\nu(1+\gamma_5)b \qquad \mathcal{O}^{\mu}_{4,2} = \frac{im_s m_b}{q^2}\,\bar{s}\sigma^{\mu q}(1-\gamma_5)b \tag{E.2}$$

represents a complete basis for all operators of dimension 3 and 4 that can possibly emerge in the OPE performed for the correlator $\mathcal{K}^\mu$ in chapter 5. This holds expressly to any order in QCD [1].

For the time being, let us assume the chiral limit ($m_s = 0$). Before, however, proceeding with the actual proof by exhaustion, let us establish the following facts:

- The generic structure of any $(n+3)$-dimensional operator containing (only) the quark fields $\bar{s}_L$ and b can be written as

$$\bar{s}_L\overleftarrow{D}^n\Gamma b \qquad \text{where} \qquad \Gamma = 1, \gamma^\alpha, \sigma^{\alpha\beta} \tag{E.3}$$

  Most notably, an ansatz where the covariant derivatives act exclusively on the strange quark already covers all possibilities. In other words, adding a covariant derivative acting on the bottom quark does not yield a new, that is, independent operator – a fact that can be derived from translation invariance alone:[1]

$$\bar{s}_L\overleftarrow{D}^n\Gamma D^\mu b = \partial^\mu\big(\bar{s}_L\overleftarrow{D}^n\Gamma b\big) - \bar{s}_L\overleftarrow{D}^n\overleftarrow{D}^\mu\Gamma b \tag{E.4}$$

$$= -iq^\mu\big(\bar{s}_L\overleftarrow{D}^n\Gamma b\big) + \dim(n+4) \tag{E.5}$$

- In order to obtain operators with a single open Lorentz index μ, the Dirac-structures in (E.3) can be contracted with the metric g, the ε-tensor and factors of q.

[1] The replacement $\partial^\mu \to -iq^\mu$, based on translation invariance, implicitly assumes a $B \to K^{(*)}$ matrix element where b and s quark taken together generate a momentum q^μ pointing into the $\bar{s}_L\overleftarrow{D}^n\Gamma b$ vertex.

Contractions of the Dirac-structures $\gamma^\alpha, \sigma^{\alpha\beta}$ with q_α, however, can immediately be disregarded on a general basis:

$$\begin{aligned} \bar{s}_L \overleftarrow{D}^n \not{q} b &= i\partial_\alpha\big(\bar{s}_L \overleftarrow{D}^n \gamma^\alpha b\big) = i\bar{s}_L \overleftarrow{D}^n \Big[\overleftarrow{\not{D}} + \overrightarrow{\not{D}}\Big] b \\ &= m_b \bar{s}_L \overleftarrow{D}^n b + \dim(n+4) \end{aligned} \tag{E.6}$$

$$\bar{s}_L \overleftarrow{D}^n \sigma^{\alpha q} b = i\bar{s}_L \overleftarrow{D}^n \big(m_b \gamma^\alpha - q^\alpha\big) b + \dim(n+4) \tag{E.7}$$

They only reproduce structures that can also be obtained through contractions of other instances of Γ. In particular, this also applies to

$$\mathcal{O}^\mu_{3,2} = \mathcal{O}^\mu_{3,1} - \frac{q_\nu}{q^2} \bar{s} \sigma^{\mu\nu} \overleftarrow{\not{D}} (1 + \gamma_5) b \tag{E.8}$$

witch effectively reduces the basis at the dimension-3 level to one independent operator only.

- It is sufficient to demonstrate that all operators can be expressed in terms of

$$q^\mu \bar{s}_L b \qquad \bar{s}_L \gamma^\mu b \qquad \bar{s}_L \sigma^{\mu q} b \tag{E.9}$$

Since current conservation imposes

$$q_\mu \mathcal{O}^\mu_{d,n} = 0 \tag{E.10}$$

it is then clear that only the two linear combinations of (E.9) that match our basis (E.1) may actually appear in the OPE.

Operators of Dimension $d = 3$

Starting with $d = 3$, the operators have the general form $\bar{s}_L \Gamma b$. Thus, the following contractions have to be considered for the respective choice of Γ

$$\bar{s}_L b \quad \to \quad q^\mu \bar{s}_L b \tag{E.11}$$

$$\bar{s}_L \gamma^\alpha b \quad \to \quad \bar{s}_L \gamma^\mu b,\ q^\mu \bar{s}_L \not{q} b \tag{E.12}$$

$$\bar{s}_L \sigma^{\alpha\beta} b \quad \to \quad \bar{s}_L \sigma^{\mu q} b,\ \varepsilon^{\mu q \alpha\beta} \bar{s}_L \sigma_{\alpha\beta} b \tag{E.13}$$

While the second operator of (E.12) is a special case of (E.6), the full contraction of $\sigma^{\alpha\beta}$ with the antisymmetric tensor in (E.13) can be reduced by means of universal Dirac-identities:

$$\varepsilon^{\mu q \alpha\beta} \bar{s}_L \sigma_{\alpha\beta} b = 2i\bar{s}_L \sigma^{\mu q} \gamma_5 b = 2i\bar{s}_L \sigma^{\mu q} b \tag{E.14}$$

With this, the proof already concludes at the dimension-3 level.

Operators of Dimension $d = 4$

As far as the dimension-4 operators are concerned, the different instances of $\Gamma = 1, \gamma^\alpha 1, \sigma^{\alpha\beta}$ are better approached separately. In the course of this, operators of dimension 5 will be dropped immediately.

- For $\Gamma = 1$, the generic structure becomes $\bar{s}_L \overleftarrow{D}^\nu b$. There are two possible contractions, which can be reduced according to

$$\begin{aligned} \bar{s}_L \overleftarrow{D}^\mu b &= \frac{1}{2} \bar{s}_L \Big[\overleftarrow{\not{D}} \gamma^\mu + \gamma^\mu \overleftarrow{\not{D}} \Big] b \;=\; \frac{1}{2} \Big[\partial_\nu (\bar{s}_L \gamma^\mu \gamma^\nu b) - \bar{s}_L \gamma^\mu \overrightarrow{\not{D}} b \Big] \\ &= \frac{i}{2} m_b \bar{s}_L \gamma^\mu b - \frac{1}{2} \bar{s}_L \sigma^{\mu q} b - \frac{i}{2} q^\mu \bar{s}_L b \end{aligned} \tag{E.15}$$

$$q^\mu q_\nu \bar{s}_L \overleftarrow{D}^\nu b = \frac{i}{2} (m_b^2 - q^2) q^\mu \bar{s}_L b \tag{E.16}$$

Note that (E.16) can be obtained directly from (E.15) via contraction with q_μ.

- Next, for $\Gamma = \gamma^\alpha$, one starts with the general operator $\bar{s}_L \overleftarrow{D}^\nu \gamma^\alpha b$, which can be contracted in five different ways:

$$q^\mu \bar{s}_L \overleftarrow{\not{D}} b = 0 \tag{E.17}$$

$$\bar{s}_L \overleftarrow{D}^\mu \not{q} b = i \bar{s}_L \overleftarrow{D}^\mu \overrightarrow{\not{D}} b = m_b \bar{s}_L \overleftarrow{D}^\mu b \tag{E.18}$$

$$\begin{aligned} q_\nu \bar{s}_L \overleftarrow{D}^\nu \gamma^\mu b &= i \bar{s}_L \overleftarrow{D}^\nu \gamma^\mu D_\nu b \;=\; \frac{i}{2} \partial^\nu \partial_\nu (\bar{s}_L \gamma^\mu b) - \frac{i}{2} \bar{s}_L \gamma^\mu D^\nu D_\nu b \\ &= \frac{i}{2} (m_b^2 - q^2) \bar{s}_L \gamma^\mu b \end{aligned} \tag{E.19}$$

$$q^\mu q_\nu \bar{s}_L \overleftarrow{D}^\nu \not{q} b = \frac{i}{2} m_b (m_b^2 - q^2) q^\mu \bar{s}_L b \tag{E.20}$$

$$\begin{aligned} \varepsilon^{\mu q \alpha \nu} \bar{s}_L \overleftarrow{D}_\alpha \gamma_\nu b &= -i \bar{s}_L \overleftarrow{D}_\alpha (\gamma^\alpha \gamma^\mu \not{q} - g^{\alpha\mu} \not{q} - q^\mu \gamma^\alpha + q^\alpha \gamma^\mu) b \\ &= i m_b \bar{s}_L \overleftarrow{D}^\mu b - i q_\nu \bar{s}_L \overleftarrow{D}^\nu \gamma^\mu b \end{aligned} \tag{E.21}$$

The r.h.s. of (E.18) then reduces to the basic operators (E.9) via (E.15); the two operators on the r.h.s. of (E.21) reduce via (E.15) and (E.19), respectively.

- For $\Gamma = \sigma^{\alpha\beta}$, finally, the generic operator assumes the form $\bar{s}_L \overleftarrow{D}^{\nu} \sigma^{\alpha\beta} b$, which requires an even number of q's to be contracted. For zero q's, we have

$$\bar{s}_L \overleftarrow{D}_{\nu} \sigma^{\mu\nu} b \;=\; i\bar{s}_L \overleftarrow{D}_{\nu} (g^{\nu\mu} - \gamma^{\nu}\gamma^{\mu}) b \;=\; i\bar{s}_L \overleftarrow{D}^{\mu} b \tag{E.22}$$

$$\varepsilon^{\mu\nu\alpha\beta} \bar{s}_L \overleftarrow{D}_{\nu} \sigma_{\alpha\beta} b \;=\; 2i\bar{s}_L \overleftarrow{D}_{\nu} \sigma^{\mu\nu} b \;=\; -2\bar{s}_L \overleftarrow{D}^{\mu} b \tag{E.23}$$

Contractions with two q's always involve the ε-tensor and fall a priori into two categories. Firstly, instances where one q is contracted with the $\sigma^{\alpha\beta}$

$$\bar{s}_L \overleftarrow{D}^{\nu} \sigma^{\alpha q} b \;=\; i\bar{s}_L \overleftarrow{D}^{\nu} (m_b \gamma^{\alpha} - q^{\alpha}) b \tag{E.24}$$

and thus (E.7) applies. Secondly, full contractions of the ε-tensor and $\sigma^{\alpha\beta}$

$$\varepsilon^{q\eta\alpha\beta} \bar{s}_L \overleftarrow{D}^{\nu} \sigma_{\alpha\beta} b \;=\; 2i\bar{s}_L \overleftarrow{D}^{\nu} \sigma^{q\eta} b \tag{E.25}$$

which, however, immediately leads us back to the first case (E.24).

Through this, the completeness of the basis (E.1) up to and including operators of dimension 4 is shown by exhaustion.

General Case $m_s \neq 0$

If one takes into account the mass of the strange quark, its e.o.m. becomes

$$-i\bar{s}_L \overleftarrow{\not{D}} \;=\; m_s \bar{s}_R \;\neq\; 0 \tag{E.26}$$

This gives rise to a new type of dimension-4 operator with the general form $m_s \bar{s}_R \Gamma b$. Since this is essentially a dimension-3 operator times a constant, the prove that reduces the new operators to the second row of our basis (E.2) closely resembles the dimension-3 case. Indeed, the only difference is the replacement $\bar{s}_L \to m_s \bar{s}_R$ and a minus sign on the r.h.s. of (E.14).

Operators of Dimension $d = 5$

With respect to a similar prove for dimension-5 operators, there is one qualitative difference, which arises from the fact that covariant derivatives do not commute with one another

$$\left[\overleftarrow{D}_{\alpha}, \overleftarrow{D}_{\beta}\right] \;=\; \left[\overrightarrow{D}_{\alpha}, \overrightarrow{D}_{\beta}\right] \;=\; -igG^a_{\alpha\beta} T^a \tag{E.27}$$

As a consequence, there are two different types of dimension-5 operators. Firstly, operators that can be expressed in terms of dimension-3 operators times a purely kinematic power suppression, for instance $(m_b^2 - q^2)^2$. Secondly, operators of the general form

$$\mathcal{O}^{\mu}_{5,n} \;=\; g_s \bar{s}_L (\Gamma_n G^a T^a)^{\mu} b \tag{E.28}$$

which we recognize as genuine dimension-5 operators.

F Feynman Integrals

y-Integration

After integrating over the undetermined loop momentum l, two different types of integrals appear in the calculation of the Feynman diagrams in Fig. 9.3:

$$\tilde{Y}^l_{j,k} \;\equiv\; \iint dx\, dy\, x^j (1-x)^k y^l \ln(a_0 + (a_1 - a_0)y) \tag{F.1}$$

$$Y^l_{j,k} \;\equiv\; \iint dx\, dy\, \frac{x^j (1-x)^k y^l}{a_0 + (a_1 - a_0)y} \tag{F.2}$$

At this, the quantity a^2, defined in (9.12), has been decomposed according to

$$a^2/m_q^2 \;=\; a_0 + (a_1 - a_0)y \;=\; a_0 - x(1-x)c_{10}\, y \tag{F.3}$$

where $(c_{10} = c_1 - c_0 = \bar{u}(1-s)/t)$

$$a_i \;=\; 1 - x(1-x)c_i \qquad\qquad c_0 t \;=\; s \qquad\qquad c_1 t \;=\; su + \bar{u} \tag{F.4}$$

Note that integrals of the form (F.1) arise from the l^2-term, and integrals of the form (F.2) from the l^0-term. Both types, (F.1) and (F.2), can be reduced to integrals of the form

$$X^i_{j,k} \;\equiv\; \int dx\, x^j (1-x)^k \ln(1 - x(1-x)c_i) \tag{F.5}$$

First, the integrals (F.1) are reduced to (F.2) and (F.5) using integration by parts

$$(l+1)\tilde{Y}^l_{j,k} \;=\; X^1_{j,k} + c_{10}\, Y^{l+1}_{j+1,k+1} \tag{F.6}$$

Second, to reduce the integrals (F.2), the y-integration has to be performed explicitly. The relevant instances of l are given as $(X^{10}_{j,k} \equiv X^1_{j,k} - X^0_{j,k}, \mathrm{B}(j,k) = \Gamma(j)\Gamma(k)/\Gamma(j+k))$

$$c_{10}\, Y^0_{j,k} \;=\; -X^{10}_{j-1,k-1} \tag{F.7}$$

$$c_{10}^2\, Y^1_{j,k} \;=\; -X^{10}_{j-2,k-2} + c_0 X^{10}_{j-1,k-1} - c_{10}\,\mathrm{B}(j,k) \tag{F.8}$$

$$\begin{aligned} 2c_{10}^3\, Y^2_{j,k} \;=\;& -2X^{10}_{j-3,k-3} + 4c_0 X^{10}_{j-2,k-2} - 2c_0^2 X^{10}_{j-1,k-1} \\ & - 2c_{10}\,\mathrm{B}(j-1,k-1) + c_{10}(2c_0 - c_{10})\,\mathrm{B}(j,k) \end{aligned} \tag{F.9}$$

x-Integration

For the integration over the x parameter, it is convenient to introduce the quantities

$$c_{i\pm} = \frac{1}{2}\Big(1 \pm \sqrt{1 - 4/c_i}\Big) \tag{F.10}$$

Using the identities

$$a_i = c(x - c_+)(x - c_-) = (1 - \frac{x}{c_+})(1 - \frac{x}{c_-}) = (1 - xcc_+)(1 - xcc_-) \tag{F.11}$$

the logarithm of a_i can then be decomposed as (the subscript i on all $c_{(\pm)}$'s is dropped from (F.12) through (F.18))

$$\ln(1 - x(1 - x)c) = \ln(1 - xcc_+) + \ln(1 - xcc_-) \tag{F.12}$$

Exploiting the two basic relations $X^i_{j,k} = X^i_{k,j}$ and $X^i_{j,k} = X^i_{j,k+1} + X^i_{j+1,k}$, any integral $X^i_{j,k}$ with $j + k \leqslant 2l + 1$ and $j, k \geqslant -n$ can be described as linear combination of the integrals $X^i_{-n,0}, X^i_{1-n,0}, ..., X^i_{0,0}, X^i_{2,0}, ..., X^i_{2l,0}$. Thus, in the present context, only the following integrals have to be calculated explicitly

$$X^i_{2,0} = \frac{c - 1}{3c} X^i_{0,0} - \frac{1}{18} \tag{F.13}$$

$$X^i_{0,0} = \Big[(x - c_+)\ln(1 - x(1 - x)c) + (c_+ - c_-)\ln(1 - cc_+x) - 2x\Big]\Big|_0^1 \tag{F.14}$$

$$= (c_+ - c_-)\ln(1 - cc_+) - 2 = -\mathrm{B}_0(s, m_q) - 2 \tag{F.15}$$

$$X^i_{-1,0} = \Big[- \mathrm{Li}_2(xcc_+) - \mathrm{Li}_2(xcc_-)\Big]\Big|_0^1 = \frac{1}{2}\ln^2(1 - cc_\pm) = \frac{1}{2}\ln^2(-c_\pm/c_\mp) \tag{F.16}$$

$$X^i_{-2,0} = \Big[(cc_+ - 1/x)\ln(1 - x(1 - x)c) - c(c_+ - c_-)\ln(x - c_+) - c\ln x\Big]\Big|_0^1 \tag{F.17}$$

$$= c(c_+ - c_-)\ln(1 - cc_+) - c - c\ln x = c(X^i_{0,0} + 1 - \ln x) \tag{F.18}$$

where $\mathrm{B}_0(s, m_q)$ is the function used in [40] to express $t_\parallel(s, t, u)$. The function $F(x)$, which is used in this work and, for instance, defined in (9.30), is related to the integrals above via

$$F^2(4/c_i) = 2X^i_{-1,0} - c_1 X^i_{0,0} + (c_1^2/4)(1 - 4/c_i) \tag{F.19}$$

One then finds for the curly bracket in (9.27)

$$\Big\{...\Big\} = \frac{s}{\hat{u}}(\hat{u} + s)X^{10}_{0,0} - \frac{2st}{\hat{u}} X^{10}_{-1,0} - s = -\frac{st}{\hat{u}}(F^2(4/c_1) - F^2(4/c_0)) + \hat{u} \tag{F.20}$$

$$= -\frac{s\hat{u}}{4} t_\parallel(s, t, u) \tag{F.21}$$

Bibliography

[1] M. Beylich, G. Buchalla, and Th. Feldmann, “Theory of $B \to K^{(*)}l^+l^-$ decays at high q^2: OPE and quark-hadron duality”, *Eur. Phys. J.* **C 71** (2011) 1635, [arXiv:1101.5118 [hep-ph]].

[2] M. E. Peskin and D. V. Schroeder, “An Introduction to Quantum Field Theory”, *Westview Press* (Reading 1995), ISBN 0-201-50397-2.

[3] A. Zee, “Quantum Field Theory in a Nutshell”, *Princeton University Press* (2010), ISBN 0-691-14034-6.

[4] F. Mahmoudi, T. Hurth, and S. Neshatpour, “Present Status of $b \to s\ell^+\ell^-$ Anomalies”, (2016), [arXiv:1611.05060 [hep-ph]].

[5] W. Altmannshofer, C. Niehoff, P. Stangl, and D. M. Straub, “Present Status of $B \to K^*\mu^+\mu^-$ anomaly after Moriond 2017”, (2017), [arXiv:1703.09189 [hep-ph]].

[6] G. Buchalla, “Heavy Quark Theory”, (2002), [arXiv:hep-ph/0202092].

[7] M. Beneke, G. Buchalla, M. Neubert, and C. T. Sachrajda, “Penguins with Charm and Quark-Hadron Duality”, *Eur. Phys. J.* **C 61** (2009) 439, [arXiv:0902.4446 [hep-ph]].

[8] T. Onogi, “Lattice Determination of Semileptonic Form Factors”, (2003), [arXiv:hep-ph/0309225].

[9] P. Ball and R. Zwicky, “New Results on $B \to \pi, K, \eta$ Decay Formfactors from Light-Cone Sum Rules”, *Phys. Rev.* **D 71** (2005) 014015, [arXiv:hep-ph/0406232].

[10] G. Buchalla, A. J. Buras, and M. E. Lautenbacher, “Weak Decays Beyond Leading Logarithms”, *Rev. Mod. Phys.* **68** (1996) 1125, [arXiv:hep-ph/9512380].

[11] A. J. Buras, “Weak Hamiltonian, CP Violation and Rare Decays”, (1998), [arXiv:hep-ph/9806471].

[12] A. J. Buras and R. Fleischer, "Quark Mixing, CP Violation and Rare Decays After the Top Quark Discovery", (1997), [arXiv:hep-ph/9704376].

[13] G. 't Hooft and M. Veltman, *Nucl. Phys.* **B 44** (1972) 189.

[14] G. 't Hooft, *Nucl. Phys.* **B 61** (1973) 455.

[15] P. Gambinom, M. Gorbahn, and U. Haisch, "Anomalous Dimension Matrix for Radiative and Rare Semileptonic B Decays up to Three Loops", (2003), [arXiv:hep-ph/0306079].

[16] K. Chetyrkin, M. Misiak, and M. Münz, "$\|\Delta\| = 1$ Nonleptonic Effective Hamiltonian in a Simpler Scheme", *Nucl. Phys.* **B 520** (1998) 279, [arXiv:hep-ph/9711280].

[17] M. Gorbahn and U. Haisch, "Effective Hamiltonian for Non-Leptonic $|\Delta F| = 1$ Decays at NNLO in QCD", (2009), [arXiv:hep-ph/0411071].

[18] C. Bobeth, M. Misiak, and J. Urban, "Photonic penguins at two loops and m_t-dependence of $BR[B \to X_s l^+ l^-]$", (1999), [arXiv:hep-ph/9910220].

[19] K. Chetyrkin, M. Misiak, and M. Münz, "Weak Radiative B-Meson Decay Beyond Leading Logarithms", *Phys. Lett.* **B 400** (1997) 206, [arXiv:hep-ph/9612313].

[20] G. Buchalla and G. Isidori, "Nonperturbative Effects in $\bar{B} \to X_s l^+ l^-$ for Large Dilepton Invariant Mass", *Nucl. Phys.* **B 525** (1998) 333, [arXiv:hep-ph/9801456].

[21] B. Grinstein and D. Pirjol, "Exclusive rare $B \to K^* e^+ e^-$ decays at low recoil: controlling the long-distance effects", *Phys. Rev.* **D 70** (2004) 114005, [arXiv:hep-ph/0404250].

[22] J. Charles, A. Le Yaouanc, L. Oliver, O. Pene, and J. C. Raynal, "Heavy-to-Light Form-Factors in the Final Hadron Large Energy Limit of QCD", *Phys. Rev.* **D 60** (1999) 014001, [arXiv:hep-ph/9812358].

[23] P. Ball and R. Zwicky, "$B_{d,s} \to \rho, \omega, K^*, \phi$ Decay Form Factors from Light-Cone Sum Rules Revisited", *Phys. Rev.* **D 71** (2005) 014029, [arXiv:hep-ph/0412079].

[24] N. Isgur and M. B. Wise, *Phys. Rev.* **D 42** (1990) 2388.

[25] M. Beneke and Th. Feldmann, "Symmetry-breaking corrections to heavy-to-light B meson form factors at large recoil", *Nucl. Phys.* **B 592** (2001) 3, [arXiv:hep-ph/0008255].

[26] C. W. Bauer, S. Fleming, D. Pirjol, and I. W. Stewart, "An effective field theory for collinear and soft gluons: heavy to light decays", *Phys. Rev.* **D 63** (2001) 114020, [arXiv:hep-ph/0011336].

[27] C. W. Bauer, D. Pirjol, and I. W. Stewart, "Soft-Collinear Factorization in Effective Field Theory", *Phys. Rev.* **D 65** (2002) 054022, [arXiv:hep-ph/0109045].

[28] R. J. Hill, "Heavy-to-light meson form factors at large recoil", *Phys. Rev.* **D 73** (2006) 014012, [arXiv:hep-ph/0505129].

[29] M. Bartsch, M. Beylich, G. Buchalla, and D. N. Gao, "Precision Flavour Physics with $B \to K\nu\bar{\nu}$ and $B \to Kl^+l^-$", *JHEP* **0911** (2009) 011, [arXiv:0909.1512 [hep-ph]].

[30] G. Buchalla, "Precision flavour physics with $B \to K\nu\bar{\nu}$ and $B \to Kl^+l^-$", (2010), [arXiv:1010.2674 [hep-ph]].

[31] N. Isgur, *Phys. Rev.* **D 43** (1991) 810.

[32] M. Beneke, G. Buchalla, M. Neubert, and C. T. Sachrajda, "QCD factorization for exclusive non-leptonic B-meson decays: General arguments and the case of heavy-light final states", *Nucl. Phys.* **B 591** (2000) 313, [arXiv:hep-ph/0006124].

[33] M. Beneke, G. Buchalla, M. Neubert, and C. T. Sachrajda, "QCD Factorization in $B \to \pi K, \pi\pi$ Decays and Extraction of Wolfenstein Parameters", *Nucl.Phys.* **B 606** (2001) 245, [arXiv:hep-ph/0104110].

[34] V. M. Braun and I. E. Filyanov, "QCD sum rules in exclusive kinematics and pion wave function", *Z. Phys.* **C 44** (1989) 157.

[35] V. M. Braun and I. E. Filyanov, "Conformal Invariance And Pion Wave Functions Of Nonleading Twist", *Z. Phys.* **C 48** (1990) 239.

[36] P. Ball *et al.*, "Higher Twist Distribution Amplitudes of Vector Mesons in QCD: Formalism and Twist Three Distributions", *Nucl. Phys.* **B 529** (1998) 323, [arXiv:hep-ph/9802299].

[37] B. V. Geshkenbein and M. V. Terentev, *Phys. Lett.* **B 117** (1982) 243, Sov. J. Nucl. Phys. **40** (1984) 487 [Yad. Fiz. **40** (1984) 758]; Yad. Fiz. **39** (1984) 873.

[38] A. G. Grozin and M. Neubert, "Asymptotics of Heavy-Meson Form Factors", *Phys. Rev.* **D 55** (1997) 272, [arXiv:hep-ph/9607366].

[39] M. Beneke, G. Buchalla, M. Neubert, and C. T. Sachrajda, "QCD Factorization for $B \to \pi\pi$ Decays: Strong Phases and CP Violation in the Heavy Quark Limit", *Eur. Phys. Rev. Lett.* **83** (1999) 1914, [arXiv:hep-ph/9905312].

[40] M. Beneke, Th. Feldmann, and D. Seidel, "Systematic approach to exclusive $B \to Vl^+l^-, V\gamma$ decays", *Nucl. Phys.* **B 612** (2001) 25, [arXiv:hep-ph/0106067].

[41] A. Khodjamirian, Th. Mannel, A. A. Pivorarov, and Y. M. Wang, "Charm-loop effect in $B \to K^{(*)}\ell^+\ell^-$ and $B \to K^*\gamma$", *JHEP* **1009** (2010) 089, [arXiv:1006.4945 [hep-ph]].

[42] M. Artuso *et al.*, *Eur. Phys. J. C* **57** (2008) 309, [arXiv:0801.1833 [hep-ph]].

[43] G. Buchalla, G. Isidori, and S. J. Rey, "Corrections of Order Λ^2_{QCD}/m_c^2 to Inclusive Rare B Decays", *Nucl. Phys* **B 511** (1998) 594, [arXiv:hep-ph/9705253].

[44] D. Seidel, "Analytic two-loop virtual corrections to $b \to dl^+l^-$", *Phys. Rev.* **D 70** (2004) 094038, [arXiv:hep-ph/0403185].

[45] C. Greub, V. Pilipp, and C. Schüpbach, "Analytic calculation of two-loop QCD corrections to $b \to s\ell^+\ell^-$ in the high q^2 region", *JHEP* **0812** (2008) 040, [arXiv:0810.4077 [hep-ph]].

[46] M. Beneke, T. Feldmann, and D. Seidel, "Exclusive radiative and electroweak $b \to d$ and $b \to s$ penguin decays at NLO", *Eur. Phys. J.* **C 41** (2005) 173, [arXiv:hep-ph/0412400].

[47] N. Isgur and M. B. Wise, *Phys. Rev.* **D 41** (1990) 151.

[48] V. L. Chernyak and I. R. Zhitnitsky, "B-meson exclusive decays into baryons", *Nucl. Phys.* **B 345** (1990) 137.

[49] C. Bobeth, G. Hiller, and D. van Dyk, "The Benefits of $B \to K^*l^+l^-$ Decays at Low Recoil", *JHEP* **1007** (2010) 098, [arXiv:1006.5013 [hep-ph]].

[50] M. Beneke, G. Buchalla, and I. Dunietz, "Width Difference in the $B_s - \bar{B}_s$ System", *Phys. Rev.* **D 54** (1996) 4419, [arXiv:hep-ph/9605259].

[51] M. Beneke, G. Buchalla, A. Lenz C. Greub, and U. Nierste, "Next-to-Leading Order QCD Corrections to the Lifetime Difference of B_s Mesons", *Phys. Lett* **B 459** (1999) 631, [arXiv:hep-ph/9808385].

[52] M. A. Shifman, "In the Proceedings of QCD @ Work 2003: 2nd International

Workshop on Quantum Chromodynamics: Theory and Experiment", Conversano Italy 14-18 June 2003.

[53] B. Blok, M. A. Shifman, and D. X. Zhang, "An Illustrative Example of How Quark-Hadron Duality Might Work", *Phys. Rev.* **D 57** (1998) 2691, [arXiv:hep-ph/9709333], Erratumibid. D **59** 1999 019901.

[54] M. A. Shifman, "Quark-Hadron Duality", [arXiv:hep-ph/0009131].

[55] O. Cata, M. Golterman, and S. Peris, "Unraveling duality violations in hadronic tau decays", *Phys. Rev.* **D 77** (2008) 093006, [arXiv:0803.0246 [hep-ph]].

[56] A. B. Kaidalov, *Usp. Fiz. Nauk* **105** (1971) 97, [*Sov. Phys. Uspekhi* **14** (1972) 600].

[57] P. D. B. Collins, "An Introduction to Regge Theory and High-Energy Physics", *Cambridge University Press* (1977).

[58] A. R. Zhitnitsky, "Lessons from $QCD_2(N \to \infty)$: Vacuum structure, Asymptotic Series, Instantons and all that", *Phys. Rev* **D 53** (1996) 5821, [arXiv:hep-ph/9510366].

[59] M. Baldicchi and G. M. Prosperi, "Regge trajectories and quarkonium spectrum from a first principle Salpeter equation", *Phys. Lett.* **B 436** (1998) 145, [arXiv:hep-ph/9803390].

[60] A. V. Anisovich, V. V. Anisovich, and A. V. Sarantsev, "Systematics of q anti-q states in the (n, M^2) and (J, M^2) planes", *Phys. Rev.* **D 62** (2000) 051502, [arXiv:hep-ph/0003113].

[61] S. S. Gershtein, A. K. Likhoded, and A. V. Luchinsky, "Systematics of heavy quarkonia from Regge trajectories on (n, M^2) and (M^2, J) planes", *Phys. Rev.* **D 74** (2006) 016002, [arXiv:hep-ph/0602048].

[62] A. Casher, H. Neuberger, and S. Nussinov, "Chromoelectric Flux Tube Model of Particle Production", *Phys. Rev.* **D 20** (1979) 179.

[63] J. Z. Bai *et al.* [BES Collaboration], "Measurements of the Cross Section for $e^+e^- \to$ hadrons at Center-of-Mass Energies from 2 to 5 GeV", *Phys. Rev. Lett.* **88** (2002) 101802, [arXiv:hep-ex/0102003].

[64] M. Ablikim *et al.*, "Measurements of the continuum $R_{\rm uds}$ and R values in e^+e^-

annihilation in the energy region between 3.650 and 3.872 GeV", *Phys. Rev. Lett.* **97** (2006) 262001, [arXiv:hep-ex/0612054].

[65] J. H. Kühn, M. Steinhauser, and C. Sturm, "Heavy Quark Masses from Sum Rules in Four-Loop Approximation", *Nucl. Phys.* **B 778** (2007) 192, [arXiv:hep-ph/0702103].

[66] K. A. Olive *et al.* (Particle Data Group), "Review of Particle Physics", *Chin. Phys.* **C 38** (2014) 090001, [URL: http://pdg.lbl.gov].

[67] A. D. Martin and D. Zeppenfeld, *Phys. Lett* **B 345** (1995) 558.

[68] R. V. Harlander and M. Steinhauser, *Comout. Phys. Commun.* **153** (2003) 244.

[69] B. Chibisov, R. D. Dikeman, M. A. Shifman, and N. Uraltsev, "Operator Product Expansion, Heavy Quarks, QCD Duality and its Violations", *Int. J. Mod. Phys.* **A 12** (1997) 2075, [arXiv:hep-ph/9605465].

[70] A. Ali, A. Y. Parkhomenko, and A. V. Rusov, "Precise Calculation of the Dilepton Invariant-Mass Spectrum and the Decay Rate in $B^{\pm} \to \pi^{\pm}\mu^{+}\mu^{-}$ in the SM", *Phys. Rev.* **D 89** (2014) 094021, [arXiv:hep-ph/1312.2523 [hep-ph]].

[71] D. Becirevic and A. B. Kaidalov, "Comment on the heavy $\to$ light form factors", *Phys. Lett.* **B 478** (2000), [arXiv:hep-ph/9904490].

[72] R. Aaij *et al.* (The LHCb collaboration), "First observation of the decay $B^{+} \to \pi^{+}\mu^{+}\mu^{-}$", (2013), [arXiv:1210.2645 [hep-ex]].

[73] J. Wang, R. Wang, and Y. Yang, "The rare decays $B_u^{+} \to \pi^{+}l^{+}l^{-}$, $\rho l^{+}l^{-}$ and $B_d^{0} \to l^{+}l^{-}$", *Phys. Rev* **D 77** (2007) 014017, [arXiv:0711.0321 [hep-ph]].

[74] G. Buchalla, G. Hiller, and G. Isidori, "Phenomenology of non-standard Z couplings in exclusive semileptonic $b \to s$ transitions", *Phys. Rev.* **D 63** (2001) 014015, [arXiv:hep-ph/0006136].

[75] Heavy Flavor Averaging Group (HFAG), (2015), [http://www.slac.stanford.edu/xorg/hfag/].

[76] A. J. Buras and M. Münz, "Effective Hamiltonian for $B \to X_s e^{+}e^{-}$ Beyond Leading Logarithms in the NDR and HV Schemes", *Phys. Rev.* **D 52** (1995) 186, [arXiv:hep-ph/9501281].

[77] M. Misiak, *Nucl. Phys.* **B 393** (1993) 23, Erratum-ibid. B 439 1995 461.

[78] H. H. Asatryan, H. M. Asatrian, C. Greub, and M. Walker, "Calculation of two-loop virtual corrections to $b \to sl^+l^-$ in the standard model", *Phys. Rev.* **D 65** (2002) 074004, [arXiv:hep-ph/0109140].

[79] H. H. Asatryan, H. M. Asatrian, C. Greub, and M. Walker, "Two-loop virtual corrections to $B \to X_s l^+l^-$ in the standard model", *Phys. Lett.* **B 507** (2001) 162, [arXiv:hep-ph/0103087].

[80] H. M. Asatrian, K. Bieri C. Greub, and M. Walker, "Virtual- and bremsstrahlung corrections to $b \to dl^+l^-$ in the standard model", *Phys. Rev.* **D 69** (2004) 074007, [arXiv:hep-ph/0312063].

[81] H. H. Asatryan, H. M. Asatrian, C. Greub, and M. Walker, "Complete gluon bremsstrahlung corrections to the process $b \to sl^+l^-$", *Phys. Rev.* **D 66** (2002) 034009, [arXiv:hep-ph/0204341].

[82] Y. Amhis *et al.* (HFAG), "Averages of b-hadron, c-hadron, and τ-lepton properties as of early 2012", (2013), [arXiv:1207.1158 [hep-ex]].

[83] M. Bartsch, G. Buchalla, and C. Kraus, "$B \to V_L V_L$ Decays at Next-to-Leading Order in QCD", (2008), [arXiv:0810.0249 [hep-ph]].

[84] T. Hurth and F. Mahmoudi, "The Minimal Flavour Violation benchmark in view of the latest LHCb data", *Nucl. Phys.* **B 865** (2012) 461, [arXiv:1207.0688 [hep-ph]].

[85] M. Beneke and M. Neubert, "QCD factorization for $B \to PP$ and $B \to PV$ decays", *Nucl. Phys.* **B 675** (2003) 333, [arXiv:hep-ph/0308039].

[86] P. Ball, G. W. Jones, and R. Zwicky, "$B \to V\gamma$ Beyond QCD Factorisation", *Phys. Rev.* **D 75** (2007) 054004, [arXiv:hep-ph/0612081].

[87] A. Khodjamirian, Th. Mannel, and M. Melcher, "Kaon Distribution Amplitude from QCD Sum Rules", *Phys. Rev* **D 70** (2004) 094002, [arXiv:hep-ph/0407226].

[88] P. Ball and R. Zwicky, "SU(3) Breaking of Leading–Twist K and K^* Distribution Amplitudes - a Reprise", *Phys. Lett.* **B 633** (2006) 289, [arXiv:hep-ph/0510338].

[89] P. Ball, V. M. Braun, and A. Lenz, "Twist-4 Distribution Amplitudes of the K^* and ϕ Mesons in QCD", *JHEP* **0708** (2007) 090, [arXiv:0707.1201 [hep-ph]].

[90] P. Ball and G. W. Jones, "Twist-3 Distribution Amplitudes of K^* and ϕ Mesons", *JHEP* **0703** (2007) 069, [arXiv:hep-ph/0702100].

[91] P. Ball, V. M. Braun, and A. Lenz, "Higher-Twist Distribution Amplitudes of the K Meson in QCD", *JHEP* **0605** (2006) 004, [arXiv:hep-ph/0603063].

[92] V. M. Braun, D. Yu. Ivanov, and G. P. Korchemsky, "The B-Meson Distribution Amplitude in QCD", *Phys. Rev* **D 69** (2004) 034014, [arXiv:hep-ph/0309330].

[93] A. Khodjamirian, T., and N. Offen, "B-Meson Distribution Amplitude from the $B \to \pi$ Form Factor", *Phys. Lett* **B 620** (2005) 52, [arXiv:hep-ph/0504091].

[94] S. J. Lee and M. Neubert, "Model-Independent Properties of the B-Meson Distribution Amplitude", *Phys. Rev* **D 72** (2005) 094028, [arXiv:hep-ph/0509350].

[95] S. A. Larin and J. A. M. Vermaseren, "The three-loop QCD β-function and anomalous dimensions", *Phys. Lett.* **B 303** (1993) 334, [arXiv:hep-ph/9302208].

[96] O. V. Tarasov, A. A. Vladimirov, and A. Yu. Zharkov, *Phys. Lett.* **B 93** (1980) 429.

[97] A. J. Buras, M. Misiak, M. Münz, and S. Pokorski, "Theoretical Uncertainties and Phenomenological Aspects of $B \to X_s\gamma$ Decay", *Nucl. Phys.* **B 424** (1993) 374, [arXiv:hep-ph/9311345].

[98] G. Buchalla and A. J. Buras, "The Rare Decays $K \to \pi\nu\bar{\nu}$, $B \to X\nu\bar{\nu}$ and $B \to l^+l^-$: An Update", *Nucl. Phys.* **B 548** (1999) 309, [arXiv:hep-ph/9901288].

[99] M. Misiak and J. Urban, "QCD corrections to FCNC decays mediated by Z-penguins and W-boxes", *Phys. Lett.* **B 451** (1999) 161, [arXiv:hep-ph/9901278].

[100] G. Buchalla and A. J. Buras, *Nucl. Phys.* **B 400** (1993) 225.

[101] M. Fierz, "Zur Fermischen Theorie des β-Zerfalls", *Z. Physik* **104** (1937) 553.

[102] J. F. Nieves and P. B. Pal, "Generalized Fierz identities", *Am J. Phys.* **72** (2004) 1100, [arXiv:hep-ph/0306087].

[103] C. C. Nishi, "Simple derivation of general Fierz-type identities", *Am J. Phys.* **73** (2005) 160, [arXiv:hep-ph/0412245].

[104] S. Herrlich and U. Nierste, "Evanescent Operators, Scheme Dependences and Double Insertions", *Nucl. Phys.* **B 455** (1995) 39, [arXiv:hep-ph/9412375].

Acknowledgements

At the end, I would like to thank everybody who supported me and, in this way, contributed to the success of thesis.

First of all, I want to express my gratitude towards my advisor, Prof. Gerhard Buchalla, for supervising my thesis. I am grateful for many instructive and helpful discussions, in particular his willingness to answer my questions at any given time. I also greatly appreciate his proofreading and comments on the manuscript.

My special thanks go to my parents for their unconditional support and encouragement over the past years. In particular, I want to thank my mother for her continuous help in all of life's situations and my father for proofreading the manuscript.

This work was supported by the DFG Graduiertenkolleg GK 1054, for which I am grateful as well.